

## Ecophysiology of N<sub>2</sub>O-emitting microbial communities

Roothans, Nina

**DOI**

[10.4233/uuid:b17773eb-b404-4034-82a8-cae6d7eeced9](https://doi.org/10.4233/uuid:b17773eb-b404-4034-82a8-cae6d7eeced9)

**Publication date**

2025

**Document Version**

Final published version

**Citation (APA)**

Roothans, N. (2025). *Ecophysiology of N<sub>2</sub>O-emitting microbial communities*. [Dissertation (TU Delft), Delft University of Technology]. <https://doi.org/10.4233/uuid:b17773eb-b404-4034-82a8-cae6d7eeced9>

**Important note**

To cite this publication, please use the final published version (if applicable).  
Please check the document version above.

**Copyright**

Other than for strictly personal use, it is not permitted to download, forward or distribute the text or part of it, without the consent of the author(s) and/or copyright holder(s), unless the work is under an open content license such as Creative Commons.

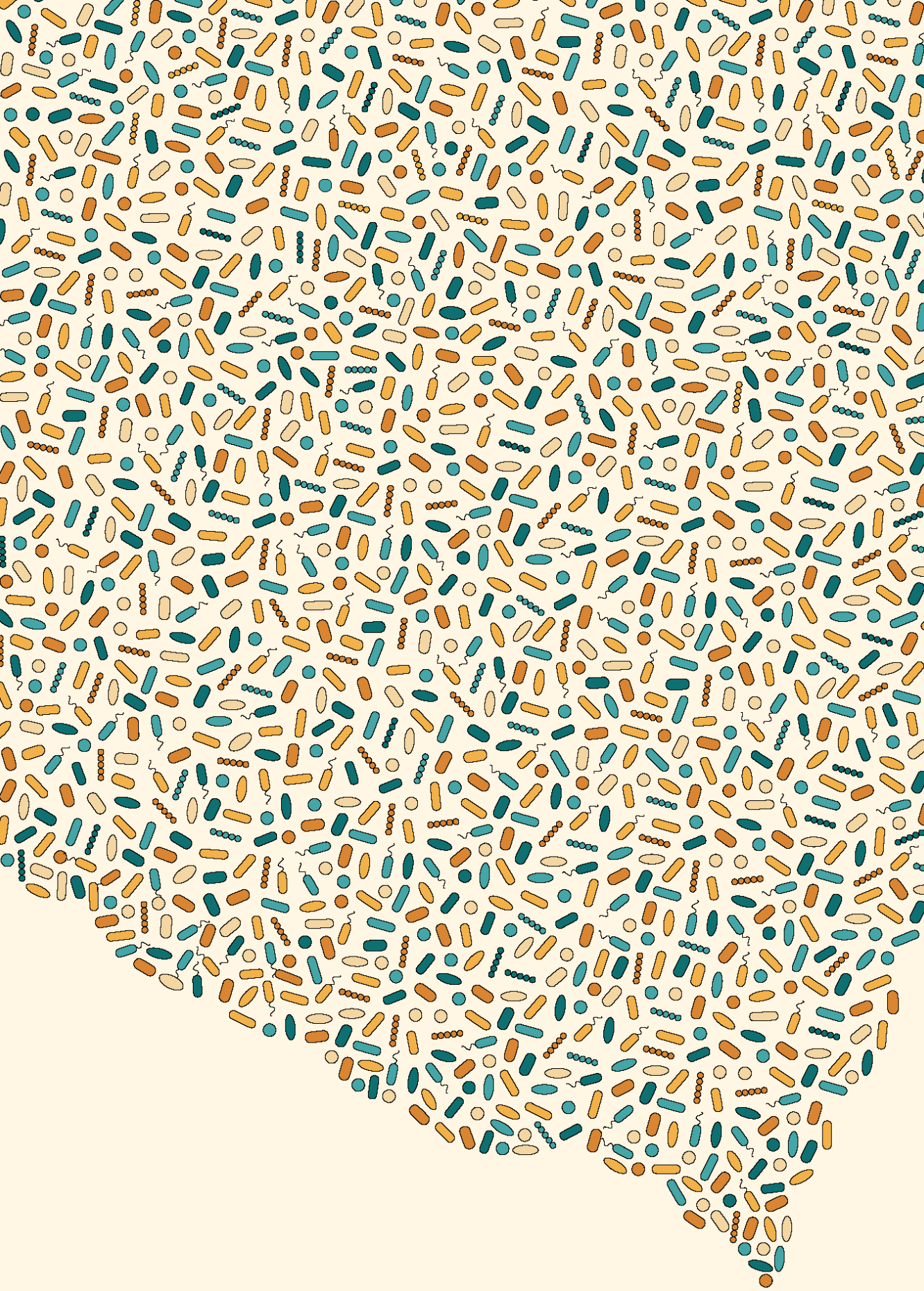
**Takedown policy**

Please contact us and provide details if you believe this document breaches copyrights.  
We will remove access to the work immediately and investigate your claim.

# ECOPHYSIOLOGY OF N<sub>2</sub>O-EMITTING MICROBIAL COMMUNITIES



Nina Roothans



# **PROPOSITIONS**

accompanying the dissertation

## **Ecophysiology of N<sub>2</sub>O-emitting microbial communities**

by

**Nina Christina Maria ROTHANS**

1. "It is not the strongest of the species that survives, nor the most intelligent; it is the one most adaptable to change." [adapted from Leon C. Megginson, 1963] (Chapters 2 and 4)
2. Partial denitrification is the rule, not the exception. (Chapter 2)
3. Metagenomics alone does not identify the most important organisms in a microbial community. (Chapter 3)
4. N<sub>2</sub>O emissions can only be minimised, not fully mitigated, and this requires understanding the underlying microbial mechanisms.
5. Aerobic denitrification will remain controversial, despite growing evidence.
6. Mixed cultures are as delicate as they are robust.
7. Correlations are used and abused in scientific literature. [Carr *et al.*, 2019]
8. "A picture is worth a thousand words" should be a guiding principle when preparing scientific figures.
9. The choice of the supervisory team is the single most important decision for a PhD.
10. The demands for self-promotion in a research career provide excellent preparation for a future in marketing.
11. While today's market prioritises computational skills, future breakthroughs will depend on the rare ability to biologically interpret data.
12. Climate change and global pollution can only be effectively addressed after solving world poverty.

These propositions are regarded as opposable and defensible, and have been approved as such by the promotor prof. dr. ir. M. C. M. van Loosdrecht and copromotor dr. M. Laureni.





# **Ecophysiology of N<sub>2</sub>O-emitting microbial communities**

Nina Roothans



# **Ecophysiology of N<sub>2</sub>O-emitting microbial communities**

## **Dissertation**

For the purpose of obtaining the degree of doctor  
at Delft University of Technology,  
by the authority of the Rector Magnificus, Prof. dr. ir. T.H.J.J. van der Hagen,  
Chair of the Board for Doctorates

to be defended publicly on Friday 11 April 2025 at 10:00

by

**Nina Christina Maria ROOTHANS**

Master of Science in Life Science and Technology,  
Delft University of Technology, the Netherlands

Born in Veldhoven, the Netherlands

This dissertation has been approved by the promotor.

Composition of the doctoral committee:

Rector Magnificus,	chairperson
Prof. dr. ir. M. C. M. van Loosdrecht,	Delft University of Technology, promotor
Dr. M. Laurenzi,	Delft University of Technology, copromotor

*Independent members:*

Prof. dr. J.T. Pronk,	Delft University of Technology
Prof. dr. S. Hallin,	Swedish University of Agricultural Sciences, Sweden
Prof. dr. D. Z. Sousa,	Wageningen University and Research
Dr. B. Kartal,	Max Planck Institute for Marine Microbiology, Germany
Dr. S. Kuehn,	University of Chicago, United States of America

*Reserve member:*

Prof. dr. D. Brdjanovic,	Delft University of Technology
--------------------------	--------------------------------



This work was part of a collaboration with Stichting Toegepast Onderzoek Waterbeheer (STOWA), Waternet, Hoogheemraadschap Hollands Noorderkwartier (HHNK), Waterschap de Dommel, and Waterschap Aa en Maas, and was funded by STOWA (18 JG191217009/732.750/CU), HHNK (19 20.0787440) and Waterschap de Dommel (Z62737/U131154).

Keywords: Nitrous oxide; greenhouse gas emissions; nitrogen cycle; microbial communities; ecophysiology; metagenomics; metaproteomics; laboratory enrichments; wastewater treatment

Printed by: Proefschriftspecialist

Cover design by: Nina Roothans

ISBN: 978-94-6518-035-9

Copyright © 2025 by Nina Roothans

An electronic version of this dissertation is available at <https://repository.tudelft.nl>.



# CONTENTS

Summary	xi
Samenvatting	xiii
Resumo	xv
<b>1</b> Introduction	1
<b>2</b> Aerobic denitrification as an N <sub>2</sub> O source from microbial communities	21
<b>3</b> Long-term multi-meta-omics resolves the ecophysiological controls of seasonal N <sub>2</sub> O emissions during wastewater treatment	77
<b>4</b> Metabolic labour division trade-offs in denitrifying microbiomes	147
<b>5</b> Outlook	175
Acknowledgements	189
Curriculum Vitae	195
Scientific contributions	197





# SUMMARY

Microbial communities drive the nitrogen cycle, a fundamental process sustaining life on Earth. However, human activities have disrupted this balance, leading to excessive emissions of nitrous oxide ( $\text{N}_2\text{O}$ ), a potent greenhouse gas with nearly 300 times the global warming potential of carbon dioxide and a significant contributor to ozone layer depletion. Despite the urgency to reduce emissions, they are projected to increase by 50% in the next 50 years. Our ability to mitigate these emissions is limited by our incomplete understanding of the microbial complexity driving them. To develop effective mitigation strategies, we must determine how microbial communities regulate nitrogen transformations across diverse environments, from natural ecosystems such as soils and oceans to managed and engineered systems like agricultural soils and wastewater treatment plants (WWTPs).

By integrating genomic, proteomic, and metabolic insights, this thesis explores the complexity of microbial nitrogen cycling and  $\text{N}_2\text{O}$  emissions.

**Chapter 1** introduces the importance of microbial nitrogen cycling and the pressing challenge of mitigating  $\text{N}_2\text{O}$  emissions.

**Chapter 2** challenges the traditional assumption that denitrification only occurs under anoxic conditions. Through lab-scale experiments, it demonstrated that microorganisms can simultaneously respire oxygen and nitrogen oxides, potentially contributing to  $\text{N}_2\text{O}$  emissions in dynamic environments such as WWTPs, sea sediments, and soils.

From a more applied perspective, in **Chapter 3** we investigated the microbial mechanisms underlying seasonal  $\text{N}_2\text{O}$  emissions in a WWTP. By analysing microbial dynamics at multiple ecophysiological levels – from genetic potential to active metabolism – we identified imbalances between ammonia-oxidising and nitrite-oxidising bacteria driving nitrite accumulation, a key precursor to  $\text{N}_2\text{O}$  formation. The findings point to dissolved oxygen as a key operational control to mitigate seasonal emissions.

Building on observations made in Chapter 3 and previous studies, **Chapter 4** addresses a broader question: why do most microorganisms in complex environments like natural ecosystems and WWTPs perform only partial denitrification? To explore this, we analysed metagenome-resolved genomes from diverse ecosystems together with experimental and theoretical insights from literature. We propose resource allocation

trade-offs between growth efficiency and adaptability as key determinants controlling the selection of complete and partial denitrifiers.

Finally, **Chapter 5** synthesises the key findings of this thesis, discusses the new questions it raises, and outlines future research directions.

By bridging *in situ* multi-level ecophysiological characterisation of microbial communities with targeted mixed culture enrichments, this work advances our understanding of microbial nitrogen cycling and provides a scientific foundation for developing more effective N<sub>2</sub>O mitigation strategies.

# SAMENVATTING

Microbiële gemeenschappen spelen een cruciale rol in de stikstofkringloop, een fundamenteel proces dat het leven op aarde ondersteunt. Echter, door menselijke activiteiten is dit natuurlijke evenwicht verstoord, wat heeft geleid tot een overmatige uitstoot van lachgas ( $\text{N}_2\text{O}$ ), een krachtig broeikasgas met een bijna 300 keer hoger opwarmingsvermogen dan koolstofdioxide en een belangrijke bijdrager aan de afbraak van de ozonlaag. Ondanks de noodzaak om deze emissies te verminderen, wordt verwacht dat ze in de komende 50 jaar met 50% zullen stijgen. Ons vermogen om deze uitstoot te beperken wordt belemmerd door een onvolledig begrip van de onderliggende microbiële processen. Om effectieve mitigatiestrategieën te ontwikkelen, moeten we beter begrijpen hoe microbiële gemeenschappen stikstofomzettingen reguleren in verschillende omgevingen, van natuurlijke ecosystemen zoals bodems en oceanen tot door mensen beheerde systemen zoals landbouwgronden en rioolwaterzuiveringsinstallaties (RWZI's).

Door een combinatie van genomische, proteomische en metabole analyses onderzoekt dit proefschrift de complexiteit van microbiële stikstofcycli en de productie van  $\text{N}_2\text{O}$ .

**Hoofdstuk 1** introduceert het belang van de microbiële stikstofkringloop en de uitdaging van  $\text{N}_2\text{O}$ -emissiereductie.

**Hoofdstuk 2** daagt de traditionele aanname uit dat denitrificatie uitsluitend in zuurstofloze omstandigheden plaatsvindt. Experimenteel onderzoek in het laboratorium toonde aan dat micro-organismen tegelijkertijd zuurstof en stikstofoxiden kunnen gebruiken, wat kan bijdragen aan  $\text{N}_2\text{O}$ -emissies in dynamische omgevingen zoals RWZI's, zeezand en bodems.

Vanuit een meer toegepaste invalshoek onderzoekt **Hoofdstuk 3** de microbiële mechanismen achter seizoensgebonden  $\text{N}_2\text{O}$ -emissies in een RWZI. Door microbiële dynamiek op meerdere ecofysiologische niveaus te analyseren – van genetisch potentieel tot actieve stofwisselingsprocessen – hebben we vastgesteld dat een onevenwicht tussen ammoniak-oxiderende en nitriet-oxiderende bacteriën leidt tot nitrietaccumulatie, een belangrijke voorloper van  $\text{N}_2\text{O}$ . De resultaten wijzen op opgeloste zuurstof als een essentiële operationele parameter voor het verminderen van seizoensgebonden emissies.

Voortbouwend op de observaties uit Hoofdstuk 3 en eerdere studies, behandelt **Hoofdstuk 4** een bredere vraag: waarom voeren de meeste micro-organismen in complexe omgevingen zoals natuurlijke ecosystemen en RWZI's slechts gedeeltelijke

denitrificatie uit? Om dit te onderzoeken, hebben we metagenomen van microbiële gemeenschappen uit diverse ecosystemen geanalyseerd en dit gecombineerd met experimentele en theoretische inzichten uit de literatuur. Wij stellen dat een afweging tussen groeiefficiëntie en aanpassingsvermogen een sleutelrol speelt in de selectie van complete versus gedeeltelijke denitrificeerders.

Tot slot brengt **Hoofdstuk 5** de belangrijkste bevindingen samen, bespreekt de nieuwe vragen die hieruit voortvloeien en stelt nieuwe onderzoeksrichtingen voor.

Door *in situ* ecologisch onderzoek op meerdere niveaus te combineren met gerichte cultuurexperimenten, draagt dit proefschrift bij aan een beter begrip van microbiële stikstofcycli en biedt het een wetenschappelijke basis voor de ontwikkeling van effectievere strategieën om N<sub>2</sub>O-emissies te verminderen.

As comunidades microbianas desempenham um papel crucial no ciclo do azoto, um processo fundamental para a manutenção da vida na Terra. No entanto, as atividades humanas têm perturbado este equilíbrio natural, resultando numa emissão excessiva de óxido nitroso ( $\text{N}_2\text{O}$ ), um gás com efeito de estufa quase 300 vezes mais potente do que o dióxido de carbono e um dos principais responsáveis pela destruição da camada de ozono. Apesar da urgência em reduzir estas emissões, prevê-se que aumentem 50% nos próximos 50 anos. A nossa capacidade de mitigar estas emissões é limitada pelo conhecimento ainda incompleto dos processos microbianos subjacentes. Para desenvolver estratégias de mitigação eficazes, é essencial compreender como as comunidades microbianas regulam as transformações do azoto em diversos ambientes, desde ecossistemas naturais como solos e oceanos a sistemas geridos e artificiais como terrenos agrícolas e estações de tratamento de águas residuais (ETARs).

Através da integração de análises genómicas, proteómicas e metabólicas, esta tese explora a complexidade do ciclo microbiano do azoto e a sua relação com a emissão de  $\text{N}_2\text{O}$ .

O **Capítulo 1** introduz a importância do ciclo do azoto e os desafios da mitigação das emissões de  $\text{N}_2\text{O}$ .

O **Capítulo 2** questiona a suposição tradicional de que a desnitrificação ocorre apenas em condições anóxicas. Experiências laboratoriais demonstram que certos microrganismos conseguem respirar simultaneamente oxigénio e óxidos de azoto, possivelmente contribuindo para a produção de  $\text{N}_2\text{O}$  em ambientes dinâmicos, como ETARs, sedimentos marinhos e solos.

De uma perspetiva mais aplicada, o **Capítulo 3** investiga os mecanismos microbianos subjacentes às emissões sazonais de  $\text{N}_2\text{O}$  numa ETAR. Através da análise da dinâmica microbiana em vários níveis ecofisiológicos – desde o potencial genético à atividade metabólica – identificaram-se desequilíbrios entre bactérias oxidantes de amoníaco e de nitrito, resultando na acumulação de nitrito, um precursor fundamental do  $\text{N}_2\text{O}$ . Os resultados indicam que a concentração de oxigénio é um fator operacional chave para mitigar as emissões sazonais.

Com base nas observações do Capítulo 3 e em estudos anteriores, o **Capítulo 4** aborda uma questão mais ampla: porque é que a maioria dos microrganismos em ambientes complexos, como ecossistemas naturais e ETARs, realiza apenas uma desnitrificação parcial? Para responder a esta questão, foram analisados metagenomas de diversos ecossistemas e dados de experiências laboratoriais e conceitos teóricos da literatura.

Propõe-se que a seleção natural entre desnitrificação completa ou parcial resulta de um equilíbrio entre eficiência de crescimento e adaptabilidade ao ambiente.

Por fim, o **Capítulo 5** sintetiza as principais conclusões desta tese, reflete sobre novas questões emergentes e propõe direções para investigação futura.

Ao combinar a caracterização ecológica multi-nível de comunidades microbianas com culturas de laboratório, este trabalho contribui para um conhecimento mais profundo do ciclo microbiano do azoto e fornece uma base científica para o desenvolvimento de estratégias mais eficazes para a mitigação das emissões de  $N_2O$ .

# Introduction







## 1.1. How microorganisms live together in communities

Over three billion years, selective pressures have driven the evolution of nearly a trillion microbial species. Yet, we have only scratched the surface of microbial diversity, with an estimated 99.999% of microorganisms still undiscovered <sup>1</sup>. Bacteria, archaea, and fungi thrive in diverse environments, from soils <sup>2</sup>, oceans <sup>3</sup>, and freshwater systems <sup>4</sup> to the gastrointestinal tracts of animals <sup>5</sup>. Microorganisms have even colonised extreme habitats, including scorching or freezing deserts <sup>6,7</sup>, highly saline and alkaline soda lakes <sup>8</sup>, acidic geothermal and mining areas <sup>9</sup>, the toxic high-pressure depths of hydrothermal vents <sup>10</sup>, the nutrient-deprived terrestrial subsurface <sup>11</sup>, and even nuclear reactors <sup>12</sup>. However, microorganisms rarely exist in isolation. Instead, they form dynamic, interdependent communities (microbiomes) within complex ecosystems.

### 1.1.1. The role of microbiomes in shaping natural ecosystems

In nature, microorganisms exist as part of large communities, engaging in both competitive and cooperative interactions. They exchange nutrients, compete for resources and space, and even produce toxins to maintain dominance within their ecological niches <sup>13</sup>. Each species behaves uniquely, preferring specific substrates, pH ranges, or temperatures. These distinct preferences allow a vast array of species to coexist within the same ecosystem, resulting in complex and highly diverse microbial communities in both taxonomy and function.

The environment selects the organisms best suited to specific conditions, and microbial communities, in turn, play a vital role in shaping their environment. In soils, for example, bacteria provide critical nutrients to plants by converting atmospheric nitrogen into ammonia and nitrate <sup>14</sup>. In return, plants supply organic carbon to microorganisms. Similarly, photosynthetic microorganisms in oceans convert carbon dioxide (CO<sub>2</sub>) into organic matter while releasing oxygen, supporting marine ecosystems and life as we know it <sup>15</sup>. These examples show how microorganisms sustain Earth's biogeochemical cycles, such as the nitrogen and carbon cycles, naturally regenerating resources to maintain ecological equilibrium. However, human activities are disrupting this balance, contributing to climate change and threatening food security and biodiversity <sup>16</sup>.

Like natural ecosystems, microorganisms in the human body form complex communities and are crucial to maintain human health <sup>17</sup>. The gut microbiome, for example, has been linked to autoimmune diseases like multiple sclerosis <sup>18</sup>, metabolic disorders such as obesity <sup>19</sup>, and even neurological conditions like autism <sup>20</sup> and depression <sup>21</sup>. Modern lifestyles, characterised by unhealthy diets and inactivity, have significantly altered these microbial communities, contributing to the rise in chronic diseases <sup>22</sup>. Ultimately,

microbial communities are vital for life on Earth, so it is essential that we learn how to sustainably manage them.

### 1.1.2. Harnessing microbial potential

Humans have been harnessing the power of microorganisms for millennia, long before we even knew they existed. One of the earliest examples is fermentation, a process used to preserve food by converting sugars into acids and alcohols using naturally present microbial communities. This ancient practice gave rise to products like cheese, yoghurt, kimchi, pickles, beer, and wine <sup>23</sup>. Over time, through trial and error and, later, scientific refinement, we learned to control fermentations with greater precision by selecting specific microbial strains or guiding native microbiomes toward desired outcomes. For example, carefully selected yeast strains are used in beer production, whereas intrinsic microbial communities still shape the flavours of wine, chocolate, and fermented vegetables <sup>23</sup>.

Microbial communities also play crucial roles in modern environmental applications, such as bioremediation, where they are used to clean environments contaminated with pesticides, oil, and heavy metals <sup>24–26</sup>. At the same time, waste streams are being repurposed to produce biogas, bioplastics (e.g. polyhydroxyalkanoates), and other valuable biopolymers (e.g. extracellular polymeric substances) <sup>27–30</sup>. Perhaps the most significant application of microbiomes for both environmental conservation and human health is biological wastewater treatment, which prevents contamination of water sources and disease spread <sup>31</sup>.

The broad range of applications of microbial communities, from food production to environmental conservation, highlights their vast potential to improve our life quality and address global challenges, such as the current environmental and health crises (highlighted in section 1.1.1). However, fully realising microbial potential depends on our ability to study and understand the complex interactions governing microbial ecosystems in both natural and engineered environments.

### 1.1.3. From traditional culturing to modern omics in microbial research

Technological advancements have boosted microbial research over the last few years. Yet, it all started 300 years ago. The discovery of microorganisms in the 17<sup>th</sup> century marked the beginning of a new scientific era, with laboratory studies taking off by the late 19<sup>th</sup> century <sup>32</sup>. Early research focused on pure cultures, where microorganisms were isolated and studied in controlled conditions. These laboratory settings, while still now invaluable for determining fundamental physiological principles, do not reflect the

complexities of natural microbial ecosystems, where microorganisms rarely grow in isolation. In fact, less than 0.00001% of all microbial species are estimated to have been cultured, and these are seldom the dominant or most functionally important organisms in nature <sup>1,33</sup>. Over time, new approaches have emerged, allowing us to explore how microorganisms interact with each other and their environment. Enrichment cultures simulate natural selection by favouring organisms adapted to specific conditions <sup>34,35</sup>. Though proving an excellent tool to study ecological principles in controlled settings, they still fall short of capturing the full complexity of natural ecosystems.

Recent advances in culture-independent molecular techniques have revolutionised the field of microbial ecology, offering new tools to investigate microorganisms directly in their environments and answer fundamental questions like “Who is there?”, “What are they doing?” and “Who is doing what?”. Particularly, high-throughput DNA sequencing and bioinformatics have significantly expanded our knowledge of microbial diversity and functional versatility. The initial focus of these techniques was on sequencing solely the 16S rRNA gene to identify microorganisms based on their evolutionary relationship <sup>36</sup>. However, this approach offered limited insight into the functional roles of each organism. With the decreasing costs of DNA sequencing, microbial ecology increasingly turned to metagenomics – analysing the entire DNA pool of a microbial community. Individual genomes can be reconstructed from the collective DNA of a community (metagenome-assembled genomes), linking genetic functions to specific species. This progress has significantly expanded our understanding of microbial diversity in humans, oceans, freshwater, and soils <sup>37</sup>. In addition to metagenomics, other omics approaches such as metatranscriptomics (RNA), metaproteomics (proteins), and metabolomics (metabolites), allow us to identify the actual metabolic activities of active members within a community (Figure 1.1) <sup>36</sup>.

By combining classical and novel approaches, we are now able to explore microbial ecosystems in unprecedented detail, boosting microbiological advancements in food production, human health, and environmental management <sup>38</sup>. The technological advancements in microbial ecophysiological research have been particularly important to resolve the microbial complexity of the Earth’s nitrogen cycle, as detailed in the following section.

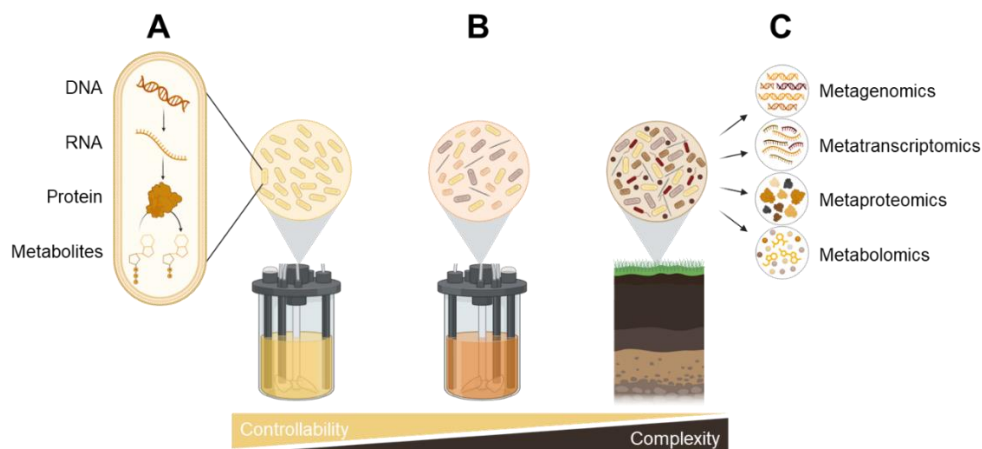


**Figure 1.1. Microbial research approaches.** **A)** Cellular elements controlling the function of the cell: DNA is transcribed into RNA and subsequently translated into proteins, which are responsible for converting metabolites. **B)** Different systems where microorganisms can be studied, ordered from more to less controlled and from low to high complexity: pure culture, mixed culture, and natural environments. **C)** Meta-omics approaches enabling the study of microbial communities in situ through the analysis of the DNA, RNA, proteins, and metabolites of the different community members. (Created with Biorender)

## 1.2. Microbial nitrogen network

The nitrogen cycle is one of Earth's main biogeochemical cycles, being primarily driven by microbial processes. Dinitrogen gas ( $N_2$ ) dominates the atmosphere, yet most organisms require more reactive nitrogen forms like ammonia ( $NH_3$ ) or nitrate ( $NO_3^-$ ) to grow<sup>14</sup>. Nitrogen is fundamental for synthesising key cellular components like DNA, RNA, and proteins. Many microorganisms also oxidise or reduce nitrogen compounds for energy conservation (Figure 1.2). These transformations sustain marine and terrestrial ecosystems, regulate greenhouse gases, and support engineered processes like wastewater treatment. Our understanding of microbial nitrogen pathways has evolved rapidly, revealing greater complexity than previously thought.

### 1.2.1. From nitrogen cycle to modular network

Historically, energy-conserving microbial nitrogen transformations were categorised into nitrification ( $NH_3 \rightarrow NO_2^- \rightarrow NO_3^-$ ), denitrification ( $NO_3^- \rightarrow N_2$ ), and nitrogen fixation ( $N_2 \rightarrow NH_3$ ), with the first occurring in oxic ( $+O_2$ ) and the latter two in anoxic ( $-O_2$ ) environments<sup>39</sup> (Figure 1.2A). Microorganisms were classified into distinct groups based on the specific nitrogen processes they carried out: nitrifiers (ammonia- and nitrite-oxidising bacteria – AOB and NOB), denitrifiers, or diazotrophs. However, the newly discovered metabolic versatility of nitrogen-transforming microorganisms

challenges their traditional classification in individual functional guilds <sup>14</sup>. The discovery of novel reactions and microorganisms have transformed our understanding of the nitrogen cycle into a modular network, where different pathways often coexist within a single organism (Figure 1.2B) <sup>39</sup>.

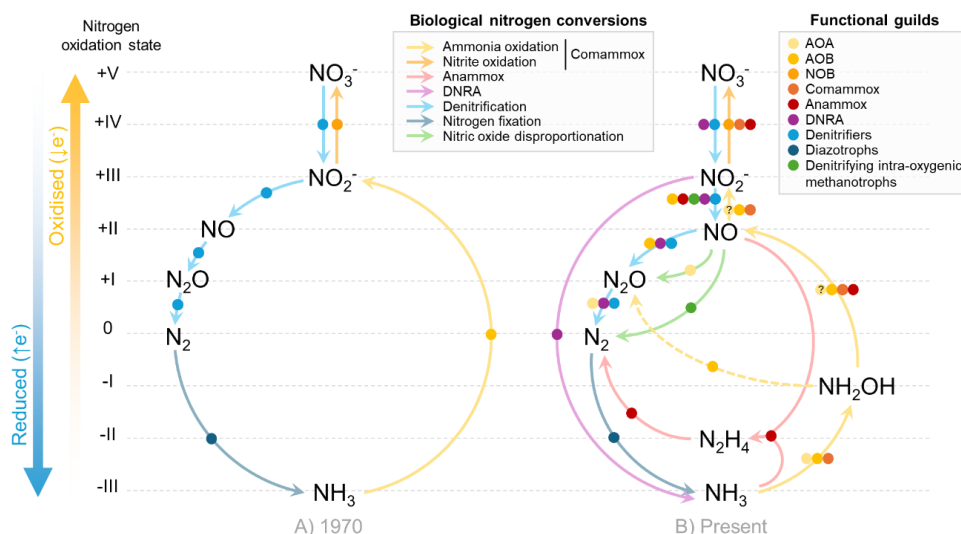


**Figure 1.2. Microbial nitrogen network as known in 1970 (A) and in the present (B)** <sup>14,39,55</sup>. The nitrogen compounds are represented from most oxidised to more reduced from top to bottom. The colour of the arrows indicate the metabolic pathways: ammonia and nitrite oxidation, anaerobic ammonia oxidation (anammox), dissimilatory nitrite reduction to ammonia (DNRA), denitrification, nitrogen fixation, and nitric oxide disproportionation. The symbols represent the functional guilds performing each conversion: ammonia-oxidising archaea and bacteria (AOA and AOB), nitrite-oxidising bacteria (NOB), complete ammonia oxidisers (comammox), anaerobic ammonia oxidisers (anammox), dissimilatory nitrite reduction to ammonia (DNRA), denitrifiers, diazotrophs, and denitrifying intra-oxygenic methanotrophs. The exact steps from hydroxylamine to nitrite in AOA are not resolved (marked with a “?” in the figure) <sup>40</sup>. The distribution of the functional guilds among the nitrogen conversions is likely incomplete, as new genes and conversions are increasingly found across functional guilds. For example, nitrogen-fixing and denitrification genes were found in the same organism <sup>56</sup>, and a nitrite reduction protein is present in several NOB <sup>57</sup> yet their physiological relevance remains to be determined.

For example, AOB not only oxidise ammonia ( $\text{NH}_3$ ) to nitrite ( $\text{NO}_2^-$ ) but can also denitrify nitrite and nitric oxide ( $\text{NO}$ ) to nitrous oxide ( $\text{N}_2\text{O}$ ) <sup>40</sup>. Only recently, nitric oxide was identified as a central intermediate in the AOB pathway, and direct conversion of hydroxylamine ( $\text{NH}_2\text{OH}$ ) to  $\text{N}_2\text{O}$  was identified as a novel biochemical reaction (Figure 1.2B) <sup>41</sup>. The discovery of ammonia-oxidising archaea (AOA) expanded the phylogenetic diversity of nitrifiers <sup>40,42</sup> and the discovery of anaerobic ammonia oxidation (anammox) demonstrated that ammonia can be oxidised without oxygen (Figure 1.2B) <sup>43</sup>. Even more recently, the discovery of organisms oxidising ammonia completely to nitrate (comammox) challenged the idea that nitrification must be divided between two

microbial guilds <sup>44,45</sup>. Certain bacteria and archaea can heterotrophically oxidise ammonia to hydroxylamine, yet this is likely not coupled to energy conservation <sup>46,47</sup>. On the reducing side of the cycle, it is now known that many microorganisms perform only some denitrification steps (partial denitrifiers), rather than completing the entire pathway (complete denitrifiers) (Figure 1.2B). As a consequence, denitrification has been variously defined in literature. Some define it *sensu stricto* as the complete reduction of nitrate ( $\text{NO}_3^-$ ) to dinitrogen gas <sup>48</sup>, others as the reduction of nitrite to gaseous nitric and nitrous oxide <sup>49</sup>, or simply as the conversion of nitrite to nitric oxide <sup>50</sup>. In this thesis, microorganisms respiring at least one of the nitrogen oxides will be referred to as “denitrifiers”. Dissimilatory nitrite reduction to ammonia (DNRA) was discovered as a “shortcut” in the nitrogen cycle by reducing nitrite directly to ammonia <sup>51,52</sup>. The disproportionation of two nitric oxide molecules to oxygen and dinitrogen, and to oxygen and nitrous oxide was recently discovered in methanotrophs and AOA, respectively <sup>53,54</sup>.

Despite these significant advances, many aspects of the microbial nitrogen network remain unknown. The ecological significance of complete versus partial denitrifiers, and the metabolic versatility of nitrifying and anammox bacteria remain to be resolved. Many enzymes remain unidentified, such as those responsible for nitric oxide oxidation to nitrite in AOB or hydroxylamine oxidation in AOA (Table 1.1) <sup>40</sup>. Entire metabolic pathways may yet remain to be discovered <sup>14</sup>. Further physiological, biochemical, and ecological research, employing advanced techniques such as meta-omics, will be crucial to uncover the full complexity of microbial nitrogen metabolism.

**Table 1.1. Main enzymes and respective catalytic subunits performing each nitrogen conversion.** Putative enzymes are represented with squared brackets. The nitrogen conversions were grouped according to the pathway they belong to (Figure 1.2B) <sup>14,58</sup>. This list will increase in complexity as new enzymes are discovered. For example,  $\text{N}_2\text{O}$  reductases different from NosZ are speculated to exist, as some bacteria and archaea can consume  $\text{N}_2\text{O}$  but seem to lack the known *nosZ* genes <sup>59,60</sup>.

Process	Conversion	Enzyme name	Enzyme complex	Catalytic subunit
Nitrification	$\text{NH}_3 \rightarrow \text{NH}_2\text{OH}$	Ammonia monooxygenase	AMO	AmoA
	$\text{NH}_2\text{OH} \rightarrow \text{NO}$	Hydroxylamine oxidoreductase/oxidase	HAO/HOX	Hao/Hox
	$\text{NH}_2\text{OH} \rightarrow \text{N}_2\text{O}$	Cytochrome P <sub>460</sub>	Cyt P <sub>460</sub>	Cyt P <sub>460</sub>
	$\text{NO} \rightarrow \text{NO}_2^-$	Nitric oxide oxidase	[NOO]	?
	$\text{NO}_2^- \rightarrow \text{NO}_3^-$	Nitrite oxidoreductase	NXR	NxrA
Denitrification	$\text{NO}_3^- \rightarrow \text{NO}_2^-$	Cytoplasmic/periplasmic nitrate reductase	NAR/NAP	NarG/NapA
	$\text{NO}_2^- \rightarrow \text{NO}$	Cytochrome cd1/copper-based nitrite reductase	cd1-NIR/Cu-NIR	NirS/NirK
	$\text{NO} \rightarrow \text{N}_2\text{O}$	Cytochrome c/quinol nitric oxide reductase	cNOR/qNOR	NorB/NorZ
	$\text{N}_2\text{O} \rightarrow \text{N}_2$	Nitrous oxide reductase	NOS	NosZ
$\text{N}_2$ fixation	$\text{N}_2 \rightarrow \text{NH}_3$	Molybdenum/vanadium/iron nitrogenase	MoFe/VFe/FeFe	NifDK/VnfDGK/AnfDGK
DNRA	$\text{NO}_2^- \rightarrow \text{N}_2$	Pentaheme/octaheme cytochrome c nitrite reductase	ccNIR/ONR	NrfA/?

Anammox	$\text{NO} + \text{NH}_3 \rightarrow \text{N}_2\text{H}_4$	Hydrazine synthase	HZS	HzsA
	$\text{N}_2\text{H}_4 \rightarrow \text{N}_2$	Hydrazine dehydrogenase	HDH	Hdh
NO dismutation	$2 \text{NO} \rightarrow \text{N}_2$	Nitric oxide dismutase	[NOD]	?
	$2 \text{NO} \rightarrow \text{N}_2\text{O}$	Nitric oxide dismutase	[NOD]	?

### 1.2.2. Nitrous oxide: a greenhouse and ozone-depleting gas

Manipulation of the nitrogen cycle, particularly through the development of synthetic fertilisers containing ammonia and nitrate <sup>61</sup>, has been vital to sustain food production and human health and prosperity, but has disrupted the natural balance of nitrogen compounds. The increased nitrogen input in natural environments has resulted in a rise of atmospheric nitrous oxide ( $\text{N}_2\text{O}$ ), currently the third most emitted greenhouse gas. Although less abundant,  $\text{N}_2\text{O}$  has nearly 300 times the global warming potential of  $\text{CO}_2$  over 100 years, persists in the atmosphere for over a century, and is a major ozone-depleting substance <sup>62,63</sup>. Despite the urgency to reduce  $\text{N}_2\text{O}$  emissions, they are projected to increase by 50% in the next 50 years <sup>62</sup>, hindering efforts to achieve the global net-zero emission targets set for 2050 <sup>64–66</sup>.

$\text{N}_2\text{O}$  emissions are primarily driven by microbial processes (Figure 1.2B). AOB generate  $\text{N}_2\text{O}$  as a byproduct via three main routes: the direct oxidation of hydroxylamine or the reduction of nitric oxide, produced from hydroxylamine (nitrification) or nitrite (nitrifier denitrification). Nitrification is a particularly important source under high oxygen and ammonia, whereas nitrifier denitrification is active under low oxygen and high nitrite concentrations <sup>67</sup>. In contrast, heterotrophic denitrifiers release  $\text{N}_2\text{O}$  as an intermediate, especially when conditions like low organic carbon or high oxygen hinder the final step of  $\text{N}_2\text{O}$  reduction <sup>68,69</sup>. AOA have also been shown to biologically produce  $\text{N}_2\text{O}$  <sup>54,59</sup>, yet their contribution to overall emissions in diverse environments remains to be resolved <sup>70,71</sup>. Organisms like NOB, and comammox and anammox bacteria are believed not to produce  $\text{N}_2\text{O}$  biologically <sup>58,72–74</sup>, yet their intermediates can undergo abiotic reactions that result in  $\text{N}_2\text{O}$  generation, particularly in the presence of metallic ions (e.g.  $\text{NH}_2\text{OH} + \text{HNO}_2 \rightarrow \text{N}_2\text{O} + 2 \text{H}_2\text{O}$ ; Fe(II/III)-mediated oxidation of  $\text{NO}_2^-$ , NO, and  $\text{NH}_2\text{OH}$ ) <sup>67,75,76</sup>. Though these chemical reactions are typically minor, they can become significant under high concentrations of reactants <sup>40,75,77</sup>.

Quantifying the contribution of various microbial processes to  $\text{N}_2\text{O}$  emissions in complex environments remains a challenge. Recent advancements in isotope analyses are gradually improving our ability to distinguish between different microbial pathways <sup>78</sup>, yet still face limitations in differentiating between nitrifier and heterotrophic denitrification (reviewed in Butterbach-Bahl et al., 2013; Domingo-Félez & Smets, 2019;

Duan et al., 2017; Hu et al., 2015; Wrage-Mönnig et al., 2018). A deeper understanding of the underlying microbial communities is needed to further elucidate N<sub>2</sub>O production and consumption mechanisms, and develop robust mitigation strategies in natural (oceans, soils), managed (agriculture), and engineered sources (wastewater treatment plants)<sup>84</sup>. Wastewater treatment plants (WWTPs) offer a key model ecosystem to study N<sub>2</sub>O-producing microbiomes, as they offer more controlled and monitored settings than natural ecosystems<sup>85</sup>.

### 1.2.3. Nitrous oxide emissions during wastewater treatment

WWTPs are key engineered ecosystems where microbial nitrogen conversions occur on a large scale. Developed in 1914, the activated sludge process remains the most widely adopted method to treat sewage, naturally selecting diverse microbial communities to remove pollutants<sup>31,86</sup>. The process typically involves two main stages: an oxic stage where nitrifiers oxidise ammonia to nitrate, and an anoxic stage where denitrifiers reduce nitrate to dinitrogen gas (Figure 1.3). N<sub>2</sub>O emissions can arise during both stages, as a byproduct of AOB or incomplete denitrification.

Although WWTPs contribute only 4% of anthropogenic N<sub>2</sub>O emissions, compared to 52% from agriculture, they can account for 80% of a WWTP's carbon footprint<sup>84,87</sup>. Decades of research have identified strategies to minimise these emissions – such as maintaining moderate oxygen levels, regulating ammonia loads, ensuring sufficient organic carbon in the anoxic stage, and avoiding abrupt changes in operational conditions<sup>88–91</sup>. However, these strategies are often plant-specific, can be challenging to implement, and are not always consistently effective due to the complexity of nitrogen-converting microbial communities<sup>88–90</sup>.

Additionally, WWTPs worldwide have reported seasonal peaks in N<sub>2</sub>O emissions for over a decade, often comprising the bulk of their annual emissions<sup>87,92,101,102,93–100</sup>. Yet, clear correlations pinpointing the cause of these emissions are often lacking due to the simultaneous influence of multiple operational factors and limited microbial insights<sup>87,93–95</sup>. A deeper understanding of the intricate microbial mechanisms that govern nitrogen conversions within WWTP microbiomes is essential to develop robust and effective N<sub>2</sub>O mitigation strategies<sup>88</sup>.



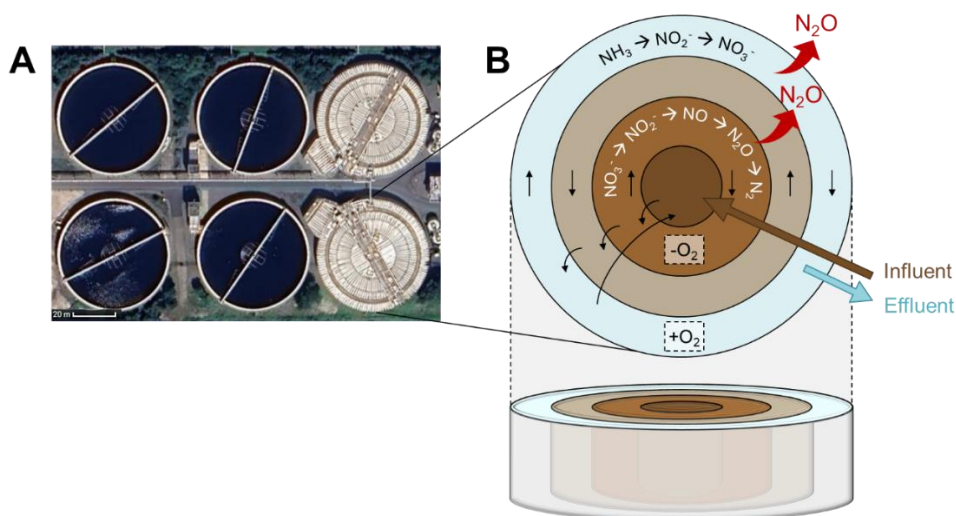


**Figure 1.3. Biological nitrogen removal at a wastewater treatment.** **A)** Satellite view of the Amsterdam-West wastewater treatment plant, showing four settling tanks and two activated sludge tanks. The scale bar represents 20 meters. **B)** Simplified representation of the biological nitrogen removal process in an activated sludge tank. Ammonia ( $\text{NH}_3$ ) is converted into nitrate ( $\text{NO}_3^-$ ) under oxic conditions and nitrate is converted to dinitrogen gas ( $\text{N}_2$ ) under anoxic conditions, with possible emission of  $\text{N}_2\text{O}$  in both stages. The arrows represent the water flow.

### 1.3. Investigating $\text{N}_2\text{O}$ -emitting microbial communities

Over a century of research on nitrogen-converting microorganisms has significantly expanded our understanding of their physiology, biochemistry, and ecology. Yet, many questions remain unresolved. This thesis aims to deepen our understanding of the ecophysiology of nitrogen-converting microbial communities underlying biological  $\text{N}_2\text{O}$  emissions by studying them at the genomic, proteomic, and metabolic levels, ultimately aiming to contribute to  $\text{N}_2\text{O}$  mitigation. The knowledge gaps addressed in each chapter range from fundamental to practical issues, exploring both simplified lab-based communities and complex microbiomes in WWTPs and natural environments (Figure 1.4).

**Chapter 2** investigates whether the strict separation between oxygen and nitrogen oxide respiration in heterotrophic denitrifiers holds in dynamic environments with frequent fluctuations between oxic and anoxic conditions, such as WWTPs. We hypothesised that microorganisms capable of aerobic denitrification (simultaneous aerobic respiration and denitrification) may have a competitive advantage by adapting more rapidly to these fluctuating conditions. Two lab-scale enrichment cultures were

employed to determine if aerobic denitrification contributes to nitrogen turnover and nitrous oxide emissions under varying oxygen levels.

**Chapter 3** addresses the unresolved seasonal  $\text{N}_2\text{O}$  emission peaks observed in WWTPs worldwide. Given the widespread occurrence of these peaks, we hypothesised that they are driven by changes in the WWTP microbiome rather than shifts in process operation alone. Therefore, we conducted a 1.5-year study at a Dutch WWTP, integrating metagenomics, metaproteomics, kinetic analyses, and operational data to identify the microbial and operational mechanisms controlling seasonal  $\text{N}_2\text{O}$  emissions.

**Chapter 4** returns to a more fundamental question by examining microbiomes from a variety of nitrogen-converting ecosystems, including laboratory cultures, WWTPs, soils, rivers, and oceans. It is becoming increasingly evident that most organisms found in natural and engineered environments perform only a subset of the four denitrification steps rather than the complete pathway. This raises the question: What ecological factors drive the selection of partial versus complete denitrifiers in these complex environments? To explore this, we synthesised theoretical perspectives and experimental evidence from literature to identify potential drivers favouring partial over complete denitrification.

Finally, **Chapter 5** presents the overarching conclusions of this research, reflecting on its broader impact, discussing unanswered questions, and considering future research directions.

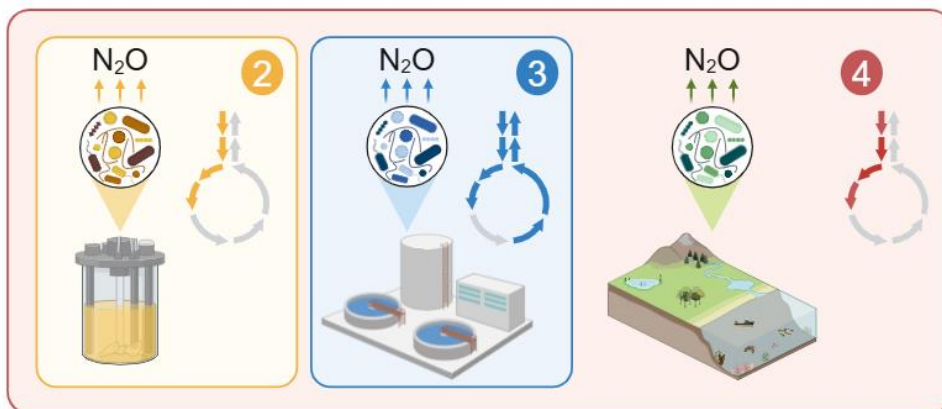


**Figure 1.4. Schematic overview of the research chapters of this thesis.** The chapters investigate microbial denitrification (2, 4) and nitrification + denitrification (3) by microbial communities in the laboratory (2, 4), wastewater treatment plants (3, 4), and natural environments (4). (Created with Biorender)

## 1.4. References

- Locey KJ, Lennon JT. Scaling laws predict global microbial diversity. *Proc Natl Acad Sci U S A*. 2016;113(21):5970-5975. doi:10.1073/pnas.1521291113
- Fierer N. Embracing the unknown: Disentangling the complexities of the soil microbiome. *Nat Rev Microbiol*. 2017;15(10):579-590. doi:10.1038/nrmicro.2017.87
- Sunagawa S, Coelho LP, Chaffron S, et al. Structure and function of the global ocean microbiome. *Science*. 2015;348(6237):1261359. doi:10.1126/science.1261359
- David C. Sigee. *Freshwater Microbiology: Biodiversity and Dynamic Interactions of Microorganisms in the Aquatic Environment*. John Wiley & Sons, Ltd; 2005. doi:10.1002/0470011254
- Groussin M, Mazel F, Sanders JG, et al. Unraveling the processes shaping mammalian gut microbiomes over evolutionary time. *Nat Commun*. 2017;8. doi:10.1038/ncomms14319
- Makhalanyane TP, Valverde A, Gunnigle E, Frossard A, Ramond JB, Cowan DA. Microbial ecology of hot desert edaphic systems. *FEMS Microbiol Rev*. 2015;39(2):203-221. doi:10.1093/femsre/fuu011
- Makhalanyane TP, Van Goethem MW, Cowan DA. Microbial diversity and functional capacity in polar soils. *Curr Opin Biotechnol*. 2016;38:159-166. doi:10.1016/j.copbio.2016.01.011
- Sorokin DY, Banciu HL, Muyzer G. Functional microbiology of soda lakes. *Curr Opin Microbiol*. 2015;25:88-96. doi:10.1016/j.mib.2015.05.004
- Johnson DB. Biodiversity and ecology of acidophilic microorganisms. *FEMS Microbiol Ecol*. 1998;27(4):307-317. doi:10.1016/S0168-6496(98)00079-8
- Dick GJ. The microbiomes of deep-sea hydrothermal vents: distributed globally, shaped locally. *Nat Rev Microbiol*. 2019;17(5):271-283. doi:10.1038/s41579-019-0160-2
- Beaver RC, Neufeld JD. Microbial ecology of the deep terrestrial subsurface. *ISME J*. 2024;18(1). doi:10.1093/ismejo/wrae091
- Bratkic A, Jazbec A, Toplak N, et al. The colonization of an irradiated environment: the case of microbial biofilm in a nuclear reactor. *Int J Radiat Biol*. 2024;100(1):108-121. doi:10.1080/09553002.2023.2258206
- Hibbing ME, Fuqua C, Parsek MR, Peterson SB. Bacterial competition: Surviving and thriving in the microbial jungle. *Nat Rev Microbiol*. 2010;8(1):15-25. doi:10.1038/nrmicro2259
- Kuypers MMM, Marchant HK, Kartal B. The microbial nitrogen-cycling network. *Nat Rev Microbiol*. 2018;16(5):263-276. doi:10.1038/nrmicro.2018.9
- Azam F, Malfatti F. Microbial structuring of marine ecosystems. *Nat Rev Microbiol*. 2007;5(10):782-791. doi:10.1038/nrmicro1747
- Cavicchioli R, Ripple WJ, Timmis KN, et al. Scientists' warning to humanity: microorganisms and climate change. *Nat Rev Microbiol*. 2019;17(9):569-586. doi:10.1038/s41579-019-0222-5
- Cryan JF, Dinan TG. Mind-altering microorganisms: The impact of the gut microbiota on brain and behaviour. *Nat Rev Neurosci*. 2012;13(10):701-712. doi:10.1038/nnr3346
- Hooper LV, Littman DR, Macpherson AJ. Interactions between the microbiota and the immune system. *Science*. 2012;336(6086):1268-1273. doi:10.1126/science.1223490

19. Ley RE, Turnbaugh PJ, Klein S, Gordon JI. Human gut microbes associated with obesity. *Nature*. 2006;444(21):1022-1023. doi:10.1038/nature4441022a
20. Hsiao EY, McBride SW, Hsien S, et al. Microbiota modulate behavioral and physiological abnormalities associated with neurodevelopmental disorders. *Cell*. 2013;155(7):1451-1463. doi:10.1016/j.cell.2013.11.024
21. Radjabzadeh D, Bosch JA, Uitterlinden AG, et al. Gut microbiome-wide association study of depressive symptoms. *Nat Commun*. 2022;13(1):1-10. doi:10.1038/s41467-022-34502-3
22. Fan Y, Pedersen O. Gut microbiota in human metabolic health and disease. *Nat Rev Microbiol*. 2021;19(1):55-71. doi:10.1038/s41579-020-0433-9
23. Bamforth CW, Cook DJ. *Food, Fermentation, and Micro-organisms*. John Wiley & Sons Ltd.; 2019. doi:10.1002/9781119557456
24. Head IM, Jones DM, Røling WFM. Marine microorganisms make a meal of oil. *Nat Rev Microbiol*. 2006;4(3):173-182. doi:10.1038/nrmicro1348
25. Atashgahi S, Sánchez-Andrea I, Heipieper HJ, Meer JR van der, Stams AJM, Smidt H. Prospects for harnessing biocide resistance for bioremediation and detoxification. *Science*. 2018;360:743-746. doi:10.1126/science.aar3778
26. Coban O, de Deyn GB, van der Ploeg M. Soil microbiota as game-changers in restoration of degraded lands. *Science*. 2022;375(6584). doi:10.1126/science.abe0725
27. Estévez-Alonso Á, Pei R, van Loosdrecht MCM, Kleerebezem R, Werker A. Scaling-up microbial community-based polyhydroxyalkanoate production: status and challenges. *Bioresour Technol*. 2021;327(January). doi:10.1016/j.biortech.2021.124790
28. Zahra SA, Persiani R, Dueholm MK, et al. Rethinking characterization, application, and importance of extracellular polymeric substances in water technologies. *Curr Opin Biotechnol*. 2024;89(August):103192. doi:10.1016/j.copbio.2024.103192
29. Kleerebezem R, van Loosdrecht MC. Mixed culture biotechnology for bioenergy production. *Curr Opin Biotechnol*. 2007;18(3):207-212. doi:10.1016/j.copbio.2007.05.001
30. Zheng M, Hu Z, Liu T, et al. Pathways to advanced resource recovery from sewage. *Nat Sustain*. Published online 2024. doi:10.1038/s41893-024-01423-6
31. Van Loosdrecht MCM, Brdjanovic D. Anticipating the next century of wastewater treatment. *Science*. 2014;344(6191):1452-1453. doi:10.1126/science.1255183
32. Collard P. *The Development of Microbiology*. Cambridge University Press; 1976.
33. Hugenholtz P. Exploring prokaryotic diversity in the genomic era. *Genome Biol*. 2002;3(2):1-8. doi:10.1186/gb-2002-3-2-reviews0003
34. Kuenen JG. Continuous cultures (chemostats). In: Schmidt TM, ed. *Encyclopedia of Microbiology*. 4th ed. Elsevier Inc.; 2019:743-761. doi:10.1016/B978-0-12-801238-3.02490-9
35. Beijerinck MW. Anhaufungsversuche mit Ureumbakterien. *Cent F Bakteriol*. 1901;7:33-61.
36. Franzosa EA, Hsu T, Sirota-Madi A, et al. Sequencing and beyond: Integrating molecular "omics" for microbial community profiling. *Nat Rev Microbiol*. 2015;13(6):360-372. doi:10.1038/nrmicro3451
37. Nayfach S, Roux S, Seshadri R, et al. A genomic catalog of Earth's microbiomes. *Nat Biotechnol*. 2021;39(4):499-509.

- doi:10.1038/s41587-020-0718-6
38. Eren AM, Banfield JF. Modern microbiology: Embracing complexity through integration across scales. *Cell*. 2024;187(19):5151-5170. doi:10.1016/j.cell.2024.08.028
  39. Stein LY, Klotz MG. The nitrogen cycle. *Curr Biol*. 2016;26(3):R94-R98. doi:10.1016/j.cub.2015.12.021
  40. Stein LY. Insights into the physiology of ammonia-oxidizing microorganisms. *Curr Opin Chem Biol*. 2019;49:9-15. doi:10.1016/j.cbpa.2018.09.003
  41. Caranto JD, Vilbert AC, Lancaster KM. Nitrosomonas europaea cytochrome P460 is a direct link between nitrification and nitrous oxide emission. *Proc Natl Acad Sci U S A*. 2016;113(51):14704-14709. doi:10.1073/pnas.1611051113
  42. Könneke M, Bernhard AE, De La Torre JR, Walker CB, Waterbury JB, Stahl DA. Isolation of an autotrophic ammonia-oxidizing marine archaeon. *Nature*. 2005;437(7058):543-546. doi:10.1038/nature03911
  43. Mulder A, van de Graaf AA, Robertson LA, Kuenen JG. Anaerobic ammonium oxidation discovered in a denitrifying fluidized bed reactor. *FEMS Microbiol Ecol*. 1995;16(3):177-183. doi:10.1016/0168-6496(94)00081-7
  44. Van Kessel MAHJ, Speth DR, Albertsen M, et al. Complete nitrification by a single microorganism. *Nature*. 2015;528(7583):555-559. doi:10.1038/nature16459
  45. Daims H, Lebedeva E V., Pjevac P, et al. Complete nitrification by Nitrospira bacteria. *Nature*. 2015;528(7583):504-509. doi:10.1038/nature16461
  46. Stein LY. Heterotrophic Nitrification and Nitrifier Denitrification. In: Ward BB, Arp DJ, Klotz MG, eds. *Nitrification*. ASM Press; 2011:95-115. doi:10.1128/9781555817145.ch5
  47. Lenferink WB, Bakken LR, Jetten MSM, van Kessel MAHJ, Lückers S. Hydroxylamine production by *Alcaligenes faecalis* challenges the paradigm of heterotrophic nitrification. *Sci Adv*. 2024;10(23):1-9. doi:10.1126/sciadv.adl3587
  48. Sanford RA, Wagner DD, Wu Q, et al. Unexpected nondenitrifier nitrous oxide reductase gene diversity and abundance in soils. *Proc Natl Acad Sci U S A*. 2012;109(48):19709-19714. doi:10.1073/pnas.1211238109
  49. Zumft WG. Cell biology and molecular basis of denitrification. *Microbiol Mol Biol Rev*. 1997;61(4):533-616. doi:10.1128/mmbr.61.4.533-616.1997
  50. Lycus P, Bøthun KL, Bergaust L, Shapleigh JP, Bakken LR, Frostegård Å. Phenotypic and genotypic richness of denitrifiers revealed by a novel isolation strategy. *ISME J*. 2017;11(10):2219-2232. doi:10.1038/ismej.2017.82
  51. Cole JA, Brown CM. Nitrite reduction to ammonia by fermentative bacteria: a short circuit in the biological nitrogen cycle. *FEMS Microbiol Lett*. 1980;7:65-72. doi:10.1016/S0378-1097(80)80001-2
  52. Hasan SM, Hall JB. The physiological function of nitrate reduction in *Clostridium perfringens*. *J Gen Microbiol*. 1975;87(1):120-128. doi:10.1099/00221287-87-1-120
  53. Ettwig KF, Butler MK, Le Paslier D, et al. Nitrite-driven anaerobic methane oxidation by oxygenic bacteria. *Nature*. 2010;464(7288):543-548. doi:10.1038/nature08883
  54. Kraft B, Jehmlich N, Larsen M, et al. Oxygen and nitrogen production by an ammonia-oxidizing archaeon. *Science*. 2022;375(6576):97-100. doi:10.1126/science.abe6733
  55. Delwiche CC. The nitrogen cycle. *Sci Am*. 1970;223(3):136-147. doi:10.1038/scientificamerican0970-

56. Yan Y, Yang J, Dou Y, et al. Nitrogen fixation island and rhizosphere competence traits in the genome of root-associated *Pseudomonas stutzeri* A1501. *Proc Natl Acad Sci U S A*. 2008;105(21):7564-7569. doi:10.1073/pnas.0801093105
57. Daims H, Lückner S, Wagner M. A new perspective on microbes formerly known as nitrite-oxidizing bacteria. *Trends Microbiol*. 2016;24(9):699-712. doi:10.1016/j.tim.2016.05.004
58. Stein LY. The Long-Term Relationship between Microbial Metabolism and Greenhouse Gases. *Trends Microbiol*. 2020;28(6):500-511. doi:10.1016/j.tim.2020.01.006
59. Hernández-Magaña E, Kraft B. Nitrous oxide production and consumption by marine ammonia-oxidizing archaea under oxygen depletion. *Front Microbiol*. 2024;15(September). doi:10.3389/fmicb.2024.1410251
60. Zumft WG, Kroneck PMH. *Respiratory Transformation of Nitrous Oxide (N2O) to Dinitrogen by Bacteria and Archaea*. Vol 52.; 2006. doi:10.1016/S0065-2911(06)52003-X
61. Erisman JW, Sutton MA, Galloway J, Klimont Z, Winiwarter W. How a century of ammonia synthesis changed the world. *Nat Geosci*. 2008;1(10):636-639. doi:10.1038/ngeo325
62. Intergovernmental Panel on Climate Change. *Climate Change 2014: Synthesis Report*. (Core Writing Team, Pachauri RK, Meyer LA, eds.). IPCC; 2015.
63. Ravishankara AR, Daniel JS, Portmann RW. Nitrous oxide (N2O): The dominant ozone-depleting substance emitted in the 21st century. *Science*. 2009;326(5949):123-125. doi:10.1126/science.1176985
64. European Commission. *The European Green Deal*; 2019.
65. United States Department of State and United States Executive Office of the President. *The Long-Term Strategy of the United States: Pathways to Net-Zero Greenhouse Gas Emissions by 2050*; 2021.
66. International Energy Agency. *Net Zero by 2050: A Roadmap for the Global Energy Sector*; 2021.
67. Schreiber F, Wunderlin P, Udert KM, Wells GF. Nitric oxide and nitrous oxide turnover in natural and engineered microbial communities: Biological pathways, chemical reactions, and novel technologies. *Front Microbiol*. 2012;3(OCT):1-24. doi:10.3389/fmicb.2012.00372
68. Morley N, Baggs EM, Dörsch P, Bakken L. Production of NO, N2O and N2 by extracted soil bacteria, regulation by NO2- and O2 concentrations. *FEMS Microbiol Ecol*. 2008;65(1):102-112. doi:10.1111/j.1574-6941.2008.00495.x
69. Pan Y, Ni BJ, Bond PL, Ye L, Yuan Z. Electron competition among nitrogen oxides reduction during methanol-utilizing denitrification in wastewater treatment. *Water Res*. 2013;47(10):3273-3281. doi:10.1016/j.watres.2013.02.054
70. Wu L, Chen X, Wei W, Liu Y, Wang D, Ni B jie. A Critical Review on Nitrous Oxide Production by Ammonia-Oxidizing Archaea. Published online 2020. doi:10.1021/acs.est.0c03948
71. Stein LY, Klotz MG, Lancaster KM, et al. Comment on "A Critical Review on Nitrous Oxide Production by Ammonia-Oxidizing Archaea" by Lan Wu, Xueming Chen, Wei Wei, Yiwen Liu, Dongbo Wang, and Bing-Jie Ni. *Environ Sci Technol*. 2021;55(1):797-798. doi:10.1021/acs.est.0c06792
72. Kits KD, Jung MY, Vierheilig J, et al. Low yield and abiotic origin of N2O formed by the complete nitrifier *Nitrospira inopinata*. *Nat Commun*. 2019;10(1):1-12. doi:10.1038/s41467-019-09790-x



73. Kozłowski JA, Stieglmeier M, Schleper C, Klotz MG, Stein LY. Pathways and key intermediates required for obligate aerobic ammonia-dependent chemolithotrophy in bacteria and Thaumarchaeota. *ISME J*. 2016;10(8):1836-1845. doi:10.1038/ismej.2016.2
74. Jetten MSM, Niftrik L Van, Strous M, Kartal B, Keltjens JT, Op Den Camp HJM. Biochemistry and molecular biology of anammox bacteria. *Crit Rev Biochem Mol Biol*. 2009;44(2-3):65-84. doi:10.1080/10409230902722783
75. Zhu-Barker X, Cavazos AR, Ostrom NE, Horwath WR, Glass JB. The importance of abiotic reactions for nitrous oxide production. *Biogeochemistry*. 2015;126(3):251-267. doi:10.1007/s10533-015-0166-4
76. Kampschreur MJ, Kleerebezem R, de Vet WWJM, Van Loosdrecht MCM. Reduced iron induced nitric oxide and nitrous oxide emission. *Water Res*. 2011;45(18):5945-5952. doi:10.1016/j.watres.2011.08.056
77. Hink L, Lycus P, Gubry-Rangin C, et al. Kinetics of NH<sub>3</sub>-oxidation, NO<sub>2</sub><sup>-</sup> turnover, N<sub>2</sub>O-production and electron flow during oxygen depletion in model bacterial and archaeal ammonia oxidisers. *Environ Microbiol*. 2017;19(12):4882-4896. doi:10.1111/1462-2920.13914
78. Ostrom NE, Ostrom PH. Mining the isotopic complexity of nitrous oxide: a review of challenges and opportunities. *Biogeochemistry*. 2017;132(3):359-372. doi:10.1007/s10533-017-0301-5
79. Butterbach-Bahl K, Baggs EM, Dannenmann M, Kiese R, Zechmeister-Boltenstern S. Nitrous oxide emissions from soils: How well do we understand the processes and their controls? *Philos Trans R Soc B*. 2013;368(1621). doi:10.1098/rstb.2013.0122
80. Domingo-Félez C, Smets BF. Regulation of key N<sub>2</sub>O production mechanisms during biological water treatment. *Curr Opin Biotechnol*. 2019;57:119-126. doi:10.1016/j.copbio.2019.03.006
81. Duan H, Ye L, Erler D, Ni B jie, Yuan Z. Quantifying nitrous oxide production pathways in wastewater treatment systems using isotope technology - A critical review. *Water Res*. 2017;122:96-113. doi:10.1016/j.watres.2017.05.054
82. Hu HW, Chen D, He JZ. Microbial regulation of terrestrial nitrous oxide formation: Understanding the biological pathways for prediction of emission rates. *FEMS Microbiol Rev*. 2015;39(5):729-749. doi:10.1093/femsre/fuv021
83. Wrage-Mönnig N, Horn MA, Well R, Müller C, Velthof G, Oenema O. The role of nitrifier denitrification in the production of nitrous oxide revisited. *Soil Biol Biochem*. 2018;123(April):A3-A16. doi:10.1016/j.soilbio.2018.03.020
84. Tian H, Xu R, Canadell JG, et al. A comprehensive quantification of global nitrous oxide sources and sinks. *Nature*. 2020;586(7828):248-256. doi:10.1038/s41586-020-2780-0
85. Daims H, Taylor MW, Wagner M. Wastewater treatment: a model system for microbial ecology. *Trends Biotechnol*. 2006;24(11):483-489. doi:10.1016/j.tibtech.2006.09.002
86. Edward A, William TL. Experiments on the oxidation of sewage without the aid of filters. *J Soc Chem Ind*. 1914;33(10):523-539. doi:10.1002/jctb.5000331005
87. Daelman MRJ, Van Voorthuizen EM, Van Dongen LGJM, Volcke EIP, Van Loosdrecht MCM. Methane and nitrous oxide emissions from municipal wastewater treatment - Results from a long-term study. *Water Sci Technol*. 2013;67(10):2350-2355. doi:10.2166/wst.2013.109
88. Desloover J, Vlaeminck SE, Clauwaert P, Verstraete W, Boon N. Strategies to

- mitigate N<sub>2</sub>O emissions from biological nitrogen removal systems. *Curr Opin Biotechnol.* 2012;23(3):474-482. doi:10.1016/j.copbio.2011.12.030
89. Vasilaki V, Massara TM, Stanchev P, Fatone F, Katsou E. A decade of nitrous oxide (N<sub>2</sub>O) monitoring in full-scale wastewater treatment processes: A critical review. *Water Res.* 2019;161:392-412. doi:10.1016/j.watres.2019.04.022
  90. Duan H, Zhao Y, Koch K, et al. Insights into nitrous oxide mitigation strategies in wastewater treatment and challenges for wider implementation. *Environ Sci Technol.* 2021;55:7208-7224. doi:10.1021/acs.est.1c00840
  91. Kampschreur MJ, Temmink H, Kleerebezem R, Jetten MSM, van Loosdrecht MCM. Nitrous oxide emission during wastewater treatment. *Water Res.* 2009;43(17):4093-4103. doi:10.1016/j.watres.2009.03.001
  92. Daelman MRJ, van Voorthuizen EM, van Dongen UGJM, Volcke EIP, van Loosdrecht MCM. Seasonal and diurnal variability of N<sub>2</sub>O emissions from a full-scale municipal wastewater treatment plant. *Sci Total Environ.* 2015;536:1-11. doi:10.1016/j.scitotenv.2015.06.122
  93. Valk L, Peces M, Singleton CM, et al. Exploring the microbial influence on seasonal nitrous oxide concentration in a full-scale wastewater treatment plant using metagenome assembled genomes. *Water Res.* 2022;219(May):118563. doi:10.1016/j.watres.2022.118563
  94. Chen X, Mielczarek AT, Habicht K, Andersen MH, Thornberg D, Sin G. Assessment of Full-Scale N<sub>2</sub>O Emission Characteristics and Testing of Control Concepts in an Activated Sludge Wastewater Treatment Plant with Alternating Aerobic and Anoxic Phases. *Environ Sci Technol.* 2019;53(21):12485-12494. doi:10.1021/acs.est.9b04889
  95. Kosonen H, Heinonen M, Mikola A, et al. Nitrous Oxide Production at a Fully Covered Wastewater Treatment Plant: Results of a Long-Term Online Monitoring Campaign. *Environ Sci Technol.* 2016;50(11):5547-5554. doi:10.1021/acs.est.5b04466
  96. Yan X, Li L, Liu J. Characteristics of greenhouse gas emission in three full-scale wastewater treatment processes. *J Environ Sci.* 2014;26(2):256-263. doi:10.1016/S1001-0742(13)60429-5
  97. Sieranen M, Hilander H, Haimi H, Larsson T, Kuokkanen A, Mikola A. Seasonality of nitrous oxide emissions at six full-scale wastewater treatment plants. *Water Sci Technol.* 2023;89(3):603-612. doi:10.2166/wst.2023.420
  98. van Dijk EJH, van Loosdrecht MCM, Pronk M. Nitrous oxide emission from full-scale municipal aerobic granular sludge. *Water Res.* 2021;198:117159. doi:10.1016/j.watres.2021.117159
  99. Bae W Bin, Park Y, Chandran K, et al. Temporal triggers of N<sub>2</sub>O emissions during cyclical and seasonal variations of a full-scale sequencing batch reactor treating municipal wastewater. *Sci Total Environ.* 2021;797:149093. doi:10.1016/j.scitotenv.2021.149093
  100. Gruber W, Villez K, Kipf M, et al. N<sub>2</sub>O emission in full-scale wastewater treatment: Proposing a refined monitoring strategy. *Sci Total Environ.* 2020;699:134157. doi:10.1016/j.scitotenv.2019.134157
  101. Gruber W, Niederdorfer R, Ringwald J, Morgenroth E, Bürgmann H, Joss A. Linking seasonal N<sub>2</sub>O emissions and nitrification failures to microbial dynamics in a SBR wastewater treatment plant. *Water Res X.* 2021;11:100098. doi:10.1016/j.wroa.2021.100098
  102. Gruber W, von Känel L, Vogt L, et al. Estimation of countrywide N<sub>2</sub>O emissions from wastewater treatment in Switzerland using long-term



monitoring data. *Water Res X*.  
2021;13(September).  
doi:10.1016/j.wroa.2021.100122



# Aerobic denitrification as an N<sub>2</sub>O source from microbial communities



## Abstract

Nitrous oxide (N<sub>2</sub>O) is a potent greenhouse gas of primarily microbial origin. Oxic and anoxic emissions are commonly ascribed to autotrophic nitrification and heterotrophic denitrification, respectively. Beyond this established dichotomy, we quantitatively show that heterotrophic denitrification can significantly contribute to aerobic nitrogen turnover and N<sub>2</sub>O emissions in complex microbiomes exposed to frequent oxic/anoxic transitions. Two planktonic, nitrification-inhibited enrichment cultures were established under continuous organic carbon and nitrate feeding, and cyclic oxygen availability. Over a third of the influent organic substrate was respired with nitrate as electron acceptor at high oxygen concentrations (> 6.5 mg/L). N<sub>2</sub>O accounted for up to one quarter of the nitrate reduced under oxic conditions. The enriched microorganisms maintained a constitutive abundance of denitrifying enzymes due to the oxic/anoxic frequencies exceeding their protein turnover - a common scenario in natural and engineered ecosystems. The aerobic denitrification rates are ascribed primarily to the residual activity of anaerobically synthesised enzymes. From an ecological perspective, the selection of organisms capable of sustaining significant denitrifying activity during aeration shows their competitive advantage over other heterotrophs under varying oxygen availabilities. Ultimately, we propose that the contribution of heterotrophic denitrification to aerobic nitrogen turnover and N<sub>2</sub>O emissions is currently underestimated in dynamic environments.

## 2.1. Introduction

Nitrous oxide (N<sub>2</sub>O) is today's third most important greenhouse gas and the main stratospheric ozone-depleting substance <sup>1</sup>. Globally, the majority of N<sub>2</sub>O originates from biological conversions in natural, managed, and engineered ecosystems <sup>2</sup>, such as oceans <sup>3</sup>, agricultural soils <sup>4</sup>, and wastewater treatment plants <sup>5</sup>. N<sub>2</sub>O emissions from anthropogenic activities are projected to reach 11.5 Tg N yr<sup>-1</sup> in 2050, double the amount emitted in 2000, if no mitigation action is taken <sup>1,2</sup>. Robust emission control strategies strongly rely on our knowledge of the microbiology underlying N<sub>2</sub>O turnover.

N<sub>2</sub>O is a metabolic by-product of autotrophic nitrification, the aerobic oxidation of ammonium (NH<sub>4</sub><sup>+</sup>) to nitrite (NO<sub>2</sub><sup>-</sup>) and nitrate (NO<sub>3</sub><sup>-</sup>), and an obligate intermediate of heterotrophic denitrification, the multi-step reduction of NO<sub>3</sub><sup>-</sup> to dinitrogen gas (N<sub>2</sub>). Conventionally, nitrification and denitrification are considered to dominate N<sub>2</sub>O emissions in the presence and absence of O<sub>2</sub>, respectively <sup>3,4,6</sup>. Oxygen is known to regulate the expression and inhibit the activity of denitrifying enzymes <sup>7-9</sup>. Besides, as most known denitrifiers are facultative aerobes, the more energetically and kinetically favourable O<sub>2</sub> respiration is expected to be prioritised over denitrification in oxic conditions <sup>10</sup>. The aerobic contribution of denitrification is thus generally neglected in soils <sup>11-13</sup>, oceans <sup>3,14</sup>, and wastewater treatment systems <sup>15-17</sup>. However, starting from the seminal work of Robertson & Kuenen <sup>18</sup>, the occurrence of denitrification under high oxygen concentrations has been documented in pure culture studies (as previously reviewed <sup>10</sup>). What remains to be resolved is the ecological significance of heterotrophic denitrification in aerobic N<sub>2</sub>O formation.

*Sensu stricto*, we refer to the simultaneous occurrence of heterotrophic denitrification and aerobic respiration as aerobic denitrification <sup>18-21</sup>. Biochemically, the co-respiration of O<sub>2</sub> and nitrogen oxides by the same organism may result from the *de novo* aerobic synthesis of denitrifying enzymes or from the residual activity of anaerobically expressed enzymes <sup>8</sup>. Based on a past literature review <sup>10</sup>, aerobic denitrification rates seem to be generally much lower than the anaerobic ones, yet are likely to provide an ecological advantage in dynamic environments. Bacteria reported to denitrify aerobically, including *Alcaligenes faecalis* and multiple *Pseudomonas* species, have indeed been successfully isolated mainly from ecosystems exposed to fluctuating O<sub>2</sub> levels such as soils, sediments, and activated sludge <sup>18,21-23</sup>. One study <sup>21</sup> employed weekly alternating oxic/anoxic conditions to enrich for aerobic denitrifiers prior to isolation, further highlighting dynamic O<sub>2</sub> conditions as key to select for bacteria capable of denitrifying under oxic conditions. However, most reported aerobic heterotrophic denitrification rates are based on a limited number of isolates

characterised primarily under continuous aeration, inherently hindering their extrapolation to complex microbiomes in dynamic  $O_2$  environments. Central challenges in open ecosystems are the co-occurrence of nitrification as potential confounding aerobic  $N_2O$  source, and the development of anoxic micro-niches in microbial aggregates<sup>24,25</sup>. Only three studies quantified denitrification in the presence of oxygen in natural communities, namely in soil bacteria extracted by density-gradient centrifugation<sup>25</sup> and intact sea sediments<sup>20,24</sup>. All authors experimentally showed nitrification to be negligible, yet anoxic niches could not be excluded in these complex ecosystems. One study<sup>24</sup> even observed a marked decrease in aerobic  $NO_x^-$  respiration upon vigorous stirring, possibly resulting from the disruption of anoxic micro-niches. The extent to which heterotrophic denitrification contributes to overall aerobic nitrogen turnover in dynamic ecosystems is currently unknown.

We enriched for two communities of heterotrophic denitrifiers co-respiring  $O_2$  and  $NO_3^-$  under alternating oxic/anoxic conditions to quantitatively resolve the ecological role of aerobic denitrification. Our underlying hypothesis was that the ability to aerobically respire nitrogen oxides provides a competitive advantage in complex microbiomes exposed to fluctuating oxygen availabilities. We use open culturing techniques that mimic natural ecosystems, allowing microbial communities to evolve under non-axenic conditions, and the fittest organisms for the imposed conditions to dominate. Highly aerated planktonic cultures were employed to exclude anoxic micro-niches, whereas continuous allylthiourea (ATU) addition ensured full suppression of nitrification, eliminating it as possible confounding  $N_2O$  source. The genetic potential and actual-metabolism of each community member was characterised by metagenomic and metaproteomic analysis. This study proves the selective advantage of oxygen and nitrogen oxides co-respiration, and quantifies its potential contribution to nitrogen turnover and  $N_2O$  emissions in complex communities. Our findings also suggest that the contribution of heterotrophic denitrification to aerobic  $N_2O$  emissions may currently be underestimated.

## 2.2. Materials and Methods

### 2.2.1. Continuous-flow stirred tank reactors operation

Two 1 L jacketed continuous-flow stirred tank reactors (Applikon, Getinge) were operated during 96 days, with continuous and vigorous mixing at 500 rpm using a six-blade turbine. The hydraulic and sludge retention times (HRT and SRT) were identical, controlled at  $2 \pm 0.1$  days by two peristaltic pumps (Masterflex) continuously feeding the two media to the system and an effluent pump removing 94 mL of broth every 6 h. The average working volume was  $0.75 \pm 0.05$  L. The temperature was controlled at 20

$\pm 0.1$  °C using a cryostat bath (Lauda). The pH and dissolved oxygen were continuously monitored by pH and dissolved oxygen probes (Applikon AppliSens, Getinge). The pH was kept at  $7.1 \pm 0.1$  by 1 M HCl or 1 M NaOH with two peristaltic pumps (Watson Marlow) controlled by a process controller (Applikon in-Control, Getinge).

Denitrifying bacteria were enriched by continuous supply of  $0.93 \pm 0.04$  N-mmol/h NO<sub>3</sub><sup>-</sup> as electron acceptor and a mixture of volatile fatty acids (VFAs) as electron donor and carbon source: acetate ( $0.94 \pm 0.08$  C-mmol/h), propionate ( $1.00 \pm 0.09$  C-mmol/h), and butyrate ( $0.75 \pm 0.07$  C-mmol/h). Ammonia served as the nitrogen source. The reactors were covered with aluminium foil to prevent the growth of phototrophic organisms. Nitrogen and carbon media were prepared separately to prevent microbial growth during storage. Nitrogen medium consisted of (per Liter): 9.14 g NaNO<sub>3</sub>, 2.84 g NH<sub>4</sub>Cl, 2.01 g KH<sub>2</sub>PO<sub>4</sub>, 1.04 g MgSO<sub>4</sub> · 7 H<sub>2</sub>O, 0.04 g NaOH, 4 mg yeast extract, 5 mL trace element solution <sup>26</sup>, and 1 mL of a 10 g/L solution of allylthiourea (ATU). ATU was added to selectively inhibit bacterial ammonium oxidation to nitrite <sup>27-29</sup> without significantly affecting denitrification <sup>30</sup>. The trace element solution consisted of (per Liter): 50 g EDTA · H<sub>2</sub> · Na<sub>2</sub> · 2 H<sub>2</sub>O, 2.5 g FeSO<sub>4</sub> · 7 H<sub>2</sub>O, 1.1 g ZnSO<sub>4</sub> · 7 H<sub>2</sub>O, 4.1 g CaCl<sub>2</sub> · 2 H<sub>2</sub>O, 2.2 g MnSO<sub>4</sub> · H<sub>2</sub>O, 1.1 g Na<sub>2</sub>MoO<sub>4</sub> · 2 H<sub>2</sub>O, 0.8 g CuSO<sub>4</sub> · 5 H<sub>2</sub>O, and 0.7 g CoCl<sub>2</sub> · 6 H<sub>2</sub>O. Carbon medium consisted of (per Liter): 8.1 g NaCH<sub>3</sub>COO · 3 H<sub>2</sub>O, 1.9 mL C<sub>4</sub>H<sub>8</sub>O<sub>2</sub>, and 4.1 g NaC<sub>3</sub>H<sub>5</sub>O<sub>2</sub>, the pH was set to 6.0 with NaOH pellets. After the initial start-up phase of 27 days, the VFAs were always below detection limit in the effluent, confirming carbon limiting conditions. Drops of antifoam C emulsion (Merck Life Science NV), diluted six times, were added to the reactors when foam formation was noted.

The reactors were inoculated with activated sludge from the Amsterdam-West wastewater treatment plant, comprising 349 high-quality metagenome-assembled genomes (MAGs), 305 of which had at least one denitrification gene (genome-resolved metagenomic composition in Supplementary Figure S2.20) <sup>31</sup>. Carbon-limiting conditions were reached after an initial start-up phase of 20 days where NO<sub>3</sub><sup>-</sup> was the growth-limiting compound. During the NO<sub>3</sub><sup>-</sup>-limiting start-up phase, the concentrations of VFAs were increased by four times in the carbon medium compared to the values presented above. The two reactors were exposed to continuous cycles of alternating oxic and anoxic conditions in a time proportion of 2:1. The reactors were exposed to 4 (R<sub>4</sub>) or 32 (R<sub>32</sub>) cycles per day, with oxic periods of 4h and 30 min and anoxic periods of 2h and 15 min, respectively. Oxic and anoxic conditions were maintained by continuous sparging of compressed air and N<sub>2</sub>, respectively, at 400 mL/min, controlled by mass-flow controllers (Brooks). Oxic conditions close to air saturation were assured by maintaining average dissolved O<sub>2</sub> concentrations of  $7.5 \pm 0.2$  and  $6.8 \pm 0.3$  mg/L in R<sub>4</sub> and R<sub>32</sub>, respectively. The reactors reached fully anoxic or oxic conditions within 5

min after switching the influent gas. The 6-hourly reactor broth removal coincided with the end of an anoxic phase. The net amount of oxic ( $\geq 1\%$  air saturation) and anoxic ( $< 1\%$  air saturation) hours per day were 16:8 and 17:7 for  $R_4$  and  $R_{32}$ , respectively. Throughout the operation, visual and microscopic analysis confirmed that the cultures remained planktonic and homogeneous (Supplementary Figure S2.4). For  $R_{32}$ , small biomass aggregates were progressively washed out reaching an entirely homogeneous and suspended culture after 63 days of operation. Occasional biomass accumulation in the splash zone of the bioreactor was always removed with no noticeable consequential changes in the reactors' operation (Supplementary Figure S2.2), confirming that it played no role in the nitrogen conversions. The measured  $O_2$  conversion rates were 7.5-fold lower than the maximum  $O_2$  transfer rate (Supplementary Table S2.1 and eq. S2.9), reflecting the significant aeration over-capacity in the reactors.

For metabolite and biomass analysis, quadruplicate samples of 2 mL were taken from both reactors at three moments within a cycle: at the start and end of the oxic phase, and at the end of the anoxic phase. The samples were placed on ice and immediately filtered using 0.22  $\mu\text{m}$  PVDF Millex-GV syringe filters (Merck) or centrifuged at 16,200  $\times g$  for 5 minutes at 4  $^{\circ}\text{C}$  to separate the biomass from the supernatant. The pellets were stored at -80  $^{\circ}\text{C}$  and the supernatant at -20  $^{\circ}\text{C}$  until further analysis. Feed substrate concentrations were confirmed by occasionally sampling the reactor influent, with storage at -20  $^{\circ}\text{C}$  until analysis.

### 2.2.2. Analytical methods

The concentrations of  $\text{NH}_4^+$ ,  $\text{NO}_2^-$ , and  $\text{NO}_3^-$  in the influent and effluent supernatant were spectrophotometrically measured with the Gallery Discrete Analyzer (Thermo Fisher Scientific) or cuvette test kits (Hach Lange) immediately after sampling or within 24h after storage at 4  $^{\circ}\text{C}$ . The concentrations of acetate, propionate, and butyrate in the influent and effluent supernatant were measured after storage at -20  $^{\circ}\text{C}$  by high-pressure liquid chromatography (Vanquish Core HPLC, Thermo Fisher Scientific) using an Aminex HPX-87H column (300  $\times$  7.8 mm) (Bio-Rad), calibrated with solutions ranging from 0 to 250 mM. The concentrations of  $O_2$ ,  $\text{N}_2\text{O}$ , and  $\text{CO}_2$  in the off-gas were continuously monitored online (every minute) by a Rosemount NGA 2000 off-gas analyser (Emerson). Before reaching the analyser, the off-gas was dried in a condenser, operated with water at 4 $^{\circ}\text{C}$  using a cryostat bath (Lauda).



### 2.2.3. Calculations

The calculations of consumption and production rates of all compounds are detailed in Supplementary Section 2.5.2. Briefly, the overall consumption and production rates of dissolved compounds ( $R_i$ , with  $i = \text{NH}_4^+$ ,  $\text{NO}_2^-$ ,  $\text{NO}_3^-$ , acetate, propionate, and butyrate) were calculated via a mass balance of the volumetric influent and effluent ( $F_{i,\text{in}}$  and  $F_{i,\text{out}}$ ) flow rates, and the influent and effluent concentrations ( $C_{i,\text{in}}$  and  $C_{i,\text{out}}$ ) measured in triplicate:

$$R_i^{\text{overall}} = F_{i,\text{out}} \cdot C_{i,\text{out}} - F_{i,\text{in}} \cdot C_{i,\text{in}} \quad (\text{eq. 2.1})$$

The overall rates ( $R_i^{\text{overall}}$ ) are, in practice, a weighted average of the aerobic and anaerobic consumption and production rates ( $R_i^{\text{aerobic}}$  and  $R_i^{\text{anaerobic}}$ ), so these three rates are related according to the following equation:

$$R_i^{\text{overall}} = \frac{t_{\text{aerobic}}}{24} \cdot R_i^{\text{aerobic}} + \frac{t_{\text{anaerobic}}}{24} \cdot R_i^{\text{anaerobic}} \quad (\text{eq. 2.2})$$

The biomass (X) production rate was estimated from the ammonium consumption rates, assuming complete assimilation into biomass at a ratio of 0.2 N-mol/C-mol. The same estimation was obtained when calculating the biomass rates from the carbon balance (i.e. from the CO<sub>2</sub> and organic carbon rates), validating the previous assumption. The estimated biomass concentrations were  $1.8 \pm 0.2$  (R<sub>4</sub>) and  $2.1 \pm 0.3$  (R<sub>32</sub>) g·L<sup>-1</sup>. The overall, oxic, and anoxic accumulation rates of gaseous compounds ( $R_{\text{gas},i}$ ,  $i = \text{N}_2\text{O}$  and CO<sub>2</sub>) were calculated from continuous measurements of the molar fractions in the gas inlet and outlet ( $y_{i,\text{in}}$  and  $y_{i,\text{out}}$ ), the atmospheric pressure ( $P_{\text{atm}}$ ), the volumetric gas flow ( $F_{V,\text{gas}}$ ), the ideal gas constant (R), and the reactor temperature (T).

$$R_{\text{gas},i} = (y_{i,\text{out}} - y_{i,\text{in}}) \cdot \frac{P_{\text{atm}} \cdot F_{V,\text{gas}}}{R \cdot T} \quad (\text{eq. 2.3})$$

The overall N<sub>2</sub> production rate was estimated from the nitrate and N<sub>2</sub>O rates, as the accumulation of nitrite and nitric oxide was negligible throughout steady-state. The O<sub>2</sub> consumption rates ( $R_{\text{O}_2}$ ) during the oxic phase were calculated from the experimentally determined volumetric mass transfer coefficient ( $k_{\text{La}}$ , Supplementary Section 2.5.1), the O<sub>2</sub> Henry coefficient ( $H_{\text{O}_2}$ ), the atmospheric pressure ( $P_{\text{atm}}$ ), the O<sub>2</sub> molar fraction in the off-gas ( $y_{\text{O}_2}$ ), the continuous dissolved oxygen measurements (DO), and the average broth volume (V).

$$R_{\text{O}_2} = k_{\text{La}} \cdot H_{\text{O}_2} \cdot P_{\text{atm}} \cdot y_{\text{O}_2} \cdot (1 - \text{DO}) \cdot V \quad (\text{eq. 2.4})$$

For consistency, an “overall” consumption rate was also calculated for O<sub>2</sub>, by averaging its aerobic consumption over the entire cycle duration (eq. 2.2). For all compounds, steady-state rates were determined by averaging the rates measured during the entire steady-state period. Overall carbon and electron balances were calculated from the consumption and production rates of all substrates (R<sub>in</sub>) and products (R<sub>out</sub>), and electron donors (R<sub>eD</sub>) and acceptors (R<sub>eA</sub>), respectively.

$$\text{C balance (\%)} = \frac{R_{in}}{R_{out}} = \frac{|R_{Ace} + R_{Pro} + R_{But}|}{R_X + R_{CO_2}} \quad (\text{eq. 2.5})$$

$$\text{e}^- \text{ balance (\%)} = \frac{R_{eD}}{R_{eA}} = \frac{|4 \cdot R_{Ace} + 4.7 \cdot R_{Pro} + 5 \cdot R_{But}|}{-8 \cdot R_{NO_3^-} - 4 \cdot R_{N_2O} - 3 \cdot R_{N_2} - 4 \cdot R_{O_2} + 4.2 \cdot R_X} \quad (\text{eq. 2.6})$$

The specific aerobic and anaerobic NO<sub>3</sub><sup>-</sup> consumption rates were estimated from the available measurements, mass balances, and eq. 2.2, as explained in Supplementary Section 2.5.2. These values were validated with direct calculations from measured concentration profiles throughout each phase (Supplementary Figures S2.8-2.9). Possible deviations in the estimated rates due to potential PHA accumulation were negligible (Supplementary Section 2.5.2).

#### 2.2.4. DNA extraction, library preparation, and sequencing

DNA was extracted from biomass samples taken at the end of the anoxic period after 68 days of operation using the DNeasy PowerSoil Pro Kit (Qiagen), according to the manufacturer's instructions with the following exceptions. The pelleted biomass, stored at -80 °C, was resuspended in 800 µL of solution CD1 by vortexing before transferring to the PowerBead tube. Samples were homogenised by 4 x 40s bead-beating using the Beadbeater-24 (Biospec) alternated with 2 min incubation on ice. Tubes were gently inverted 10x instead of vortexing to avoid DNA shearing. Elution of the extracted DNA was performed with 50 µL solution C6. The DNA concentration was 710 and 605 ng/µL for R<sub>4</sub> and R<sub>32</sub>, respectively, as measured with the Qubit 4 Fluorometer (Thermo Fisher Scientific). DNA quality was assessed with the BioTek Synergy HTX multi-mode microplate reader (Agilent). For differential coverage binning and increased bin recovery, DNA was also extracted from samples taken after 41 days of operation using the Dneasy UltraClean Microbial Kit (Qiagen), following the manufacturer's instructions. The extraction yielded 224 and 267 ng/µL for R<sub>4</sub> and R<sub>32</sub>, respectively.

Library preparation of the extracted DNA from day 68 for long-read sequencing was performed using the Ligation Sequencing Kit V14 (Oxford Nanopore Technologies Ltd). The NEBNext Companion Module for Oxford Nanopore Technologies Ligation Sequencing (New England BioLabs Inc.) and UltraPure BSA (50 mg/mL) (Thermo

Fisher Scientific) were additionally used for the DNA repair and end-prep, and the flow cell priming steps. All steps were performed as instructed by the manufacturer, except the incubations in the Hula mixer were replaced with slow manual inversions (~5 s per inversion). All resuspension steps were performed by flicking the tube. MinION R10.4 version flow cells (Oxford Nanopore), starting with 1345 and 461 active pores, were loaded with 132 and 150 ng DNA for R<sub>4</sub> and R<sub>32</sub>, respectively. Samples were sequenced in accurate mode (260 bps) for 46 and 40 h, respectively, yielding 14.7 and 4.3 Gbp of sequenced data. Samples from day 41 were sequenced on a NovaSeq 6000 platform (Illumina) by Novogene Ltd. (UK). Approximately 10 Gbp of 150 bp paired-end reads with an insert size of 350 bp were generated.

### 2.2.5. Metagenomic data processing

The raw Nanopore data was basecalled using Guppy v6.4.2 (Oxford Nanopore) with the configuration file “dna\_r10.4.1\_e8.2\_260bps\_sup.cfg” and --do\_read\_splitting option. Duplex reads were identified and filtered using the pairs\_from\_summary and filter\_pairs settings from Duplex tools v0.2.19 (Oxford Nanopore), and basecalled with the duplex basecaller of Guppy, using identical settings to the simplex basecalling. The simplex reads, not part of a pair, were merged with the duplex basecalled reads using SeqKit v2.3.0 <sup>32</sup>, generating a single fastq file containing all unique reads. Sequences belonging to the Lambda control DNA were removed with NanoLyse v1.2.1 <sup>33</sup>. The basecalled data was inspected and processed with NanoPlot v1.41.0 <sup>33</sup>, NanoFilt -q 10 -l 1000 (v2.8.0 <sup>33</sup>), and Porechop v0.2.4 (<https://github.com/rrwick/Porechop>). Reads assembly was performed with Flye v2.9.1 <sup>34</sup> in --meta mode. Assembly quality was assessed with MetaQUAST v5.0.2 <sup>35</sup> using the --fragmented option. Reads were aligned to the assembly with Minimap2 v2.24 <sup>36</sup>. The assembly was polished with Racon v1.4.3 (<https://github.com/isovic/racon>) and two rounds of Medaka v1.5.0 (<https://github.com/nanoporetech/medaka>) with default settings. Nanopore and Illumina reads were mapped to the final assembly using Minimap2 <sup>36</sup>, the alignments were converted from SAM to BAM and sorted with SAMtools v1.10 <sup>37</sup>, and the contig coverage was calculated with jgi\_summarize\_bam\_contig\_depths <sup>38</sup>. Automatic differential coverage binning was independently performed with MetaBAT2 v2.15 <sup>38</sup>, MaxBin2 v2.2.7 <sup>39</sup>, and CONCOCT v1.1.0 <sup>40</sup>, with a minimum contig length of 2000 bp. The output of all binning tools was combined with DAS Tool v1.1.3 <sup>41</sup>, using Prodigal v2.6.3 <sup>42</sup> and DIAMOND v2.0.8 <sup>43</sup> for single copy gene prediction and identification, resulting in an optimised non-redundant set of bins. Bin completeness and contamination was determined with CheckM v1.1.3 <sup>44</sup> using the lineage\_wf workflow. Nanopore and Illumina bins from each reactor were dereplicated with dRep v3.2.2 <sup>45</sup> with the options -comp 70 -con 10 --S\_algorithm gANI, using the default thresholds for average nucleotide identity (ANI). The final set of non-redundant bins (completeness

above 70% and contamination under 10%) contained all Nanopore bins and the Illumina bins that did not cluster with any Nanopore bins (gANI < 99%). The bins were taxonomically classified with the `classify_wf` workflow of GTDB-Tk v.2.2.5<sup>46</sup> using the GTDB release 207 (`gtdbtk_r207_v2_data.tar.gz`<sup>47</sup>). The relative abundance of each bin in the metagenome was determined with CoverM v0.6.1 (<https://github.com/wwood/CoverM>) in `relative_abundance` mode.

Genes were predicted from the assembly using Prodigal v2.6.3<sup>42</sup> and functionally annotated with DRAM v1.3 in `annotate_genes` mode<sup>48</sup>, using the default settings and the KOfam<sup>49</sup>, MEROPS<sup>50</sup>, Pfam<sup>51</sup>, dbCAN<sup>52</sup>, and VOGDB (<https://vogdb.org/>) databases. Genes of interest were identified by their KO identifier (Supplementary Tables S2.9-2.11). The genes encoding the alpha and beta subunits of the respiratory nitrate reductase (Nar) have the same KO identifiers as the alpha and beta subunits of the nitrite oxidoreductase (Nxr). We could confidently attribute all genes identified with K00370 and K00371 to the nitrate reductase (encoded by *narGHI* or *narZYV*), as the gamma subunit of this enzyme (K00374, exclusive to Nar) was present in all bins containing the alpha and beta subunits. Distinction between clade I and clade II N<sub>2</sub>O reductase (NosZ) was determined by, respectively, identifying the twin-arginine translocation (Tat, IPR006311) or the general secretory (Sec, IPR026468) pathway-specific signal peptides on InterPro v92.0<sup>53</sup>. The quinol-dependent nitric oxide reductase (qNor, encoded by *norZ*) has a fused quinol oxidase domain on the N-terminal<sup>54</sup>, unlike the cytochrome c-dependent reductase (cNor, encoded by *norBC*). Yet, the *norZ* genes were annotated as *norB*, so qNor was distinguished by identifying the quinol oxidase domain through a multiple sequence alignment (COBALT<sup>55</sup>) of putative NorB protein sequences (K04561) with reference sequences of NorB (*Pseudomonas stutzeri*, P98008) and NorZ (*Cupriavidus necator*, Q0JYR9), extracted from UniProtKB<sup>56</sup>.

Quality control of the Illumina paired-end reads was performed with FastQC v0.11.7 (<https://www.bioinformatics.babraham.ac.uk/projects/fastqc/>). Reads were filtered and trimmed with Trimmomatic v0.39<sup>57</sup> using the options `LEADING:3 TRAILING:3 SLIDINGWINDOW:4:15 MINLEN:35 HEADCROP:5`. Reads were assembled into contigs using `metaspades.py` from SPAdes v3.14.1<sup>58</sup>. The assembly was inspected with MetaQUAST v5.0.2<sup>35</sup> using the `--fragmented` option. Contigs smaller than 500 bp were removed with `filterContigByLength.pl`<sup>59</sup>. Gene prediction and functional annotation was performed identically to the Nanopore data. The paired-end reads were mapped to the contigs using BWA-MEM2 v2.1<sup>60</sup>. The paired-end reads were mapped to the contigs using BWA-MEM2 v2.1<sup>60</sup> and the alignments were processed as described above. Automatic binning and bin analysis was identical as described for the Nanopore data, except no differential coverage binning was performed and the default minimum

contig length of each binning software was used. The generated bins were further dereplicated with the Nanopore bins as described above. Nonpareil v3.401<sup>61</sup>, ran with the kmer algorithm, estimated that the Illumina reads covered 98.6% and 99.2% of the sample diversity. Raw DNA reads were deposited on the NCBI Sequence Read Archive and medium- and high-quality MAGs were deposited in Genbank under BioProject PRJNA977937.

### 2.2.6. Protein extraction, precipitation, digestion, and clean-up

Preparation of protein samples was performed as previously described<sup>62</sup>. Briefly, biomass samples were homogenised with glass beads (150 - 212 µm, Sigma Aldrich), 50 mM TEAB buffer with 1% (w/w) NaDOC, and B-PER reagent (Thermo Scientific) through three cycles of vortexing and ice incubation. The samples were incubated at 80°C and sonicated. The supernatant was collected after centrifuging at 14,000 g. Proteins were precipitated with 1:4 trichloroacetic acid solution (TCA, Sigma Aldrich) and washed with acetone. The pellet was re-dissolved in 6 M Urea (Sigma Aldrich) in 200 mM ammonium bicarbonate, reduced in 10 mM dithiothreitol (Sigma Aldrich) at 37°C for 60 min, and alkylated with 20 mM iodoacetamide (Sigma Aldrich) in the dark for 30 min, at room temperature. Samples were diluted to reach a urea concentration under 1 M. Proteins were digested overnight (21 h) at 37°C with 0.1 µg/µL trypsin (sequencing grade, Promega) dissolved in 1 mM HCl. Samples were desalted and cleaned through solid phase extraction using an Oasis HLB 96-well µElution Plate (2mg sorbent per well, 30 µm, Waters) and a vacuum pump. The columns were conditioned with MeOH, equilibrated with two rounds of water, loaded with the digested samples, and washed with two rounds of 5% MeOH. Peptide samples were sequentially eluted with 2% formic acid in 80% MeOH and 1 mM ammonium bicarbonate in 80% MeOH, dried at 50°C in an Integrated SpeedVac System (Thermo Scientific), and stored at -20°C until shotgun proteomic analysis.

### 2.2.7. Shotgun metaproteomics

Briefly, samples were dissolved in 20 µL of 3% acetonitrile and 0.01% trifluoroacetic acid. The samples were incubated at room temperature for 30 min and vortexed thoroughly. The protein concentration was measured on a NanoDrop ND-1000 spectrophotometer (Thermo Scientific) at 280 nm wavelength. If needed, samples were diluted to a concentration of 0.5 mg/mL.

Shotgun metaproteomics experiments were performed as recently described<sup>62,63</sup>. Briefly, aliquots corresponding to approximately 0.5 µg protein digest were analysed using a nano-liquid-chromatography system consisting of an EASY nano-LC 1200,

equipped with an Acclaim PepMap RSLC RP C18 separation column (50  $\mu\text{m}$  x 150 mm, 2  $\mu\text{m}$ , Cat. No. 164568), and a QE plus Orbitrap mass spectrometer (Thermo Fisher Scientific). The flow rate was maintained at 350 nL/min over a linear gradient from 5% to 25% solvent B over 90 min, then from 25% to 55% over 60 min, followed by back equilibration to starting conditions. Solvent A was  $\text{H}_2\text{O}$  containing 0.1% formic acid (FA), and solvent B consisted of 80% ACN in  $\text{H}_2\text{O}$  and 0.1% FA. The Orbitrap was operated in data dependent acquisition (DDA) mode acquiring peptide signals from 385–1250 m/z at 70 K resolution in full MS mode with a maximum ion injection time (IT) of 75 ms and an automatic gain control (AGC) target of  $3\text{E}6$ . The top 10 precursors were selected for MS/MS analysis and subjected to fragmentation using higher-energy collisional dissociation (HCD) at a normalised collision energy of 28. MS/MS scans were acquired at 17.5 K resolution with AGC target of  $2\text{E}5$  and IT of 75 ms, 1.2 m/z isolation width. Raw mass spectrometric data from each reactor were analysed against a protein reference sequence database respectively constructed from the metagenomic data, including the all MAGs and unbinned portion of the samples taken at day 68 and the additional dereplicated MAGs from day 41, using PEAKS Studio X (Bioinformatics Solutions Inc.) allowing for 20 ppm parent ion and 0.02 m/z fragment ion mass error, 3 missed cleavages, and iodoacetamide as fixed, and methionine oxidation and N/Q deamidation as variable modifications. Peptide spectrum matches were filtered against 1% false discovery rates (FDR) and protein identifications with  $\geq 2$  unique peptide sequences.

For each protein, the peptide spectral counts were normalised by dividing them with the protein molecular weight. The relative abundance of each protein in the samples was calculated by dividing its normalised spectral counts by the sum of normalised spectral counts of all proteins of that respective sample. The technical duplicates were then averaged. The total relative contribution of each bin to the proteome was determined by summing the relative abundances of its proteins. Similarly, the total relative abundance of functionally identical proteins was determined by summing the relative contribution of all proteins with the same functional annotation. The exclusion of any NapA and NapB peptides in the proteomic data was concluded from the absence of corresponding sequences within the obtained peptide spectrum matches. RStudio v22.0.3 <sup>64</sup> with R v4.2.2 <sup>65</sup>, with the plyr v1.8.8 <sup>66</sup>, tidyverse v2.0.0 <sup>67</sup>, readxl v1.4.2 <sup>68</sup>, and ggplot2 v3.4.2 <sup>69</sup> packages, was used for data processing and visualisation. Mass spectrometric raw data and unprocessed search files are publicly available via the PRIDE repository under the project code PXD042057.

## 2.3. Results

### 2.3.1. Stable denitrifying cultures under alternating oxygen availability

2

Two planktonic denitrifying microbial communities were enriched under alternating anoxic and fully oxic conditions to quantitatively resolve the role of aerobic heterotrophic denitrification, i.e. the co-respiration of nitrogen oxides and oxygen, in mixed communities. A mixture of volatile fatty acids (acetate, propionate, butyrate) served as carbon and energy source, and  $\text{NO}_3^-$  as electron acceptor. All dissolved substrates were continuously provided (Supplementary Table S2.1). The  $\text{O}_2$  supply was controlled to ensure a 1:2 ratio of anoxic to oxic time, split in 4 ( $\text{R}_4$ ) and 32 ( $\text{R}_{32}$ ) cycles per day. Fully anoxic conditions were ensured by continuous  $\text{N}_2$  sparging. In the oxic phase, dissolved oxygen was maintained above 6.5 mg/L (>75% air saturation), and both  $\text{NO}_3^-$  and  $\text{O}_2$  served as electron acceptors. Continuous supply of allylthiourea (ATU) ensured complete suppression of nitrification, as confirmed by the absence of ammonium oxidation activity (day 61, Supplementary Figure S2.10) and nitrification genes in the recovered metagenomes (Figure 2.3).

After a start-up period of 20 days, the reactors were run for 76 days (equivalent to 38 volume changes) under carbon-limiting conditions with a dilution rate of  $0.02 \text{ h}^{-1}$ . The operational steady-state was reached after day 37, as confirmed by constant overall substrates and products conversion rates (Figure 2.1, panels A-B). These overall rates represent the weighted average of the aerobic and anaerobic rates within one cycle (eq. 2.2). For consistency, an “overall” consumption rate was also calculated for  $\text{O}_2$ , by averaging its aerobic consumption over the entire cycle duration (Supplementary Section 2.5.2). The overall  $\text{NH}_4^+$ ,  $\text{CO}_2$ , organic carbon, and biomass conversion rates (Supplementary Table S2.1), as well as the resulting stoichiometric yields (Table 2.1), were comparable between the two reactors. The enrichments differed only in terms of the overall  $\text{NO}_3^-$  ( $Y_{\text{NO}_3/\text{s}}$ ) and  $\text{O}_2$  ( $Y_{\text{O}_2/\text{s}}$ ) yields (Table 2.1). Over the combined oxic and anoxic periods,  $56 \pm 4\%$  and  $39 \pm 4\%$  of the total catabolic electron flow was used for  $\text{NO}_3^-$  reduction in  $\text{R}_4$  and  $\text{R}_{32}$  respectively, with the remaining being used for  $\text{O}_2$  reduction (Supplementary Table S2.3).  $\text{NO}$  accumulation was absent and  $\text{NO}_2^-$  accumulation was negligible ( $4 \pm 6\%$  and  $2 \pm 3\%$  of the total consumed  $\text{NO}_3^-$  for  $\text{R}_4$  and  $\text{R}_{32}$  respectively, Supplementary Tables S2.1-2.2) during the entire steady-state period. The carbon and electrons balances closed, further confirming that all involved substrates and products were measured, and supporting  $\text{N}_2\text{O}$  and  $\text{N}_2$  as the primary products of  $\text{NO}_3^-$  reduction (Table 2.1).

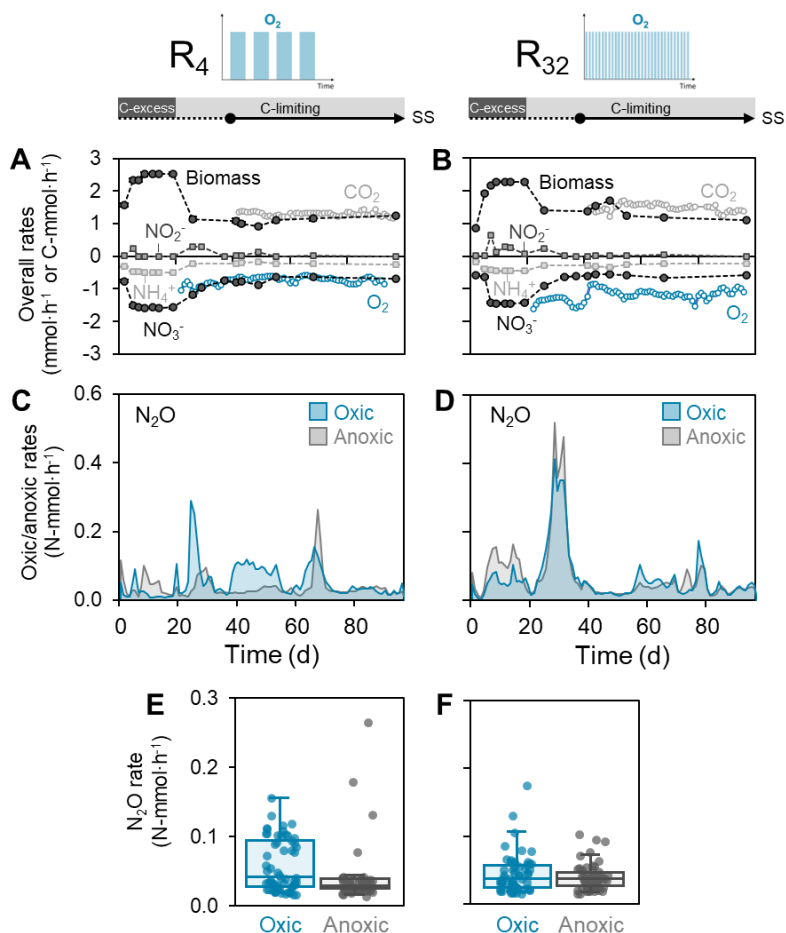


**Figure 2.1. Conversion rates (mmol·h<sup>-1</sup>) in the low- ( $R_4$ ) and high-frequency ( $R_{32}$ ) oxic/anoxic cycling reactors over the entire operational period.** Prior to the target carbon limiting conditions, the reactors were started up for 20 days under carbon excess. The steady-state (SS), was reached on day 37 and maintained for over two months (equivalent to 30 generation times). Negative rates represent consumption whereas positive rates represent production. Panels A and B: overall (i.e. combined aerobic and anaerobic)  $NO_3^-$ ,  $NH_4^+$ , and  $O_2$  consumption, and  $NO_2^-$ ,  $CO_2$ , and biomass production rates (in mmol·h<sup>-1</sup> or C·mmol·h<sup>-1</sup> for the carbon compounds). The latter was calculated from the  $NH_4^+$  consumption rate. For consistency, an “overall”  $O_2$  consumption rate was calculated by averaging its aerobic consumption over the entire cycle duration. Error bars of all rates are smaller than the symbols and represent the standard deviation of triplicate samples (nitrogen substrates) or of daily averages of continuous measurements ( $CO_2$  and  $O_2$ ). Panels C and D: Daily average  $N_2O$  production rates (N·mmol/h) during the oxic and anoxic phases. Panels E and F: boxplots summarising the daily  $N_2O$  emission rates (N·mmol/h) in both phases during the steady-state period.



**Table 2.1. Average overall steady-state stoichiometric yields, and carbon and electron balances in the low- (R<sub>4</sub>) and high-frequency (R<sub>32</sub>) reactors.** The yields were calculated using the overall consumption and production rates (i.e. weighted average of the aerobic and anaerobic rates, eq. 2.2). X and S represent biomass and organic substrate, respectively. The standard deviations were calculated from the standard deviation of the consumption and production rates (Supplementary Table S2.1) using linear error propagation (Supplementary eq. S2.3).

Reactor	Y <sub>N<sub>2</sub>O/N<sub>O3</sub>-</sub> (Nmol/Nmol)	Y <sub>X/S</sub> (Cmol/Cmol)	Y <sub>N<sub>O3</sub>-/S</sub> (Nmol/Cmol)	Y <sub>O<sub>2</sub>/S</sub> <sup>a</sup> (mol/Cmol)	Y <sub>CO<sub>2</sub>/S</sub> (Cmol/Cmol)	C bal (%)	e <sup>-</sup> bal (%)
R <sub>4</sub>	0.07 ± 0.04	0.44 ± 0.04	0.30 ± 0.04	0.29 ± 0.03	0.53 ± 0.03	103 ± 5	101 ± 8
R <sub>32</sub>	0.07 ± 0.04	0.46 ± 0.06	0.20 ± 0.01	0.40 ± 0.05	0.51 ± 0.05	103 ± 8	100 ± 8

<sup>a</sup> For consistency, the O<sub>2</sub> respiration yield was calculated using the “overall” (i.e. combined aerobic and anaerobic) instead of the aerobic rates.

### 2.3.2. Comparable average oxic and anoxic N<sub>2</sub>O production rates

N<sub>2</sub>O emission by the enrichments was measured throughout the oxic and anoxic phases to assess the ecological significance of denitrification in aerobic N<sub>2</sub>O formation. The aerobic and anaerobic N<sub>2</sub>O production rates remained highly variable throughout the entire operation (Figure 2.1, panels C-D, with standard deviations in Supplementary Figure S2.1), despite both systems being at operational steady-state (after day 37), defined by constant conversion rates of the other metabolites. The daily average N<sub>2</sub>O emission rates fluctuated between 0.02 and 0.16 N-mmol·h<sup>-1</sup> in the two systems. The average N<sub>2</sub>O production rate in R<sub>4</sub> was higher in the oxic than in the anoxic phase (0.057±0.037 vs. 0.037±0.039 N-mmol/h), whereas these were nearly identical in R<sub>32</sub> (0.042±0.029 vs. 0.038±0.019 N-mmol/h) (Figure 2.1, panels E-F). Throughout the oxic/anoxic cycles, oxic N<sub>2</sub>O accumulation was higher or, at most, equal to the accumulation during anoxia (Figure 2.2).

The high aerobic N<sub>2</sub>O production implies that denitrification was active at fully oxic conditions (> 6.5 mg O<sub>2</sub>/L). The aerobic and anaerobic NO<sub>3</sub><sup>-</sup> consumption rates were estimated based on the aerobic and anaerobic organic substrate and oxygen consumption, CO<sub>2</sub> production and N<sub>2</sub>O accumulation rates, and the electron balances in each phase (Supplementary Section 2.5.2). The estimated aerobic NO<sub>3</sub><sup>-</sup> consumption rates were only 2.4- and 7.7-fold lower than the anaerobic rates in R<sub>4</sub> and R<sub>32</sub>, respectively. This is equivalent to 36±7% and 11±11% of the total aerobic electron flow in each reactor. These values were validated with direct calculations from measured concentration profiles throughout each phase (Supplementary Figures S2.8-2.9). The fraction of NO<sub>3</sub><sup>-</sup> emitted as N<sub>2</sub>O during aeration was estimated to be 12±8% (R<sub>4</sub>) and 24±29% (R<sub>32</sub>).

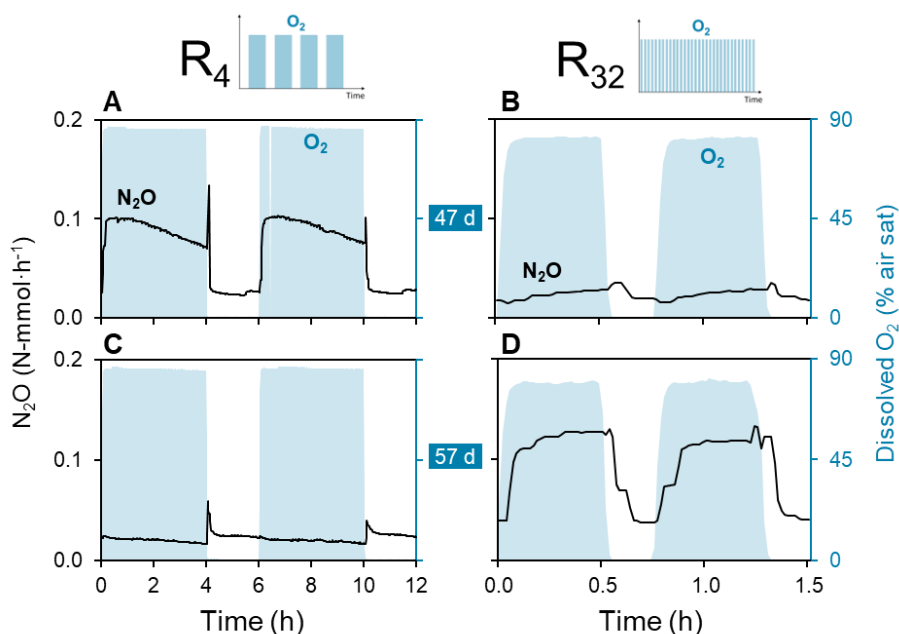


**Figure 2.2. Representative  $\text{N}_2\text{O}$  profiles during oxidic/anoxic periods at steady-state after 47 and 57 days of operation.** Left axes:  $\text{N}_2\text{O}$  accumulation rates in  $\text{N-mmol}\cdot\text{h}^{-1}$  (black lines). Right axes: dissolved oxygen concentrations (shaded area). (A,C) Low-frequency reactor ( $\text{R}_4$ ). (B,D) High-frequency reactor ( $\text{R}_{32}$ ).

### 2.3.3. Denitrifiers-enriched microbial communities

A metagenomic analysis of the enrichments identified the taxonomy and metabolic potential of microbial community members. Long-read sequencing of the whole community DNA (day 68) yielded over 2 and 0.5 million reads with N50 of 5.9 and 6.2 kb for  $\text{R}_4$  and  $\text{R}_{32}$ , respectively, after quality filtering and trimming. Reads assembly resulted in 2747 and 2002 contigs with N50 of 151 and 240 kb. After binning, we recovered a total of 21 ( $\text{R}_4$ ) and 18 ( $\text{R}_{32}$ ) high-quality metagenome-assembled genomes (MAGs) with over 90% completeness and under 5% contamination (Supplementary Tables S2.7-2.8). The top 10 most abundant high-quality MAGs accounted for 78% ( $\text{R}_4$ ) and 57% ( $\text{R}_{32}$ ) of the mapped reads normalised to the corresponding MAG length (Figure 2.3). We considered only the 10 most abundant high-quality MAGs for further analysis (Figure 2.3), and grouped all low-abundant high-quality and all medium-quality MAGs (< 90% completeness and > 5% contamination) into “others” (Supplementary Tables S2.7-2.8 and Figures S2.11-2.18). Low-quality bins (<70% completeness or >10% contamination) were grouped with the unbinned fraction, accounting for 18% ( $\text{R}_4$ ) and 26% ( $\text{R}_{32}$ ) of the community. MAG-based taxonomic analysis revealed two distinct communities, both dominated by the *Proteobacteria* phylum (Supplementary Tables S2.7-2.8).  $\text{R}_4$  was co-dominated by members of the

*Denitromonas* (Gammaproteobacteria) and *Wagnerdoeblera* (Alphaproteobacteria) genera (Figure 2.3). In R<sub>32</sub>, the two most abundant MAGs belonged to the *Castellaniella* genus (Gammaproteobacteria).

All high-quality MAGs contained at least one gene of the denitrification pathway, and full denitrifiers (with genes encoding for all denitrifications steps) dominated the community in R<sub>32</sub> (Figure 2.3 and Supplementary Section 2.5.5). The membrane-bound NO<sub>3</sub><sup>-</sup> reductase gene (*narGHI*) was annotated in most MAGs, whereas only a few also possessed the periplasmic reductase gene (*napAB*). Most MAGs had either a Cu-type (*nirK*) or *cd1*-type (*nirS*) NO<sub>2</sub><sup>-</sup> reductase gene, with some possessing both. Overall, the cytochrome c-dependent nitric oxide reductase genes (*norBC*) were more frequent than the quinol-dependent reductase genes (*norZ*). *norZ* in members of the *Castellaniella* genus were always accompanied with an additional *norB* gene. The N<sub>2</sub>O reductase gene (*nosZ*) was widespread in both reactors, and was dominated by the clade I type. No subunits of the ammonia monooxygenase (*amoABC*) and hydroxylamine oxidoreductase (*hao*) genes were found. Also, the *nrfAH* genes, catalysing the dissimilatory reduction of NO<sub>2</sub><sup>-</sup> to NH<sub>4</sub><sup>+</sup>, were essentially absent in the MAGs (Supplementary Section 2.5.5). All denitrifying MAGs also contained the genes encoding the O<sub>2</sub>-reducing terminal oxidases (complex IV) (Supplementary Section 2.5.5), and enzymes protecting against reactive oxygen species (ROS), including superoxide dismutases (SOD) and catalases/peroxidases (Figure 2.3).

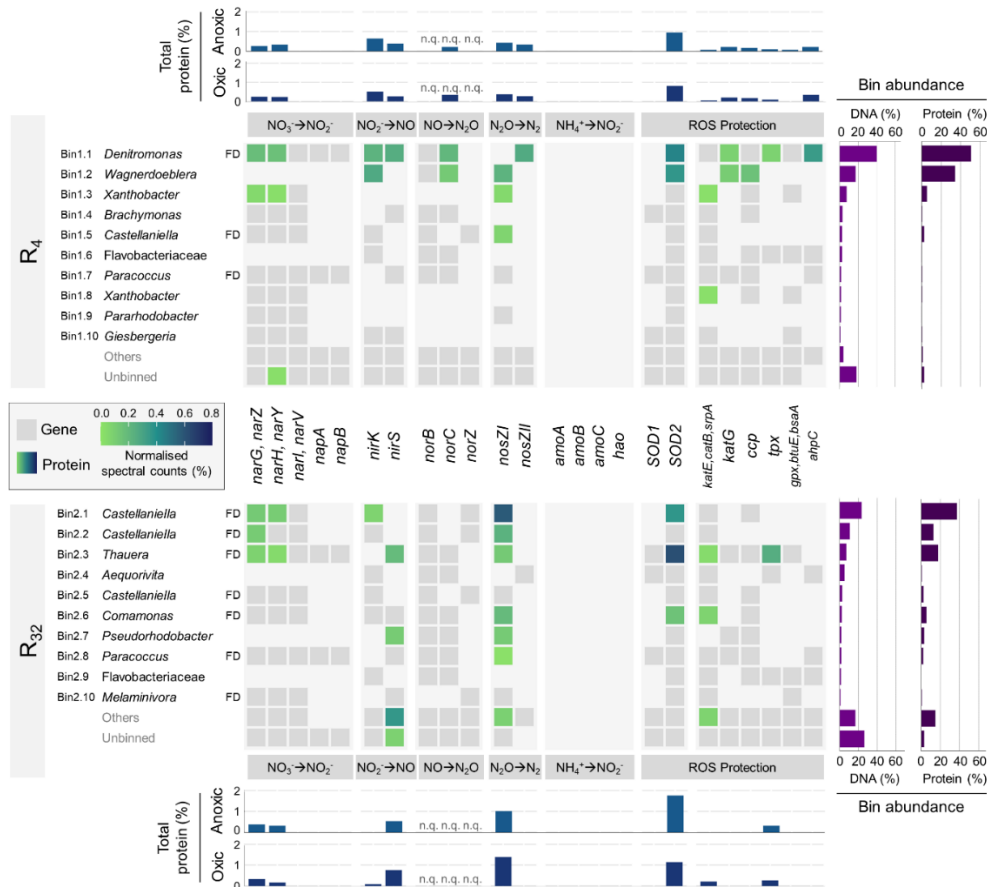


**Figure 2.3. Genomic and proteomic profiles of the top 10 most abundant high-quality MAGs in both enrichments.** Gene presence and protein expression in high-quality MAGs (completeness > 90% and contamination < 5%) in the low- ( $R_4$ ) and high-frequency ( $R_{32}$ ) reactors (top panel –  $R_4$  – and lower panel –  $R_{32}$ ), with their respective taxonomic classification at genus (or family if unclassified genus) level. Full denitrifying organisms, with genes encoding for all denitrification steps, are highlighted (FD). Low-abundant high-quality and all medium-quality MAGs (< 90% completeness and > 5% contamination) were grouped into “others” and low-quality bins (< 70% completeness and > 10% contamination) were grouped with the unbinned fraction. The presence of genes (grey tiles) and the abundance of their corresponding protein under oxic conditions (coloured tiles) are represented for denitrification ( $\text{NO}_3^- \rightarrow \text{N}_2$ ), nitrification ( $\text{NH}_4^+ \rightarrow \text{NO}_2^-$ ), and protection against reactive oxygen species (ROS). The abundance of each protein was determined from peptide spectral sequence counts. Right bar charts: total relative abundance of each MAG in the metagenome (based on relative reads alignment normalised to the corresponding MAG length) and the metaproteome (summed relative abundance of normalised spectral counts of peptides matching to predicted proteins in each MAG). Top/bottom bar charts: total relative abundance of each protein in the oxic and anoxic phases (summed relative abundance of normalised spectral counts); not quantifiable (n.q.): the used methods are not optimised for membrane proteins such as the nitric oxide reductase.

### 2.3.4. Highly comparable anoxic and oxic proteomic profiles

Shotgun metaproteomics of the steady-state enrichments (day 68) revealed the oxic and anoxic presence of key denitrification and ROS-protecting enzymes by each MAG (Figure 2.3 and Supplementary Section 2.5.5). Over 70% (R<sub>4</sub>) and 50% (R<sub>32</sub>) of the detected total peptide intensity (peak area) uniquely matched with proteins predicted from the respective metagenomes. A total of 750/849 and 724/576 proteins of R<sub>4</sub> and R<sub>32</sub> (oxic/anoxic) were identified by at least two unique peptides. The protein-based relative abundance of most MAGs was consistent with their genome-based abundance (Figure 2.3, right bar charts). The contribution to the overall proteome of the unbinned and others fraction combined, accounting for 22% and 43% of the metagenomes, was only 4% and 23% for R<sub>4</sub> and R<sub>32</sub>, respectively.

The overall and MAG-specific relative abundances of the detected denitrification enzymes was highly comparable between the oxic and anoxic phase in each enrichment (Figure 2.3 and Supplementary Section 2.5.5). The catalytic subunits of the membrane-bound NO<sub>3</sub><sup>-</sup> reductase (NarG), Cu-type (NirK) or *cd1*-type (NirS) NO<sub>2</sub><sup>-</sup> reductase, and N<sub>2</sub>O reductase (NosZ) were consistently present. NosZ I and NosZ II were both expressed in R<sub>4</sub>, but only NosZ I was detected in R<sub>32</sub>. In R<sub>4</sub>, the two most abundant MAGs (bin1.1 and bin1.2) accounted for most of the expressed denitrification proteins. On the contrary, in R<sub>32</sub>, lower abundant MAGs significantly contributed to the expression of NirS and NosZ. Moreover, NirS was the dominant type of NO<sub>2</sub><sup>-</sup> reductase detected in R<sub>32</sub>. The periplasmic NO<sub>3</sub><sup>-</sup> reductase (NapAB) was not detected in either of the communities (Figure 2.3). With respect to oxygen, the abundance of the superoxide dismutase SOD2 and different catalases and peroxidases were detected primarily in the dominant MAGs (Figure 2.3). The used protocol was not optimised for membrane-bound proteins, such as the cytochrome c- (cNor) and quinol-dependent (qNor) NO reductases, and the membrane-bound O<sub>2</sub>-reducing terminal oxidases (Cta, Cco, Cyo, Cyd) (Supplementary Section 2.5.5).

## 2.4. Discussion

Two planktonic, nitrification-inhibited denitrifying communities co-respiring O<sub>2</sub> and nitrogen oxides were enriched under alternating oxic/anoxic conditions at frequencies representative of both natural (e.g. coastal sediments<sup>20</sup>) and engineered (e.g. wastewater treatment, Supplementary Section 2.5.6) ecosystems. Significant denitrification occurred at high oxygen concentrations, with almost 40% of the electrons from organic carbon being respired with NO<sub>3</sub><sup>-</sup> in the reactor with longer oxic/anoxic periods (R<sub>4</sub>). The high aerobic NO<sub>3</sub><sup>-</sup> reduction rates in this reactor - only half of the anaerobic rates - suggest the enrichment of a more O<sub>2</sub>-tolerant denitrifying

community than under more frequent oxic/anoxic transitions (R<sub>32</sub>). Typically, the co-respiration of nitrogen oxides and oxygen is characterized in monocultures under continuous aeration, resulting in relatively low reported rates (as previously reviewed<sup>10</sup>). Only one study<sup>21</sup> emphasised the significance of alternating oxic/anoxic conditions for enhanced aerobic denitrification. However, most studies are based on a limited number of isolates, making their extrapolation to complex communities challenging. Few works quantified the contribution of aerobic heterotrophic denitrification in natural ecosystems with fluctuating oxic/anoxic conditions, namely aggregate-forming extracted soil bacteria<sup>25</sup>, sea sediments<sup>24</sup>, and coastal sediments<sup>20</sup>, yet at usually lower oxygen concentrations. The study with coastal sediments<sup>20</sup> reported peaks of aerobic NO<sub>3</sub><sup>-</sup> reduction rates up to 60% of the anaerobic rates at alternating oxic/anoxic conditions above 3 mg O<sub>2</sub>/L. However, only up to 5% of the electrons were respired via denitrification during aeration<sup>20</sup>, and anoxic niches could not be completely ruled out in any of the abovementioned studies. Instead, microscopy confirmed that our cultures were planktonic (Supplementary Figure S2.4) and the aeration overcapacity was 7.5-fold the actual respiration rates, so we can confidently exclude anoxic micro-niches to have significantly contributed to the overall rate. Besides, to maintain the high aerobic NO<sub>3</sub><sup>-</sup> conversion rate measured in R<sub>4</sub>, at least 40% of the active biomass would have had to be in anoxic micro-niches, which would have been unequivocally visible. Overall, we quantitatively show that aerobic denitrification is ecologically relevant in microbial communities exposed to O<sub>2</sub> fluctuations. Furthermore, we estimated that on average 12% (R<sub>4</sub>) and 24% (R<sub>32</sub>) of NO<sub>3</sub><sup>-</sup> was emitted as N<sub>2</sub>O during aeration, highlighting that heterotrophic denitrification also holds the potential to be a major contributor to aerobic N<sub>2</sub>O emissions.

The oxic and anoxic proteomic profiles were nearly identical within each enrichment. The three most abundant MAGs in R<sub>4</sub> and R<sub>32</sub> accounted for 90% and 68% of the respective proteomes, proving their prominent functional role. All denitrification enzymes remained present and, at least partially, active under oxic conditions. In contrast, in continuous monocultures, most denitrifying proteins are generally detected exclusively in anaerobically grown cells, and their abundance and activity is negligible under solely oxic conditions<sup>7,70,71</sup>. Traditionally, oxygen is believed to suppress the transcription of denitrifying genes<sup>7,9,72</sup>, even if denitrification transcripts have also been detected during aeration (for example, *narG* and *nosZ* at 100 μM O<sub>2</sub><sup>8</sup>; *narG*, *norB*, and *nosZ* at 235 μM O<sub>2</sub><sup>72,73</sup>). Besides, prolonged exposure to alternating conditions has been hypothesised to reduce the direct impact of O<sub>2</sub><sup>18,20,21,25</sup>. We worked at oxic/anoxic transition frequencies significantly higher than the imposed growth rates, i.e. the O<sub>2</sub> cycling was faster than protein turnover. Consequently, denitrifying enzymes synthesised in the anoxic period most likely persisted and

remained active in the oxic phase, masking the influence of any potential oxygen-mediated transcriptional regulation on protein abundances. Yet, it would be of interest to determine the protein regulation mechanisms of denitrifying organisms under highly dynamic oxygen conditions. From an ecological perspective, open culture cultivation as applied here selects, by design, for the organisms that are the fittest for the imposed conditions <sup>74</sup>. Therefore, we postulate that organisms capable of maintaining a significant denitrification activity in the presence of oxygen can outcompete (i.e. have a competitive advantage over) other heterotrophs in environments with fluctuating oxygen availabilities. In analogy, relevant aerobic residual denitrification potentials are to be expected in environments with rapid O<sub>2</sub> fluctuations, such as sediments <sup>20</sup> and wastewater treatment plants (Supplementary Section 2.5.6).

The lower aerobic denitrification rates, compared to the anaerobic ones, can thus reasonably be ascribed to reversible enzyme inhibition or electron competition with O<sub>2</sub>, rather than to transcriptional or translational regulation <sup>8,10,75</sup>. The O<sub>2</sub> impact differed for each denitrification step, in line with previous observations <sup>7,76</sup>. Even though NO<sub>2</sub><sup>-</sup> and NO were hardly detected, N<sub>2</sub>O consistently accumulated, possibly as a result of the often reported higher relative oxygen sensitivity of NosZ <sup>25,76,77</sup>. The marked N<sub>2</sub>O accumulation at the onset of anoxia implies a slower post-aerobiosis recovery of Nos compared to the other reductases. The progressive N<sub>2</sub>O accumulation under full aeration suggests a gradual yet incomplete inhibition of N<sub>2</sub>O reduction, as previously observed <sup>8</sup>. In fact, we estimated that 80-90% of the produced N<sub>2</sub>O was still reduced during aeration. Based on such a high N<sub>2</sub>O consumption, one may argue that heterotrophic denitrification could function as a sink for nitrifier-produced N<sub>2</sub>O during intermittent oxic conditions. However, N<sub>2</sub>O did accumulate, indicating higher production than consumption rates, and suggesting that aerobic denitrification likely acts as a net N<sub>2</sub>O source rather than a sink in dynamic O<sub>2</sub> environments. Unexpectedly, N<sub>2</sub>O accumulation fluctuated throughout the operational steady-state of both reactors despite the consistency of all other conversion rates. N<sub>2</sub>O accumulation results from the unbalance between its production and consumption rates. Minor variations in the latter two lead to significant fluctuations in the comparably lower net N<sub>2</sub>O accumulation. Such fluctuations may result from stochastic micro-oscillations in microbial composition, as documented in functionally redundant communities <sup>78-80</sup>. Taken together, these results highlight the need for more research on the impact of variable O<sub>2</sub> availability on denitrification and, from a physiological perspective, further support the long-term competitive advantage of metabolic preparedness in dynamic environments.

Contrary to the long-standing assumption that the periplasmic reductase Nap is required for aerobic nitrate respiration<sup>20,21,23,25,81</sup>, only the membrane-bound Nar was detected in our metaproteomes. Although preferential extraction or sequencing, and biases towards more abundant species can impact protein recovery<sup>82</sup>, both Nap subunits are soluble<sup>83</sup> and are usually detected with equivalent protocols (e.g. in *Paracoccus denitrificans*<sup>71</sup>). Also, the *napAB* genes were found in the most abundant MAGs, e.g. bin1.1 accounting for 50% of the proteome in R<sub>4</sub>. Therefore, although the presence of Nap at very low abundance cannot be completely ruled out, NO<sub>3</sub><sup>-</sup> reduction in our cultures was evidently driven by Nar and thus contributed directly to proton translocation under oxic conditions. Studies on pure cultures of *Paracoccus pantotrophus* and *P. denitrificans* reported Nar and Nap to be preferentially expressed under continuous anoxic or oxic conditions, respectively<sup>71,81,84</sup>. The excess NO<sub>3</sub><sup>-</sup> in our cultures may have alleviated the potential oxygen inhibition of NO<sub>3</sub><sup>-</sup> uptake<sup>85,86</sup>, favouring the lower-affinity Nar over Nap<sup>87</sup>. However, high levels of *nap* transcription and Nap activity were measured in *P. pantotrophus* grown in oxic NO<sub>3</sub><sup>-</sup>-excess chemostats<sup>88</sup>, suggesting that factors other than NO<sub>3</sub><sup>-</sup> affinity determined the preferential Nar expression in our enrichments. Overall, the here observed consistent and exclusive expression of Nar suggests a higher versatility under alternating oxic/anoxic conditions, and challenges the use of *nap* as specific marker gene for aerobic heterotrophic denitrification<sup>19,20</sup>.

The subsequent nitrogen oxides reduction steps featured different degrees of labour-division among the MAGs in the two enrichments. Both nitrite reductases (NirK and NirS), and both clade I and II N<sub>2</sub>O reductases (NosZ) were primarily expressed by the dominant MAGs in R<sub>4</sub>. Conversely, the proteomic profile of R<sub>32</sub> revealed a more prominent role of lower abundant MAGs in NO<sub>2</sub><sup>-</sup> and N<sub>2</sub>O reduction. Also, despite the widespread presence of the *nirK* gene in R<sub>32</sub>, mainly NirS was expressed. The preferential expression of NirK in R<sub>4</sub> and NirS in R<sub>32</sub> may account for the conflicting accumulation of nitrite in the anoxic (R<sub>4</sub>) and oxic (R<sub>32</sub>) phases (Figure S2.8). Although O<sub>2</sub>-driven preferential expression and activity of either NirK or NirS is plausible, conflicting O<sub>2</sub>-sensitivities have been reported<sup>76</sup>, warranting further research on the determinants of functional homologues preferences. The expression of NirK and NirS by several MAGs without nitrate reductase may explain the low nitrite accumulation in both cultures. In line with previous proteomic studies<sup>71,89</sup>, the detection of the membrane-bound hydrophobic qNor and cNor, intrinsically challenging to detect in proteomic analyses, was negligible. The *nosZ I* was annotated in most MAGs, with many expressing the encoded NosZ I. In turn, NosZ II was exclusively detected in R<sub>4</sub>. It is here tempting to speculate that the higher aerobic denitrification rates in R<sub>4</sub> related to the reported lower O<sub>2</sub> inhibition of clade II NosZ<sup>73</sup>. However, these observations were limited to one *nosZ II*-harbouring *Azospira* strain and no evident clade-dependent



differences in O<sub>2</sub>-tolerance were observed in a more recent study <sup>90</sup>. Furthermore, different physiological mechanisms such as strain-specific ability to scavenge O<sub>2</sub> may impact the O<sub>2</sub>-tolerance of N<sub>2</sub>O-reducers <sup>90</sup>.

In conclusion, beyond decades of research based on pure cultures, we show that organisms capable of co-respiring nitrogen oxides and oxygen have a competitive advantage in complex ecosystems exposed to time-varying oxygen availabilities. We posit that the aerobic denitrification rates, comparable to the anaerobic ones, likely resulted from the activity of anaerobically produced enzymes, as the imposed oxic/anoxic frequencies exceeded the organisms growth rate, a scenario often observed in natural and engineered microbiomes. Our findings also suggest that heterotrophic denitrification may be an important aerobic N<sub>2</sub>O source alongside nitrification in O<sub>2</sub> fluctuating environments.

## 2.5. Supplementary information

### 2

#### 2.5.1. Reactor operation

**Table S2.1. Measured average substrate loading and steady-state conversion rates of the low- ( $R_4$ ) and high-frequency ( $R_{32}$ ) reactors.** Overall rates refer to rates estimated over the total duration of an oxic/anoxic cycle, and considers the average of three effluent concentrations (beginning and end of oxic phase, and end of anoxic one). Only for the gaseous compounds ( $\text{CO}_2$  and  $\text{N}_2\text{O}$ ) individual rates for each phase (oxic and anoxic) were measured on top of the overall rates.  $\text{O}_2$  was only added and consumed in the oxic phase, yet an “overall” rate was also calculated by averaging the aerobic  $\text{O}_2$  consumption over the entire cycle duration (eq. S2.9) for further balancing purposes.

Compound	Phase	Units	Loading		Conversion	
			$R_4$	$R_{32}$	$R_4$	$R_{32}$
$\text{CO}_2$	Oxic	C-mmol/h	-	-	$1.37 \pm 0.07$	$1.5 \pm 0.1$
	Anoxic	C-mmol/h	-	-	$1.15 \pm 0.08$	$1.4 \pm 0.1$
	Overall	C-mmol/h	-	-	$1.30 \pm 0.06$	$1.5 \pm 0.1$
$\text{N}_2\text{O}$	Oxic	N-mmol/h	-	-	$0.06 \pm 0.04$	$0.04 \pm 0.03$
	Anoxic	N-mmol/h	-	-	$0.04 \pm 0.04$	$0.04 \pm 0.02$
	Overall	N-mmol/h	-	-	$0.05 \pm 0.03$	$0.04 \pm 0.03$
$\text{NO}_3^-$	Overall	N-mmol/h	$0.96 \pm 0.02$	$0.91 \pm 0.02$	$-0.73 \pm 0.08$	$-0.60 \pm 0.04$
$\text{NO}_2^-$	Overall	N-mmol/h	-	-	$0.03 \pm 0.05$	$0.01 \pm 0.02$
$\text{NH}_4^+$	Overall	N-mmol/h	$0.49 \pm 0.02$	$0.47 \pm 0.01$	$-0.22 \pm 0.02$	$-0.27 \pm 0.04$
$\text{O}_2$	Oxic	mmol/h	210	210	$-1.0 \pm 0.1$	$-1.6 \pm 0.2$
	“Overall”	mmol/h	141	149	$-0.70 \pm 0.07$	$-1.2 \pm 0.2$
Biomass <sup>a</sup>	Overall	C-mmol/h	-	-	$1.08 \pm 0.09$	$1.4 \pm 0.2$
Acetate <sup>b</sup>	Overall	C-mmol/h	$0.85 \pm 0.02$	$1.02 \pm 0.01$	$-0.85 \pm 0.02$	$-1.02 \pm 0.01$
Propionate <sup>b</sup>	Overall	C-mmol/h	$0.91 \pm 0.02$	$1.09 \pm 0.01$	$-0.91 \pm 0.02$	$-1.09 \pm 0.01$
Butyrate <sup>b</sup>	Overall	C-mmol/h	$0.68 \pm 0.02$	$0.82 \pm 0.01$	$-0.69 \pm 0.02$	$-0.83 \pm 0.01$

<sup>a</sup> Calculated from the  $\text{NH}_4^+$  consumption rates.

<sup>b</sup> Always 0 in the effluent.

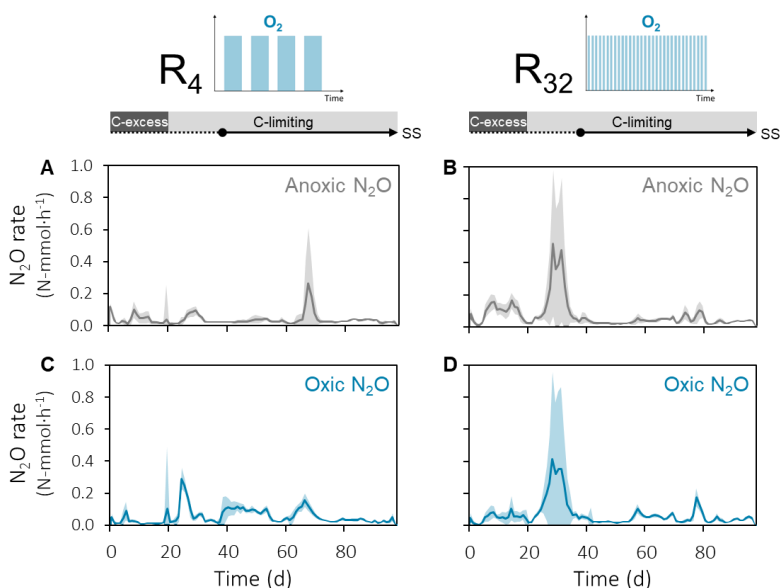


**Figure S2.1.** Daily average anoxic (top, grey) and oxic (bottom, blue) N<sub>2</sub>O production rates in the low- ( $R_4$ ) and high-frequency ( $R_{32}$ ) reactors. The shaded areas are the standard deviation of the daily averages, representing the fluctuation of N<sub>2</sub>O rates within each day.

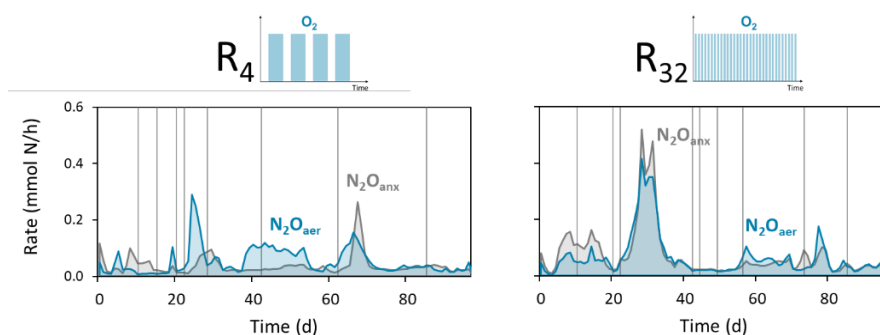


**Figure S2.2.** Headspace wall-growth cleaning events (vertical lines) did not affect the profile of the oxic (blue) and anoxic (grey) N<sub>2</sub>O emissions in the low- ( $R_4$ ) and high-frequency ( $R_{32}$ ) reactors.

**Table S2.2.** Nitrite concentrations throughout the steady-state period.

$R_4$		$R_{32}$	
Day	NO <sub>2</sub> <sup>-</sup> (mM)	Day	NO <sub>2</sub> <sup>-</sup> (mM)
37	0.3 ± 0.3	37	0.0004 ± 0.0009
41	0.6 ± 0.4	41	0.02 ± 0.02
43	0.8 ± 0.3	44	0.04 ± 0.01
49	8.0 ± 0.2	49	0.05 ± 0.02
55	0.2 ± 0.2	55	0.83 ± 0.01
68	0.2 ± 0.3	68	2.85 ± 0.06

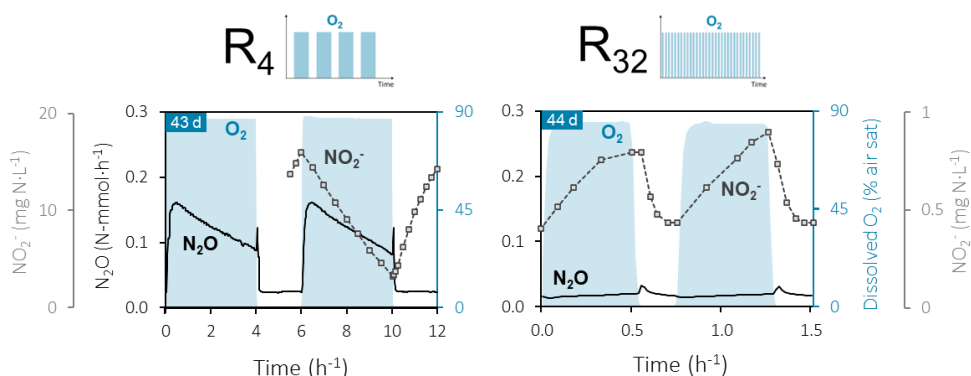


**Figure S2.3. Concentration profiles during one or two oxic/anoxic cycles after 43 ( $R_4$ ) or 44 ( $R_{32}$ ) days of operation.** The nitrite (symbols) and dissolved oxygen concentrations (blue area), as well as the  $N_2O$  production rate measured every minute (black line) are represented. In this case, nitrite accumulated in the anoxic phase in  $R_4$  and in the oxic phase in  $R_{32}$ .

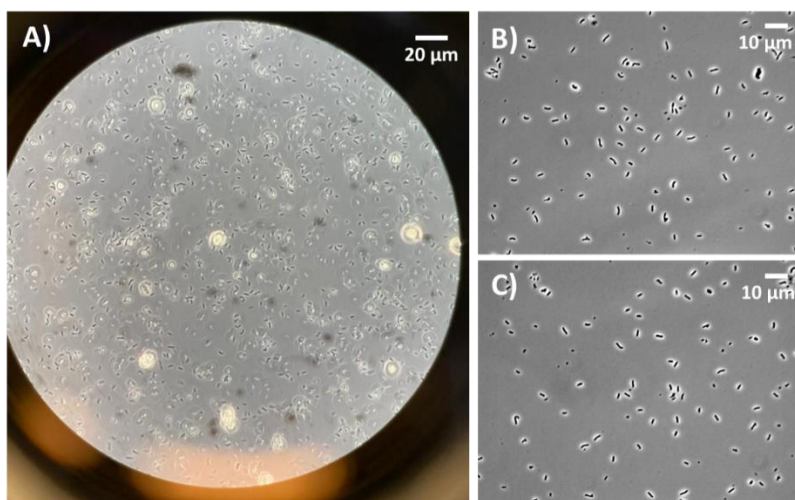


**Figure S2.4. Microscopic pictures of the broth of  $R_4$ .** (A) Undiluted culture after 35 days of operation, 400x amplified. (B, C) 8-fold diluted culture after 55 days of operation, 1000x amplified.

**$k_{La}$  determination.** The oxygen volumetric mass transfer coefficient ( $k_{La}$ ) was determined to calculate the oxygen transfer rate in the oxic phase. The  $k_{La}$  of  $R_4$  and  $R_{32}$  were determined under identical conditions as the enrichments (500 rpm stirring, 400 mL/min gas flow), but with water instead of biomass. The  $O_2$  transfer rates were determined by following the dissolved oxygen concentration during the sparging of air (400 mL/min) in anoxic water. The  $k_{La}$  was obtained by fitting the integrated mass transfer equation to the dissolved  $O_2$  concentration profile over time, with  $C_{O_2}^*$  the solubility of  $O_2$  at 20°C:

$$C_{O_2} = C_{O_2}^* \cdot (1 - e^{-k_L a \cdot t}) \quad (\text{eq. S2.1})$$

The obtained  $k_L a$  values were 36.2 (R<sub>4</sub>) and 37.0 h<sup>-1</sup> (R<sub>32</sub>).

2

### 2.5.2. Calculation of consumption and production rates

Consumption and production rates of all dissolved and gaseous compounds were measured or estimated in the oxic and anoxic phases, and overall (combined oxic and anoxic). Consumption rates are negative and production rates are positive.

**Overall consumption and production rates in the liquid.** Consumption and production rates of NO<sub>3</sub><sup>-</sup>, NO<sub>2</sub><sup>-</sup> ( $C_{in} = 0$ ), NH<sub>4</sub><sup>+</sup> and the organic compounds acetate, propionate and butyrate ( $C_{out} = 0$ ) were calculated from a mass balance:

$$R_i (\text{mmol} \cdot \text{h}^{-1}) = F_{i,out} \cdot C_{i,out} - F_{i,in} \cdot C_{i,in} \quad (\text{eq. S2.2})$$

with  $R_i$  the molar rate (mmol·h<sup>-1</sup>),  $F_i$  the influent and effluent flow rates (L·h<sup>-1</sup>), and  $C_i$  the concentration of compound  $i$  (mmol·L<sup>-1</sup>).  $C_{out}$  was the average of three effluent measurements (taken at the beginning and end of the oxic phase, and end of the anoxic phase). The sample for  $C_{in}$  was taken directly at the entry point of the reactors, yet differences with stock feed solution remained negligible throughout the experimental period. The flow rates were the average of the measured flow rates during the entire operation. Linear error propagation was applied to determine the standard deviation in the rates (eq. S2.3), using the standard deviations of  $F_{in}$ ,  $F_{out}$ , and  $C_{out}$  (deviation between the three measurements).

Linear error propagation of a function  $f$  dependent on multiple variables ( $x, y, \dots$ ):

$$f(x, y, \dots): \sigma_f = \sqrt{\left(\frac{\partial f}{\partial x}\right)^2 \cdot \sigma_x^2 + \left(\frac{\partial f}{\partial y}\right)^2 \cdot \sigma_y^2 + \dots} \quad (\text{eq. S2.3})$$

with  $\sigma_f$ ,  $\sigma_x$ , and  $\sigma_y$  the standard deviations of  $f$ ,  $x$ , and  $y$ , respectively, and  $\partial f / \partial x$  and  $\partial f / \partial y$  the partial derivatives of  $f$  with respect to  $x$  and  $y$ , respectively.

**Overall, aerobic, and anaerobic consumption and production rates in the gas phase.** A script was written in RStudio to calculate the overall, and separate aerobic and anaerobic N<sub>2</sub>O and CO<sub>2</sub> rates from continuous measurements recorded every minute. The molar gas flow leaving the reactor was calculated for each time point based on the constant influent volumetric gas flow rate (400 mL·min<sup>-1</sup>) and the measured temperature and atmospheric pressure:

$$N_{\text{gas}}(\text{mmol} \cdot \text{h}^{-1}) = \frac{P_{\text{atm}} \cdot F_{V,\text{gas}}}{R \cdot T} \quad (\text{eq. S2.4})$$

With  $N_{\text{gas}}$  the molar gas flow rate ( $\text{mmol} \cdot \text{h}^{-1}$ ),  $P_{\text{atm}}$  the atmospheric pressure (mbar),  $F_{V,\text{gas}}$  the volumetric gas flow rate,  $R$  the ideal gas constant ( $\text{L} \cdot \text{mbar} \cdot \text{K}^{-1} \cdot \text{mmol}^{-1}$ ), and  $T$  the reactor temperature (K). The molar gas fractions were normalized to the zero measurement before further calculations, by subtracting the corresponding value measured for the zero concentration. For each of the gases, the molar flow rates in the off-gas were calculated at each time point from measured gas fractions and the total molar gas flow rate:

$$N_{\text{CO}_2}(\text{mmol} \cdot \text{h}^{-1}) = y_{\text{CO}_2} \cdot N_{\text{gas}} \quad (\text{eq. S2.5})$$

The  $\text{N}_2\text{O}$  rate was normalized per mole of nitrogen:

$$N_{\text{N}_2\text{O}}(\text{Nmmol} \cdot \text{h}^{-1}) = 2 \cdot y_{\text{N}_2\text{O}} \cdot N_{\text{gas}} \quad (\text{eq. S2.6})$$

with  $N_i$  the molar gas flow rates ( $\text{mmol} \cdot \text{h}^{-1}$ ),  $N_{\text{gas}}$  the molar gas flow rate ( $\text{mmol} \cdot \text{h}^{-1}$ ), and  $y_i$  the molar fractions of each compound in the off-gas. The accumulation rates at every time point were calculated with the following mass balance:

$$R_{\text{CO}_2, \text{N}_2\text{O}}((\text{N})\text{mmol} \cdot \text{h}^{-1}) = N_{i,\text{out}} - N_{i,\text{in}} \quad (\text{eq. S2.7})$$

The average fraction of  $\text{CO}_2$  in the influent air was 450 ppm. The dataset containing the rates at every minute was split in oxic and anoxic periods, with the oxic period defined for time points with  $\text{DO} > 1\%$  ( $0.08 \text{ mg O}_2 \cdot \text{L}^{-1}$ ). Daily average aerobic, anaerobic, and overall rates were calculated with the corresponding dataset. The standard deviation of these averages was taken as the uncertainty in the rates.

**Overall and aerobic consumption and production rates of oxygen.** The  $\text{O}_2$  consumption rates during the oxic phase were calculated from the dissolved oxygen measurements during maximum aeration periods ( $> 20\% \text{ O}_2$  in the off-gas and dissolved oxygen  $> 70\%$ ):

$$R_{\text{O}_2}(\text{mmol} \cdot \text{h}^{-1}) = k_{\text{L}}a \cdot H_{\text{O}_2} \cdot P_{\text{atm}} \cdot y_{\text{O}_2} \cdot (1 - \text{DO}) \cdot V \quad (\text{eq. S2.8})$$

With  $k_{\text{L}}a$  the experimentally measured transfer coefficient ( $\text{h}^{-1}$ ),  $H_{\text{O}_2}$  the Henry coefficient for  $\text{O}_2$  ( $0.001283 \text{ mmol} \cdot \text{L}^{-1} \cdot \text{mbar}^{-1}$ ),  $P_{\text{atm}}$  the atmospheric pressure (mbar),

$y_{O_2}$  the O<sub>2</sub> molar fraction in the off-gas, DO the measured dissolved oxygen, and V the broth volume (L).

The aeration over-capacity in the reactors was determined by comparing the maximum O<sub>2</sub> transfer rate from the gas to the liquid (equivalent to the maximum possible O<sub>2</sub> microbial respiration rate) to the actual O<sub>2</sub> respiration rates. The maximum possible O<sub>2</sub> transfer rates, *i.e.* the maximum microbial respiration capacity, would be achieved when the DO is 0, so eq. S2.8 can be simplified into eq. S2.9. These rates were calculated to be 7.5-fold higher than the actual O<sub>2</sub> respiration rates, reflecting the aeration over-capacity in the reactors.

$$R_{O_2}^{\max} (\text{mmol} \cdot \text{h}^{-1}) = k_L a \cdot H_{O_2} \cdot P_{\text{atm}} \cdot y_{O_2} \cdot V \quad (\text{eq. S2.9})$$

Daily averages were calculated and taken for further calculations. The standard deviation of these averages were taken as the uncertainty of the rates. The “overall” consumption rate of O<sub>2</sub> for further electron balancing purposes over an entire cycle was taken as the weighted average of the aerobic and anaerobic (=0) rates:

$$R_i^{\text{overall}} = \frac{t_{\text{aerobic}}}{24} \cdot R_i^{\text{aerobic}} + \frac{t_{\text{anaerobic}}}{24} \cdot R_i^{\text{anaerobic}} \quad (\text{eq. S2.10})$$

with  $t_{\text{aerobic}}$  and  $t_{\text{anaerobic}}$  (h) the total time in one day in which the dissolved oxygen was above or below 1%, respectively.

**Overall respiratory electron flow to nitrogen oxides and O<sub>2</sub>.** The absolute and relative overall flows of electrons from organic electron donors to the electron acceptors NO<sub>3</sub><sup>-</sup> and O<sub>2</sub> were calculated from the overall rates considering four and five electrons for the conversion of NO<sub>3</sub><sup>-</sup> to N<sub>2</sub>O and N<sub>2</sub>, respectively, and four electrons for the reduction of O<sub>2</sub> to H<sub>2</sub>O (Table S2.3). NO<sub>3</sub><sup>-</sup> and O<sub>2</sub> were the sole electron acceptors and NH<sub>4</sub><sup>+</sup> fully sustained biomass growth (detailed in the following section), minimizing NO<sub>3</sub><sup>-</sup> assimilation. Thus, both substrates account for the entirety of the catabolic electron flow.

**Table S2.3. Absolute (mmol e<sup>-</sup>/h) and relative (%) overall electron flows from organic carbon to the electron acceptors NO<sub>3</sub><sup>-</sup> and O<sub>2</sub> in the low- (R<sub>4</sub>) and high-frequency (R<sub>32</sub>) reactors.** The electron flows were calculated from the NO<sub>3</sub><sup>-</sup> and O<sub>2</sub> consumption and the N<sub>2</sub>O accumulation rates.

Electron flow	e <sup>-</sup>	R <sub>4</sub> (mmol e <sup>-</sup> /h)	R <sub>32</sub> (mmol e <sup>-</sup> /h)
NO <sub>3</sub> <sup>-</sup> → N <sub>2</sub> O	4	0.2 ± 0.1	0.2 ± 0.1
NO <sub>3</sub> <sup>-</sup> → N <sub>2</sub>	5	3.4 ± 0.4	2.8 ± 0.2
O <sub>2</sub> → H <sub>2</sub> O	4	2.8 ± 0.3	4.7 ± 0.6
% NO <sub>3</sub> <sup>-</sup> / Total		56 ± 4%	39 ± 4%
% O <sub>2</sub> / Total		44 ± 4%	61 ± 4%

**Biomass production rates.** The biomass concentration was estimated from  $\text{NH}_4^+$  measurements and carbon balances. In the studied system, ammonia oxidation was fully inhibited via continuous ATU addition, thus the assimilation into biomass (0.2 N-mol/C-mol) was the sole  $\text{NH}_4^+$  consumption process. The biomass production rate was calculated as follows:

$$R_X = |R_{\text{NH}_4^+}/0.2| \quad (\text{eq. S2.11})$$

The carbon balance included only the organic carbon substrates (acetate, propionate, and butyrate),  $\text{CO}_2$  and biomass, as no other products were detected in the HPLC. Therefore, the biomass production rate could also be directly calculated according to the following equation:

$$R_X (\text{Cmmol} \cdot \text{h}^{-1}) = |R_{\text{Ace}} + R_{\text{Pro}} + R_{\text{But}} + R_{\text{CO}_2}| \quad (\text{eq. S2.12})$$

For all calculations, an empirical biomass formula of  $\text{CH}_{1.8}\text{N}_{0.2}\text{O}_{0.6}$  was used. The biomass concentration ( $C_X$  in  $\text{C-mmol} \cdot \text{L}^{-1}$ ) was then estimated from the production rate ( $R_X$ ) and the flow rate ( $F_{\text{out}}$  in  $\text{L} \cdot \text{h}^{-1}$ ):

$$C_X = R_X/F_{\text{out}} \quad (\text{eq. S2.13})$$

Both methods resulted in similar estimations, showing that the biomass concentration and its production rate can be determined through either one of the methods (Figure S2.5). The biomass rates and concentrations based on  $\text{NH}_4^+$  measurements were used for further calculations. Error propagation was applied to determine the standard deviation in the rates, using the standard deviations of  $F_{\text{out}}$ , and  $\text{NH}_4^+$ , organic carbon, and  $\text{CO}_2$  rates.

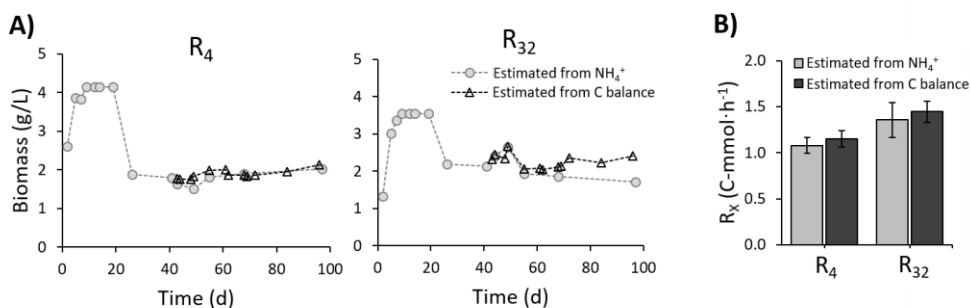


**Figure S2.5. Highly comparable biomass concentrations and production rates in the low- ( $R_4$ ) and high-frequency ( $R_{32}$ ) reactors estimated with two different methods. Panel A: Biomass concentration over time in both the low- and high-frequency reactors, expressed as g/L. Panel B: average biomass**



production rates during the steady-state. The estimated concentrations and rates were determined from the NH<sub>4</sub><sup>+</sup> measurements (light grey) and the carbon balance (dark grey), i.e. the organic substrate and CO<sub>2</sub> measurements.

**Overall carbon, nitrogen, and electron balances.** Mass balances were performed using the consumption and production rates averaged over the steady-state period to ensure that all substrates and products were recovered. The overall carbon balance was calculated from the consumption and production rates of acetate, propionate, butyrate, biomass (estimated from the NH<sub>4</sub><sup>+</sup> rates), and CO<sub>2</sub>:

$$\text{C balance (\%)} = \frac{R_{\text{in}}}{R_{\text{out}}} = \frac{|R_{\text{Ace}} + R_{\text{Pro}} + R_{\text{But}}|}{R_{\text{X}} + R_{\text{CO}_2}} \quad (\text{eq. S2.14})$$

The nitrogen compounds involved in the nitrogen balance would be NH<sub>4</sub><sup>+</sup>, biomass, NO<sub>3</sub><sup>-</sup>, NO<sub>2</sub><sup>-</sup>, NO, N<sub>2</sub>O, and N<sub>2</sub>. All compounds were measured (or estimated, in the case of biomass) except N<sub>2</sub>. NO and NO<sub>2</sub><sup>-</sup> accumulation was absent or negligible throughout the entire experiment, so we could assume that the missing nitrogen was recovered as N<sub>2</sub>, representing full denitrification from NO<sub>3</sub><sup>-</sup>:

$$R_{\text{N}_2} = |R_{\text{NO}_3^-}| - R_{\text{N}_2\text{O}} \quad (\text{eq. S2.15})$$

Based on all calculated and estimated rates, an electron balance was calculated.

$$\text{e}^- \text{ balance (\%)} = \frac{R_{\text{eD}}}{R_{\text{eA}}} = \frac{|4 \cdot R_{\text{Ace}} + 4.7 \cdot R_{\text{Pro}} + 5 \cdot R_{\text{But}}|}{-8 \cdot R_{\text{NO}_3^-} - 4 \cdot R_{\text{N}_2\text{O}} - 3 \cdot R_{\text{N}_2} - 4 \cdot R_{\text{O}_2} + 4.2 \cdot R_{\text{X}}} \quad (\text{eq. S2.16})$$

Uncertainty of the balances were calculated through linear error propagation from the standard deviations of the respective rates (eq. S2.3).

**Table S2.4. Overall carbon, and electron balances over the entire steady-state period of the low- (R<sub>4</sub>) and high-frequency (R<sub>32</sub>) oxic/anoxic cycling denitrifying reactors.**

Reactor	Low-frequency	High-frequency
Carbon balance	103 ± 5%	101 ± 9%
Electrons balance	103 ± 8%	100 ± 8%

**Estimation of the NO<sub>3</sub><sup>-</sup> consumption and production rates in the oxic and anoxic phases.** Separate aerobic and anaerobic rates were calculated for all compounds continuously measured in the gas (N<sub>2</sub>O and CO<sub>2</sub>) or liquid phase (O<sub>2</sub>). In turn, grab samples for the quantification of all other compounds were less sensitive to the small concentration changes occurring during each phase, so consumption and production rates could not be determined directly with high confidence. Instead, aerobic and anaerobic rates were calculated from the overall mass balance and the phase-specific

$\text{N}_2\text{O}$ ,  $\text{CO}_2$ , and  $\text{O}_2$  rates as detailed below. In short, as the overall balances closed (Table S2.4), all biological processes taking place in the controlled environments of the reactor are known. Also, the overall rates are the sum of the aerobic and anaerobic ones weighted by their corresponding time fractions.

The calculation of aerobic and anaerobic conversion rates detailed below were based on carbon, nitrogen, and electron balances, so one needs to know which processes occurred in the reactor broth in each phase. Specifically, from the closed carbon and electron balances (Table S2.4) we know that denitrification occurred, with  $\text{N}_2\text{O}$  and  $\text{N}_2$  as end-products. We do not know, however, which fraction of this conversion occurred in the oxic and anoxic phases. To determine this, three scenarios were considered (Figure S2.6). The rationale underlying these scenarios is briefly explained:

- 1) **Scenario 1** was developed based on past literature. Aerobic denitrification was widely considered to be absent or negligible under fully oxic conditions. Nevertheless, we measured aerobic production of  $\text{N}_2\text{O}$  in our reactors, which means that at least part of the  $\text{NO}_3^-$  was aerobically converted to  $\text{N}_2\text{O}$ . For this scenario, we assumed that this was the only fraction of  $\text{NO}_3^-$  converted aerobically, with the remaining converted under anoxic conditions.
- 2) The aerobic and anaerobic electron balances did not close in **scenario 1**, which means that our assumption was incorrect.
- 3) Based on the electron gaps observed in scenario 1, we developed **scenario 2**. In this case, we rationalized that the missing or surplus of electrons in scenario 1 must belong to a “blind” amount of  $\text{NO}_3^-$  aerobically reduced to  $\text{N}_2$ . In other words, for **scenario 2**, we considered that part of the  $\text{NO}_3^-$  was aerobically converted to  $\text{N}_2\text{O}$  (directly measured, same as scenario 1) and an additional part was converted to  $\text{N}_2$  (estimated).
- 4) The estimations made in **scenario 2** were validated with measurements, so we could confidently estimate the aerobic and anaerobic  $\text{NO}_3^-$  consumption rates.
- 5) Even though scenario 2 seems to accurately describe the microbial conversions in our reactors, we considered the possibility of PHA accumulation in the anoxic phase. **Scenario 3** was developed to evaluate if the potential PHA accumulation would affect the estimated aerobic and anaerobic  $\text{NO}_3^-$  consumption rates in scenario 2. We concluded that even large amounts of PHA accumulation would not affect the estimated rates.

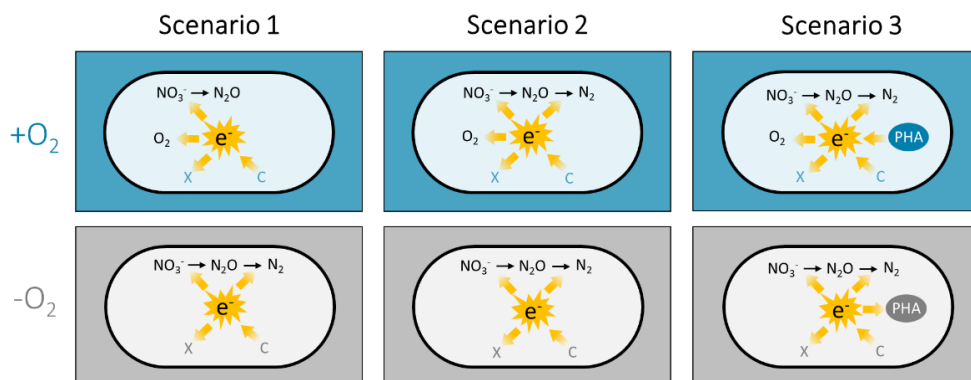


**Figure S2.6. Schematic representation of the three scenarios considered to calculate the aerobic and anaerobic conversion rates of soluble substrates.** The compounds/conversions included in the electron balance in each scenario in the anoxic (grey) and oxic (blue) conditions are represented. All scenarios considered the organic carbon © as electron donor and biomass (X) production as electron sink. Under oxic conditions, all scenarios considered O<sub>2</sub> reduction to H<sub>2</sub>O. Under anoxic conditions, all scenarios considered full denitrification from NO<sub>3</sub><sup>-</sup> to N<sub>2</sub>. The different conversions considered for each scenario under oxic conditions were: (1) partial denitrification of NO<sub>3</sub><sup>-</sup> to N<sub>2</sub>O, no PHA pool; (2) full denitrification of NO<sub>3</sub><sup>-</sup> to N<sub>2</sub>, no PHA pool; (3) full denitrification of NO<sub>3</sub><sup>-</sup> to N<sub>2</sub> with consumption of a PHA pool generated under anoxic conditions. The different conversions considered under anoxic conditions were: (1) and (2) no PHA pool; (3) PHA accumulation. We had experimental measurements of the N<sub>2</sub>O and CO<sub>2</sub> production and O<sub>2</sub> consumption rates in each phase, in addition to the overall consumption and production rates of all compounds.

Detailed calculations performed in each scenario are also explained:

- **Scenario 1: no aerobic conversion NO<sub>3</sub><sup>-</sup> to N<sub>2</sub>, only to N<sub>2</sub>O.** From literature, it is known that aerobic denitrification is not commonly observed in a denitrifying microbial community, at least not at a significant rate. However, in this study, significant N<sub>2</sub>O production was observed during the aerated periods. So, at first, the aerobic NO<sub>3</sub><sup>-</sup> consumption rate was assumed equal to the observed N<sub>2</sub>O production, excluding any N<sub>2</sub> production:

$$R_{\text{NO}_3^-}^{\text{aerobic}} = -R_{\text{N}_2\text{O}}^{\text{aerobic}} \quad (\text{eq. S2.17})$$

The anaerobic NO<sub>3</sub><sup>-</sup> consumption rate was calculated from the measured overall rate and the supposed aerobic rate, knowing that the overall consumption rate comes from a balance between the aerobic and the anaerobic rates (eq. S2.10). The N<sub>2</sub> production rate in the anoxic phase was calculated from the NO<sub>3</sub><sup>-</sup> and the N<sub>2</sub>O rates (eq. S2.15). Similarly to NO<sub>3</sub><sup>-</sup>, the NH<sub>4</sub><sup>+</sup> consumption rates could not be determined in each phase individually. Therefore, differently from the overall mass balance approach, the biomass production rates in each phase were derived from the carbon mass balances (eq. S2.12). The validity of this estimation was

proven above (Figure S2.5). The  $\text{NH}_4^+$  consumption rate was then estimated from the biomass production rate (eq. S2.11).

**Table S2.5. Summarized explanation of how the overall, aerobic, and anaerobic rates were determined in the first scenario.**

Compound	Overall rate	Aerobic rate	Anaerobic rate
Organic substrate	Measured	Measured	Measured
$\text{CO}_2$	Measured	Measured	Measured
$\text{N}_2\text{O}$	Measured	Measured	Measured
$\text{O}_2$	Measured	Measured	Measured (= 0)
$\text{NH}_4^+$	Measured	Estimated from aerobic biomass	Estimated from anaerobic biomass
Biomass	Estimated from overall $\text{NH}_4^+$ (= C balance)	Estimated from aerobic C balance	Estimated from anaerobic C balance
$\text{NO}_3^-$	Measured	Estimated from aerobic N balance (= $\text{N}_2\text{O}$ )	Estimated from aerobic and overall $\text{NO}_3^-$ (Eq. S2.10)
$\text{N}_2$	Estimated from overall N balance	Assumed to be 0	Estimated from anaerobic N balance

The electron balance (eq. S2.16) and electron gap were then calculated for both the oxic and anoxic phases (Table S2.6):

$$e^- \text{ gap} = R_{eD} - R_{eA} \quad (\text{eq. S2.18})$$

**Table S2.6. Electron balances and gaps in the oxic and anoxic phases of the low-frequency and high-frequency reactors, assuming the exclusive conversion of  $\text{NO}_3^-$  to  $\text{N}_2\text{O}$  under oxic conditions.**

Reactor	Low-frequency		High-frequency	
Phase	Oxic	Anoxic	Oxic	Anoxic
Electrons balance	$124 \pm 9\%$	$69 \pm 10\%$	$105 \pm 7\%$	$81 \pm 7\%$
Electron gap ( $e^- \text{mmol} \cdot \text{h}^{-1}$ )	$2.1 \pm 0.7$	$-5.0 \pm 2.3$	$0.7 \pm 0.8$	$-3.2 \pm 1.4$

The electron balances did not close in either of the phases in both reactors. The balances show an underestimation of electrons accepted in the oxic phase and an overestimation in the anoxic phase. This suggests that more  $\text{NO}_3^-$  was reduced in the oxic phase than accounted for, whereas an excess  $\text{NO}_3^-$  reduction was accounted for in the anoxic phase.

- **Scenario 2: yes aerobic conversion of  $\text{NO}_3^-$  to both  $\text{N}_2$  and  $\text{N}_2\text{O}$  - closing the electron mass balance.** From the electron balances in the previous scenario and the symmetric electron gaps of the two phases, it was hypothesized that the surplus of reduced  $\text{NO}_3^-$  accounted for in the anoxic phase was actually reduced in the oxic phase. New aerobic and anaerobic  $\text{NO}_3^-$  consumption rates were estimated

by closing the respective electron gaps, assuming full conversion of NO<sub>3</sub><sup>-</sup> to N<sub>2</sub> (5 e<sup>-</sup> transfer):

$$R_{\text{NO}_3}^{\text{Scenario 2}} = R_{\text{NO}_3}^{\text{Scenario 1}} - \frac{e_{\text{gap}}^-}{5} \quad (\text{eq. S2.19})$$

Linear error propagation was applied to estimate the standard deviations of the derived rates (eq. S2.3). With the estimations of the aerobic and anaerobic NO<sub>3</sub><sup>-</sup> conversion rates, we estimated the overall NO<sub>3</sub><sup>-</sup> consumption rate (eq. S2.10). Considering that we also have the actual measured value for this rate, we could validate the calculation of the aerobic and anaerobic NO<sub>3</sub><sup>-</sup> consumption rates by comparing the recalculated overall NO<sub>3</sub><sup>-</sup> consumption rates in scenario 2 (eq. S2.10) to the measured rates (Figure S2.7, panel B). Therefore, we confidently estimated the aerobic and anaerobic NO<sub>3</sub><sup>-</sup> consumption rates as 0.48 ± 0.14 and 1.13 ± 0.54 N-mmol/h (R<sub>4</sub>) and 0.17 ± 0.17 and 1.34 ± 0.31 N-mmol/h (R<sub>32</sub>), respectively. From the total aerobic electron flow, 36±7% and 11±11% went to denitrification. These values were validated with direct calculations from measured concentration profiles throughout each phase, including the NO<sub>2</sub><sup>-</sup> accumulation rates (Supplementary Figures S2.8-2.9).

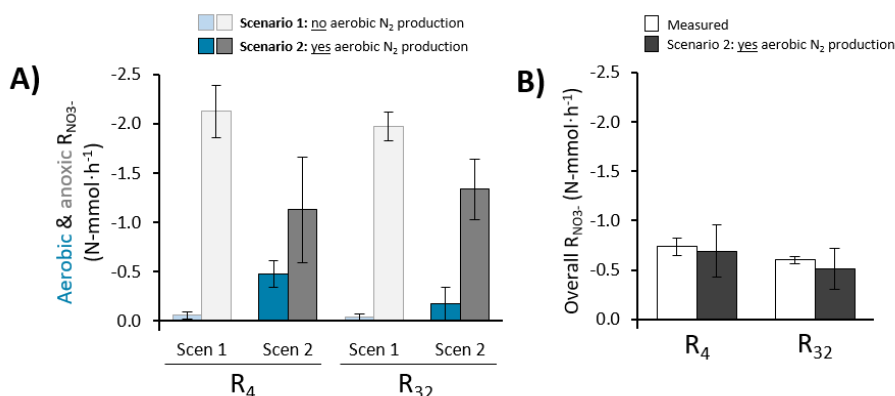


**Figure S2.7. Nitrate consumption rates in the oxic (blue) and anoxic (grey) phases of the low- (R<sub>4</sub>) and high-frequency (R<sub>32</sub>) reactors. Panel A:** comparison between the predicted rates according to scenario 1 (light, assuming no aerobic N<sub>2</sub> production) and scenario 2 (dark, assuming yes aerobic N<sub>2</sub> production). **Panel B:** The measured and estimated overall nitrate consumption rates were also compared to validate the calculations.

- **Scenario 3: yes aerobic conversion of NO<sub>3</sub><sup>-</sup> to both N<sub>2</sub> and N<sub>2</sub>O, and simultaneous PHA accumulation.** Cyclic conditions may select for populations accumulating storage compounds, such as polyhydroxyalkanoates (PHAs). We assessed the potential impact on the estimated aerobic NO<sub>3</sub><sup>-</sup> consumption rates in

scenario 2 of PHA accumulation in the anoxic phase and its subsequent consumption in the oxic period. Biomass contains 4.2 electrons per carbon, whereas polyhydroxybutyrate (PHB, the most common form of PHA) contains 4.5 electrons per carbon, so changes in the electron balance were minimal. Assuming that 50% of the biomass growth in the anoxic phase was actually PHA accumulation, the estimated aerobic and anaerobic  $\text{NO}_3^-$  consumption rates were  $0.50 \pm 0.14$  and  $1.09 \pm 0.53$  N-mmol/h ( $R_4$ ) and  $0.20 \pm 0.18$  and  $1.29 \pm 0.30$  N-mmol/h ( $R_{32}$ ), nearly identical to scenario 2. Therefore, our conclusions would remain unchanged even in the case of significant PHA accumulation.

### Confirmation of the aerobic denitrification rates through concentration profiles.

The aerobic denitrification rates obtained in scenario 2 using mass balances, and reported in the main text, were confirmed with cycle measurements performed after 43-44 days of operation (Figure S2.8).

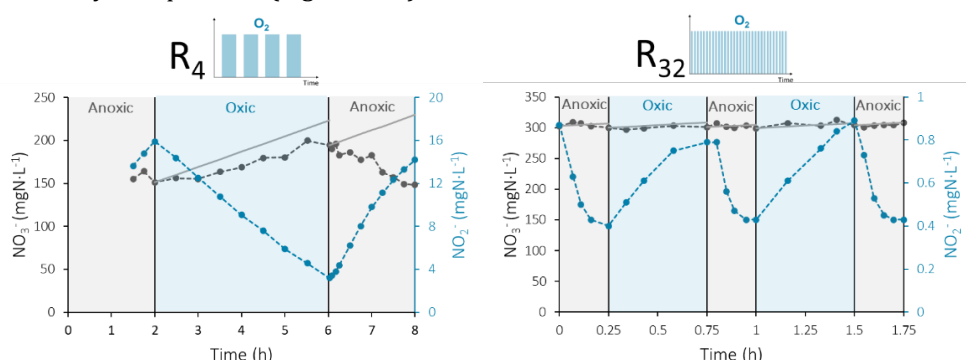


**Figure S2.8. Nitrate and nitrite concentration profiles used to confirm the aerobic denitrification rates.** Nitrate concentrations (grey symbols), expected nitrate concentrations if there was no consumption (grey lines), and nitrite concentrations (blue symbols) during the anoxic (grey area) and oxic (blue area) periods are represented. The measurements were performed after 43 ( $R_4$ ) and 44 ( $R_{32}$ ) days of operation.

The aerobic nitrate and nitrite net accumulation rates were determined by calculating the slope of the linear regression of the concentration profiles (Figure S2.8) and multiplying by the broth volume. For  $R_{32}$ , the rates measured during two cycles were averaged. The error of these rates was assumed to be the error in the slope ( $R_4$ ) or the standard deviation of replicates ( $R_{32}$ ). The nitrate consumption rates were calculated from these accumulation rates and the influent rate (Table S2.1):

$$R_{\text{NO}_3^-, \text{cons}} = R_{\text{NO}_3^-, \text{accum}} - R_{\text{NO}_3^-, \text{in}} \quad (\text{eq. S2.20})$$

There was no nitrite in the influent but it was continuously produced from nitrate reduction, so the net consumption rates were equal to the accumulation rates added to the nitrate consumption rates ( $R_{\text{NO}_2^-, \text{prod}} = R_{\text{NO}_3^-, \text{cons}}$ ).

$$R_{\text{NO}_2^-, \text{cons}} = R_{\text{NO}_2^-, \text{accum}} - R_{\text{NO}_2^-, \text{prod}} \quad (\text{eq. S2.21})$$

The obtained aerobic NO<sub>x</sub><sup>-</sup> denitrification rates were 0.47±0.07 (R<sub>4</sub>) and 0.33±0.16 mmol-N·h<sup>-1</sup> (R<sub>32</sub>), similar to the rates obtained through mass balances with eq. S2.19. The percentage of aerobic electrons used in denitrification vs. O<sub>2</sub> respiration, 33±4% (R<sub>4</sub>) and 27±9% (R<sub>32</sub>), were also similar to the values obtained through mass balances (Figure S2.9).

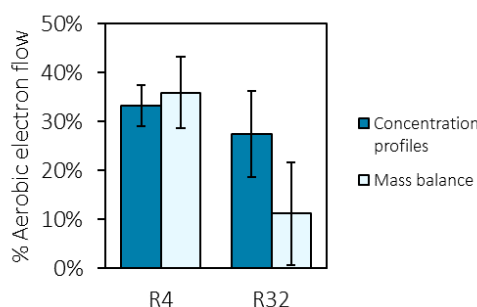


**Figure S2.9.** Percentage of aerobic electron flow used in denitrification in both reactors, as calculated through concentration profiles measured on a single day and overall steady-state mass balances (scenario 2 in Figure S2.6).

The calculated values were determined from relatively small fluctuations in nitrate concentrations, so they were only used to validate the values obtained through the alternative method (mass balances).

### 2.5.3. Nitrification assays

NH<sub>4</sub><sup>+</sup> oxidation activity tests were performed with biomass extracted from R<sub>4</sub> and R<sub>32</sub>, in the presence and absence of the NH<sub>4</sub><sup>+</sup> oxidation inhibitor ATU. A negative control replaced biomass with water and a positive control contained biomass from an enriched nitrifying microbial community. The nitrifying culture at pH 7 with a biomass concentration of 0.04 gVSS/L was enriched from activated sludge in a 2 L continuously-stirred tank reactor for 53 days, with an HRT of 4.2 days, using NH<sub>4</sub><sup>+</sup> as energy source (supplied at 34 NH<sub>4</sub><sup>+</sup>-N mmol/d), bicarbonate as carbon source, and O<sub>2</sub> as electron acceptor (provided as air at 500 mL/min). The nitrifying biomass was centrifuged and the pellet was resuspended in PBS buffer and added to rubber sealed bottles (filled with air) to prevent excessive evaporation. The bottles were incubated

overnight in a shaker at room temperature after addition of 10 mg-N/L  $\text{NH}_4^+$  to start the batches.  $\text{NH}_4^+$  consumption and  $\text{NO}_2^-$  and  $\text{NO}_3^-$  production were observed only in the positive control.  $\text{NH}_4^+$  concentrations increased in the experiments with biomass from  $R_4$  and  $R_{32}$ , indicating biomass decay. Identical concentration profiles between experiments performed with or without ATU further confirm the absence of  $\text{NH}_4^+$  oxidation activity in  $R_4$  and  $R_{32}$ .

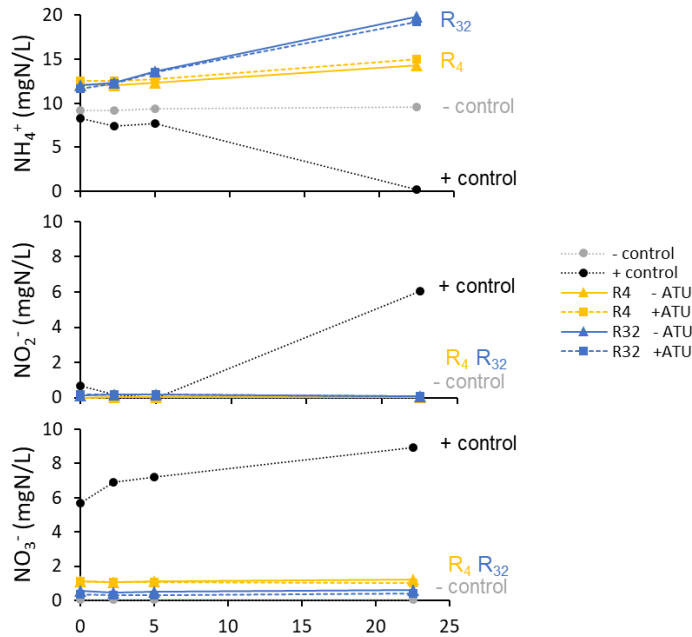


**Figure S2.10. Ammonium, nitrite, and nitrate concentration profiles during ammonium oxidation activity tests with biomass extracted from low- ( $R_4$ , yellow) and high-frequency ( $R_{32}$ , blue) reactors, alongside a negative (water) and a positive control (nitrifying mixed culture). Batches were performed with 10 mg  $\text{NH}_4^+$ -N/L, in the presence or absence of ATU.**



## 2.5.4. Metagenomics

**Table S2.7. Characteristics of the draft genomes recovered from R<sub>4</sub> ordered from high to low abundance (top 10 + others):** Genbank accession number, genome completeness, contamination, and size, GC content, number of predicted genes, relative abundance at 68 days of operation, and taxonomic classification. Bins with a completeness lower than 70% or contamination above 10% were grouped with the unbinned portion. All medium- (MQ) and low-abundant high-quality (HQ) bins were grouped into “others” (grey) in the main manuscript.

	Bin	Genome accession	Comp(%)	Cont(%)	Genome (Mbp)	GC(%)	Genes	Abund(%)	Phylum	Class	Order	Family	Genus	Species
HQ	Bin1.1	JAUCBR000000000	98.96	0.00	5.0	66.1	4695	40.00	Proteobacteria	Gammaproteobacteria	Burkholderiales	Rhodocyclaceae	Denitromonas	
HQ	Bin1.2	JAUCBS000000000	98.96	0.91	5.5	66.7	5347	17.37	Proteobacteria	Alphaproteobacteria	Rhodobacterales	Rhodobacteraceae	Wagnerdoeblera	
HQ	Bin1.3	JAUCBT000000000	95.89	1.05	3.8	60.8	3400	7.57	Proteobacteria	Alphaproteobacteria	Rhizobiales	Xanthobacteraceae	Xanthobacter	
HQ	Bin1.4	JAUCBU000000000	99.61	0.00	2.8	63.9	2582	3.01	Proteobacteria	Gammaproteobacteria	Burkholderiales	Burkholderiaceae	Brachymonas	Brachymonas denitrificans
HQ	Bin1.5	JAUCBV000000000	99.53	2.24	3.9	59.4	3859	2.37	Proteobacteria	Gammaproteobacteria	Burkholderiales	Burkholderiaceae	Castellaniella	
HQ	Bin1.6	JAUCBW000000000	98.13	0.29	2.9	36.3	2601	2.35	Bacteroidota	Bacteroidia	Flavobacteriales	Flavobacteriaceae		
HQ	Bin1.7	JAUCBX000000000	99.44	0.81	4.7	63.2	4678	1.62	Proteobacteria	Alphaproteobacteria	Rhodobacterales	Rhodobacteraceae	Paracoccus	Paracoccus sp002359815
HQ	Bin1.8	JAUCBY000000000	94.12	0.00	3.3	60.5	2965	1.24	Proteobacteria	Alphaproteobacteria	Rhizobiales	Xanthobacteraceae	Xanthobacter	
HQ	Bin1.9	JAUCBZ000000000	98.48	3.89	4.5	62.5	4466	1.23	Proteobacteria	Alphaproteobacteria	Rhodobacterales	Rhodobacteraceae	Pararhodobacter	
HQ	Bin1.10	JAUCCA000000000	100	1.67	4.1	61.7	3805	1.20	Proteobacteria	Gammaproteobacteria	Burkholderiales	Burkholderiaceae	Giesbergeria	
HQ	Bin1.11	JAUCCB000000000	99.51	0.49	2.7	34.5	2528	1.01	Bacteroidota	Bacteroidia	Chitinophagales	Chitinophagaceae	Ginsengibacter	
HQ	Bin1.12	JAUCCC000000000	97.59	1.09	3.8	48.1	3649	0.57	Proteobacteria	Gammaproteobacteria	Pseudomonadales	Pseudomonadaceae	Pseudomonas_C	
MQ	Bin1.13	JAUCCD000000000	94.83	6.90	3.7	63.3	3666	0.46	Proteobacteria	Gammaproteobacteria	Burkholderiales	Rhodocyclaceae	Thauera	
HQ	Bin1.14	JAUCCE000000000	97.05	1.14	4.0	38.9	3659	0.40	Bacteroidota	Bacteroidia	Flavobacteriales	Flavobacteriaceae	Aequorivita	
HQ	Bin1.15	JAUCCF000000000	90.82	3.82	3.7	64.7	3856	0.26	Proteobacteria	Gammaproteobacteria	Burkholderiales	Burkholderiaceae	Giesbergeria	
MQ	Bin1.16	JAUCCG000000000	81.01	0.55	2.8	67.2	3490	0.25	Proteobacteria	Alphaproteobacteria	Caulobacteriales	Caulobacteraceae	Brevundimonas	
MQ	Bin1.17	JAUCCH000000000	78.5	1.27	2.9	60.0	3425	0.24	Actinobacteriota	Actinomycetia	Actinomycetales	Microbacteriaceae	Leucobacter	
MQ	Bin1.18	JAUCCI000000000	75.66	6.85	2.5	66.5	2765	0.23	Proteobacteria	Gammaproteobacteria	Burkholderiales	Burkholderiaceae	Castellaniella	
HQ	Bin1.19	JAUC CJ000000000	91.89	0.26	4.2	55.2	3800	0.10	Proteobacteria	Gammaproteobacteria	Burkholderiales	Burkholderiaceae	Pusillimonas_B	Pusillimonas_B sp013416395
MQ	Bin1.20	JAUCKK000000000	87.25	2.93	3.2	64.7	3091	0.09	Proteobacteria	Gammaproteobacteria	Burkholderiales	Burkholderiaceae	Giesbergeria	
HQ	Bin1.21	JAUCKL000000000	99.97	0.16	3.9	67.5	3572	0.08	Proteobacteria	Gammaproteobacteria	Burkholderiales	Burkholderiaceae	Castellaniella	
MQ	Bin1.22	JAUCCM000000000	81.14	2.96	2.7	64.5	2521	0.08	Proteobacteria	Gammaproteobacteria	Burkholderiales	Burkholderiaceae	Comamonas	
MQ	Bin1.23	JAUCCN000000000	79.66	0.00	1.3	25.7	1183	0.07	Patescibacteria	JAEDAM01	BD1-5	UBA6164	UBA7396	
HQ	Bin1.24	JAUCCO000000000	96.16	1.83	3.6	34.1	3183	0.07	Bacteroidota	Bacteroidia	NS11-12g	UKL13-3	UBA6183	
HQ	Bin1.25	JAUCCP000000000	91.25	1.21	3.6	63.5	3680	0.05	Proteobacteria	Alphaproteobacteria	Rhodobacterales	Rhodobacteraceae	Paracoccus	Paracoccus sp002359815
HQ	Bin1.26	JAUC CQ000000000	94.75	2.21	4.7	68.1	4687	0.05	Proteobacteria	Alphaproteobacteria	Rhodobacterales	Rhodobacteraceae	Pararhodobacter	
HQ	Bin1.27	JAUC CR000000000	94.12	1.23	3.5	63.9	3394	0.03	Proteobacteria	Gammaproteobacteria	Burkholderiales	Burkholderiaceae	Giesbergeria	Giesbergeria suum
HQ	Bin1.28	JAUC CS000000000	99.17	1.64	4.7	37.9	4055	0.02	Bacteroidota	Bacteroidia	Flavobacteriales	Flavobacteriaceae	Gelidibacter	Gelidibacter japonicus
MQ	Bin1.29	JAUCCT000000000	86.78	0.99	2.7	32.7	2849	0.01	Bacteroidota	Bacteroidia	Chitinophagales	JADIYW01		
Unbinned								17.99						

**Table S2.8. Characteristics of the draft genomes recovered from R<sub>32</sub> ordered from high to low abundance (top 10 + others):** Genbank accession number, genome completeness, contamination, and size, GC content, number of predicted genes, relative abundance at 68 days of operation, and taxonomic classification. Bins with a completeness lower than 70% or contamination above 10% were grouped with the unbinned portion. All medium- (MQ) and low-abundant high-quality (HQ) bins were grouped into “others” (grey) in the main manuscript.

	Bin	Genome accession	Comp(%)	Cont(%)	Genome (Mbp)	GC(%)	Genes	Abund(%)	Phylum	Class	Order	Family	Genus	Species
HQ	Bin2.1	JAUCCU0000000000	98.85	0.00	3.2	59.3	3036	23.52	Proteobacteria	Gammaproteobacteria	Burkholderiales	Burkholderiaceae	Castellaniella	
HQ	Bin2.2	JAUCCV0000000000	99.37	2.40	3.1	62.2	2902	10.61	Proteobacteria	Gammaproteobacteria	Burkholderiales	Burkholderiaceae	Castellaniella	
HQ	Bin2.3	JAUCCW0000000000	98.81	1.76	4.3	63.0	3964	7.32	Proteobacteria	Gammaproteobacteria	Burkholderiales	Rhodocyclaceae	Thaueria	
HQ	Bin2.4	JAUCCX0000000000	98.29	0.40	3.6	36.9	3206	5.02	Bacteroidota	Bacteroidia	Flavobacteriales	Flavobacteriaceae	Aequorivita	
HQ	Bin2.5	JAUCCY0000000000	99.41	0.47	3.9	68.9	3479	2.67	Proteobacteria	Gammaproteobacteria	Burkholderiales	Burkholderiaceae	Castellaniella	Castellaniella defragrans
HQ	Bin2.6	JAUCCZ0000000000	93.95	2.25	3.1	61.8	2958	2.13	Proteobacteria	Gammaproteobacteria	Burkholderiales	Burkholderiaceae	Comamonas	
HQ	Bin2.7	JAUCDA0000000000	98.99	0.91	3.8	59.2	3671	1.65	Proteobacteria	Alphaproteobacteria	Rhodobacterales	Rhodobacteraceae	Pseudorhodobacter	
HQ	Bin2.8	JAUCDB0000000000	97.73	3.66	5.0	63.0	5008	1.52	Proteobacteria	Alphaproteobacteria	Rhodobacterales	Rhodobacteraceae	Paracoccus	Paracoccus sp002359815
HQ	Bin2.9	JAUCDC0000000000	96.7	2.46	3.0	37.2	2922	1.44	Bacteroidota	Bacteroidia	Flavobacteriales	Flavobacteriaceae		
HQ	Bin2.10	JAUCDD0000000000	96.36	4.9	3.9	68.8	3558	0.95	Proteobacteria	Gammaproteobacteria	Burkholderiales	Burkholderiaceae	Melaminivora_A	
MQ	Bin2.11	JAUCDE0000000000	80.22	0.00	1.3	26.6	1250	6.53	Patescibacteria	JAEDAM01	BD1-5	UBA6164	UBA7396	UBA7396 sp002470645
MQ	Bin2.12	JAUCDF0000000000	94.69	7.47	3.8	62.7	3530	3.76	Proteobacteria	Gammaproteobacteria	Burkholderiales	Burkholderiaceae	Comamonas	Comamonas sp019104825
MQ	Bin2.13	JAUCDG0000000000	97.7	7.04	4.1	48.4	3929	2.18	Proteobacteria	Gammaproteobacteria	Pseudomonadales	Pseudomonadaceae	Pseudomonas_C	
MQ	Bin2.14	JAUCDH0000000000	88.51	2.61	3.1	65.9	3002	0.95	Proteobacteria	Gammaproteobacteria	Xanthomonadales	Xanthomonadaceae	Stenotrophomonas	
MQ	Bin2.15	JAUCDI0000000000	77.08	1.63	1.8	43.1	1964	0.89	Proteobacteria	Alphaproteobacteria	Paracaeobacterales	Paracaeobacteraceae		
MQ	Bin2.16	JAUCDJ0000000000	92.88	5.36	3.7	64.8	3865	0.81	Proteobacteria	Gammaproteobacteria	Burkholderiales	Burkholderiaceae	Giesbergeria	
MQ	Bin2.17	JAUCDK0000000000	81.35	0.00	1.2	25.9	1111	0.35	Patescibacteria	JAEDAM01	BD1-5	UBA6164	UBA7396	
HQ	Bin2.18	JAUCDL0000000000	98	0.03	3.3	68.8	3065	0.33	Proteobacteria	Gammaproteobacteria	Burkholderiales	Burkholderiaceae	Castellaniella	
HQ	Bin2.19	JAUCDM0000000000	90.25	3.15	3.1	64.1	2759	0.27	Proteobacteria	Gammaproteobacteria	Burkholderiales	Burkholderiaceae	Comamonas	
HQ	Bin2.20	JAUCDN0000000000	92.18	2.05	3.5	64.6	3616	0.20	Proteobacteria	Alphaproteobacteria	Rhizobiales	Devosiaceae	Devosia	
HQ	Bin2.21	JAUCDO0000000000	97.98	1.84	3.9	38.7	3378	0.16	Bacteroidota	Bacteroidia	Flavobacteriales	Flavobacteriaceae	Aequorivita	
HQ	Bin2.22	JAUCDP0000000000	97.27	3.95	4.5	62.3	4359	0.10	Proteobacteria	Gammaproteobacteria	Burkholderiales	Rhodocyclaceae	Azoarcus_C	
HQ	Bin2.23	JAUCDQ0000000000	93.02	1.94	3.8	60.2	3838	0.05	Proteobacteria	Alphaproteobacteria	Rhizobiales	Rhizobiaceae	Hoeflea	
MQ	Bin2.24	JAUCDR0000000000	78.42	3.71	3.2	67.1	3605	0.04	Proteobacteria	Alphaproteobacteria	Sphingomonadales	Sphingomonadaceae	Sphingopyxis	Sphingopyxis granuli
HQ	Bin2.25	JAUCDS0000000000	99.29	0.5	3.2	64.5	3015	0.04	Proteobacteria	Gammaproteobacteria	Burkholderiales	Burkholderiaceae	Castellaniella	
HQ	Bin2.26	JAUCDT0000000000	92.51	1.00	3.1	68.1	2884	0.04	Proteobacteria	Gammaproteobacteria	Burkholderiales	Burkholderiaceae	Comamonas_C	Comamonas_C sp002894305
MQ	Bin2.27	JAUCDU0000000000	77.62	2.16	2.6	64.0	2734	0.04	Proteobacteria	Gammaproteobacteria	Burkholderiales	Burkholderiaceae	Giesbergeria	
MQ	Bin2.28	JAUCDV0000000000	77.69	0.98	2.0	61.5	2259	0.03	Actinobacteriota	Actinomycetia	Actinomycetales	Microbacteriaceae	Leucobacter	
MQ	Bin2.29	JAUCDW0000000000	88.65	2.51	2.9	48.0	3153	0.02	Proteobacteria	Gammaproteobacteria	Pseudomonadales	Pseudomonadaceae	Pseudomonas_C	
	Unbinned							26.38						

**Table S2.9. Reference KO-numbers of the genes from the nitrogen metabolism.**

KO ID	Gene	Description	Pathway
K00362	nirB	nitrite reductase (NADH) large subunit [EC:1.7.1.15]	DNRA
K00363	nirD	nitrite reductase (NADH) small subunit [EC:1.7.1.15]	
K03385	nrfA	nitrite reductase (cytochrome c-552) [EC:1.7.2.2]	
K15876	nrfH	cytochrome c nitrite reductase small subunit	
K00370	narG, narZ, nxrA	nitrate reductase / nitrite oxidoreductase, alpha subunit [EC:1.7.5.1 1.7.99.-]	Denitrification
K00371	narH, narY, nxrB	nitrate reductase / nitrite oxidoreductase, beta subunit [EC:1.7.5.1 1.7.99.-]	
K00373	narJ, narW	chaperone	
K00374	narI, narV	nitrate reductase gamma subunit [EC:1.7.5.1 1.7.99.-]	
K07673	narX	nitrate/nitrite sensor	
K07684	narL	response regulator	
K02575	NRT, narK, nrtP, nasA	MFS transporter, NNP family, nitrate/nitrite transporter	
K02567	napA	nitrate reductase (cytochrome) [EC:1.9.6.1]	
K02568	napB	nitrate reductase (cytochrome), electron transfer subunit	
K02570	napD	nitrate reductase (cytochrome)	
K02571	napE	nitrate reductase (cytochrome)	
K00367	narB	ferredoxin-nitrate reductase	
K10850	narT	putative nitrate transporter	
K15576	nrtA, nasF, cynA	nitrate/nitrite transport system substrate-binding protein	
K15577	nrtB, nasE, cynB	nitrate/nitrite transport system permease protein	
K15578	nrtC, nasD	nitrate/nitrite transport system ATP-binding protein [EC:7.3.2.4]	
K15579	nrtD, cynD	nitrate/nitrite transport system ATP-binding protein	
K21563	dnr	CRP/FNR family transcriptional regulator, dissimilatory nitrate respiration regulator	
K01420	fnr	CRP/FNR family transcriptional regulator, anaerobic regulatory protein	
K00368	nirK	nitrite reductase (NO-forming) [EC:1.7.2.1]	
K15864	nirS	nitrite reductase (NO-forming) / hydroxylamine reductase [EC:1.7.2.1 1.7.99.1]	
K04561	norB	nitric oxide reductase subunit B [EC:1.7.2.5]	
K02305	norC	nitric oxide reductase subunit C	
KnorZ	norZ	quinol-dependent nitric oxide reductase	
K02448	norD	nitric oxide reductase D protein	
K02164	norE	nitric oxide reductase E protein	
K04747	norF	nitric oxide reductase F protein	
K04748	norQ	nitric oxide reductase Q protein	
K12266	treg	transcription regulator	
K13771	trep	NO-sensitive transcription repressor	
K00376	nosZ I	nitrous-oxide reductase [EC:1.7.2.4]	Nitrification
KnosZII	nosZ II	nitrous-oxide reductase [EC:1.7.2.4]	
K19339	nosR	nitrous-oxide reductase transcriptional regulator	
K19342	nosL	copper chaperone	
K07218	nosD	accessory protein	
K10944	amoA	methane/ammonia monooxygenase subunit A [EC:1.14.18.3 1.14.99.39]	
K10945	amoB	methane/ammonia monooxygenase subunit B	
K10946	amoC	methane/ammonia monooxygenase subunit C	
K10535	hao	hydroxylamine dehydrogenase [EC:1.7.2.6]	

Table S2.10. Reference KO-numbers of the genes from the respiratory chain.

KO ID	Gene	Description	Reaction type
K00330	nuoA	NADH-quinone oxidoreductase subunit A [EC:7.1.1.2]	NADH oxidation
K00331	nuoB	NADH-quinone oxidoreductase subunit B [EC:7.1.1.2]	
K00332	nuoC	NADH-quinone oxidoreductase subunit C [EC:7.1.1.2]	
K00333	nuoD	NADH-quinone oxidoreductase subunit D [EC:7.1.1.2]	
K00334	nuoE	NADH-quinone oxidoreductase subunit E [EC:7.1.1.2]	
K00335	nuoF	NADH-quinone oxidoreductase subunit F [EC:7.1.1.2]	
K00336	nuoG	NADH-quinone oxidoreductase subunit G [EC:7.1.1.2]	
K00337	nuoH	NADH-quinone oxidoreductase subunit H [EC:7.1.1.2]	
K00338	nuoI	NADH-quinone oxidoreductase subunit I [EC:7.1.1.2]	
K00339	nuoJ	NADH-quinone oxidoreductase subunit J [EC:7.1.1.2]	
K00340	nuoK	NADH-quinone oxidoreductase subunit K [EC:7.1.1.2]	
K00341	nuoL	NADH-quinone oxidoreductase subunit L [EC:7.1.1.2]	
K00342	nuoM	NADH-quinone oxidoreductase subunit M [EC:7.1.1.2]	
K00343	nuoN	NADH-quinone oxidoreductase subunit N [EC:7.1.1.2]	
K03885	ndh	NADH:quinone reductase (non-electrogenic) [EC:1.6.5.9]	
K00411	petA	ubiquinol-cytochrome c reductase iron-sulfur subunit [EC:7.1.1.8]	Cyt c reduction
K00412	petB	ubiquinol-cytochrome c reductase cytochrome b subunit	
K00413	petC	ubiquinol-cytochrome c reductase cytochrome c1 subunit	
K00410	fbcH	ubiquinol-cytochrome c reductase cytochrome b/c1 subunit	
K03890	qcrA	ubiquinol-cytochrome c reductase iron-sulfur subunit	
K03891	qcrB	ubiquinol-cytochrome c reductase cytochrome b subunit	
K03889	qcrC	ubiquinol-cytochrome c reductase cytochrome c subunit	
K02274	coxA,ctaD	cytochrome <i>aa</i> <sub>3</sub> oxidase subunit I [EC:7.1.1.9]	O <sub>2</sub> reduction
K02275	coxB,ctaC	cytochrome <i>aa</i> <sub>3</sub> oxidase subunit II [EC:7.1.1.9]	
K02276	coxC,ctaE	cytochrome <i>aa</i> <sub>3</sub> oxidase subunit III [EC:7.1.1.9]	
K02277	coxD,ctaF	cytochrome <i>aa</i> <sub>3</sub> oxidase subunit IV [EC:7.1.1.9]	
K00404	ccoN	cytochrome <i>cbb</i> <sub>3</sub> oxidase subunit I [EC:7.1.1.9]	
K00405	ccoO	cytochrome <i>cbb</i> <sub>3</sub> oxidase subunit II	
K15862	ccoNO	cytochrome <i>cbb</i> <sub>3</sub> oxidase subunit I/II [EC:7.1.1.9]	
K00407	ccoQ	cytochrome <i>cbb</i> <sub>3</sub> oxidase subunit IV	
K00406	ccoP	cytochrome <i>cbb</i> <sub>3</sub> oxidase subunit III	
K02297	cyoA	cytochrome <i>bo</i> <sub>3</sub> ubiquinol oxidase subunit I [EC:7.1.1.3]	
K02298	cyoB	cytochrome <i>bo</i> <sub>3</sub> ubiquinol oxidase subunit II [EC:7.1.1.3]	
K02299	cyoC	cytochrome <i>bo</i> <sub>3</sub> ubiquinol oxidase subunit III	
K02300	cyoD	cytochrome <i>bo</i> <sub>3</sub> ubiquinol oxidase subunit IV	
K00425	cydA	cytochrome <i>bd</i> ubiquinol oxidase subunit I [EC:7.1.1.7]	
K00426	cydB	cytochrome <i>bd</i> ubiquinol oxidase subunit II [EC:7.1.1.7]	
K00424	cydX	cytochrome <i>bd</i> ubiquinol oxidase subunit X [EC:7.1.1.7]	
K08738	CYC	cytochrome c	Cytochrome c
K02111	atpA	F-type H <sup>+</sup> /Na <sup>+</sup> -transporting ATPase subunit alpha [EC:7.1.2.2 7.2.2.1]	ATP synthesis
K02108	atpB	F-type H <sup>+</sup> -transporting ATPase subunit a	
K02114	atpC	F-type H <sup>+</sup> -transporting ATPase subunit epsilon	
K02112	atpD	F-type H <sup>+</sup> /Na <sup>+</sup> -transporting ATPase subunit beta [EC:7.1.2.2 7.2.2.1]	
K02110	atpE	F-type H <sup>+</sup> -transporting ATPase subunit c	
K02109	atpF	F-type H <sup>+</sup> -transporting ATPase subunit b	
K02115	atpG	F-type H <sup>+</sup> -transporting ATPase subunit gamma	
K02113	atpH	F-type H <sup>+</sup> -transporting ATPase subunit delta	

**Table S2.11. Reference KO-numbers of the genes from the ROS-protection pathway.**

KO ID	Gene	Description	Reaction type
K04565	SOD1	superoxide dismutase, Cu-Zn family [EC:1.15.1.1]	$O_2^- \rightarrow H_2O_2$
K04564	SOD2	superoxide dismutase, Fe-Mn family [EC:1.15.1.1]	
K03781	katE, catB, srpA	catalase [EC:1.11.1.6]	$H_2O_2 \rightarrow H_2O$
K07217	Mn-cat	Mn-catalase	
K03782	katG	catalase-peroxidase [EC:1.11.1.21]	
K00428	ccp	cytochrome c peroxidase [EC:1.11.1.5]	
K00430	px	peroxidase	
K11065	tpx	thiol peroxidase	
K00432	gpx, btuE, bsaA	glutathione peroxidase	
K05910	npr	NADH peroxidase	
K14171	ahp1	alkyl hydroperoxide reductase	
K03386	ahpC	alkyl hydroperoxide reductase	

## 2.5.5. Heatmaps with gene presence and protein expression

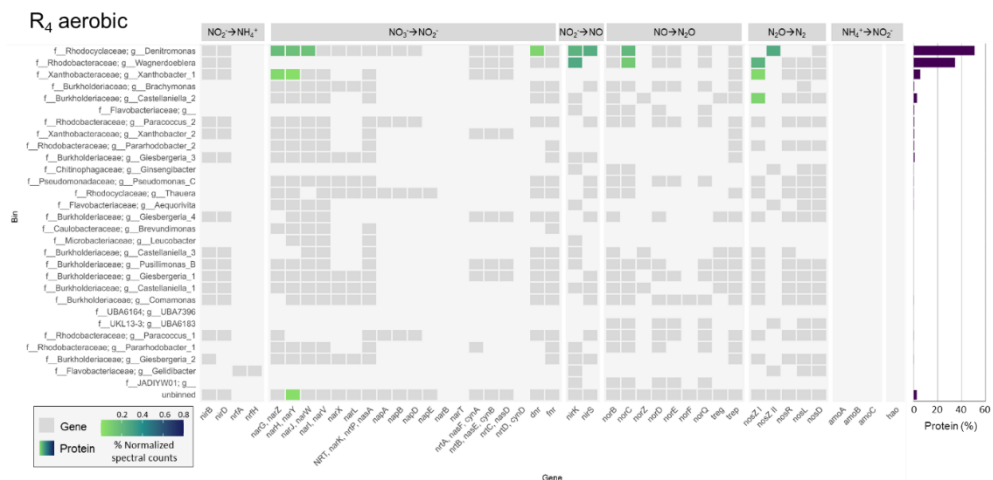


**Figure S2.11.** Heatmap with gene presence (grey) and protein expression (coloured) of the nitrogen metabolism, represented as relative abundance of the total proteome, of all MAGs (ordered from high to low abundance in the metagenome) at the end of the oxic phase of R4. **Right bar charts:** total relative abundance of each MAG in the metaproteome.



**Figure S2.12.** Heatmap with gene presence (grey) and protein expression (coloured) of the nitrogen metabolism, represented as relative abundance of the total proteome, of all MAGs (ordered from high to low abundance in the metagenome) at the end of the anoxic phase of R<sub>4</sub>. **Right bar charts:** total relative abundance of each MAG in the metaproteome.

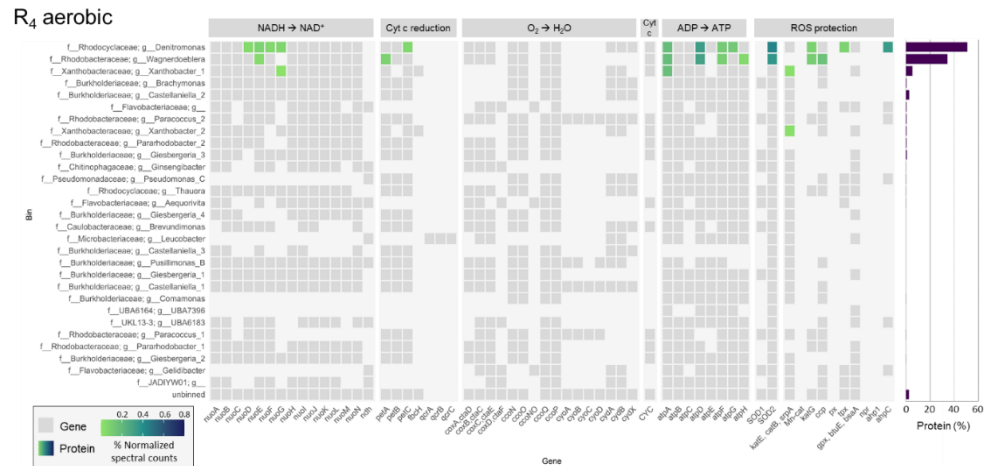


**Figure S2.13.** Heatmap with gene presence (grey) and protein expression (coloured) of the respiratory chain and ROS-protection pathway, represented as relative abundance of the total proteome, of all MAGs (ordered from high to low abundance in the metagenome) at the end of the oxic phase of R<sub>4</sub>. **Right bar charts:** total relative abundance of each MAG in the metaproteome.

# R<sub>4</sub> anoxic



**Figure S2.14.** Heatmap with gene presence (grey) and protein expression (coloured) of respiratory chain and ROS-protection pathway, represented as relative abundance of the total proteome, of all MAGs (ordered from high to low abundance in the metagenome) at the end of the anoxic phase of R<sub>4</sub>. **Right bar charts:** total relative abundance of each MAG in the metaproteome.

# R<sub>32</sub> aerobic

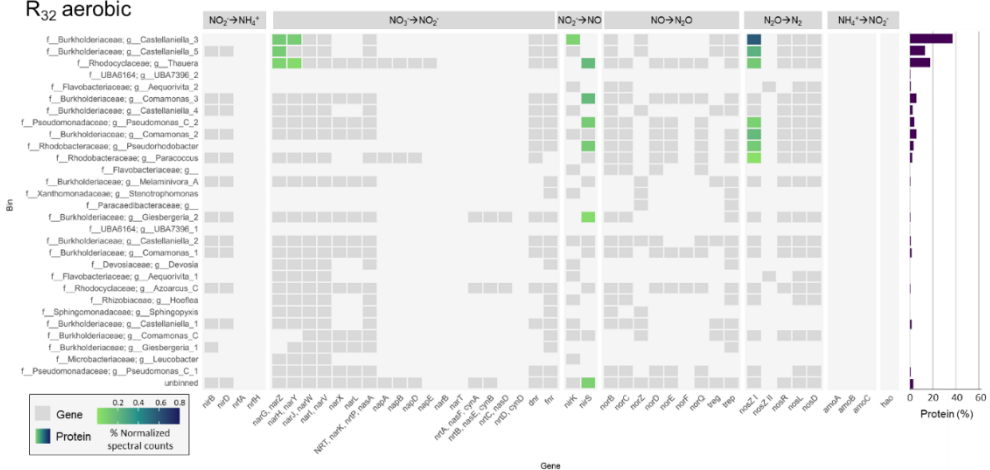


**Figure S2.15.** Heatmap with gene presence (grey) and protein expression (coloured) of the nitrogen metabolism, represented as relative abundance of the total proteome, of all MAGs (ordered from high to low abundance in the metagenome) at the end of the oxic phase of R<sub>32</sub>. **Right bar charts:** total relative abundance of each MAG in the metaproteome.

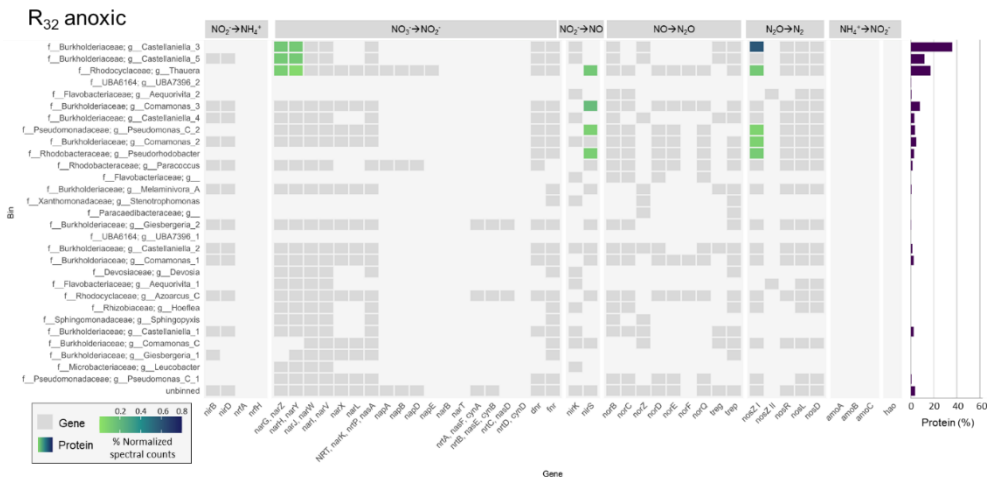


**Figure S2.16.** Heatmap with gene presence (grey) and protein expression (coloured) of the nitrogen metabolism, represented as relative abundance of the total proteome, of all MAGs (ordered from high to low abundance in the metagenome) at the end of the anoxic phase of R<sub>32</sub>. **Right bar charts:** total relative abundance of each MAG in the metaproteome.

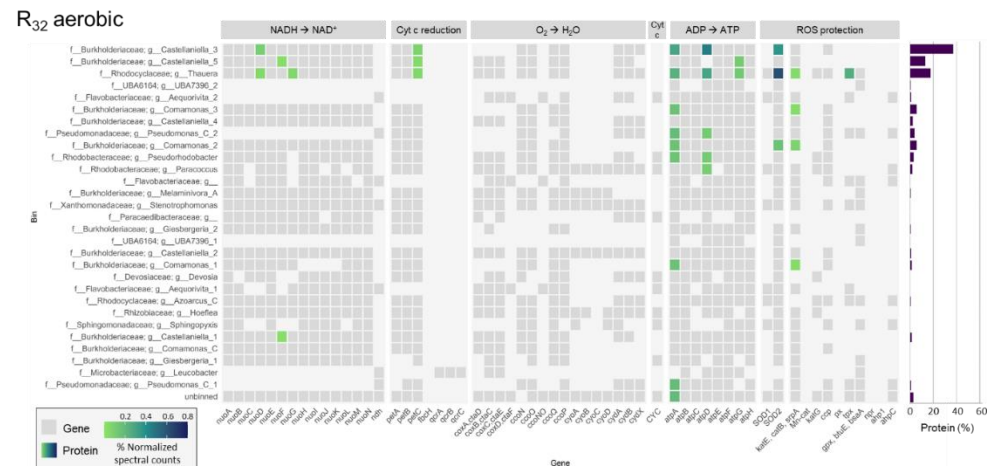


**Figure S2.17.** Heatmap with gene presence (grey) and protein expression (coloured) of respiratory chain and ROS-protection pathway, represented as relative abundance of the total proteome, of all MAGs (ordered from high to low abundance in the metagenome) at the end of the oxic phase of R<sub>32</sub>. **Right bar charts:** total relative abundance of each MAG in the metaproteome.



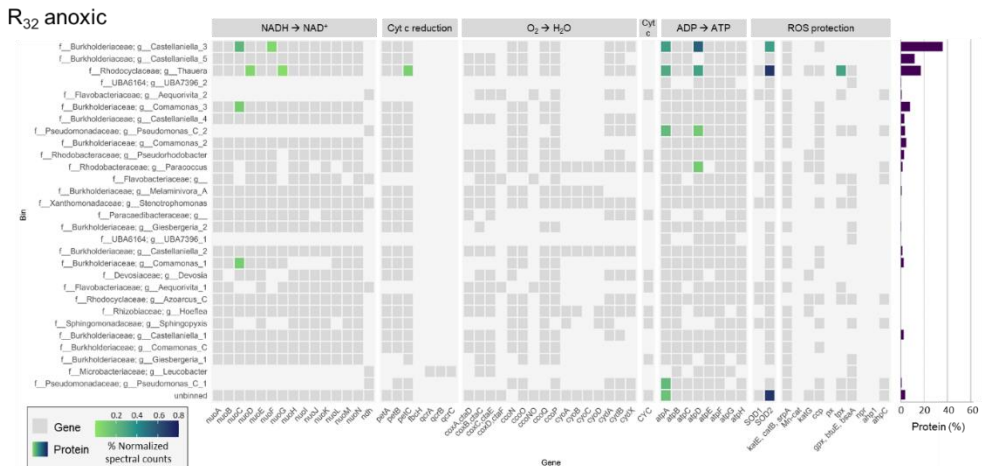


**Figure S2.18.** Heatmap with gene presence (grey) and protein expression (coloured) of respiratory chain and ROS-protection pathway, represented as relative abundance of the total proteome, of all MAGs (ordered from high to low abundance in the metagenome) at the end of the anoxic phase of R<sub>32</sub>. **Right bar charts:** total relative abundance of each MAG in the metaproteome.

## 2.5.6. Oxic/anoxic cycling in 5 reference Dutch WWTPs

The exposure frequency of activated sludge to oxic/anoxic cycles in wastewater treatment plants (WWTPs) cannot exactly be determined, but estimations were made for different WWTPs using flow rates and tank volumes. The hydraulic residence time in each of the tanks was determined (Figure S2.19): anaerobic (no O<sub>2</sub>, no NO<sub>x</sub>), anoxic (no O<sub>2</sub>), facultative (can function as anoxic or aerobic tank, according to the treatment needs), and aerobic (with O<sub>2</sub>). The sludge residence time in the anoxic tanks varied between 11 and 142 minutes, whereas this was 13-155 min for the aerobic zones. The biomass that passes through the settler experiences approximately one oxic/anoxic transition per day, which is equivalent to 15-42 transitions per sludge retention time (SRT, equivalent to the cell generation time, normally 15-20 days in a WWTP). If cells remain in a recycling loop between the aerobic and anoxic zones they can experience up to 9-36 transitions per day, i.e. 132-756 switches per SRT (Table S2.12). Similarly to the activated sludge in the WWTPs, the biomass in our reactors experienced 4 (R<sub>4</sub>) and 32 (R<sub>32</sub>) oxic/anoxic transitions per day, equalling 8 and 64 transitions within one SRT. Experiments with even higher frequency of oxic/anoxic transitions within one SRT should be performed to assess the extent of aerobic denitrification in the highest frequency ranges observed in WWTPs.

**Table S2.12. Number of oxic/anoxic transitions experienced by the biomass in our reactors and in five different WWTP configurations (Figure S2.19), in one day and within one sludge retention time (SRT).**

System	SRT (d)	Cycles/day	Cycles/SRT
R <sub>4</sub>	2	4	8
R <sub>32</sub>	2	32	64
WWTP A	15	1 - 35	15 - 315
WWTP B	21	2 - 36	42 - 756
WWTP C	22	1 - 19	22 - 418
WWTP D	15	1 - 14	15 - 210
WWTP E	15	1 - 9	15 - 135

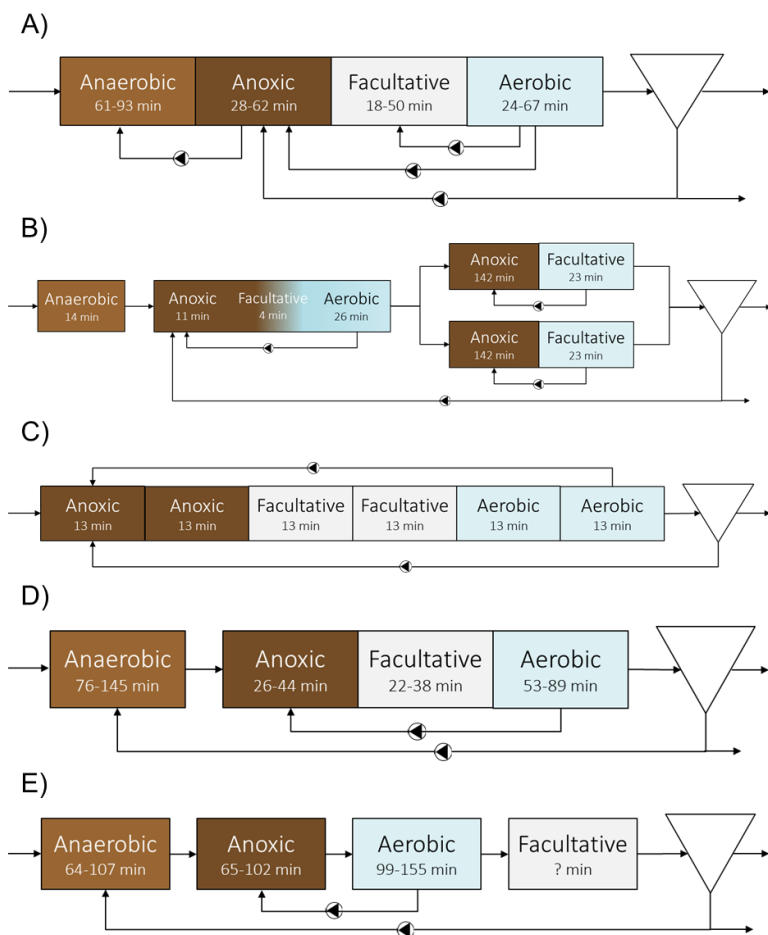


**Figure S2.19. Hydraulic residence time in tanks with different conditions in five different Dutch WWTPs, representing the time that the sludge experiences those conditions. The anaerobic tanks do not contain O<sub>2</sub> nor nitrogen oxides, the anoxic tanks have no oxygen, the aerobic tanks are aerated with air and the facultative tanks can function either as anoxic or aerobic tanks.**

## 2.5.7. Microbial composition of the inoculum



**Figure S2.20. DNA composition of the inoculum (activated sludge).** 349 high-quality metagenome-assembled genomes were identified, 305 of these had at least one denitrification gene<sup>31</sup>. The most abundant 50 MAGs are represented here. The activated sludge sample from the full-scale treatment plant was taken two weeks after the inoculation.

## 2.6. References

2

1. Intergovernmental Panel on Climate Change. *Climate Change 2014: Synthesis Report*. (Core Writing Team, Pachauri RK, Meyer LA, eds.). IPCC; 2015.
2. Tian H, Xu R, Canadell JG, et al. A comprehensive quantification of global nitrous oxide sources and sinks. *Nature*. 2020;586(7828):248-256. doi:10.1038/s41586-020-2780-0
3. Freing A, Wallace DWR, Bange HW. Global oceanic production of nitrous oxide. *Philos Trans R Soc B*. 2012;367:1245-1255. doi:10.1098/rstb.2011.0360
4. Zhu X, Burger M, Doane TA, Horwath WR. Ammonia oxidation pathways and nitrifier denitrification are significant sources of N<sub>2</sub>O and NO under low oxygen availability. *Proc Natl Acad Sci*. 2013;110(16):6328-6333. doi:10.1073/pnas.1219993110
5. Duan H, van den Akker B, Thwaites BJ, et al. Mitigating nitrous oxide emissions at a full-scale wastewater treatment plant. *Water Res*. 2020;185. doi:10.1016/j.watres.2020.116196
6. Duan H, Zhao Y, Koch K, et al. Insights into nitrous oxide mitigation strategies in wastewater treatment and challenges for wider implementation. *Environ Sci Technol*. 2021;55:7208-7224. doi:10.1021/acs.est.1c00840
7. Korner H, Zumft WG. Expression of denitrification enzymes in response to the dissolved oxygen levels and respiratory substrate in continuous culture of *Pseudomonas stutzeri*. *Appl Environ Microbiol*. 1989;55(7):1670-1676. doi:10.1128/aem.55.7.1670-1676.1989
8. Qu Z, Bakken LR, Molstad L, Frostegård Å, Bergaust LL. Transcriptional and metabolic regulation of denitrification in *Paracoccus denitrificans* allows low but significant activity of nitrous oxide reductase under oxic conditions. *Environ Microbiol*. 2016;18(9):2951-2963. doi:10.1111/1462-2920.13128
9. Gaimster H, Alston M, Richardson DJ, Gates AJ, Rowley G. Transcriptional and environmental control of bacterial denitrification and N<sub>2</sub>O emissions. *FEMS Microbiol Lett*. 2018;365:fnx277. doi:10.1093/femsle/fnx277
10. Chen J, Strous M. Denitrification and aerobic respiration, hybrid electron transport chains and co-evolution. *Biochim Biophys Acta*. 2013;1827(2):136-144. doi:10.1016/j.bbabi.2012.10.002
11. Braker G, Conrad R. Diversity, structure, and size of N<sub>2</sub>O-producing microbial communities in soils - What matters for their functioning? *Adv Appl Microbiol*. 2011;75:33-70. doi:10.1016/B978-0-12-387046-9.00002-5
12. Baggs EM. Soil microbial sources of nitrous oxide: recent advances in knowledge, emerging challenges and future direction. *Curr Opin Environ Sustain*. 2011;3(5):321-327. doi:10.1016/j.cosust.2011.08.011
13. Butterbach-Bahl K, Baggs EM, Dannenmann M, Kiese R, Zechmeister-Boltenstern S. Nitrous oxide emissions from soils: How well do we understand the processes and their controls? *Philos Trans R Soc B*. 2013;368(1621). doi:10.1098/rstb.2013.0122
14. Battaglia G, Joos F. Marine N<sub>2</sub>O Emissions from nitrification and denitrification constrained by modern observations and projected in multimillennial global warming simulations. *Global Biogeochem Cycles*. 2018;32(1):92-121. doi:10.1002/2017GB005671
15. Kampschreur MJ, Temmink H, Kleerebezem R, Jetten MSM, van Loosdrecht MCM. Nitrous oxide emission during wastewater treatment. *Water Res*. 2009;43(17):4093-4103.

- doi:10.1016/j.watres.2009.03.001
16. van Loosdrecht MCM, Jetten MSM. Microbiological conversions in nitrogen removal. *Water Sci Technol.* 1998;38(1):1-7. doi:10.2166/wst.1998.0002
17. Gruber W, Magyar PM, Mitrovic I, et al. Tracing N<sub>2</sub>O formation in full-scale wastewater treatment with natural abundance isotopes indicates control by organic substrate and process settings. *Water Res X.* 2022;15. doi:10.1016/j.wroa.2022.100130
18. Robertson LA, Kuenen JG. Aerobic denitrification: a controversy revived. *Arch Microbiol.* 1984;139(4):351-354. doi:10.1007/BF00408378
19. Yang J, Feng L, Pi S, et al. A critical review of aerobic denitrification: insights into the intracellular electron transfer. *Sci Total Environ.* 2020;731. doi:10.1016/j.scitotenv.2020.139080
20. Marchant HK, Ahmerkamp S, Lavik G, et al. Denitrifying community in coastal sediments performs aerobic and anaerobic respiration simultaneously. *ISME J.* 2017;11(8):1799-1812. doi:10.1038/ismej.2017.51
21. Patureau D, Zumstein E, Delgenes JP, Moletta R. Aerobic denitrifiers isolated from diverse natural and managed ecosystems. *Microb Ecol.* 2000;39(2):145-152. doi:10.1007/s002480000009
22. Frette L, Gejlsbjerg B, Westermann P. Aerobic denitrifiers isolated from an alternating activated sludge system. *FEMS Microbiol Ecol.* 1997;24:363-370. doi:10.1111/j.1574-6941.1997.tb00453.x
23. Carter JP, Ya Hsin Hsiao, Spiro S, Richardson DJ. Soil and sediment bacteria capable of aerobic nitrate respiration. *Appl Environ Microbiol.* 1995;61(8):2852-2858. doi:10.1128/aem.61.8.2852-2858.1995
24. Gao H, Schreiber F, Collins G, et al. Aerobic denitrification in permeable Wadden Sea sediments. *ISME J.* 2010;4(3):417-426. doi:10.1038/ismej.2009.127
25. Morley N, Baggs EM, Dörsch P, Bakken L. Production of NO, N<sub>2</sub>O and N<sub>2</sub> by extracted soil bacteria, regulation by NO<sub>2</sub>- and O<sub>2</sub> concentrations. *FEMS Microbiol Ecol.* 2008;65(1):102-112. doi:10.1111/j.1574-6941.2008.00495.x
26. Vishniac W, Santer M. The Thiobacilli. *Bacteriol Rev.* 1957;21:195-213. doi:10.1128/br.21.3.195-213.1957
27. van Loosdrecht MCM, Nielsen PH, Lopez-Vazquez CM, Brdjanovic D. *Experimental Methods in Wastewater Treatment.* IWA; 2016. doi:10.2166/9781780404752
28. Hooper AB, Terry KR. Photoinactivation of ammonia oxidation in Nitrosomonas. *J Bacteriol.* 1974;119(3):899-906. doi:10.1128/jb.119.3.899-906.1974
29. Ginestet P, Audic JM, Urbain V, Block JC. Estimation of nitrifying bacterial activities by measuring oxygen uptake in the presence of the metabolic inhibitors allylthiourea and azide. *Appl Environ Microbiol.* 1998;64(6):2266-2268. doi:10.1128/aem.64.6.2266-2268.1998
30. Jensen MM, Thamdrup B, Dalsgaard T. Effects of specific inhibitors on anammox and denitrification in marine sediments. *Appl Environ Microbiol.* 2007;73(10):3151-3158. doi:10.1128/AEM.01898-06
31. Roothans N, Pabst M, van Diemen M, et al. Long-term multi-meta-omics resolves the ecophysiological controls of seasonal N<sub>2</sub>O emissions. *bioRxiv.* Published online 2024:2024.04.17.589950. doi:10.1101/2024.04.17.589950
32. Shen W, Le S, Li Y, Hu F. SeqKit: A cross-platform and ultrafast toolkit for FASTA/Q file manipulation. *PLoS One.* 2016;11(10). doi:10.1371/journal.pone.0163962

33. De Coster W, D'Hert S, Schultz DT, Cruts M, Van Broeckhoven C. NanoPack: visualizing and processing long-read sequencing data. *Bioinformatics*. 2018;34(15):2666-2669. doi:10.1093/bioinformatics/bty149
34. Kolmogorov M, Bickhart DM, Behsaz B, et al. metaFlye: scalable long-read metagenome assembly using repeat graphs. *Nat Methods*. 2020;17(11):1103-1110. doi:10.1038/s41592-020-00971-x
35. Mikheenko A, Saveliev V, Gurevich A. MetaQUAST: evaluation of metagenome assemblies. *Bioinformatics*. 2016;32(7):1088-1090. doi:10.1093/bioinformatics/btv697
36. Li H. Minimap2: pairwise alignment for nucleotide sequences. *Bioinformatics*. 2018;34(18):3094-3100. doi:10.1093/bioinformatics/bty191
37. Li H, Handsaker B, Wysoker A, et al. The Sequence Alignment/Map format and SAMtools. *Bioinformatics*. 2009;25(16):2078-2079. doi:10.1093/bioinformatics/btp352
38. Kang DD, Li F, Kirton E, et al. MetaBAT 2: an adaptive binning algorithm for robust and efficient genome reconstruction from metagenome assemblies. *PeerJ*. 2019;7. doi:10.7717/peerj.7359
39. Wu YW, Simmons BA, Singer SW. MaxBin 2.0: an automated binning algorithm to recover genomes from multiple metagenomic datasets. *Bioinformatics*. 2016;32(4):605-607. doi:10.1093/bioinformatics/btv638
40. Alneberg J, Bjarnason BS, De Bruijn I, et al. Binning metagenomic contigs by coverage and composition. *Nat Methods*. 2014;11(11):1144-1146. doi:10.1038/nmeth.3103
41. Sieber CMK, Probst AJ, Sharrar A, et al. Recovery of genomes from metagenomes via a dereplication, aggregation and scoring strategy. *Nat Microbiol*. 2018;3(7):836-843. doi:10.1038/s41564-018-0171-1
42. Hyatt D, Chen GL, LoCascio PF, Land ML, Larimer FW, Hauser LJ. Prodigal: prokaryotic gene recognition and translation initiation site identification. *BMC Bioinformatics*. 2010;11. doi:10.1186/1471-2105-11-119
43. Buchfink B, Xie C, Huson DH. Fast and sensitive protein alignment using DIAMOND. *Nat Methods*. 2014;12(1):59-60. doi:10.1038/nmeth.3176
44. Parks DH, Imelfort M, Skennerton CT, Hugenholtz P, Tyson GW. CheckM: assessing the quality of microbial genomes recovered from isolates, single cells, and metagenomes. *Genome Res*. 2015;25(7):1043-1055. doi:10.1101/gr.186072.114
45. Olm MR, Brown CT, Brooks B, Banfield JF. DRep: a tool for fast and accurate genomic comparisons that enables improved genome recovery from metagenomes through de-replication. *ISME J*. 2017;11(12):2864-2868. doi:10.1038/ismej.2017.126
46. Chaumeil PA, Mussig AJ, Hugenholtz P, Parks DH. GTDB-Tk v2: memory friendly classification with the genome taxonomy database. *Bioinformatics*. 2022;38(23):5315-5316. doi:10.1093/bioinformatics/btac672
47. Parks DH, Chuvochina M, Rinke C, Mussig AJ, Chaumeil PA, Hugenholtz P. GTDB: an ongoing census of bacterial and archaeal diversity through a phylogenetically consistent, rank normalized and complete genome-based taxonomy. *Nucleic Acids Res*. 2022;50:785-794. doi:10.1093/nar/gkab776
48. Shaffer M, Borton MA, McGivern BB, et al. DRAM for distilling microbial metabolism to automate the curation of microbiome function. *Nucleic Acids Res*. 2020;48(16):8883-8900. doi:10.1093/nar/gkaa621
49. Aramaki T, Blanc-Mathieu R, Endo H, et

- al. KofamKOALA: KEGG Ortholog assignment based on profile HMM and adaptive score threshold. *Bioinformatics*. 2020;36(7):2251-2252. doi:10.1093/bioinformatics/btz859
50. Rawlings ND, Waller M, Barrett AJ, Bateman A. MEROPS: the database of proteolytic enzymes, their substrates and inhibitors. *Nucleic Acids Res*. 2014;42:503-509. doi:10.1093/nar/gkt953
51. Mistry J, Chuguransky S, Williams L, et al. Pfam: the protein families database in 2021. *Nucleic Acids Res*. 2021;49:412-419. doi:10.1093/nar/gkaa913
52. Yin Y, Mao X, Yang J, Chen X, Mao F, Xu Y. DbCAN: a web resource for automated carbohydrate-active enzyme annotation. *Nucleic Acids Res*. 2012;40:445-451. doi:10.1093/nar/gks479
53. Paysan-Lafosse T, Blum M, Chuguransky S, et al. InterPro in 2022. *Nucleic Acids Res*. 2023;51:418-427. doi:10.1093/nar/gkac993
54. Zumft WG. Nitric oxide reductases of prokaryotes with emphasis on the respiratory, heme-copper oxidase type. *J Inorg Biochem*. 2005;99(1):194-215. doi:10.1016/j.jinorgbio.2004.09.024
55. Papadopoulos JS, Agarwala R. COBALT: constraint-based alignment tool for multiple protein sequences. *Bioinformatics*. 2007;23(9):1073-1079. doi:10.1093/bioinformatics/btm076
56. The UniProt Consortium. UniProt: the universal protein knowledgebase in 2023. *Nucleic Acids Res*. 2023;51:523-531. doi:doi.org/10.1093/nar/gkac1052
57. Bolger AM, Lohse M, Usadel B. Trimmomatic: a flexible trimmer for Illumina sequence data. *Bioinformatics*. 2014;30(15):2114-2120. doi:10.1093/bioinformatics/btu170
58. Nurk S, Meleshko D, Korobeynikov A, Pevzner PA. MetaSPAdes: a new versatile metagenomic assembler. *Genome Res*. 2017;27(5):824-834. doi:10.1101/gr.213959.116
59. Dong X, Strous M. An integrated pipeline for annotation and visualization of metagenomic contigs. *Front Genet*. 2019;10. doi:10.3389/fgene.2019.00999
60. Vasimuddin M, Misra S, Li H, Aluru S. Efficient Architecture-Aware Acceleration of BWA-MEM for Multicore Systems. *IEEE Parallel Distrib Process Symp*. Published online 2019:314-324. doi:10.1109/IPDPS.2019.00041
61. Rodriguez-R LM, Konstantinidis KT. Nonpareil: a redundancy-based approach to assess the level of coverage in metagenomic datasets. *Bioinformatics*. 2014;30(5):629-635. doi:10.1093/bioinformatics/btt584
62. Kleikamp HBC, Pronk M, Tugui C, et al. Database-independent de novo metaproteomics of complex microbial communities. *Cell Syst*. 2021;12(5):375-383. doi:10.1016/j.cels.2021.04.003
63. den Ridder, van den Brandeler W, Altiner M, Daran-Lapujade P, Pabst M. Proteome dynamics during transition from exponential to stationary phase under aerobic and anaerobic conditions in yeast. *Mol Cell Proteomics*. 2023;22(6). doi:10.1016/j.mcpro.2023.100552
64. RStudio Team. RStudio: integrated development environment for R. RStudio, PBC, Boston, MA. Published 2021. <https://www.rstudio.com/>
65. R Core Team. R: A language and environment for statistical computing. R Foundation for Statistical Computing, Vienna, Austria. Published 2022. <https://www.r-project.org/>
66. Wickham H. The split-apply-combine strategy for data analysis. *J Stat Softw*. 2011;40(1). doi:10.18637/jss.v040.i01



67. Wickham H, Averick M, Bryan J, et al. Welcome to the Tidyverse. *J Open Source Softw.* 2019;4(43):1686. doi:10.21105/joss.01686
68. Wickham H, Bryan J. readxl: read excel files. Published 2023. <https://cran.r-project.org/package=readxl>
69. Wickham H. *Ggplot2: Elegant Graphics for Data Analysis*. Second. Springer; 2016.
70. Moir JWB, Richardson DJ, Ferguson SJ. The expression of redox proteins of denitrification in *Thiosphaera pantotropha* grown with oxygen, nitrate, and nitrous oxide as electron acceptors. *Arch Microbiol.* 1995;164(1):43-49. doi:10.1007/BF02568733
71. Olaya-Abril A, Hidalgo-Carrillo J, Luque-Almagro VM, et al. Exploring the denitrification proteome of *Paracoccus denitrificans* PD1222. *Front Microbiol.* 2018;9. doi:10.3389/fmicb.2018.01137
72. Giannopoulos G, Sullivan MJ, Hartop KR, et al. Tuning the modular *Paracoccus denitrificans* respirome to adapt from aerobic respiration to anaerobic denitrification. *Environ Microbiol.* 2017;19(12):4953-4964. doi:10.1111/1462-2920.13974
73. Suenaga T, Riya S, Hosomi M, Terada A. Biokinetic characterization and activities of N<sub>2</sub>O-reducing bacteria in response to various oxygen levels. *Front Microbiol.* 2018;9:697. doi:10.3389/fmicb.2018.00697
74. Gijs Kuenen J, Johnson OJ. Continuous cultures (chemostats). In: Schaechter M, ed. *Encyclopedia of Microbiology (Third Edition)*. Academic Press; 2009:130-147. doi:10.1016/B978-012373944-5.00112-7
75. Conthe M, Parchen C, Stouten G, Kleerebezem R, van Loosdrecht MCM. O<sub>2</sub> versus N<sub>2</sub>O respiration in a continuous microbial enrichment. *Appl Microbiol Biotechnol.* 2018;102(20):8943-8950. doi:10.1007/s00253-018-9247-3
76. Otte S, Grobbsen NG, Robertson LA, Jetten MSM, Kuenen JG. Nitrous oxide production by *Alcaligenes faecalis* under transient and dynamic aerobic and anaerobic conditions. *Appl Environ Microbiol.* 1996;62(7):2421-2426. doi:10.1128/aem.62.7.2421-2426.1996
77. Wüst A, Schneider L, Pomowski A, Zumft WG, Kroneck PMH, Einsle O. Nature's way of handling a greenhouse gas: the copper-sulfur cluster of purple nitrous oxide reductase. *Biol Chem.* 2012;393(10):1067-1077. doi:10.1515/hsz-2012-0177
78. Conthe M, Wittorf L, Kuenen JG, Kleerebezem R, Van Loosdrecht MCM, Hallin S. Life on N<sub>2</sub>O: deciphering the ecophysiology of N<sub>2</sub>O respiring bacterial communities in a continuous culture. *ISME J.* 2018;12(4):1142-1153. doi:10.1038/s41396-018-0063-7
79. Roeselers G, Zippel B, Staal M, Van Loosdrecht M, Muyzer G. On the reproducibility of microcosm experiments - different community composition in parallel phototrophic biofilm microcosms. *FEMS Microbiol Ecol.* 2006;58(2):169-178. doi:10.1111/j.1574-6941.2006.00172.x
80. Louca S, Polz MF, Mazel F, et al. Function and functional redundancy in microbial systems. *Nat Ecol Evol.* 2018;2(6):936-943. doi:10.1038/s41559-018-0519-1
81. Bell LC, Richardson DJ, Ferguson SJ. Periplasmic and membrane-bound respiratory nitrate reductases in *Thiosphaera pantotropha*. *FEBS.* 1990;265:85-87.
82. Kleiner M, Thorson E, Sharp CE, et al. Assessing species biomass contributions in microbial communities via metaproteomics. *Nat Commun.* 2017;8(1). doi:10.1038/s41467-017-01544-x
83. Arnoux P, Sabaty M, Alric J, et al. Structural and redox plasticity in the



- p>heterodimeric periplasmic nitrate reductase.
- Nat Struct Biol.*
- 2003;10(11):928-934. doi:10.1038/nsb994
84. Richardson DJ, Berks BC, Russell DA, Spiro S, Taylor CJ. Functional, biochemical and genetic diversity of prokaryotic nitrate reductases. *Cell Mol Life Sci.* 2001;58(2):165-178. doi:10.1007/PL00000845
85. Hernandez D, Rowe JJ. Oxygen inhibition of nitrate uptake is a general regulatory mechanism in nitrate respiration. *J Biol Chem.* 1988;263(17):7937-7939. doi:10.1016/s0021-9258(18)68423-6
86. Moir JWB, Wood NJ. Nitrate and nitrite transport in bacteria. *Cell Mol Life Sci.* 2001;58(2):215-224. doi:10.1007/PL00000849
87. Potter LC, Millington P, Griffiths L, Thomas GH, Cole JA. Competition between *Escherichia coli* strains expressing either a periplasmic or a membrane-bound nitrate reductase: does Nap confer a selective advantage during nitrate-limited growth? *Biochem J.* 1999;344(1):77-84. doi:10.1042/0264-6021:3440077
88. Ellington MJK, Sawers G, Sears HJ, Spiro S, Richardson DJ, Ferguson SJ. Characterization of the expression and activity of the periplasmic nitrate reductase of *Paracoccus pantotrophus* in chemostat cultures. *Microbiology.* 2003;149(6):1533-1540. doi:10.1099/mic.0.26277-0
89. Zorz JK, Kozlowski JA, Stein LY, Strous M, Kleiner M. Comparative proteomics of three species of ammonia-oxidizing bacteria. *Front Microbiol.* 2018;9. doi:10.3389/fmicb.2018.00938
90. Wang Z, Vishwanathan N, Kowaliczko S, Ishii S. Clarifying microbial nitrous oxide reduction under aerobic conditions: tolerant, intolerant, and sensitive. *Microbiol Spectr.* 2023;11(2):e04709-22. doi:doi.org/10.1128/spectrum.04709-22



Long-term multi-meta-omics  
resolves the ecophysiological  
controls of seasonal  
N<sub>2</sub>O emissions during  
wastewater treatment



## Abstract

Nitrous oxide (N<sub>2</sub>O) is the third most important greenhouse gas, and originates primarily from natural and engineered microbiomes. Effective emission mitigations are currently hindered by the largely unresolved ecophysiological controls of coexisting N<sub>2</sub>O-converting metabolisms in complex communities. We use biological wastewater treatment as model ecosystem, and combine long-term metagenome-resolved metaproteomics with *ex situ* kinetic and full-scale operational characterisation over nearly two years. By leveraging the evidence independently obtained at multiple ecophysiological levels, from individual genetic potential to actual metabolism and emergent community phenotype, the cascade of environmental and operational triggers driving seasonal N<sub>2</sub>O emissions is ultimately resolved. We identify nitrifier denitrification as the dominant N<sub>2</sub>O-producing pathway and the dissolved O<sub>2</sub> as the prime operational parameter, paving the way to design and foster robust emission control strategies. This work exemplifies the untapped potential of multi-meta-omics in the mechanistic understanding and ecological engineering of microbiomes towards reducing anthropogenic impacts and advancing sustainable biotechnological developments.

Accepted as: Roothans N, Pabst M, van Diemen M, Herrera Mexicano C, Zandvoort M, Abeel T, van Loosdrecht MCM, Laureni M. Long-term multi-meta-omics resolves the ecophysiological controls of seasonal N<sub>2</sub>O emissions during wastewater treatment. *Nat Water* 2025

### 3.1. Introduction

The yearly anthropogenic emissions of nitrous oxide (N<sub>2</sub>O), currently the third most important greenhouse gas, are projected to increase by 50% in the coming 50 years if no mitigation strategies are employed <sup>1</sup>. N<sub>2</sub>O is mainly produced by microbial communities in natural, managed and engineered ecosystems <sup>2</sup>. Yet, the mechanisms governing biological N<sub>2</sub>O emissions in these ecosystems remain largely unknown. The main challenge lies in the coexistence of nitrogen-converting guilds in complex microbiomes, each emitting N<sub>2</sub>O under a range of complementary conditions that alternate or overlap in most ecosystems (e.g. alternating oxic-anoxic conditions in wastewater treatment plants <sup>3</sup> and sea sediments <sup>4</sup>; substrate concentration gradients in oceans <sup>5</sup>, soils <sup>6</sup> and wastewater treatment biofilms <sup>7</sup>). In general, high ammonium (NH<sub>4</sub><sup>+</sup>) and oxygen (O<sub>2</sub>) concentrations stimulate N<sub>2</sub>O production through hydroxylamine (NH<sub>2</sub>OH) oxidation by ammonia-oxidising bacteria (AOB), while high nitrite (NO<sub>2</sub><sup>-</sup>) and low O<sub>2</sub> concentrations enhance the nitrifier denitrification pathway <sup>8,9</sup> (Figure 3.1A). High NO<sub>2</sub><sup>-</sup> and high O<sub>2</sub> concentrations result in N<sub>2</sub>O accumulation from imbalanced denitrification by heterotrophic denitrifying bacteria (DEN) <sup>8,10</sup> (Figure 3.1A). High concentrations of reactive intermediates (NO<sub>2</sub><sup>-</sup>, NH<sub>2</sub>OH, NO) and metals (e.g. Fe and Mn) can lead to abiotic N<sub>2</sub>O formation (previously reviewed <sup>11</sup>), particularly in ammonia-oxidising archaea (AOA)-dominated marine environments <sup>12-14</sup>. Yet, in soils and conventional wastewater treatment plants (WWTPs), abiotic rates have been shown to be minor compared to biological N<sub>2</sub>O production by AOB and DEN <sup>15-18</sup>. Seemingly ubiquitous is the strong seasonality of N<sub>2</sub>O emissions in many natural and managed environments, such as oceans <sup>19,20</sup>, soils <sup>21-23</sup>, lakes <sup>24,25</sup> and rivers <sup>26</sup>, and engineered systems such as wastewater treatment plants <sup>27-34</sup> (summarised in Table S3.1). This indicates that seasonally-impacted macroscopic factors directly influence biological N<sub>2</sub>O turnover. Yet, studying the interactions between environmental conditions, complex microbiome dynamics and N<sub>2</sub>O emissions, and capturing the underlying ecological principles is inherently challenging. To this end, we use biological wastewater treatment as a more tractable model ecosystem, as the N<sub>2</sub>O seasonality is well-represented, while other variables (e.g. aeration, biomass concentration) are controlled or extensively monitored <sup>35</sup>.

Most WWTPs emit the majority of their yearly N<sub>2</sub>O during a winter or spring peak lasting 3-4 months, with simultaneous NO<sub>2</sub><sup>-</sup> accumulation <sup>27,31-34,36</sup> (Table S3.1). Similarly, higher N<sub>2</sub>O emissions during colder seasons are widely reported for oceans <sup>20</sup>, soils <sup>22,23</sup>, and lakes <sup>24</sup>. Low or increasing temperatures have been hypothesised as the underlying causes for the seasonal N<sub>2</sub>O emissions, but a clear correlation is often missing <sup>20,23,24,28,29,37,38</sup>. The immediate effect of diverse environmental and process parameters

on the N<sub>2</sub>O production rates of AOB and DEN largely explain the short-term N<sub>2</sub>O dynamics in WWTPs<sup>3,39</sup> and natural environments<sup>5,6,40,41</sup>, but fail to describe the widely observed seasonality. Emblematic is the reported higher N<sub>2</sub>O production by AOB at high temperatures<sup>42</sup>, while most seasonal emissions occur in winter. Broadly applied correlation analyses between N<sub>2</sub>O and environmental and operational parameters have proved insufficient to explain seasonal emissions in WWTPs<sup>28,34,43</sup>, oceans<sup>19,20</sup>, soils<sup>21–23</sup> and freshwater systems<sup>24–26</sup>. Despite the evident central microbial role in N<sub>2</sub>O conversions, most studies do not take potential seasonal dynamics of the microbiome's metabolism into account, likely overlooking key mechanisms linking environmental triggers and emissions. A delay between triggers, metabolic adaptations, and emergent phenotype is expected in slow-growing natural and WWTP communities<sup>38</sup>. Only few studies investigated microbial dynamics during seasonal nitrogen oxides peaks in WWTPs with seemingly contradicting results. Seasonal NO<sub>2</sub><sup>−</sup> and N<sub>2</sub>O accumulation events have been attributed to decreased nitrite-oxidising bacteria (NOB) 16S rRNA gene abundances<sup>29,33</sup> and increased difference between AOB and NOB activity<sup>27,32</sup>, while in other instances no seasonal fluctuations were observed in the nitrifying community<sup>44</sup>. To date, the operational and metabolic mechanisms controlling seasonal N<sub>2</sub>O emissions remain largely unknown, hindering effective mitigation.

We combine long-term metagenomic-resolved metaproteomic analyses with *ex situ* kinetic and full-scale process characterisations to address the mechanistic gap in seasonal N<sub>2</sub>O emissions. The cascade of environmental and operational triggers underlying N<sub>2</sub>O emissions is resolved by leveraging the evidence obtained at multiple ecophysiological levels, from individual genetic potential to actual metabolism and emergent community phenotype. We identify nitrifier denitrification as the prime N<sub>2</sub>O-producing pathway, and the dissolved O<sub>2</sub> as the central operational parameter to minimise emissions. This work exemplifies the yet-to-be-realised potential of multi-meta-omics approaches to inform ecologically-driven microbiomes management and engineering, ultimately reducing anthropogenic emissions and advancing sustainable biotechnological developments.

## 3.2. Methods

### 3.2.1. WWTP operation

The covered Amsterdam-West WWTP has the daily capacity to treat 200,000 m<sup>3</sup> municipal wastewater under dry weather conditions (1 million population equivalents). After fine screening and primary sedimentation, carbon, phosphorus and nitrogen are biologically removed in a modified University of Cape Town configuration in seven independent parallel cylindric plug-flow activated sludge tanks (Figure S3.1). Nutrient

removal occurred in four compartments: anaerobic (biological phosphorus removal), anoxic (denitrification), facultative (aerated when additional nitrification capacity was required), and aerobic (nitrification) (Figure S3.1). The setpoint for the dissolved O<sub>2</sub> concentration in the aerobic and facultative zones was set as function of the measured NH<sub>4</sub><sup>+</sup> concentration in the aerated compartment. The average sludge retention time (SRT) was 11-15 days and was controlled to maintain an average total suspended solids of 4.2 g·L<sup>-1</sup>. N<sub>2</sub>O was measured in the combined gas exhaust of all compartments (anaerobic + anoxic + facultative + aerobic) of a single lane using an Rosemount™ X-STREAM gas analyser (Emerson). NH<sub>4</sub><sup>+</sup>, NO<sub>3</sub><sup>-</sup> and N<sub>2</sub>O were measured in a single biological nutrient removal lane of the WWTP, NO<sub>2</sub><sup>-</sup> was measured in the pooled effluent of seven lanes.

### 3.2.2. *Ex situ* batch activity tests with full-scale activated sludge

The maximum nitrification and denitrification activities of the activated sludge were measured every two weeks between January 2021 and May 2022. For consistency, the sludge sampling, handling and storage, and the activity tests were always performed in the same manner. Samples were collected from the aerated compartment of the monitored full-scale activated sludge reactor and stored in two litre glass bottles in the fridge for a maximum of four hours. The sludge was transported under cold conditions (never reaching a temperature above 10 °C) and immediately placed in a 3 L jacketed glass bioreactor with a 2 L working volume (Applikon, Getinge). The sludge was made anoxic by sparging with N<sub>2</sub> for 1 h at 0.5 L·min<sup>-1</sup> (after which the bioreactor was sealed) and was incubated overnight with 50 mg N·L<sup>-1</sup> NaNO<sub>3</sub> to consume the internal carbon storages. During overnight storage and subsequent activity tests, the sludge was stirred at 750 rpm by two six-blade turbines, the temperature was maintained at 20 ± 1 °C using a cryostat bath (Lauda), and the pH was automatically maintained at 7.0 ± 0.1 by 1 M HCl and 1 M NaOH with two peristaltic pumps (Watson Marlow) controlled by an in-Control process controller (Applikon, Getinge). The pH and dissolved oxygen were continuously monitored with probes (Applikon AppliSens, Getinge). Influent gas flows were controlled by mass-flow controllers (Brooks). After overnight incubation with NO<sub>3</sub><sup>-</sup>, the sludge was activated by adding a spike of NaNO<sub>3</sub> (5 mg N·L<sup>-1</sup>) and a mixture of organic carbon (acetate, pyruvate, glucose, 37.5 mg COD·L<sup>-1</sup> each). The batch activity tests were sequentially performed on the same day in the following order: N<sub>2</sub>O, NO<sub>2</sub><sup>-</sup> and NO<sub>3</sub><sup>-</sup> reduction (denitrification), and NH<sub>4</sub><sup>+</sup> and NO<sub>2</sub><sup>-</sup> oxidation (nitrification) (Table 3.2). Before each batch, the depletion of the previous nitrogen compound was ensured. Substrates were added to the bioreactor with a syringe and needle through a rubber septum, marking the start of the batches. The batches' progress was monitored with NO<sub>2</sub><sup>-</sup> and NO<sub>3</sub><sup>-</sup> MQuant® colorimetric test strips (Merck).

Nitrogen compounds were added at 12 mg N·L<sup>-1</sup>, in the form of N<sub>2</sub>O (sparging 1.5% N<sub>2</sub>O + 98.5% N<sub>2</sub> at 0.5 L·min<sup>-1</sup> during 15-20 min), NaNO<sub>2</sub> (1.2 mL), NaNO<sub>3</sub> (1.2 mL) and NH<sub>4</sub>HCO<sub>3</sub> (1.2 mL) from concentrated stocks. The proportion bicarbonate to nitrogen was kept the same for the two nitrification batches by supplying 0.9 mM NaHCO<sub>3</sub> to the NO<sub>2</sub><sup>-</sup> oxidation batch. The organic carbon compounds were added at the start of the denitrification batches (each 75 mg COD·L<sup>-1</sup>, at least 2-fold higher than stoichiometrically needed) from anoxic concentrated stock solutions: sodium acetate (C<sub>2</sub>H<sub>3</sub>NaO<sub>2</sub>, 3 mL), sodium pyruvate (C<sub>3</sub>H<sub>3</sub>NaO<sub>3</sub>, 3 mL) and glucose (C<sub>6</sub>H<sub>12</sub>O<sub>6</sub>, 3 mL). The concentration of pyruvate was 4-fold lower in the batch tests from January until mid-August 2021, but this had no effect on the measured activities. Before each denitrification test, anoxic conditions were ensured by sparging N<sub>2</sub> at 0.5 L·min<sup>-1</sup> for 20 min, after which the reactor was sealed off from the exterior. The transition from anoxic to oxic conditions was achieved by sparging air at 0.5 L·min<sup>-1</sup> for at least 1 h. During each nitrification test, oxic conditions (> 70% air saturation) were ensured by continuously sparging air at 0.5 L·min<sup>-1</sup>. When necessary, foam formation was reduced with a few drops of six times diluted antifoam C 391 emulsion (Merck Life Science NV). For supernatant analysis, samples were taken every 3, 5, 10 or 15 min (depending on the length of the batches), and immediately filtered with a 0.45 µm PVDF Millex syringe filter (Merck) and placed on ice. The samples were stored at 4 °C until analysis on the following day.

**Table 3.1. Order and details of the nitrification and denitrification activity tests performed on a single day, every second week.** The denitrification tests (N<sub>2</sub>O, NO<sub>2</sub><sup>-</sup> and NO<sub>3</sub><sup>-</sup> reduction) were performed under anoxic conditions, with a mixture of organic carbon compounds as electron donor. Prior to each denitrification batch the broth was sparged with N<sub>2</sub> during 20 min to ensure anoxic conditions and remove intermediate nitrogenous gases. The nitrification tests (NH<sub>4</sub><sup>+</sup> and NO<sub>2</sub><sup>-</sup> oxidation) were performed with O<sub>2</sub> as electron acceptor, under continuous aeration. Between the denitrification and nitrification batches, the broth was made oxic by sparging air for 60 min. Each nitrogen compound was added at a final concentration of 12 mg N·L<sup>-1</sup>.

Batch	Electron donor	Electron acceptor	Length (min)	Sparging	Conditions
N <sub>2</sub> O reduction (DEN)	Acetate, pyruvate, glucose	N <sub>2</sub> O	24 - 105	Off	Anoxic
NO <sub>2</sub> <sup>-</sup> reduction (DEN)	Acetate, pyruvate, glucose	NO <sub>2</sub> <sup>-</sup>	25 - >150	Off	
NO <sub>3</sub> <sup>-</sup> reduction (DEN)	Acetate, pyruvate, glucose	NO <sub>3</sub> <sup>-</sup>	35 - >150	Off	
NH <sub>4</sub> <sup>+</sup> oxidation (AOB)	NH <sub>4</sub> <sup>+</sup>	O <sub>2</sub>	30 - >150	Air	Oxic
NO <sub>2</sub> <sup>-</sup> oxidation (NOB)	NO <sub>2</sub> <sup>-</sup>	O <sub>2</sub>	45 - >150	Air	

### 3.2.3. Analytical methods

The concentrations of NH<sub>4</sub><sup>+</sup>, NO<sub>2</sub><sup>-</sup> and NO<sub>3</sub><sup>-</sup> in the filtered supernatant were spectrophotometrically measured on the day following the batches, using the Gallery™ Discrete Analyzer (Thermo Fisher Scientific) or cuvette test kits (LCK339, LCK342 and LCK304, Hach Lange). When measuring NO<sub>3</sub><sup>-</sup> with the cuvette test kits, the samples were



diluted 1:1 with 20 g·L<sup>-1</sup> sulfamic acid to remove NO<sub>2</sub><sup>-</sup> as interference. The volatile suspended solids concentration (ash content subtracted from the dried biomass), measured in triplicate, was taken as proxy for the biomass concentration. Immediately upon arrival, 3x 25 mL of sludge was centrifuged at 4200 rpm for 20 min, the pellet was resuspended in 15 mL MilliQ water, dried at 105 °C (24 h) and burned at 550 °C (2 h). The concentrations of O<sub>2</sub>, CO<sub>2</sub> and N<sub>2</sub>O in the condenser-dried reactor off-gas were monitored by a Rosemount NGA 2000 off-gas analyser (Emerson). The dissolved N<sub>2</sub>O concentrations were monitored and recorded every minute with a standard N<sub>2</sub>O-R microsensor (customised concentration range 0.4 – 2 mM, Unisense) and a picoammeter PA2000 (Unisense). The dissolved N<sub>2</sub>O concentrations were calculated using the average of all calibrations performed 1-2 days before every batch series.

### 3.2.4. Calculations activity tests

The maximum NO<sub>2</sub><sup>-</sup> and NO<sub>3</sub><sup>-</sup> reduction and NH<sub>4</sub><sup>+</sup> and NO<sub>2</sub><sup>-</sup> oxidation rates were obtained through linear regression of the substrate concentration profiles over time. The slope was determined using at least four concentration points in the linear range. The maximum N<sub>2</sub>O reduction rate was calculated in Spyder IDE v5.1.5 using Python v3.9.12 and the NumPy v1.21.5<sup>45</sup>, SciPy v1.7.3<sup>46</sup> and Pandas v1.4.2<sup>47</sup> packages, taking into account the gas-liquid transfer between the reactor broth and headspace throughout the batch test (Supplementary Section 3.13). A system of ordinary differential equations (ODEs), representing the liquid and headspace mass balances, was defined to describe the gas-liquid transfer over time:

$$\frac{dc_{N_2O,liq}}{dt} = r_{N_2O} - k_L a \cdot (c_{N_2O,liq} - c_{N_2O,gas} \cdot \frac{K_{H,N_2O} \cdot R \cdot T}{p}) \quad (\text{eq. 3.1})$$

$$\frac{dc_{N_2O,gas}}{dt} = \frac{V_{liq}}{V_{gas}} k_L a \cdot (c_{N_2O,liq} - c_{N_2O,gas}) \quad (\text{eq. 3.2})$$

With  $c_{N_2O,liq}$  and  $c_{N_2O,gas}$  the N<sub>2</sub>O concentration in the liquid and headspace,  $r_{N_2O}$  the unknown N<sub>2</sub>O consumption rate,  $k_L a$  the experimentally determined volumetric mass transfer coefficient (5 h<sup>-1</sup>),  $K_{H,N_2O}$  the Henry coefficient (27.05 mM/atm),  $R$  the ideal gas constant (8.206 x 10<sup>-5</sup> L·atm·K<sup>-1</sup>·mmol),  $T$  the temperature,  $p$  the pressure, and  $V_{liq}$  and  $V_{gas}$  the broth and headspace volumes. The rates were obtained by fitting the model to the experimental data, i.e. by minimising the sum of squared errors between the experimentally measured and calculated (eq. 3.1-3.2) N<sub>2</sub>O concentrations (see code in Supplementary Section 3.13).

### 3.2.5. DNA extraction, library preparation and sequencing

Samples of 2 mL were taken immediately after cold transport of the sludge, and centrifuged at  $16,200 \times g$  for 5 min at 4 °C to separate the biomass from the supernatant. The biomass pellets were stored at -80 °C until DNA extraction. The DNA of the 12 Nov 2020, 9 Jun, 16 Dec 2021 and 11 May 2022 samples was extracted with the DNeasy PowerSoil Pro Kit (Qiagen). The manufacturer's instructions were followed, with exception of these steps: approximately 50 mg biomass was resuspended in the CD1 solution by vortexing before transferring to the PowerBead tube; 3 x 40 s bead-beating (Beadbeater-24, Biospec) was alternated with 2 min incubation on ice; tubes were gently inverted instead of vortexed to prevent DNA shearing<sup>48</sup>. The DNA of the 20 Jan and 3 Mar 2021 samples (1/3 pellet) was extracted with the DNeasy UltraClean Microbial Kit (Qiagen) following the manufacturer's instructions. The DNA concentration and quality were assessed with the Qubit 4 Fluorometer (Thermo Fisher Scientific) and the BioTek Synergy HTX multimode microplate reader (Agilent), respectively.

The samples of 12 Nov 2020 (np1), 9 Jun (np2), 16 Dec 2021 (np3) and 11 May 2022 (np4) were prepared for long-read sequencing using the Ligation Sequencing Kit V14 (Oxford Nanopore Technologies Ltd), the NEBNext® Companion Module for Oxford Nanopore Technologies® Ligation Sequencing (New England BioLabs) and UltraPure™ BSA (50 mg/mL) (Thermo Fisher Scientific). The incubations in the Hula mixer were replaced with slow manual inversions, all resuspensions were performed by flicking the tube, and the last room temperature incubation step was performed at 37 °C to improve the recovery of long DNA fragments. Four MinION R10.4 flow cells (Oxford Nanopore Technologies), one for each sample, were used to sequence on a MinION for 89-96 h in accurate mode (260 bps), yielding 21-29 Gbp per sample. The sample of 20 Jan 2021 (np1.5) was prepared with a Ligation Sequencing Kit V12 and sequenced on a GridION with MinION R9.4 flow cells (Oxford Nanopore Technologies), generating 11.2 Gbp. Short-read sequencing was also performed on the samples of 20 Jan (il1) and 3 Mar 2021 (il2) on an Illumina NovaSeq 6000 platform by Novogene Ltd. (UK), resulting in over 20 Gbp (per sample) of 150 bp paired-end reads with a 350 bp insert.

### 3.2.6. Processing of metagenomic data and MAG recovery

After sequencing, the DNA data was processed to obtain metagenome-assembled genomes (MAGs). The final set of MAGs was obtained from the five nanopore-sequenced samples (np1-4 and np1.5). The Illumina reads (il1 and il2) were solely used for differential coverage binning and to estimate the relative abundance of each MAG on the respective dates. The raw long reads were basecalled in super-accurate mode with the

“dna\_r10.4.1\_450bps\_sup.cfg” configuration file and --do\_read\_splitting option using Guppy v6.4.2 (np1-4) or with “dna\_r9.4.1\_450bps\_sup.cfg” using Guppy v5.0.7 (Oxford Nanopore Technologies) (np1.5). The duplex reads of np1-4 were filtered using pairs\_from\_summary and filter\_pairs from Duplex tools v0.2.19 (Oxford Nanopore Technologies). The duplex reads were basecalled using the duplex basecaller of Guppy and merged with the remaining simplex reads using SeqKit v2.3.0 <sup>49</sup>. The reads were filtered, trimmed and inspected with NanoFilt v2.8.0 <sup>50</sup> (options -q 10 -l 200), Porechop v0.2.4 (<https://github.com/rrwick/Porechop>) and NanoPlot v1.41.0 <sup>50</sup>. The Illumina reads were filtered and trimmed using Trimmomatic v0.39 <sup>51</sup> with the options LEADING:3 TRAILING:3 SLIDINGWINDOW:4:15 MINLEN:35 HEADCROP:5. The kmer algorithm of Nonpareil v3.401 <sup>52</sup> estimated a diversity coverage of 69.9% (il1) and 71.3% (il2) for the trimmed Illumina reads.

The long reads were individually assembled and pairwise co-assembled (np1-np2, np2-np3, np3-np4) with Flye v2.9.1 <sup>53</sup> in --meta mode. The reads were mapped on the assembly with Minimap2 v2.24 <sup>54</sup>. The individual assemblies were polished with Racon v1.4.3 (<https://github.com/isovic/racon>) and two times with Medaka v1.5.0 (<https://github.com/nanoporetech/medaka>). The reads from all samples were mapped to each assembly using Minimap2, the alignments were converted from SAM to BAM and sorted with SAMtools v1.10 <sup>55</sup> and the contig coverage in each sample was calculated with jgi\_summarize\_bam\_contig\_depths <sup>56</sup>. The differential coverages were used for automatic binning of each assembly with MetaBAT2 v2.15 <sup>56</sup>, MaxBin2 v2.2.7 <sup>57</sup> and CONCOCT v1.1.0 <sup>58</sup>, setting the minimum contig length at 2000 bp. The outputs were combined into an optimized set of non-redundant bins with DAS Tool v1.1.3 <sup>59</sup>, which used Prodigal v2.6.3 <sup>60</sup> and DIAMOND v2.0.8 <sup>61</sup>. The bins obtained from all assemblies (np1, np1.5, np2, np3, np4, np1-np2, np2-np3, np3-np4) were dereplicated with the 1083 HQ MAGs from Singleton *et al.* (2021) <sup>48</sup> at 95% average nucleotide identity of open reading frames using dRep v3.2.2 <sup>62</sup> with the options -comp 70 -con 10 -sa 0.95 --S\_algorithm gANI.

Bin completeness and contamination was assessed with the lineage\_wf workflow of CheckM v1.1.3 <sup>63</sup>. The relative abundance of the bins in each sample (np1, np2, np3, np4, il1, il2) was determined with CoverM v0.6.1 (<https://github.com/wwood/CoverM>), using the options --methods relative\_abundance mean --min-read-percent-identity 95 --min-read-aligned-percent 50. Bins with completeness < 90%, contamination > 5% or with zero abundance in all samples were discarded, resulting in a non-redundant set of 349 HQ MAGs. The HQ MAGs were taxonomically classified using the classify\_wf mode of GTDB-Tk v2.3.0 <sup>64</sup> and the GTDB release 207 <sup>65</sup> (gtdbtk\_r207\_v2\_data.tar.gz). The presence of 16S rRNA genes was verified with barrnap v0.9 (<https://github.com/tseemann/barrnap>). A bacterial phylogenetic tree was made with

FastTree v2.1.11 <sup>66</sup> using the multiple sequence alignment generated with the identify and align modes of GTDB-Tk, adjusted with the TreeTools v1.10.0 <sup>67</sup> package in RStudio v22.0.3 <sup>68</sup> with R v4.2.2 <sup>69</sup> and visualised with iTol v6.8.2 <sup>70</sup>.

## 3

### 3.2.7. Gene prediction and functional annotation

Genes were predicted in all assemblies using Prodigal v2.6.3 <sup>60</sup> with the -p meta option. The gene sequences were concatenated and duplicates were removed using grep and rmdup from SeqKit v2.3.1 <sup>49</sup>, resulting in a unique set of genes covering all metagenomic samples. The predicted genes were functionally annotated with the annotate pipeline of EnrichM v0.6.5 (<https://github.com/geronimp/enrichM>), using DIAMOND v2.0.8 <sup>61</sup> and HMMER v3.2.1 (<http://hmmerr.org/>) and the EnrichM v10 database, including a KO-annotated UniRef100 2018\_11 <sup>71</sup> DIAMOND database and HMM libraries of the KEGG 88.2 <sup>72</sup>, PFAM 32.0 <sup>73</sup>, and TIGRFAMs 15.0 <sup>74</sup> databases. In general, the genes of interest from the nitrogen cycle were identified by their KO identifier (Table S3.3). Cytochrome P460 was identified through its PFAM identifier PF16694. The genes encoding the alpha- and beta-subunit of the cytoplasmic nitrate reductase (*narG* and *narH*) and the nitrite oxidoreductase (*nxrA* and *nxrB*) have the same KO identifier, so these were distinguished through a phylogenetic analysis using the graft command of GraftM <sup>75</sup> and the respective packages (7.70.nxrA\_narG and 7.69.nxrB). If the alpha-subunit was classified as *narG* or *nxrA*, the putative beta-subunit located in the same contig was manually annotated. The unclassified sequences were left with the *narGH* annotation. The *nxrAB* genes from the *Ca. Nitrotoga* MAG (NOB) could not be distinguished with GraftM, but were confirmed with a BLAST on UniProt <sup>76</sup>. Similarly, the alpha-subunit of the ammonia monooxygenase gene (*amoA*) was distinguished from the methane monooxygenase gene (*pmoA*) using the 20170316\_pmoA package of GraftM. Unidentified sequences remained annotated as *pmoA*. The beta- and gamma-subunits located in the same contig as *amoA* were manually annotated as *amoB* and *amoC*. Distinction between the quinol-dependent nitric oxide reductase (qNor, encoded by *norZ*) and the alpha subunit of the cytochrome c-dependent reductase (cNor, encoded by *norB*), was made by identifying the fused quinol oxidase domain on the N-terminal of *norZ* <sup>77</sup>. A multiple sequence alignment was performed between putative NorB and NorZ protein sequences found in the metagenomes (K04561), and reference sequences of NorB (*Pseudomonas stutzeri*, P98008) and NorZ (*Cupriavidus necator*, Q0JYR9), extracted from UniProtKB <sup>76</sup>, using Clustal Omega v1.2.4 <sup>78</sup>. The alignment was visualised and analysed, and the quinol oxidase domain was identified with Jalview v2.11.3.2. The distinction between clade I and II nitrous oxide reductase, respectively TAT- and Sec-dependent, was made by combining the TIGRFAM annotation of EnrichM and the phylogenetic analysis of GraftM with the 7.45.nosZ package. The sequences not classified as either clade I or II remained annotated as unclassified *nosZ*. Data processing

was performed using RStudio v22.0.3 <sup>68</sup> with R v4.2.2 <sup>69</sup>, and the plyr v1.8.8 <sup>79</sup>, tidyverse v2.0.0 <sup>80</sup>, readxl v1.4.2 <sup>81</sup>, data.table v1.15.0 <sup>82</sup>, applot v0.2.2 <sup>83</sup> and reshape2 v1.4.4 <sup>84</sup> packages.

### 3.2.8. Protein extraction

Biomass samples were taken and stored as detailed in the DNA extraction section. Proteins were extracted from 12 samples, as previously described <sup>85</sup>. Briefly, around 60 mg of the biomass pellet were homogenised in three cycles of vortexing and ice incubation with glass beads (150 – 212 µm, Sigma Aldrich), 50 mM TEAB buffer 1% (w/w) NaDOC and B-PER reagent (Thermo Scientific). Proteins in the supernatant were precipitated with 1:4 trichloroacetic acid (Sigma Aldrich). The pellet was washed and disrupted with acetone two times and re-dissolved in 200 mM ammonium bicarbonate with 6 M Urea (Sigma Aldrich). Human serum albumin (0.1 µg, Sigma Aldrich) was added to all samples to control the digestion efficiency. The mixture was reduced with 10 mM dithiothreitol (Sigma Aldrich) at 37 °C for 60 min, and alkylated with 20 mM iodoacetamide (Sigma Aldrich) in the dark for 30 min. Samples were diluted with 100 mM ammonium bicarbonate to obtain a urea concentration lower than 1 M. Protein digestion occurred overnight at 37 °C and 300 rpm with 1.5 µg sequencing grade trypsin (Promega). 0.5 pmol of the Pierce™ Peptide Retention Time Calibration mix (Thermo Scientific) was added to all samples to control the chromatographic performance. Solid phase extraction was performed with an Oasis HLB 96-well µElution Plate (2 mg sorbent per well, 30 µm, Waters) and a vacuum pump. The columns were conditioned with MeOH, equilibrated with water two times, loaded with the peptide samples, washed with two rounds of 5% MeOH and sequentially eluted with 2% formic acid in 80% MeOH and 1 mM ammonium bicarbonate in 80% MeOH. The samples were dried in a centrifuge Concentrator plus (Eppendorf) at 45 °C and stored at -20 °C until analysis.

### 3.2.9. Shotgun metaproteomics

Peptide samples were dissolved in 20 µL of 3% acetonitrile and 0.01% trifluoroacetic acid, incubated at room temperature for 30 min and vortexed thoroughly. The protein concentration was measured at 280 nm wavelength with a NanoDrop ND-1000 spectrophotometer (Thermo Scientific) and samples were diluted to a concentration of 0.5 mg/mL. Shotgun metaproteomics was performed as previously described <sup>85</sup>, with a randomised sample order. Briefly, approximately 0.5 µg protein digest was analysed using a nano-liquid-chromatography system consisting of an EASY nano-LC 1200, equipped with an Acclaim PepMap RSLC RP C18 separation column (50 µm x 150 mm, 2 µm, Cat. No. 164568), and a QE plus Orbitrap mass spectrometer (Thermo Fisher Scientific). The flow rate was maintained at 350 nL/min over a linear gradient from 5%

to 25% solvent B over 90 min, from 25% to 55% over 60 min, followed by back equilibration to starting conditions. Solvent A was a 0.1% formic acid solution in water (FA), and solvent B consisted of 80% ACN in water and 0.1% FA. The Orbitrap was operated in data dependent acquisition (DDA) mode acquiring peptide signals from 385–1250  $m/z$  at 70 K resolution in full MS mode with a maximum ion injection time (IT) of 75 ms and an automatic gain control (AGC) target of 3E6. The top 10 precursors were selected for MS/MS analysis and subjected to fragmentation using higher-energy collisional dissociation (HCD) at a normalised collision energy of 28. MS/MS scans were acquired at 17.5 K resolution with AGC target of 2E5 and IT of 75 ms, 1.2  $m/z$  isolation width. The protein reference sequence database was generated through whole metagenome sequencing of the microbial samples, which included all metagenome-assembled genomes (MAGs) and unique unbinned sequences from all samples. The raw mass spectrometric data from each sample were analysed against this database using PEAKS Studio X (Bioinformatics Solutions Inc.) in a two-round database search process. The initial round was conducted without considering variable modifications and missed cleavages. Subsequently, the focused database was further searched, allowing for a 20 ppm parent ion and a 0.02  $m/z$  fragment ion mass error tolerance, up to 3 missed cleavages, and iodoacetamide as a fixed modification, with methionine oxidation and N/Q deamidation as variable modifications.

### 3.2.10. Metaproteomic data analysis

Peptide spectrum matches were filtered against 5% false discovery rates (FDR) and protein identifications with  $\geq 2$  unique peptide sequences were considered significant. The human serum albumin added as internal process control was filtered out. Proteins were grouped according to their unique protein group identification. The peptide spectral counts were divided by their molar mass for normalisation and technical duplicates were averaged. The relative abundance of each protein in a certain sample was determined by dividing the respective normalised spectral counts by the sum of normalised spectral counts of all proteins detected in that sample. The total relative abundance of each MAG in the metaproteome was calculated by summing the relative abundance of all proteins belonging to that MAG. The same was performed to calculate the total relative abundance of functionally identical proteins. Some functionally identical proteins belonging to different MAGs from the same genus could not be distinguished because of their high similarity. Therefore, these proteins were grouped by their functional annotation and genus for the data analysis. Proteins that simultaneously matched unbinned sequences and one or more MAGs from a certain genus, were classified as belonging to that genus. The catalytic subunits of the nitrogen-converting enzymes of interest were used as representative of that protein during data analysis, with exception of the ammonia monooxygenase (AMO). The catalytic alpha-

subunit (AmoA) is located in the cell membrane <sup>86</sup>, and is thus hydrophobic, so it is not well detected in the proteomic analysis (Figure S3.16). The beta-subunit (AmoB), only partially in the membrane, was detected in much higher amounts so it was here used as proxy for AMO. In any case, the results were similar for AmoA and AmoB, suggesting that both subunits are reliable for proteomic analysis (Figure S3.18). Data processing was performed using RStudio v22.0.3 <sup>68</sup> with R v4.2.2 <sup>69</sup>, and the plyr v1.8.8 <sup>79</sup>, tidyverse v2.0.0 <sup>80</sup>, readxl v1.4.2 <sup>81</sup>, data.table v1.15.0 <sup>82</sup>, applot v0.2.2 <sup>83</sup>, reshape2 v1.4.4 <sup>84</sup> and matrixStats v1.2.0 <sup>87</sup> packages.

### 3.3. Results

#### 3.3.1. Signature metabolite accumulation profiles

The ecophysiological response of N<sub>2</sub>O-emitting complex microbial communities to seasonal environmental and operational dynamics was studied using the Amsterdam-West wastewater treatment plant (WWTP) as model ecosystem (Figure 3.1A-B). The monitoring and sampling period lasted eighteen months and covered two highly comparable N<sub>2</sub>O emission peaks (Figure 3.2). The peaks occurred during periods with low water temperatures, namely Feb – May 2021 and Nov 2021 – Mar 2022, and were preceded by the sequential accumulation of NH<sub>4</sub><sup>+</sup>, O<sub>2</sub>, and NO<sub>2</sub><sup>-</sup> (Figures 3.2 and S3.2, Supplementary Data 1 [available online]). Central to the plant operation is the control of the dissolved O<sub>2</sub> (DO) concentration as a function of the residual NH<sub>4</sub><sup>+</sup> concentration in the aerated compartment. To counteract the temperature-induced nitrification rate reduction, and consequent NH<sub>4</sub><sup>+</sup> concentration increase, the weekly average DO concentration was increased from 1 up to almost 3 mg O<sub>2</sub>·L<sup>-1</sup> (Figure 3.2). In spite of this, O<sub>2</sub> remained the rate-limiting substrate for nitrification during low temperature periods with high N<sub>2</sub>O emissions, as evidenced by a lower O<sub>2</sub>/NH<sub>4</sub><sup>+</sup> ratio in the aerated compartment compared to warmer periods with low N<sub>2</sub>O (Figure S3.3). Following the increase in DO, the average NO<sub>2</sub><sup>-</sup> concentration in the pooled effluent rapidly increased up to 1.1 mg N·L<sup>-1</sup>. Finally, N<sub>2</sub>O started to accumulate, reaching maximum daily rates of 110 (1<sup>st</sup> peak) and 101 kg N·d<sup>-1</sup> (2<sup>nd</sup> peak) (Figures 3.2 and S3.2). The delay between the maximum DO concentration and the maximum N<sub>2</sub>O emission rate ranged between six and seven weeks for both peaks (Figure 3.2). This timeframe aligns with the imposed average sludge retention time of 11-15 days, indicating that seasonal N<sub>2</sub>O emissions are driven by changes in microbial composition and/or protein expression, rather than solely by shifts in microbial activity. Statistically, NO<sub>2</sub><sup>-</sup> strongly correlated with the O<sub>2</sub> concentration (Pearson correlation coefficient of 0.8), and N<sub>2</sub>O with NO<sub>2</sub><sup>-</sup> (correlation coefficient 0.7), while they only weakly correlated with all other parameters including the temperature (Figure S3.4 and Table S3.2).



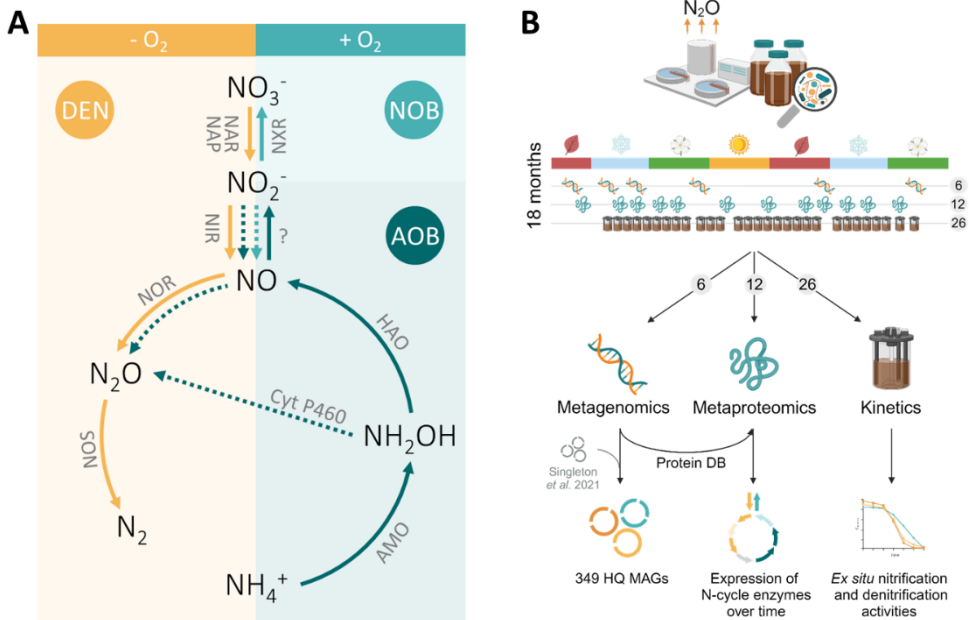


**Figure 3.1. Schematic representation of the nitrogen cycle, experimental approach and obtained datasets. (A)** Nitrogen conversions in the biological nitrogen removal process and respective enzyme complexes. Ammonia-oxidising bacteria (AOB) aerobically oxidise ammonium ( $\text{NH}_4^+$ ) to hydroxylamine ( $\text{NH}_2\text{OH}$ ) with the ammonia monooxygenase (AMO),  $\text{NH}_2\text{OH}$  to nitric oxide (NO) with the hydroxylamine oxidoreductase (HAO), and NO to nitrite ( $\text{NO}_2^-$ ) with a yet unknown enzyme. AOB can biologically produce  $\text{N}_2\text{O}$  through the oxidation of  $\text{NH}_2\text{OH}$  with cytochrome P460 (cyt P460) or through the reduction of NO – produced from  $\text{NH}_2\text{OH}$  oxidation or nitrifier denitrification ( $\text{NO}_2^-$  reduction with the nitrite reductase NIR) – with the nitric oxide reductase (NOR) (dotted arrows). Nitrite-oxidising bacteria (NOB) aerobically oxidise  $\text{NO}_2^-$  to nitrate ( $\text{NO}_3^-$ ) with the nitrite oxidoreductase (NXR) and encode NIR, but its activity and function remain to be resolved<sup>88–92</sup>. Normally under anoxic conditions, denitrifying bacteria (DEN) reduce  $\text{NO}_3^-$  to  $\text{NO}_2^-$  with the membrane-bound or periplasmic nitrate reductase (NAR, NAP),  $\text{NO}_2^-$  to NO with NIR, NO to  $\text{N}_2\text{O}$  with NOR and  $\text{N}_2\text{O}$  to  $\text{N}_2$  with the nitrous oxide reductase (NOS). Some DEN perform only some steps of the denitrification pathway while others perform the entire pathway. **(B)** Overview of the methodological approach adopted in this study for the eighteen-months characterisation of a full-scale WWTP to resolve the microbial mechanisms underlying seasonal  $\text{N}_2\text{O}$  emissions. Sludge samples were used for metagenomics (6 samples), metaproteomics (12 samples) and *ex situ* activity tests at 20 °C (26 samples). (Created with BioRender.com.)



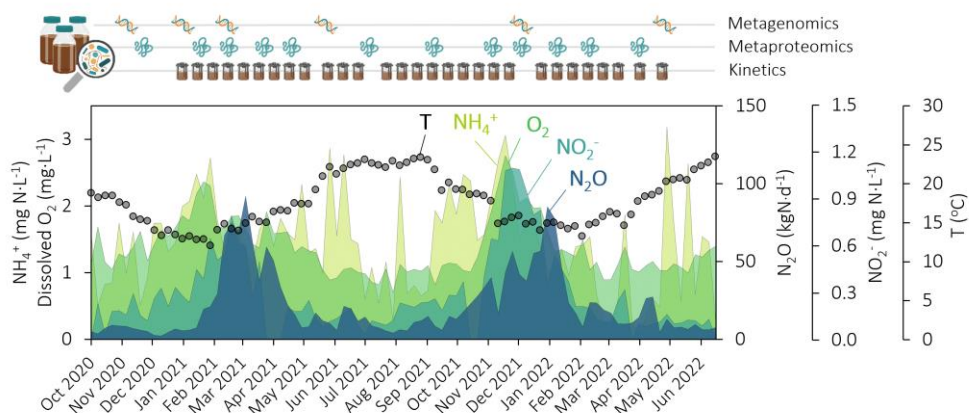


**Figure 3.2. Performance of the wastewater treatment plant (WWTP) monitored during nearly two years (Oct 2020 – Jul 2022).** Weekly average parameters at the WWTP, from back to front (light green to dark blue): concentration of  $\text{NH}_4^+$  and dissolved  $\text{O}_2$  in the nitrification compartment (left axis), pooled effluent  $\text{NO}_2^-$  concentrations (right axis),  $\text{N}_2\text{O}$  emission rates measured in the off-gas from all reactor compartments (right axis). The water temperature inside the reactor is represented on the right axis (symbols). All metabolites were measured in a single biological nutrient removal lane of the WWTP, except the effluent  $\text{NO}_2^-$  (seven lanes pooled together). Occasional sharp  $\text{NH}_4^+$  peaks were caused by outliers on rainy days (Figure S3.2). The scheme above the plot represents the sampling time points for metagenomic (DNA), metaproteomic (protein) and *ex situ* activity tests (bioreactor).

### 3.3.2. Maximum nitrogen metabolites conversion rates

To quantify seasonal changes in the microbiome metabolic potential, we estimated every second week the maximum oxidation and reduction rates of the main nitrification (i.e.  $\text{NH}_4^+$  and  $\text{NO}_2^-$ ) and denitrification (i.e.  $\text{NO}_3^-$ ,  $\text{NO}_2^-$  and  $\text{N}_2\text{O}$ ) intermediates, respectively. The maximum  $\text{NH}_4^+$  oxidation rate almost always exceeded the  $\text{NO}_2^-$  oxidation rate, with their difference being the highest in correspondence to the seasonal full-scale metabolite accumulation peaks (Figure S3.5, Supplementary Data 1 [available online]). No clear seasonality emerged in the  $\text{NO}_3^-$ ,  $\text{NO}_2^-$ , and  $\text{N}_2\text{O}$  maximum reduction rates, and the  $\text{N}_2\text{O}$  reduction capacity was 1.4 to 2.1-fold higher than all other nitrifying and denitrifying rates (Figure S3.5). The average  $\text{N}_2\text{O}$  accumulation rates remained negligible or constant during  $\text{NO}_3^-$  and  $\text{NO}_2^-$  reduction tests, respectively, throughout the seasons. In turn, the available data on  $\text{N}_2\text{O}$  accumulation rates during  $\text{NH}_4^+$  and  $\text{NO}_2^-$  oxidation tests show a higher degree of fluctuation (Figure S3.6A-D, Supplementary Data 1). The average  $\text{NO}_2^-$  accumulation rates were 6-fold higher during  $\text{NH}_4^+$  oxidation compared to  $\text{NO}_3^-$  reduction tests (Figure S3.6E).

### 3.3.3. Genome-resolved taxonomic diversity

3

The WWTP metagenome was sequenced at six time points to follow the dynamics in microbial composition and functional potential, and to serve as database for the metaproteomic analysis (Figure 3.1B). Combined short-read (two samples; average 147 million reads per sample) and long-read DNA sequencing (five samples, one of which also sequenced with short-reads; average 4.3 million reads per sample) resulted in 143 Gbp data, after quality filtering and trimming. A total of 349 high-quality metagenome-assembled genomes (HQ MAGs,  $\geq 90\%$  completeness and  $\leq 5\%$  contamination) (Figure 3.3, Supplementary Data 1 [available online]) were obtained. The 89 MAGs generated from the five long-read samples were dereplicated with the HQ MAGs from Singleton *et al.*<sup>48</sup> at 95% average nucleotide identity of open reading frames to increase the genome-resolved read coverage. From the final 349 HQ MAGs, 44 were unique to our dataset, 268 were unique to the dataset of Singleton *et al.*<sup>48</sup>, and 37 overlapped between both datasets (Figure S3.7). Overall, the HQ MAGs covered 31 phyla and 272 different genera, and included two archaeal species (only bacterial MAGs are represented in Figure 3.3). The full 16S rRNA gene was identified in 347 (99.4%) MAGs. The relative abundance of the individual MAGs showed no marked seasonal trend and little variation over the six time points (Figure S3.8 and Supplementary Data 1). We therefore discuss the average of their relative abundance among all samples. The two most abundant MAGs belonged to the *Ca. Microthrix* (4.0%) and *Nitrospira* (2.7%) genera (Figure 3.3). All other MAGs had an average relative abundance lower than 1%. The majority of the non-nitrifying MAGs contained at least one denitrification gene (DEN, 304) (Figure 3.3, Supplementary Data 1 [available online]). 51 MAGs had the genetic potential to perform dissimilatory nitrite reduction to ammonia (DNRA, containing the *nrfAH* genes), 46 of these also had at least one denitrification gene (Figure S3.15, Supplementary Data 1). Seven MAGs harboured the *amoABC* genes (AOB) and eight harboured the *nxrAB* genes (NOB), most of these also had at least one denitrification gene, mainly *nir* and *nor* encoding the NO<sub>2</sub><sup>-</sup> and NO reductases, respectively (Figure S3.15, Supplementary Data 1). Neither complete ammonia-oxidising (comammox), AOA, nor anaerobic ammonia-oxidising (anammox) MAGs were found in the metagenomes.

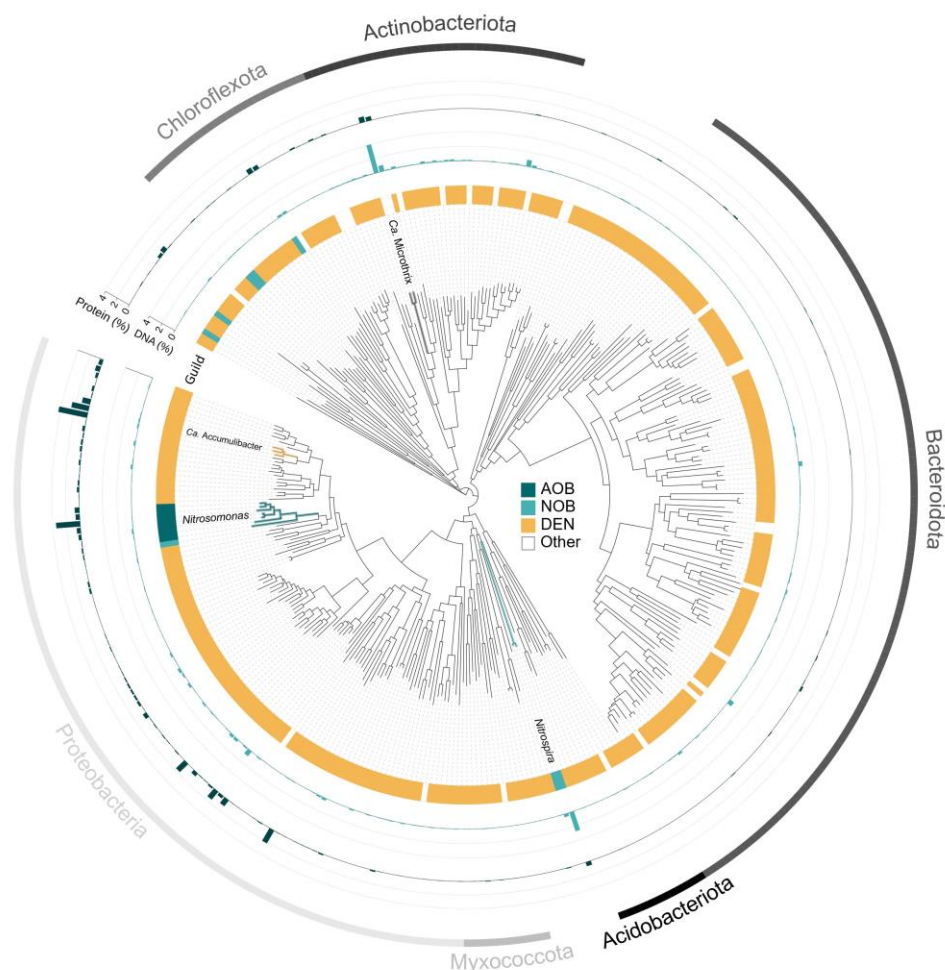


**Figure 3.3. Phylogenetic tree of the 347 bacterial high-quality MAGs extracted from activated sludge (the only two archaeal MAGs are not represented).** From the inner to the outer circle: (i) circular phylogenetic tree with the identification of key activated sludge genera *Nitrosomonas*, *Nitrospira*, *Ca. Accumulibacter* and *Ca. Microthrix*; (ii) identification of ammonia-oxidising bacteria (AOB, containing *amoABC* genes, dark blue), nitrite-oxidising bacteria (NOB, containing *nrxAB* genes, light blue) and denitrifying organisms (DEN, non-AOB and non-NOB MAGs harbouring at least one denitrification gene, yellow). Some of the AOB and NOB MAGs also contained one or more denitrification genes (Supplementary Data 1); (iii) average DNA relative abundance of each MAG in the community; (iv) average protein relative abundance of each MAG in the community; (v) identification of the six most abundant phyla.

### 3.3.4. Metaproteomic-based functional profile

The dynamics in protein expression of the entire microbial community across twelve samples was assessed by shotgun metaproteomics. We used the protein expression as proxy for active metabolisms and to estimate the protein-based relative abundance of

each MAG. In total, 3868 unique protein groups were detected, and 1884 had at least two unique peptides (accounting for  $44 \pm 1\%$  of the total mass-normalised spectral counts). 1105 of the identified proteins (accounting for  $68 \pm 1\%$  of the two unique peptides filtered normalised spectral counts) uniquely matched with a single protein predicted in the metagenome (including all MAGs and unbinned sequences). The remaining 779 proteins (accounting for  $32 \pm 1\%$  of the two unique peptides filtered normalised spectral counts) matched multiple highly similar proteins and could not be linked to a single MAG, yet could be functionally and taxonomically annotated at the genus level. Out of the 349 HQ MAGs, proteins from 143 MAGs (101 genera) were detected (Supplementary Data 1). The HQ MAGs covered  $39 \pm 1\%$  of the total protein pool, higher than the  $28 \pm 4\%$  coverage of the total community DNA (Figure 3.4A). On average, the relative abundance of key activated sludge taxa (e.g. *Ca. Microthrix*, *Ca. Accumulibacter*, *Nitrosomonas* and *Nitrospira*,) differed up to 20-fold between the metagenomic and metaproteomic approaches (Figure S3.13). For example, the AOB:NOB ratio was 0.1 in the metagenome and 3.6 in the metaproteome (discussed in Supplementary Section 3.6). Taxonomically, the diversity was greatest within the DEN guild (proteins from 124 MAGs were detected) with no clear dominant MAG (Figure 3.4B). Owing to this high diversity, many DEN organisms were present in too low abundance to be recovered as MAGs even at the already high sequencing depth employed here (20-25 Gbp per sample). Consequently, DNA sequences from many DEN remained in the unbinned portion of the metagenomes, resulting in the majority of the detected denitrification enzymes, namely nitrate, nitrite and nitrous oxide reductases being assigned to the unbinned fraction (Figure S3.16). Proteins from all seven AOB and four NOB MAGs were detected in the metaproteome. The AOB consisted entirely of *Nitrosomonas* MAGs, and were dominated by one MAG (Figure 3.4B). NOB were dominated by a *Nitrospira* and a *Chloroflexota* MAG belonging to the *Promineofilaceae* family (Figure 3.4B), but the alpha- and beta-subunits of the nitrite oxidoreductase (NxrA and NxrB) were only expressed by *Nitrospira* and *Ca. Nitrotoga* (Figure S3.16). Almost all detected nitrifying enzymes belonged entirely to the recovered MAGs, highlighting the nearly full coverage of the active nitrifying community by the MAGs (Figure S3.16). Throughout the monitoring period, the relative proteomic abundance of DEN hardly fluctuated, and the AOB and NOB guilds fluctuated similarly over time (Figure 3.4C). The maximum guild-specific fold change in the proteome was 1.1 (DEN), 1.8 (AOB) and 2.5 (NOB). Overall, there were no major shifts in the MAG-based composition of each guild, at both DNA and protein level (Figures S3.9-S3.11), and there were no significant correlations between protein-level taxa abundance and WWTP performance (Table S3.4).

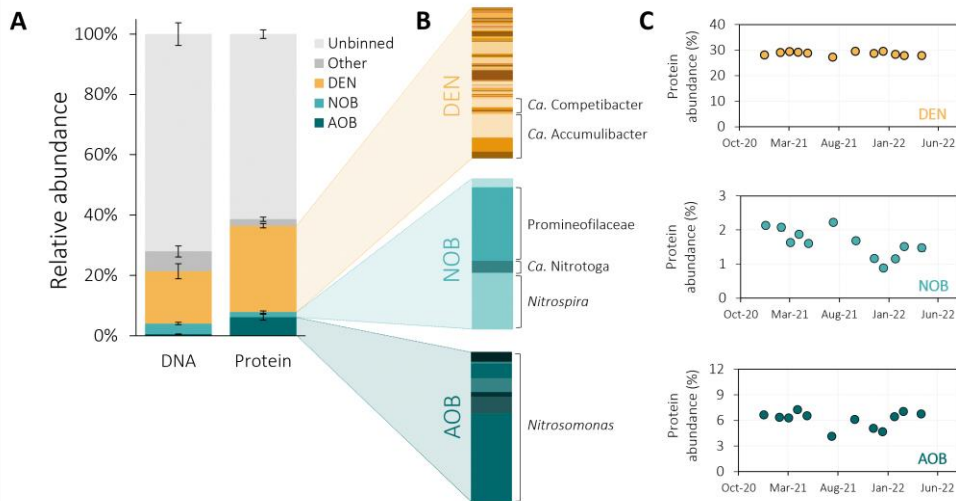


**Figure 3.4. MAG-based functional guild distribution in the metagenomes and metaproteomes of the activated sludge.** **(A)** Average relative abundance of denitrifying bacteria (DEN, non-AOB and -NOB MAGs containing at least one denitrification gene, yellow), nitrite-oxidising bacteria (NOB, containing *nxrAB* genes, light blue), ammonia-oxidising bacteria (AOB, containing *amoABC* genes, dark blue), other metagenome-assembled genomes (dark grey) and unbinned sequences (light grey) in the total metagenome (DNA) and metaproteome (Protein) of the activated sludge. Some of the AOB and NOB MAGs also contained one or more denitrification genes (Supplementary Data 1). The boxes represent the mean and the error bars represent the standard deviation within six (DNA) and twelve (protein) activated sludge samples taken at different time points throughout eighteen months. **(B)** MAG-based composition of the DEN, NOB and AOB guilds. The most abundant genera in the DEN (*Ca. Accumulibacter* and *Ca. Competibacter*), NOB (unidentified *Promineofilaceae* genus, *Ca. Nitrotoga*, *Nitrospira*) and AOB (*Nitrosomonas*) guilds are highlighted. **(C)** Temporal fluctuations in the relative protein abundance of the DEN (yellow), NOB (light blue) and AOB (dark blue) guilds. The error bars represent standard deviations between technical duplicates and are all smaller than the symbols.

### 3.3.5. Unbalanced nitrification drives seasonal nitrite accumulation

The net accumulation and potential emission of any nitrogen intermediate results from the unbalance between its production and consumption rates. Nitrite, a central metabolite exchanged between AOB, NOB and DEN (Figure 3.1A), always accumulated prior to the N<sub>2</sub>O peaks (Figure 3.2). To understand the NO<sub>2</sub><sup>-</sup> flux balance dynamics, we focused on the DNA, expressed proteins and *ex situ* activity ratios of NO<sub>2</sub><sup>-</sup>-producing and -consuming guilds. At all levels (genomic, proteomic and kinetic), the DEN guild did not display significant seasonal dynamics (Figures 3.4C, S3.9 and S3.20). Contrastingly, the (un)balance between AOB (NO<sub>2</sub><sup>-</sup> producer) and NOB (NO<sub>2</sub><sup>-</sup> consumer) fluctuated the most during the monitored period. The ratio between the total abundances of AOB and NOB, both at DNA and protein level, was up to 3-fold higher during periods of high effluent NO<sub>2</sub><sup>-</sup> concentrations, compared to the rest of the year (Figure 3.5A-B). At individual protein level, including MAG and unbinned proteins, the ratio between the

expression of the key  $\text{NH}_3$ -consuming enzyme (represented by the beta-subunit of the ammonia monooxygenase – AmoB) and  $\text{NO}_2^-$ -producing enzyme (represented by the hydroxylamine oxidoreductase – Hao) of AOB relative to the catalytic subunit of the  $\text{NO}_2^-$  oxidoreductase of NOB (NxrA) were also higher (Figure 3.5C, Supplementary Data 1 [available online]). Consistently, the ratio between the maximum  $\text{NH}_4^+$  and  $\text{NO}_2^-$  oxidation activities was larger during high  $\text{NO}_2^-$  concentration periods (Figure 3.5D).

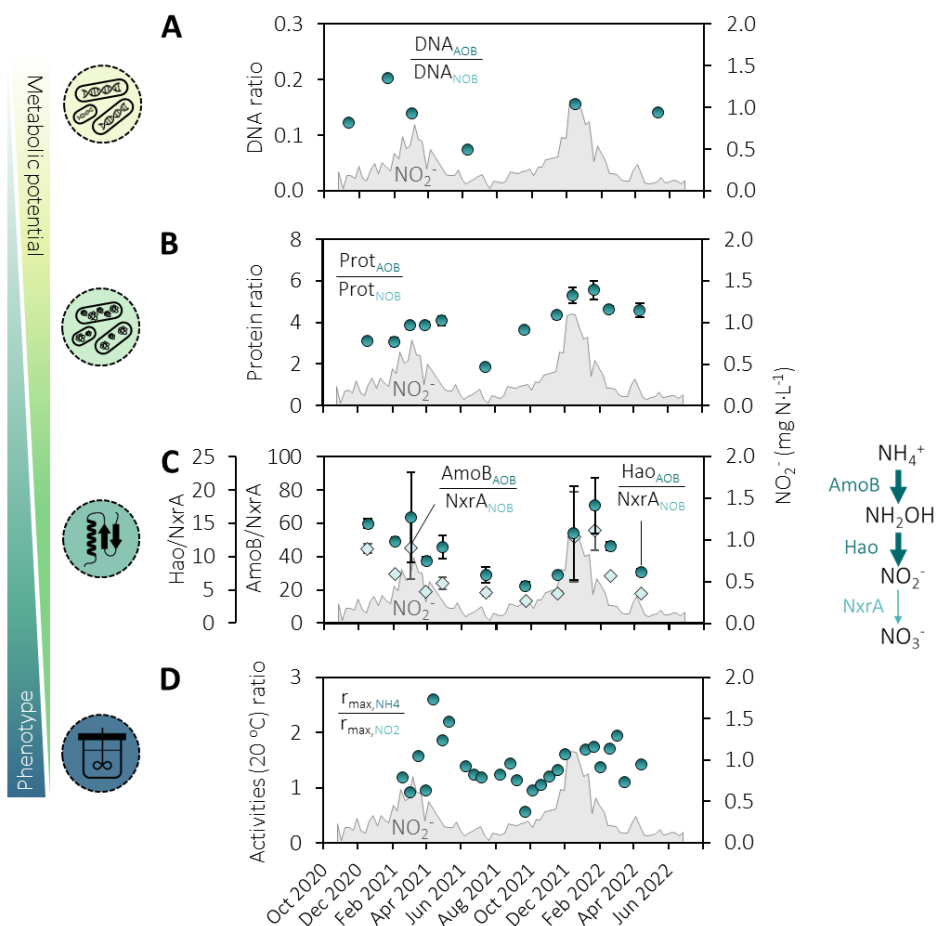


**Figure 3.5. Genomic, proteomic and maximum activity fluctuations of AOB and NOB in activated sludge during periods of high and low nitrite accumulation.** Left axes: **(A)** Ratio between the total relative DNA abundance of ammonia- (AOB) and nitrite-oxidising bacteria NOB (circles). **(B)** Ratio between the total relative protein abundance of AOB and NOB (circles). The symbols represent the mean and the error bars represent standard deviations of technical duplicates independently injected in the LC-MS/MS, some are smaller than the symbols. **(C)** Ratios between the relative abundance of  $\text{NO}_2^-$ -producing and -consuming enzymes of AOB and NOB, respectively: beta-subunit of the ammonia monooxygenase (AmoB) divided by the catalytic subunit of nitrite oxidoreductase (NxrA) (diamonds); and hydroxylamine oxidoreductase (Hao) divided by NxrA (circles). The enzyme abundances include the proteins belonging to the MAGs and the unbinned fraction. The symbols represent the mean and the error bars represent standard deviations of



technical duplicates independently injected in the LC-MS/MS, some are smaller than the symbols. The respective enzymatic conversions are represented on the right. **(D)** Ratio between the maximum *ex situ* NH<sub>4</sub><sup>+</sup> and NO<sub>2</sub><sup>-</sup> oxidation rates measured at 20 °C (circles). **Right axes: (A-D)** Weekly average NO<sub>2</sub><sup>-</sup> concentration in the effluent (seven parallel lanes pooled together, grey area). The correlation coefficients between WWTP parameters and the microbial ratios represented here and their statistical significance can be found in supplementary information (Table S3.6).

### 3.3.6. Overexpressed nitrifier denitrification during N<sub>2</sub>O accumulation

In analogy to nitrite, we used ratios between the relative abundance of enzymes directly or indirectly producing and consuming N<sub>2</sub>O as proxy for the N<sub>2</sub>O flux balance. The total enzyme abundances include MAG and unbinned protein abundances (Supplementary Data 1). The seasonally accumulated NO<sub>2</sub><sup>-</sup> can be reduced to N<sub>2</sub>O by both AOB and DEN, sequentially using the Cu- (NirK) or *cd1*-type (NirS) NO<sub>2</sub><sup>-</sup> reductases and the nitric oxide reductase (Figure 3.1A). Here, NirK and NirS were exclusively expressed by nitrifiers and DEN, respectively (Figure S3.16). Four *Nitrosomonas* (AOB) and one *Nitrospira* MAG (NOB) accounted for most of the NirK expression (75% and 17%, respectively) (Figure S3.16). Within the nitrifying community, the relative abundance of NirK over the key AOB enzymes AmoB and Hao was the highest during periods of high NO<sub>2</sub><sup>-</sup> and N<sub>2</sub>O accumulation (Figure 3.6A). The ratio of total relative abundance of NirK over the competing NO<sub>2</sub><sup>-</sup>-oxidising NxrA (NOB) and NO<sub>2</sub><sup>-</sup>-reducing NirS (DEN) followed a similar trend (Figure 3.6B). NosZ is the only known N<sub>2</sub>O-reducing enzyme, and the ratio NirK/NosZ clearly reflected the seasonal dynamics, being higher during seasonal peaks (Figure 3.6C). Similarly, yet to a significantly lower extent, also the ratio between the hydroxylamine (NH<sub>2</sub>OH) producing AmoB and consuming Hao and CytP<sub>460</sub> (Figure S3.19), and the ratio NirS/NosZ (Figure S3.20C) displayed some seasonality. The here employed protein extraction protocol does not allow for the quantification of membrane-bound proteins, such as the nitric oxide reductases<sup>93</sup>, which were therefore not included in the discussion. All microbial ratios (Figures 3.5 and 3.6) negatively correlate with temperature, and overall positively correlate with ammonia, dissolved oxygen, nitrite, and nitrous oxide emissions (Table S3.6).

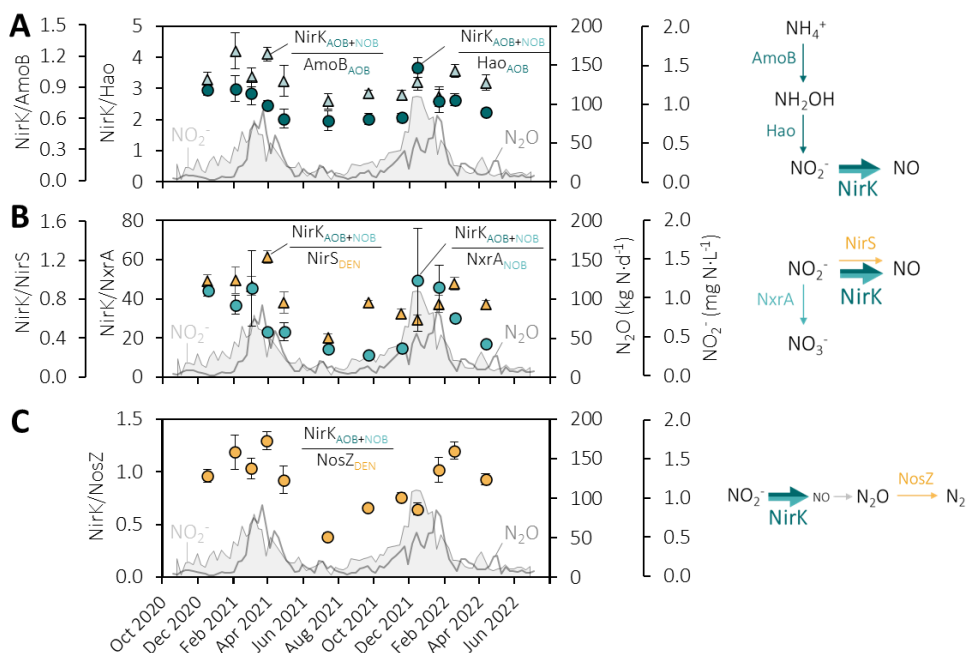


**Figure 3.6. NirK overexpression relative to other nitrogen enzymes during periods of high NO<sub>2</sub><sup>-</sup> concentrations and N<sub>2</sub>O emissions.** Left axes (symbols): The symbols represent the mean and the error bars represent standard deviations of technical duplicates independently injected in the LC-MS/MS, some are smaller than the symbols. **(A)** NirK vs. other AOB enzymes. Ratio between the total relative abundance of NO<sub>2</sub><sup>-</sup>-consuming NirK and the other key AOB enzymes Hao (circles) and AmoB (triangles). **(B)** NirK vs. competing NO<sub>2</sub><sup>-</sup> consuming enzymes. Ratio between the total relative abundance of NO<sub>2</sub><sup>-</sup>-consuming NirK and the NO<sub>2</sub><sup>-</sup> competing NxrA (circles, NOB) and NirS (triangles, DEN). **(C)** NirK in N<sub>2</sub>O balance. Ratio between the total relative abundance of NirK (producing the N<sub>2</sub>O precursor NO) and the only known enzymatic N<sub>2</sub>O-sink N<sub>2</sub>O reductase (NosZ) (circles). The enzyme abundances include the proteins belonging to the MAGs and the unbinned fraction. The error bars in the protein ratios were propagated from standard deviations of technical duplicates. All enzymatic conversions are schematically represented on the right. NirK is expressed by both AOB and NOB, but the activity and function of the enzyme in NOB are yet unknown. **Right axes: (A-C)** Weekly average NO<sub>2</sub><sup>-</sup> concentration in the effluent of the WWTP (seven parallel lanes pooled together, grey area) and N<sub>2</sub>O emission rates measured in the off-gas from all the reactor compartments in one lane at the WWTP (grey line). The correlation coefficients between WWTP parameters and the microbial ratios represented here and their statistical significance can be found in supplementary information (Table S3.6).

### 3.4. Discussion

We postulate that the seasonal accumulation of NO<sub>2</sub><sup>-</sup> and subsequent emissions of the potent greenhouse gas N<sub>2</sub>O at a full-scale WWTP are related to fluctuations in the balance of key nitrogen-converting populations, rather than their individual abundance or activity. No major changes in the DNA and protein composition, nor significant correlations with plant performance, were observed throughout eighteen months of operation. This is consistent with previous metagenomic and 16S rRNA gene amplicon



sequencing reports in WWTPs<sup>94–97</sup>. The microbiome was dominated by a taxonomically diverse DEN community (74% of the binned community proteome), in line with most genomic and transcriptional analyses of conventional WWTPs<sup>29,98,99</sup>. While the high DEN abundance may have masked fluctuations at guild level, the absence of significant changes at the activity and individual protein level further supports the DEN stability. Instead, the DNA and protein abundances of the nitrifying community, dominated by one AOB and two NOB MAGs, fluctuated over time, yet not consistently with the observed nitrogen oxides accumulation dynamics. This aligns with most studies reporting limited to no correlation between AOB and NOB 16S rRNA gene abundances and seasonal nitrification failures<sup>44</sup>, or AOB and NOB conversion rates and N<sub>2</sub>O production<sup>32</sup>. Only few studies observed a correlation between increased N<sub>2</sub>O emissions and increased relative AOB abundances (16S)<sup>100</sup>, AOB *ex situ* activities<sup>101</sup>, or decreased NOB abundances (16S)<sup>29,33</sup>. Yet evidence remains sparse and seemingly conflicting, ultimately hindering mechanistic generalisations. This lack of general consensus resides in the fundamental dependency between metabolite dynamics and the trade-off between their production and consumption rates (i.e. the balance between the producing and consuming guilds), rather than their individual magnitudes.

Against a relatively stable DEN community, featuring a fairly constant nitrite production and reduction potential, we identified the unbalance between AOB (NO<sub>2</sub><sup>-</sup> producer) and NOB (NO<sub>2</sub><sup>-</sup> consumer) as the primary cause for seasonal nitrite accumulation. During the nitrite peaks preceding the N<sub>2</sub>O ones, a higher ratio of AOB over NOB was observed at genomic, proteomic and kinetic levels. To date, only Bae et al.<sup>32</sup> quantitatively linked N<sub>2</sub>O emissions with increased AOB/NOB *ex situ* activity ratios in an otherwise stable nitrifying community based on 16S rRNA gene sequencing. Gruber et al.<sup>33</sup> observed stable AOB but lower NOB and filamentous bacteria 16S rRNA gene abundances during winter N<sub>2</sub>O emissions, and hypothesised a selective NOB washout due to compromised floc integrity. Here, the fluctuations in the sludge settleability (representing floc integrity) and in the DNA and protein abundances of *Ca. Microthrix* (filamentous bacteria) did not follow the full-scale metabolite profiles, nor the NOB abundance or the AOB/NOB ratio (Figures S3.2, S3.12 and Table S3.2). The known higher sensitivity of NOB to the toxic free ammonia and nitrous acid compared to AOB<sup>102–104</sup> has also been suggested as potential cause for nitrite accumulation<sup>103</sup>. However, in our case, the estimated concentration of free ammonia (0.03 mg N·L<sup>-1</sup>) and nitrous acid (0.001 mg N·L<sup>-1</sup>) were far below the NOB toxicity thresholds (Tables S3.6–S3.7)<sup>102–105</sup>. Instead, we argue that the unbalanced AOB/NOB ratio results from a cascade of separate environmental and operational perturbations differentially impacting their respective growth rates (Figure 3.7). The decrease in temperature reduces both AOB and NOB growth rates, and may alone promote the selective washout of the slower-growing NOB (as estimated in this work and consistent with literature values; Table S3.9, Figure

S3.22). In addition, reduced AOB rates lead to the accumulation of ammonium, with the operationally undesired worsening of effluent quality. In response, most WWTPs increase the operational dissolved O<sub>2</sub> set point to promote nitrification. The increased availability of ammonium selectively favours AOB, while, in principle, the increase in dissolved O<sub>2</sub> positively impacts the growth rate of both AOB and NOB. However, the reported lower AOB apparent affinity for O<sub>2</sub> in activated sludge<sup>106–109</sup> likely favours AOB over NOB, further enhancing the initial differential temperature impact on their growth rates. Ultimately, nitrite accumulation is the result of the progressive relative enrichment of AOB over NOB. To test our hypothesis, we developed and implemented a mathematical model based on the experimentally estimated kinetic parameters and literature-derived stoichiometric parameters (Tables S3.9–S3.12). The model comprised all three known metabolic pathways leading to N<sub>2</sub>O formation, and reproduced all observed seasonal metabolites peaks induced by decreasing temperatures and consequent increase in ammonium and operational dissolved O<sub>2</sub>. The simulations also captured the progressive relative biomass increase of AOB over NOB (Figure S3.24). These results strongly indicate that the sequential seasonal nitrogen oxides peaks result from a cascade of distinguishable events, where temperature is the initial trigger but not the sole direct cause, as commonly hypothesised. The absence of a single parameter correlating with nitrite and subsequent N<sub>2</sub>O emissions likely explains the difficulties of past studies to identify direct correlations<sup>28,34,43</sup>. Importantly, the dissolved O<sub>2</sub> concentration emerged as the central operational parameter to act upon, and we posit that the AOB/NOB unbalance may be largely prevented by anticipating in time, i.e. before measurable NH<sub>4</sub><sup>+</sup> accumulation, the operational O<sub>2</sub> increase.

The last metabolite to accumulate along the reconstructed ecophysiology cascade is N<sub>2</sub>O. Relative increases in nitrite concentrations are well-known to lead to N<sub>2</sub>O emissions through both nitrifier and heterotrophic denitrification<sup>3</sup>, yet the dominant pathway underlying seasonal N<sub>2</sub>O emissions remains unclear<sup>31,34,101</sup>. Abiotic conversions can reasonably be neglected in conventional WWTPs such as the one analysed here<sup>8,18</sup>, as the precursor reactive nitrogen species (NH<sub>2</sub>OH, NO, NO<sub>2</sub><sup>-</sup>) are known to accumulate primarily at lower pHs in systems treating higher-strength wastewaters, such as digester supernatant, and partial nitrification reactors<sup>8,18,110</sup>. We use the nitrite reductases (NirK and NirS) as proxy for N<sub>2</sub>O production, and their genome-resolved taxonomy to differentiate between nitrifier and heterotrophic denitrification. Considering the fast turnover of NO<sup>8</sup>, the use of Nir allows to overcome the challenges in detecting the membrane-bound hydrophobic nitric oxide reductase in metaproteomic analyses<sup>111,112</sup>. Unbalanced heterotrophic denitrification is unlikely to be the main N<sub>2</sub>O producing pathway during the seasonal emissions, owing to the relatively constant ratio between NirS and NosZ, both exclusively expressed by DEN, and their rates. The marginal contribution of denitrification to N<sub>2</sub>O emissions under the WWTP conditions

is further supported by the developed mathematical model, where denitrification was always a net consumer of N<sub>2</sub>O (Figure S3.24). The nitrite reductase NirK was exclusively expressed by nitrifiers, primarily by AOB, so it was used as proxy for nitrifier denitrification. NOB *Nitrospira* contributed to about one fifth of the total detected NirK, but its activity and function remain to be experimentally verified (hitherto measured activities are low)<sup>88-92</sup>. A marked increase in the ratio of NirK over other AOB enzymes (AmoB and Hao) and the competing NO<sub>2</sub><sup>-</sup>-consuming enzymes (NxrA from NOB and NirS from DEN) was observed during the seasonal nitrogen oxide peaks. The higher expression of NirK could have been induced by the seasonally increased ammonia, nitrite, and/or nitric oxide concentrations<sup>112-115</sup>, and may suggest an increased relative nitrite flux towards nitrifier denitrification rather than nitrite oxidation or heterotrophic nitrite reduction. Emissions also coincided with periods in which O<sub>2</sub> was identified as the metabolically limiting substrate for AOB (i.e. lower O<sub>2</sub>/NH<sub>4</sub><sup>+</sup> ratios compared to the rest of the year), likely forcing AOB to resort to nitrifier denitrification as additional electron sink<sup>116,117</sup>. The potential existence of an alternative nitrite reductase warrants caution on the use of NirK as the sole proxy for nitrite reduction in AOB. Sustained nitrite reduction and N<sub>2</sub>O production by *nirK*-deficient *Nitrosomonas europaea* mutant cells has been documented in batch experiments<sup>118-121</sup>. Yet, the hypothesised alternative nitrite reduction mechanism is suggested to be solely stimulated in the absence of NirK<sup>118</sup>. Moreover, another study showed that *nirK*-deficient *N. europaea* did not reduce nitrite in a chemostat and produced N<sub>2</sub>O abiotically from hydroxylamine<sup>122</sup>. The universal existence and physiological role of an alternative nitrite reductase in AOB remains therefore to be confirmed. Importantly, consistent across all studies is the centrality of NirK for efficient NH<sub>3</sub> oxidation and AOB growth<sup>118,119,122</sup>. NirK can quickly regenerate electron carriers needed for Hao, avoiding nitrosative stress caused by NH<sub>2</sub>OH (and NO) accumulation during high NH<sub>3</sub> turnover<sup>112,118,119,123</sup>. In line with this, the observed slight imbalance between hydroxylamine-producing AmoB and -consuming Hao and Cyt P460 in the metaproteome suggests that hydroxylamine accumulated as a result of the kinetic O<sub>2</sub> limitation<sup>116</sup>, further supporting an electron unbalance in the AOB metabolism and the increased need for NirK as electron sink. Optimised membrane metaproteomics could fill the gap in the nitrifier denitrification pathway by clarifying whether the Nor dynamics aligns with NirK<sup>124,125</sup>. To date, only one report suggested a correlation between N<sub>2</sub>O emissions in WWTPs and *nirK* gene transcripts abundance, quantified by RT-qPCR<sup>126</sup>. Yet, the *nirK* transcripts were not taxonomically classified and were assumed to entirely belong to heterotrophic denitrifiers<sup>126</sup>. All other studies discussing seasonal N<sub>2</sub>O emissions in WWTPs infer the main N<sub>2</sub>O-producing pathways based on metabolite profiles, and a general consensus is still lacking<sup>28,30,31,34,101</sup> (Table S3.1). Most studies identified nitrifier or heterotrophic denitrification as the main N<sub>2</sub>O-producing pathway in WWTPs using isotopic signatures<sup>127-129</sup>, but seasonal dynamics were not captured. Even more

importantly, the isotopic signatures of the produced  $\text{N}_2\text{O}$  (from natural abundance or  $^{15}\text{N}/^{18}\text{O}$  tracers) largely overlap when nitrite is the starting substrate, since the biochemical pathways of nitrifier and heterotrophic denitrification are identical and rely on the same enzymes. This challenges the possibility to univocally distinguish the two pathways in ecosystems where they potentially co-occur (previously reviewed <sup>9,130,131</sup>). Instead, by integrating metagenomic-guided metaproteomics with kinetic analyses and full-scale operational data we provide independent evidence on multiple ecophysiological levels, further supported by mathematical modelling, identifying nitrifier denitrification as the prime  $\text{N}_2\text{O}$ -producing pathway during seasonal emissions. More broadly, our results demonstrate the untapped potential of multi-meta-omics integration in biotechnological developments to reduce anthropogenic impacts by resolving the complexity and advancing the engineering of microbiomes.

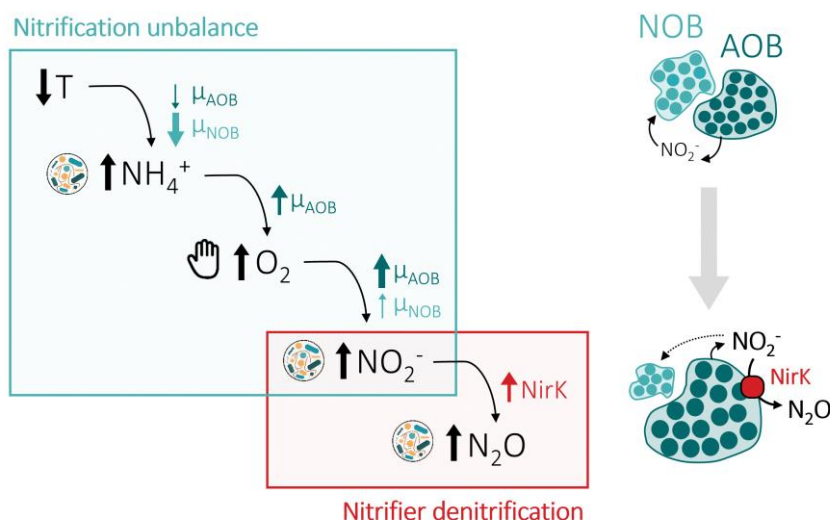


**Figure 3.7. Schematic representation of the proposed ecophysiological cascade underlying seasonal  $\text{N}_2\text{O}$  emissions in WWTPs.** A decrease in temperature causes lower growth rates of ammonia- (AOB) and nitrite-oxidising bacteria (NOB), promoting ammonium accumulation and a selective washout of the slower-growing NOB; the resulting increased ammonium concentrations stimulate the growth of AOB and induce the process control to increase the operational dissolved  $\text{O}_2$  concentration; the increased  $\text{O}_2$  concentrations increase the growth rates of both AOB and NOB, but may selectively benefit AOB with a lower apparent affinity for  $\text{O}_2$ . The resulting increased AOB/NOB ratio causes the accumulation of nitrite and consequent stimulation of nitrifier denitrification by AOB, as observed in the overexpression of the Cu-type nitrite reductase (NirK). The ammonium, nitrite and  $\text{N}_2\text{O}$  concentration increases are a result of changes in the microbial community metabolism, while the increase in  $\text{O}_2$  concentration is the only manually controlled parameter in the cascade.

### 3.5. Supplementary information

### 3.5.1. Summary of literature on seasonal N<sub>2</sub>O emissions in WWTPs

**Table S3.1. Summary of literature on worldwide seasonal N<sub>2</sub>O emission events in WWTPs.** Information of the WWTPs and the monitoring campaigns: location, type of WWTP (SBR = sequencing batch reactor; AI = intermittent aeration; BNR = biological nitrogen removal; OD = oxidation ditch; CarR = carrousel reactor; Den = denitrification; Nit = nitrification; PF = plug-flow; GS = granular sludge; A2O = anaerobic-anoxic-oxic; AO = anoxic-oxic; MBR = membrane bioreactor; CAS = conventional activated sludge), N<sub>2</sub>O monitoring period, water temperature (T), dissolved O<sub>2</sub> (DO), and the period of seasonal N<sub>2</sub>O emissions. The main conclusions of each paper – observations, hypotheses and main N<sub>2</sub>O producing pathways (NN = nitrifier nitrification/hydroxylamine oxidation; ND = nitrifier denitrification; HD = heterotrophic denitrification) – are also described. All plants were activated sludge (AS) plants except Dinxperlo WWTP (granular sludge).

Country	WWTP	Monitoring period	T (°C)	DO (mg/L)	Seasonal N <sub>2</sub> O emissions	Observations/Hypotheses	N <sub>2</sub> O pathway	Ref.
<b>Southern hemisphere (Winter: Jun-Sep)</b>								
Australia (Adelaide)	SBR A/I	N <sub>2</sub> O: Feb – Mar 2014 NO <sub>2</sub> <sup>-</sup> : Jan 2014 – Jun 2017	-	0.5-2.8	No long-term N <sub>2</sub> O data	3x NO <sub>2</sub> <sup>-</sup> peak in Jun – Sep. No long-term N <sub>2</sub> O measurement, so no hypotheses for seasonal peak.	-	132
Brasil (Rio de Janeiro)	Non-BNR	Jan – Jul (< 1 year)	24-32	0-7	Jan - Apr	Simultaneous high NO <sub>2</sub> <sup>-</sup> . Strong positive correlation N <sub>2</sub> O vs. T. Hypothesis: AOB outcompete NOB at higher T, leading to NO <sub>2</sub> <sup>-</sup> accumulation and N <sub>2</sub> O emissions.	-	27
<b>Northern hemisphere (Winter: Dec-Mar)</b>								
China (Beijing)	OD (a), A2O (b), reversed A2O (c)	Mar-Nov (< 1 year)	-	-	Mar - Jun (a), Mar-Apr (b), Jun-Jul (c)	No hypotheses for N <sub>2</sub> O seasonality.	-	133
Denmark (Avedøre WWTP)	CarR AI	Mar 2018 – Feb 2019	10-20	0.5-1.5	3x Mar - July	N <sub>2</sub> O peaks during increasing T, but likely not main cause. Negative correlation N <sub>2</sub> O vs. DNA abundance of N <sub>2</sub> O reducers and NOB (16S rRNA genes).	NN	28,29
Finland (Viikinmäki WWTP)	Den/Nit	Jul 2012 – Jun 2013	9-21	3.5 <sup>a</sup>	↑ Emissions in winter and spring	No clear relationship between T and N <sub>2</sub> O emissions.	-	37
Finland	Den/Nit	Jan 2019 – Nov 2022	10-18	-	Dec-Apr	NO <sub>2</sub> <sup>-</sup> linked to winter N <sub>2</sub> O emissions. Hypothesis: seasonal emissions partly due to T.	NN/ND	30
Netherlands (Kralingseveer WWTP)	PF (Den/Nit) + carR (Den/Nit)	Oct 2010 – Jan 2012	10-20	0.5-2	Feb - Jun	Positive correlation N <sub>2</sub> O vs. maximum NO <sub>2</sub> <sup>-</sup> concentration (negatively correlated with T). Seasonal N <sub>2</sub> O lags 2-3 months behind T. N <sub>2</sub> O correlated with NH <sub>4</sub> <sup>+</sup> , NO <sub>2</sub> <sup>-</sup> and NO <sub>3</sub> <sup>-</sup> .	ND/HD	31,38,43
Netherlands (Dinxperlo WWTP)	GS Nereda®	Aug 2017 – Mar 2018 (< 1 year)	8-22	0-3	Dec – Feb	NO <sub>2</sub> <sup>-</sup> in effluent remained low.	ND/HD	134

South Korea (3 WWTPs in Gwangju)	A2O (a), AO MBR (b), SBR (c)	Apr 2018 – Jan 2019 ( $< 1$ year)	15-30	4.3 $\pm$ 2.2	Not clear, $\uparrow$ emissions in Aug (a), Apr (b), Dec (c)	DIC/VSS and $sOUR_{AOB}$ (ex situ) positively correlated with $N_2O$ in the aerobic AS. $DOC/NO_3^-$ negatively correlated with $N_2O$ in the anoxic AS.	NN/HD	101
South Korea (Gockseong)	SBR (only Nit)	Apr 2018 – Jul 2019	9-30	$> 3$	Dec - Mar	Seasonal $NO_2^-$ accumulation. $\uparrow sOUR_{AOB}/sOUR_{NOB}$ (ex situ) during $N_2O$ peak. Hypothesis: difference between AOB and NOB activity results in $NO_2^-$ and $N_2O$ emissions.	-	32
Switzerland (3 WWTPs)	AI (a), CAS (b), SBR (c)	Mar 2014 – Sep 2015 (a) Dec 2015 – Mar 2017 (b) Feb 2018 – Apr 2019 (c)	10-20 (a), 12-23 (b), 12-21 (c)	2 (a,b), 2-3 (c)	Dec-Mar (a), Dec – Apr (b), Jan – May (c)	Simultaneous $NO_2^-$ accumulation. $\downarrow$ NOB and filamentous bacteria (16S rRNA genes) during peaks. Hypothesis: compromised floc integrity led to NOB washout and consequent $NO_2^-$ and $N_2O$ accumulation. Increasing SRT and DO did not improve the plant performance. <sup>b</sup>	-	33,36
Switzerland (5 WWTPs)	AO (a,b), A2O (c), SBR (d), AI (e)	$> 1$ year	-	-	Jan-Apr (a), Apr- Jul (c), No seasonality (b,d,e)	WWTPs with seasonal $N_2O$ had higher emission factor. Hypothesis: reduced NOB performance causes $NO_2^-$ and $N_2O$ accumulation. Propose all-year denitrification (no nitrification-only periods) to avoid $NO_2^-$ accumulation.	ND/HD	34

<sup>a</sup> Average values

<sup>b</sup> Measures were only applied as contingency instead of prevention, it may have been too late.

### 3.5.2. Full-scale WWTP configuration and operational parameters

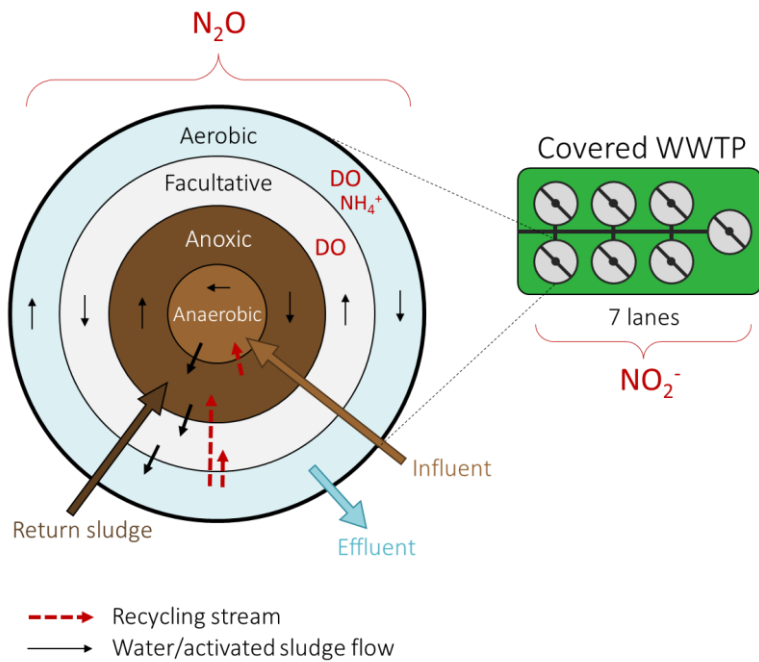


**Figure S3.1. Schematic representation of the configuration of the monitored activated sludge reactor.** The dissolved oxygen (DO) and  $NH_4^+$  concentrations were measured in the aerobic compartment, the  $N_2O$  was measured in the combined off-gas of all compartments, and  $NO_2^-$  was measured in the pooled effluent of all seven lanes of the WWTP.



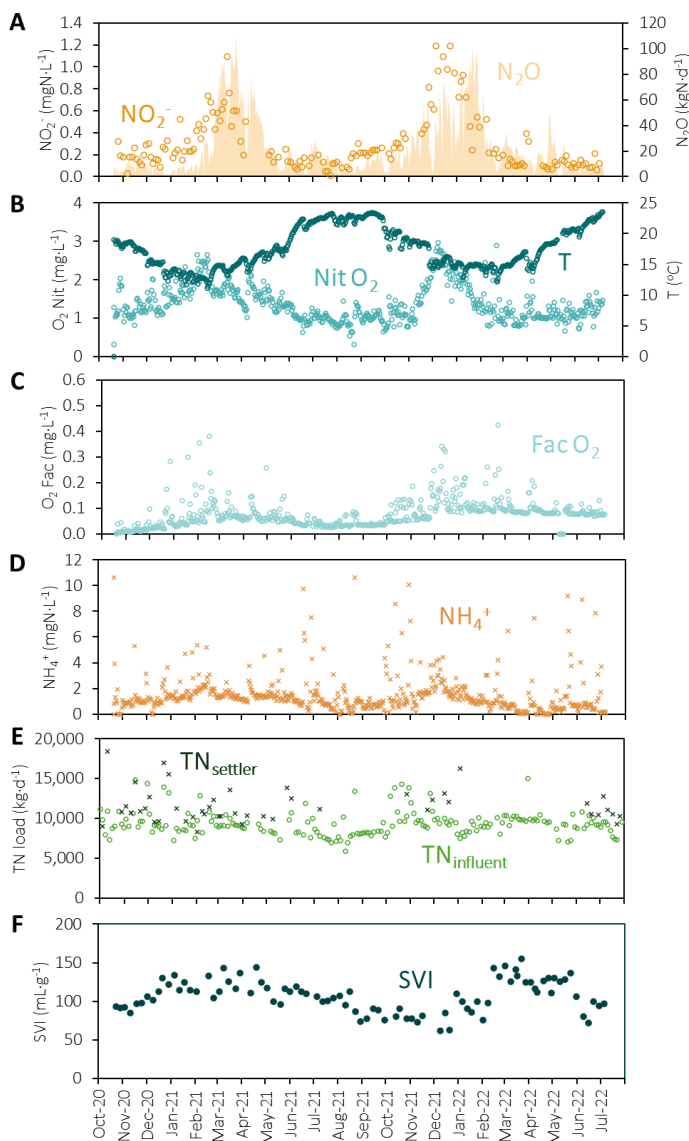


**Figure S3.2. Daily averages of the wastewater treatment plant (WWTP) parameters between Oct 2020 and Jul 2022. (A)** Nitrite concentration in the effluent (seven lanes pooled together, symbols, left axis) and N<sub>2</sub>O emission rates measured from off-gas measurements of all compartments of a single covered biological nutrient removal lane of the WWTP (area, right axis). **(B)** Dissolved O<sub>2</sub> concentration in the aerated compartment (light blue, left axis) and water temperature inside the reactor (dark blue, right axis). **(C)** Dissolved O<sub>2</sub> concentration in the facultative compartment, which depends on the nitrogen removal performance of the system. **(D)** NH<sub>4</sub><sup>+</sup> concentration in the nitrification compartment. Outliers above 12 mg N·L<sup>-1</sup> were omitted for clarity. High NH<sub>4</sub><sup>+</sup> concentrations often coincided with rainy days. All metabolites were measured in a single biological nutrient removal lane of the WWTP, except the effluent NO<sub>2</sub><sup>-</sup> (seven lanes pooled together). **(E)** Total nitrogen load of the WWTP (seven lanes) in the raw influent and after primary settling. **(F)** Sludge volume index representing the settleability of the sludge.

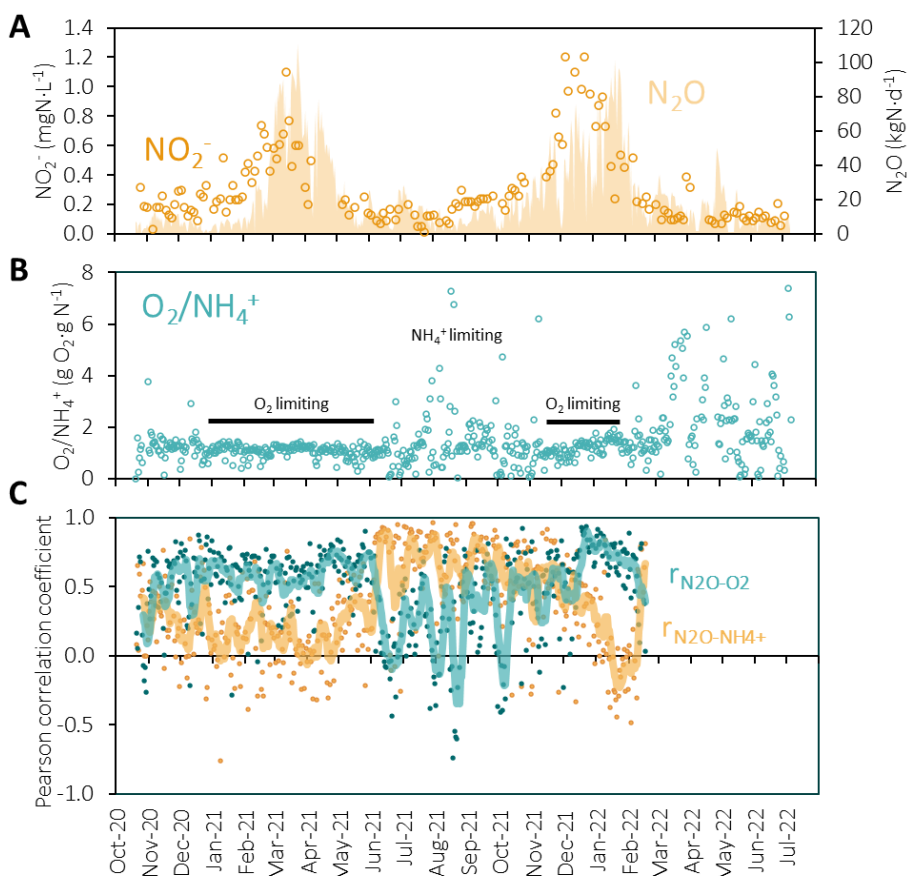


**Figure S3.3. Seasonal variations in  $\text{O}_2$  and  $\text{NH}_4^+$  limiting conditions.** (A) Daily averages: Nitrite concentration in the effluent (seven lanes pooled together, symbols, left axis) and  $\text{N}_2\text{O}$  emission rates measured from off-gas measurements of all compartments of a single covered biological nutrient removal lane of the WWTP (area, right axis). (B) Ratio between the daily average dissolved  $\text{O}_2$  and  $\text{NH}_4^+$  concentrations in the nitrification compartment. During the seasonal nitrogen oxides peak the  $\text{O}_2/\text{NH}_4^+$  reaches a plateau, suggesting that the  $\text{O}_2$  is limiting. In the summer months this plateau is not observed, suggesting that there is enough  $\text{O}_2$  to fully consume the influent  $\text{NH}_4^+$ . Outliers above  $8 \text{ g O}_2 \cdot \text{g N}^{-1}$  were omitted for clarity. (C) The Pearson correlation coefficient ( $r$ ) between the continuously measured (every 15 min) concentrations of  $\text{N}_2\text{O}-\text{O}_2$  (blue symbols) and  $\text{N}_2\text{O}-\text{NH}_4^+$  (yellow symbols) was calculated for each day. The weekly averages are represented with a line. The high values for  $\text{N}_2\text{O}-\text{O}_2$  in winter suggest a direct dependence of  $\text{N}_2\text{O}$  production on the  $\text{O}_2$  concentration, supporting  $\text{O}_2$  as the rate-determining (limiting) substrate during the nitrogen oxides peaks. The opposite is observed in summer, with mainly the  $\text{NH}_4^+$  concentrations determining the  $\text{N}_2\text{O}$  production.

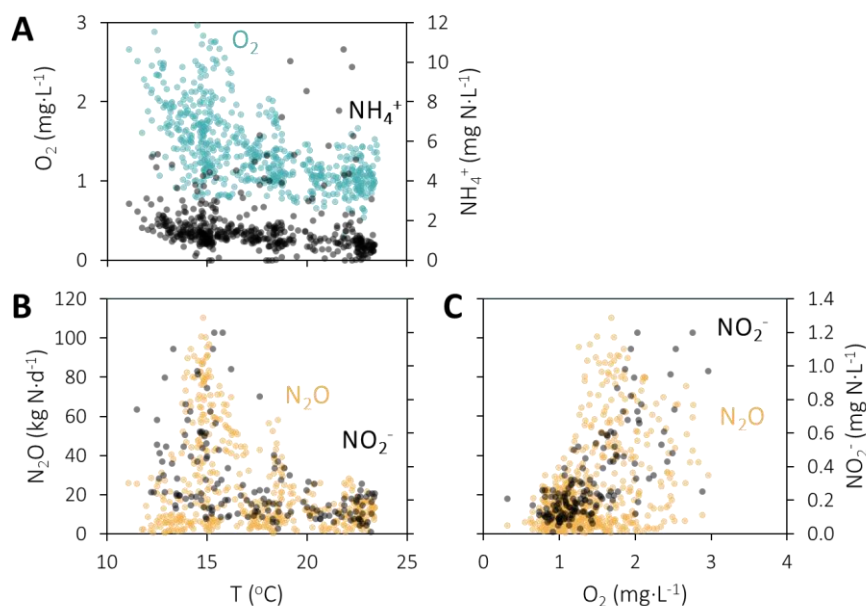


**Figure S3.4. Correlation between key parameters of the full-scale WWTP. (A)** Dissolved O<sub>2</sub> concentration (blue, left axis) and NH<sub>4</sub><sup>+</sup> concentration in the nitrification compartment (black, right axis) as function of the water temperature. **(B)** N<sub>2</sub>O emission rate (orange, left axis) and effluent NO<sub>2</sub><sup>-</sup> concentration (black, right axis) as function of the water temperature. **(C)** N<sub>2</sub>O emission rate (orange, left axis) and effluent NO<sub>2</sub><sup>-</sup> concentration (black, right axis) as function of the dissolved O<sub>2</sub> concentration in the nitrification compartment.

**Table S3.2. Pearson correlation coefficients between NO<sub>2</sub><sup>-</sup> and N<sub>2</sub>O and the weekly averages of several WWTP parameters:** N<sub>2</sub>O emission rate, nitrite concentration in the effluent, temperature in the nitrification tank, total suspended solids (TSS), ammonium concentration in the nitrification tank, nitrate concentration in the nitrification tank, dissolved oxygen concentration in the nitrification tank and the sludge volume index. Negative correlations are highlighted in red, and positive correlations are highlighted in green. Strong correlations are highlighted in bold.

	NO <sub>2</sub> <sup>-</sup>	T	TSS	NH <sub>4</sub> <sup>+</sup>	NO <sub>3</sub> <sup>-</sup>	O <sub>2</sub>	SVI
N <sub>2</sub> O	<b>0.7</b>	-0.4	-0.2	0.1	0.0	0.5	0.0
NO <sub>2</sub> <sup>-</sup>		-0.5	0.0	0.4	0.0	<b>0.8</b>	-0.2

### 3.5.3. Maximum nitrifying and denitrifying activities

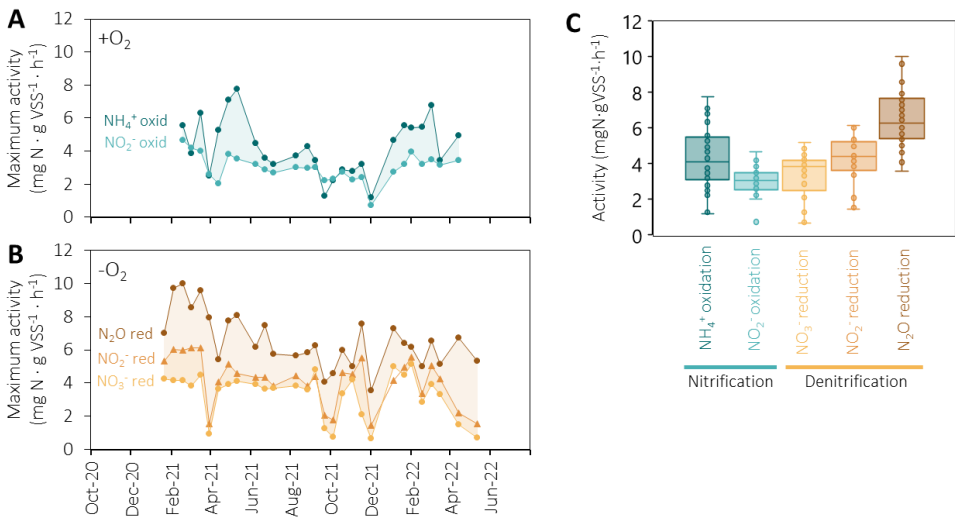


**Figure S3.5. Ex situ maximum nitrifying and denitrifying activity of activated sludge measured at 20 °C. (A)**  $NH_4^+$  and  $NO_2^-$  oxidation measured under oxic conditions. **(B)**  $N_2O$ ,  $NO_2^-$  and  $NO_3^-$  reduction measured under anoxic conditions. **(C)** Boxplots summarising the ex situ nitrifying and denitrifying activities of activated sludge ( $n=26$  for nitrification,  $n=29$  for denitrification). Boxplots display the median (line inside the box), interquartile range (box edges, first and third quartile), whiskers ( $1.5 \times$  interquartile range), and outliers (individual points beyond whiskers).

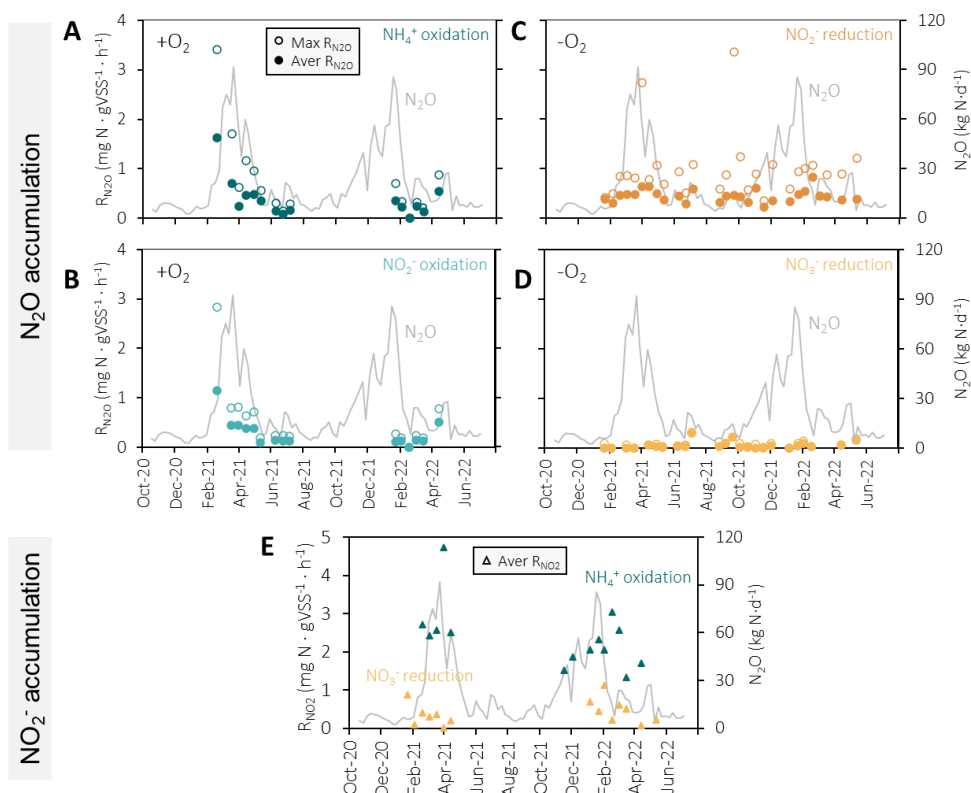


**Figure S3.6. Maximum and average  $\text{N}_2\text{O}$  and  $\text{NO}_2^-$  accumulation rates during the ex situ nitrifying and denitrifying activity measurements of activated sludge at 20 °C (left axes, symbols). (A, B)  $\text{N}_2\text{O}$  accumulation rates during  $\text{NH}_4^+$  and  $\text{NO}_2^-$  oxidation batches conducted under fully oxic conditions. The reactor was aerated, so the  $\text{N}_2\text{O}$  rates were derived from off-gas measurements (missing points correspond to periods when off-gas analyser was not available). (C, D)  $\text{N}_2\text{O}$  accumulation rates during  $\text{NO}_2^-$  and  $\text{NO}_3^-$  reduction batches conducted under anoxic conditions. The reactor was not sparged during the batches, so the  $\text{N}_2\text{O}$  rates were derived from liquid sensor measurements. (E)  $\text{NO}_2^-$  accumulation rates during  $\text{NH}_4^+$  oxidation (nitrification) and  $\text{NO}_3^-$  reduction (denitrification) batches. For reference, weekly average  $\text{N}_2\text{O}$  emission rates measured in the off-gas from all the reactor compartments in one lane at the WWTP are also presented (right axes, line).**

### 3.5.4. Metagenomic data processing

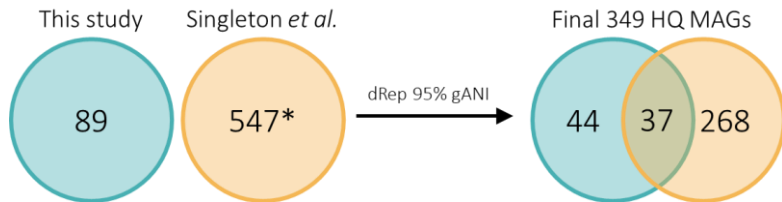


**Figure S3.7. Number of HQ MAGs before and after dereplication with the MAGs from Singleton et al.** <sup>48</sup> **at 95% average nucleotide identity of open reading frames (gANI).** In the final set of HQ MAGs, there were 37 overlapping MAGs between our original set and the original Singleton et al. set, from which 10 of our MAGs and 27 of Singleton et al.'s MAGs were kept by the dereplication software. So, in total, the final set contained 54 of our MAGs and 295 of Singleton et al.'s MAGs. \*After dereplicating the Singleton et al. 1083 MAGs at 95% gANI and before filtering out MAGs that were not present in our samples (the 252 MAGs from Singleton et al. with zero abundance in our samples were filtered out after dereplication).

**Table S3.3. Nitrogen metabolism genes and KO identifiers.**

KO ID	Gene	Description
K10944	amoA	methane/ammonia monooxygenase subunit A [EC:1.14.18.3 1.14.99.39]
K10945	amoB	methane/ammonia monooxygenase subunit B
K10946	amoC	methane/ammonia monooxygenase subunit C
K10535	hao	hydroxylamine dehydrogenase [EC:1.7.2.6]
K00370	narG, narZ, nxrA	nitrate reductase / nitrite oxidoreductase, alpha subunit [EC:1.7.5.1 1.7.99.-]
K00371	narH, narY, nxrB	nitrate reductase / nitrite oxidoreductase, beta subunit [EC:1.7.5.1 1.7.99.-]
K00374	narI, narV	nitrate reductase gamma subunit [EC:1.7.5.1 1.7.99.-]
K02567	napA	nitrate reductase (cytochrome) [EC:1.9.6.1]
K02568	napB	nitrate reductase (cytochrome), electron transfer subunit
K00368	nirK	nitrite reductase (NO-forming) [EC:1.7.2.1]
K15864	nirS	nitrite reductase (NO-forming) / hydroxylamine reductase [EC:1.7.2.1 1.7.99.1]
K04561	norB	nitric oxide reductase subunit B [EC:1.7.2.5]
K02305	norC	nitric oxide reductase subunit C
K00376	nosZ	nitrous-oxide reductase [EC:1.7.2.4]
K03385	nrfA	nitrite reductase (cytochrome c-552) [EC:1.7.2.2]
K15876	nrfH	cytochrome c nitrite reductase small subunit
K20932	hzsA	hydrazine synthase alpha subunit [EC:1.7.2.7]
K20933	hzsB	hydrazine synthase beta subunit [EC:1.7.2.7]
K20934	hzsC	hydrazine synthase gamma subunit [EC:1.7.2.7]
K20935	hdh	hydrazine dehydrogenase [EC:1.7.2.8]

### 3.5.5. Temporal profiles of the MAGs abundance in terms of DNA and protein

The data presented in this section can be found in Supplementary Data 1.

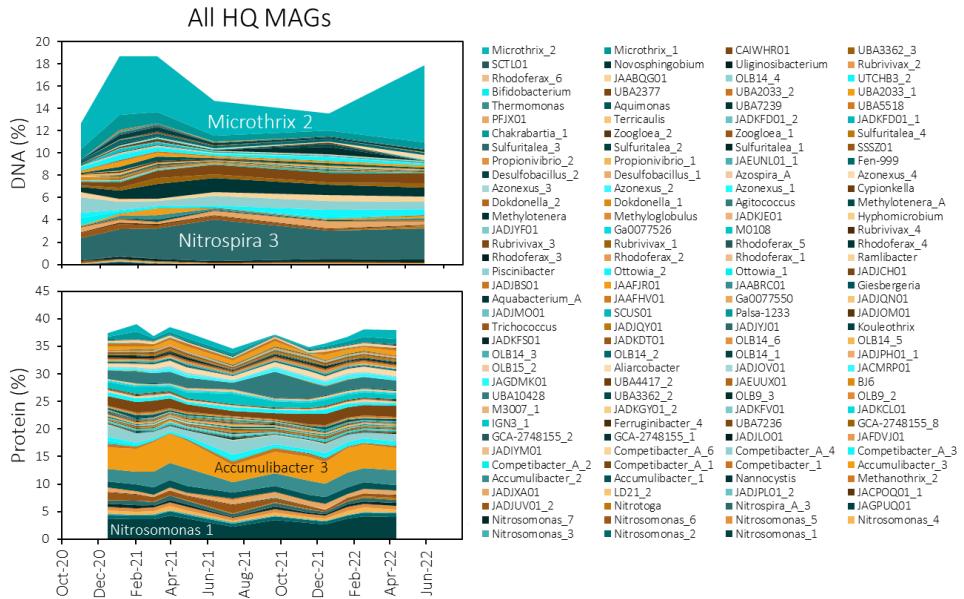


**Figure S3.8. Temporal fluctuations in the relative abundance of the 143 HQ MAGs detected in the proteome in terms of DNA and protein.**

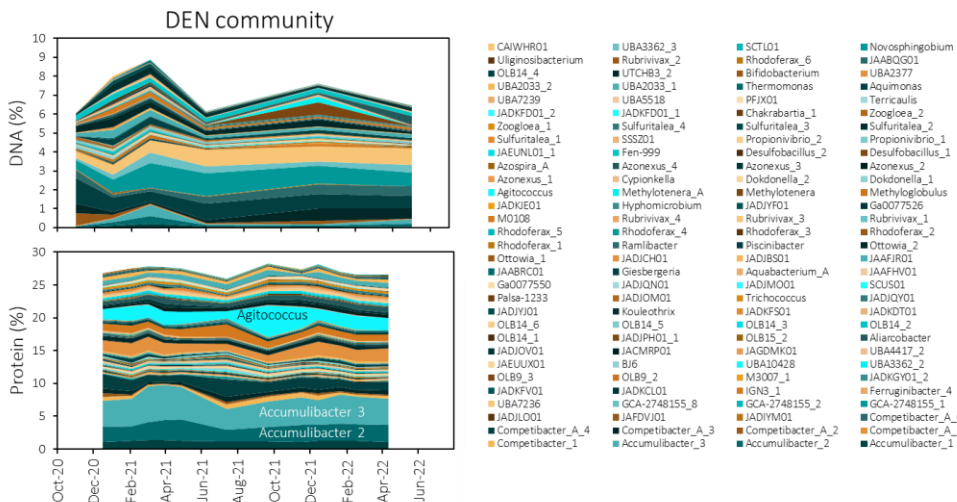


**Figure S3.9. Temporal fluctuations in the relative abundance of the 124 DEN MAGs detected in the proteome in terms of DNA and protein.**

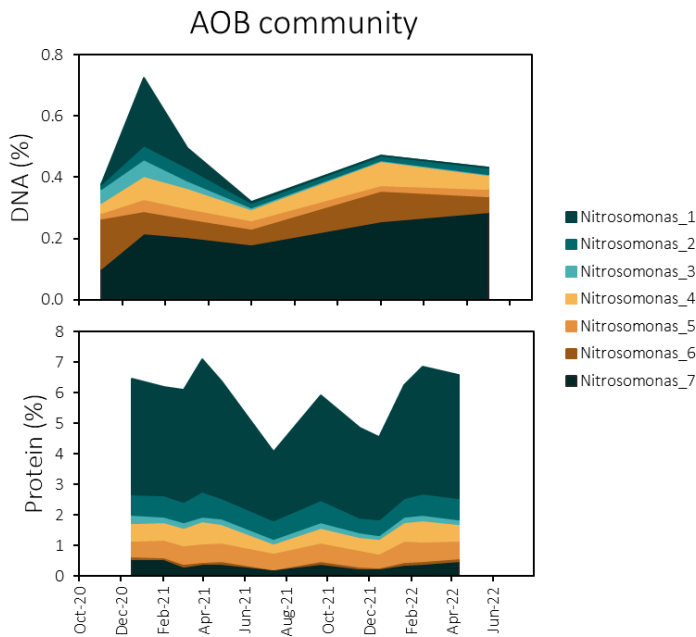


**Figure S3.10. Temporal fluctuations in the relative abundance of the seven AOB MAGs in terms of DNA and protein.**

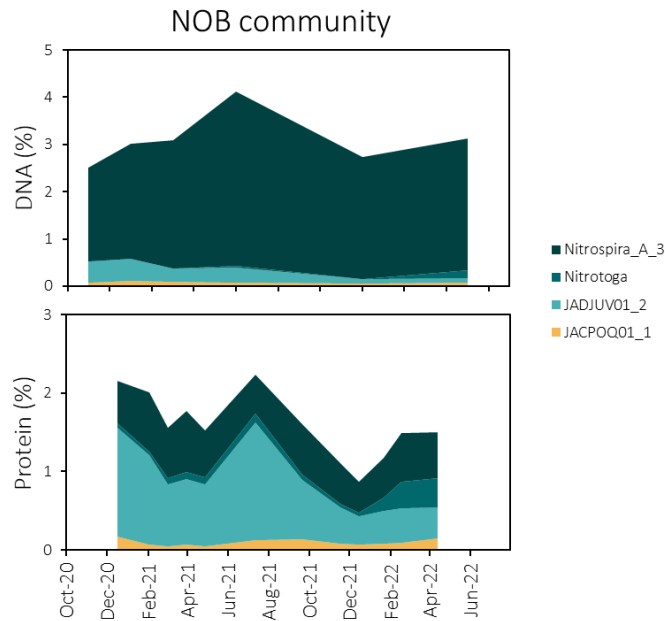


**Figure S3.11. Temporal fluctuations in the relative abundance of the four NOB MAGs detected in the proteome in terms of DNA and protein.**



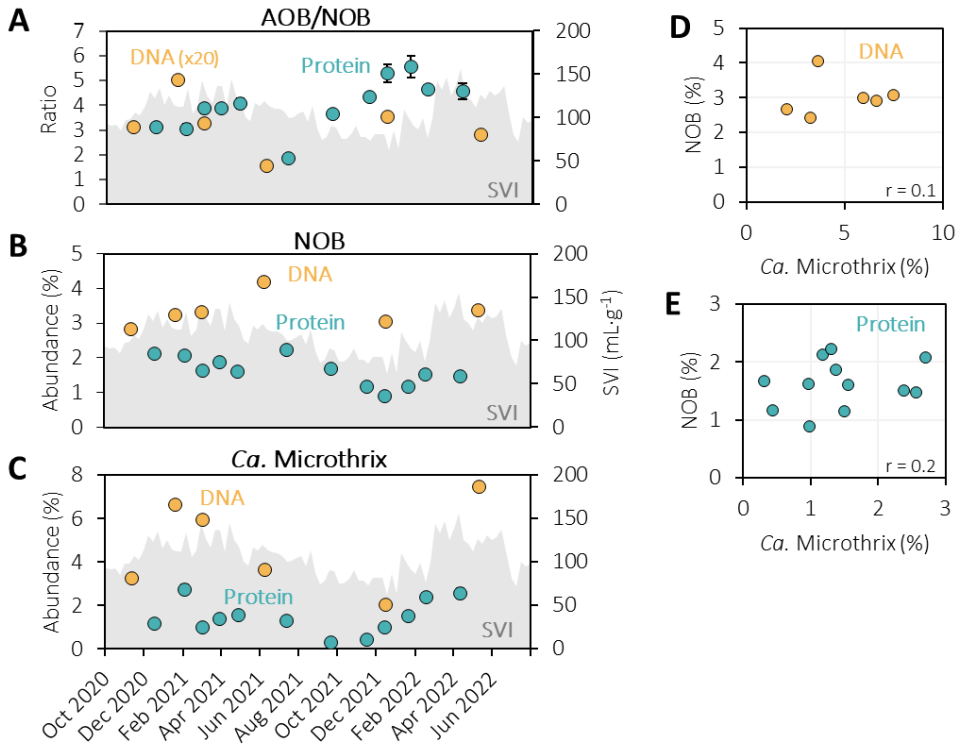


**Figure S3.12. Relative DNA and protein abundances of nitrifying and filamentous bacteria alongside the sludge volume index.** Left axis: **(A)** Ratio AOB/NOB; **(B)** NOB abundance; **(C)** *Ca. Microthrix* (filamentous) abundance. **(A-C)** The protein symbols represent the mean and the error bars represent standard deviations of technical duplicates independently injected in the LC-MS/MS, most are smaller than the symbols. **Right axis: (A-C)** Sludge volume index (SVI), representing the sludge settleability. Higher SVI stands for a worse settleability. High amounts of filamentous bacteria cause bad settleability (high SVI), this is also seen in this plot. **(D, E)** There was no correlation between the abundances of NOB and *Ca. Microthrix* ( $r =$  Pearson correlation coefficient,  $n=6$  (D) and  $n=12$  (E)).

**Table S3.4. Pearson correlation coefficients between the protein abundance of all genera with an abundance above 0.1% and weekly average WWTP operational parameters.** Twelve timepoints were used to calculate the correlation coefficients. The genera are ordered from high to low abundance. Correlation coefficients below -0.7 or above 0.7 are highlighted.

Type	Genus	Pearson correlation coefficient					
		T	NH <sub>4</sub> <sup>+</sup>	DO	N <sub>2</sub> O	NO <sub>2</sub> <sup>-</sup>	SVI
DEN	Accumulibacter	-0.5	0.0	0.2	0.6	0.0	0.5
AOB	Nitrosomonas	-0.6	-0.3	-0.2	0.0	-0.4	0.7
DEN	Competibacter	0.4	0.0	-0.1	-0.5	0.0	-0.5
DEN	Agitococcus	0.5	-0.3	-0.2	-0.1	0.0	-0.3
DEN	JADJCH01	-0.8	0.4	0.6	0.4	0.5	0.1
DEN	Azonexus	-0.1	-0.2	0.0	0.6	0.1	0.1
Other	Microthrix	-0.6	0.5	0.1	-0.3	-0.3	0.6
DEN	UBA2033	0.2	0.0	0.1	-0.1	0.1	0.0
DEN	M0108	0.5	0.1	-0.3	-0.3	-0.2	-0.2
DEN	Sulfuritalea	-0.3	-0.1	0.0	0.1	-0.1	0.4
NOB	JADJUV01	0.2	-0.1	-0.3	-0.5	-0.3	0.1
NOB	Nitrospira	-0.1	-0.2	-0.2	-0.2	-0.4	0.6
Other	JADJXA01	0.6	-0.2	-0.2	-0.2	0.2	-0.6
DEN	OLB14	0.5	-0.1	-0.3	-0.4	-0.2	-0.2
DEN	Ottowia	0.1	0.1	0.3	-0.1	0.5	-0.5
DEN	Rhodoferax	-0.7	0.4	0.4	0.2	0.3	0.4
DEN	Propionivibrio	-0.1	0.2	0.2	0.3	0.1	0.1
DEN	Zoogloea	-0.3	0.5	0.7	0.6	0.5	0.0
DEN	Giesbergeria	-0.8	0.5	0.7	0.4	0.5	0.0
DEN	SSSZ01	0.1	0.1	0.2	0.1	0.2	-0.2
DEN	JAEUUX01	0.4	0.2	0.3	0.3	0.6	-0.4
DEN	Rubrivivax	-0.9	0.2	0.5	0.2	0.3	0.3
DEN	Ga0077526	-0.4	0.6	0.5	0.2	0.1	0.2
DEN	JAABQG01	-0.7	0.3	0.2	-0.4	0.0	0.4
DEN	Fen-999	-0.5	0.1	0.5	0.6	0.4	0.0
DEN	Ramlibacter	-0.6	0.2	0.0	-0.1	-0.4	0.6
DEN	PFJX01	0.2	-0.3	-0.1	0.2	0.1	-0.2
DEN	JAELN01	0.1	0.4	0.4	0.5	0.3	-0.4
DEN	JADJBS01	-0.6	0.6	0.6	-0.1	0.6	0.0
DEN	Hyphomicrobium	0.1	0.2	-0.2	-0.2	-0.2	0.2
DEN	JADJYF01	0.0	0.6	0.6	0.0	0.5	-0.1
DEN	Dokdonella	-0.3	0.3	0.4	0.0	0.5	-0.4
DEN	JADKCL01	0.2	0.1	0.1	0.4	0.3	0.0
DEN	JAAFJR01	-0.6	-0.2	-0.2	0.1	-0.2	0.6
DEN	JADJVA01	0.2	-0.1	0.1	0.3	0.4	0.0
NOB	Nitrotoga	-0.2	-0.2	-0.4	-0.2	-0.4	0.4
DEN	JADKGY01	-0.2	-0.2	0.1	0.4	0.1	0.3
DEN	Palsa-1233	0.0	0.3	0.4	0.5	0.4	0.2
DEN	GCA-2748155	0.2	0.5	0.1	-0.4	-0.1	-0.1
DEN	Piscinibacter	-0.6	0.3	0.2	0.2	0.3	0.4
DEN	OLB9	-0.1	0.3	-0.1	0.0	0.0	0.4
DEN	IGN3	0.0	-0.1	0.1	0.2	0.2	0.2
DEN	UBA5518	-0.4	0.2	0.1	-0.4	-0.1	0.3

### 3.5.6. Taxa quantification in terms of DNA and protein

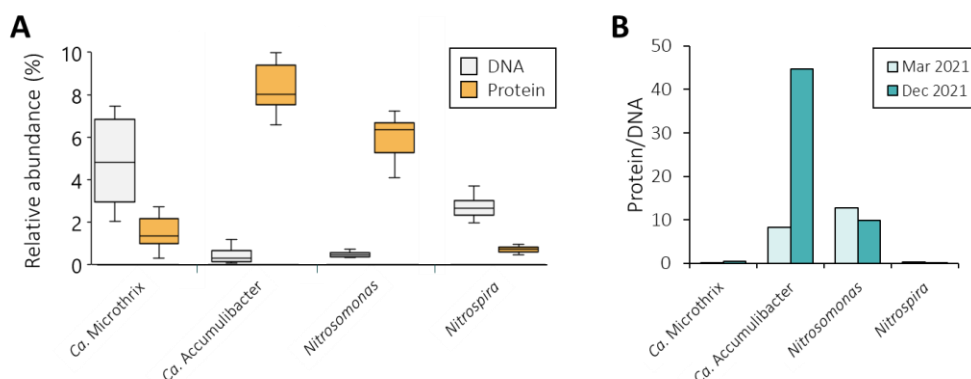


**Figure S3.13. DNA and proteomic quantification of key activated sludge genera. (A)** Overview of the relative abundance of *Ca. Microthrix* (filamentous bacteria), *Ca. Accumulibacter* (phosphate-accumulating organisms), *Nitrosomonas* (AOB) and *Nitrospira* (NOB), as quantified in the DNA (6 samples) and protein (12 samples). Boxplots display the median (line inside the box), interquartile range (box edges, first and third quartile), and whiskers (1.5× interquartile range). **(B)** Protein over DNA ratio of the same genera, measured in metagenomic and metaproteomic samples taken on the same day.

A disparity between genomic and proteomic quantification was observed for several key genera: *Ca. Microthrix* (filamentous), *Ca. Accumulibacter* (phosphate-accumulating), *Nitrosomonas* (AOB) and *Nitrospira* (NOB). Specifically, as often observed in wastewater treatment systems<sup>29,32,85,135,136</sup>, the relative contribution of AOB *Nitrosomonas* to the community's DNA pool was 7-fold lower than NOB. The opposite is expected since AOB have a higher biomass yield per g nitrogen than NOB (Table S3.9). The under- or over-representation of certain taxa in the sludge DNA pool is likely an artifact of the quantification of cell number (DNA) vs. active biomass (protein)<sup>85,97,137</sup>. The relatively higher protein-based quantification of AOB compared to NOB likely reflects the larger AOB cell size (Table S3.5, Figure S3.14).

**Table S3.5.** The cell volumes of several AOB and NOB species were estimated based on cell sizes described in literature.

Guild	Species	D (μm)	L (μm)	Estimated volume (μm <sup>3</sup> )*	Reference
AOB	<i>Nitrosomonas europaea</i>	0.8-1.1	1.0-1.7	0.50-1.6	138
	<i>Nitrosomonas eutropha</i>	1.0-1.3	1.6-2.3	1.3-3.1	138
	<i>Nitrosomonas halophila</i>	1.1-1.5	1.5-2.2	1.4-3.9	138
	<i>Nitrosomonas mobilis</i>	1.5-1.7	1.5-2.1	2.7-4.8	138
	<i>Nitrosomonas communis</i>	1.0-1.4	1.7-2.2	1.3-3.4	138
NOB	<i>Nitrospira marina</i>	0.3-0.4	0.8-1.0	0.06-0.13	139
	<i>Nitrospira moscoviensis</i>	0.2-0.4	0.9-2.2	0.03-0.28	140
	<i>Nitrospira defluvii</i>	0.2-0.4	0.7-1.7	0.02-0.21	141
	<i>Nitrospira calida</i>	0.3-0.5	1.0-2.2	0.07-0.43	142
	<i>Ca. Nitrospira inopinata</i>	0.2-0.3	0.7-1.6	0.02-0.11	143

\*Assuming cylindrical shape:  $V = \pi \cdot L \cdot D^2 / 4$

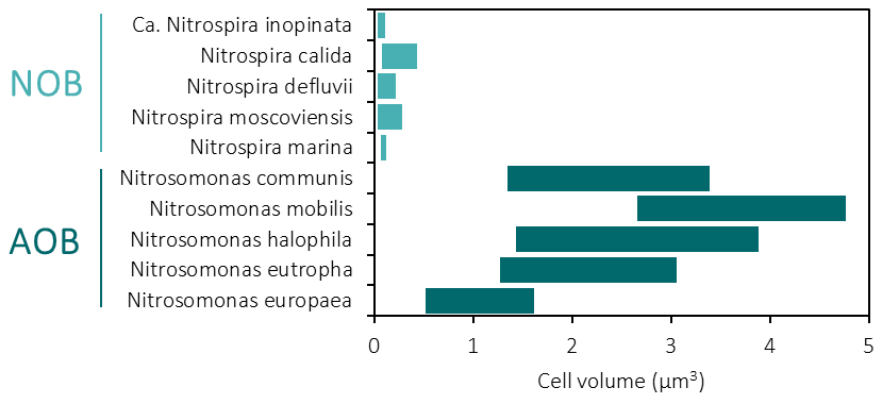


**Figure S3.14.** Estimated cell volumes of *Nitrospira* (light blue) and *Nitrosomonas* species (dark blue).

### 3.5.7. Functional characterisation of the HQ MAGs

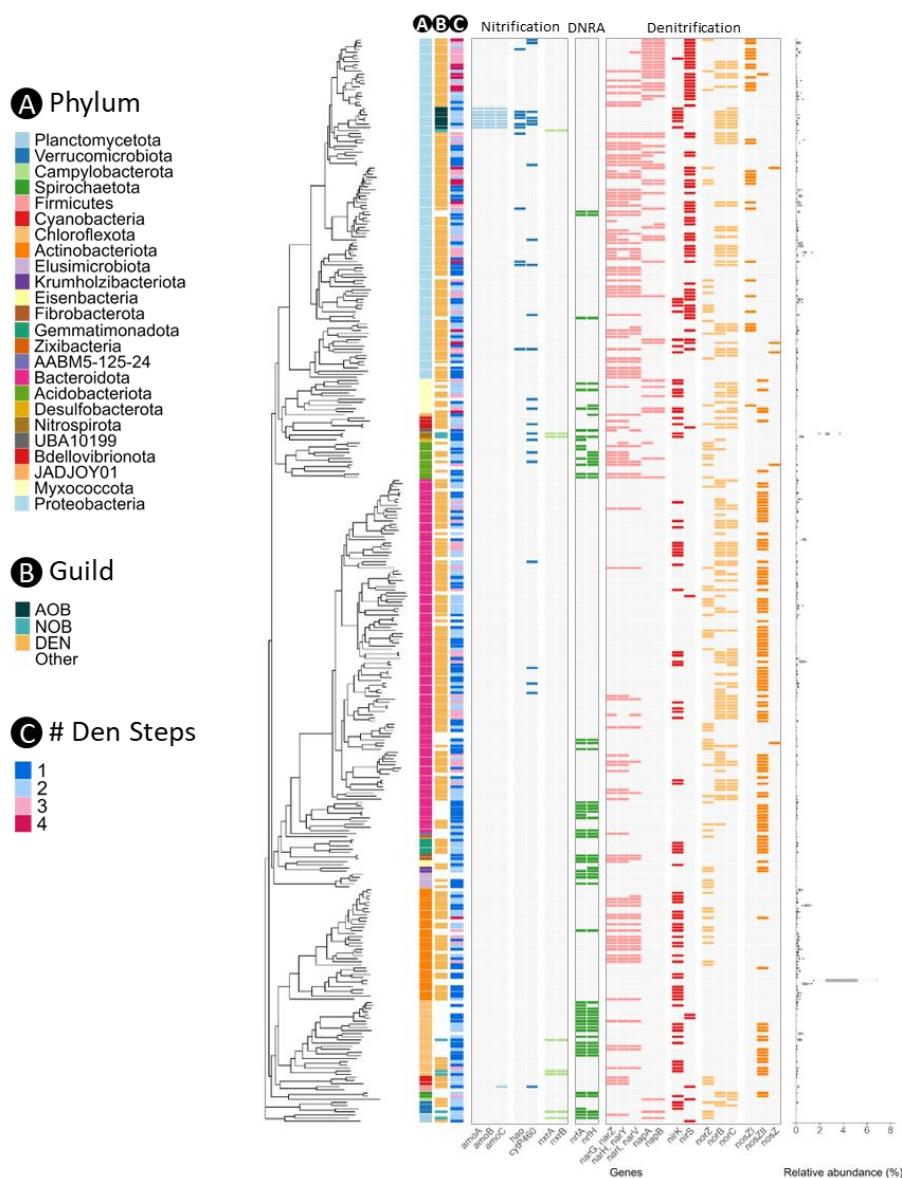


**Figure S3.15. Nitrogen gene content of the 347 bacterial HQ MAGs.** The MAGs are identified by the phylum (A), guild (B) and number of denitrification steps encoded in the genome (C). The heatmap shows the presence (coloured) or absence (light grey) of nitrogen cycle genes: ammonia oxidation (light blue), hydroxylamine oxidation (dark blue), nitrite oxidation (light green), dissimilatory nitrite reduction to ammonia (dark green), nitrate reduction (pink), nitrite reduction (red), nitric oxide reduction (light orange) and nitrous oxide reduction (dark orange). The *nosZ* genes were identified as clade I (*nosZI*), clade II (*nosZII*) or unknown (*nosZ*). The boxplot on the right represents the relative abundance of each MAG at the six time points that were sequenced. The abundance of the unbinned fraction (72%) was omitted for clarity. The full set of nitrogen cycle genes in the HQ MAGs is in Supplementary Data 1.

### 3.5.8. Protein expression profiles

The relative abundance of the nitrogen enzymes in all twelve proteomic samples can be found in Supplementary Data 1.

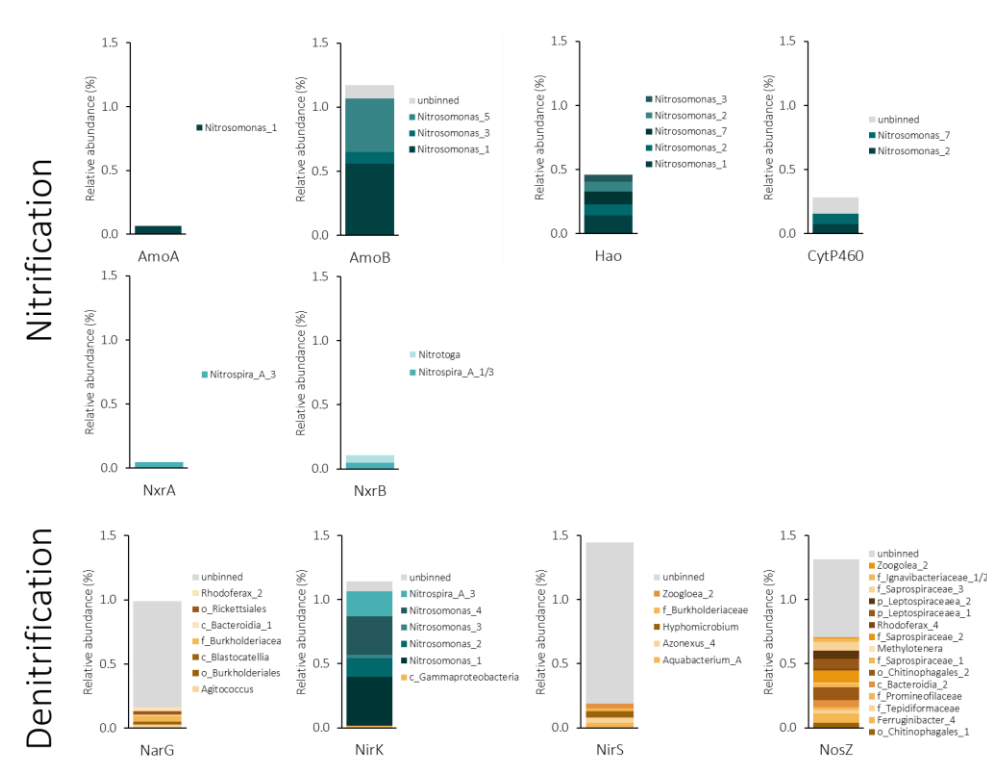


**Figure S3.16. Average protein abundances (12 samples) and distribution per MAG.** The top two rows represent the enzymes involved in the oxidation of ammonium to nitrite and nitrate: alpha- and beta-subunits of the ammonia monooxygenase (AmoA and AmoB), hydroxylamine oxidoreductase (Hao), the hydroxylamine oxidising cytochrome P460 (CytP460) and the alpha- and beta- subunits of the nitrite oxidoreductase (NxrA and NxrB). The bottom row represents the enzymes involved in the reduction of nitrogen oxides to dinitrogen gas: catalytic subunit of the nitrate reductase (NarG), copper- and cd1-type nitrite reductase (NirK and NirS) and catalytic subunit of the nitrous oxide reductase (NosZ). The coloured portion of the bars correspond to proteins belonging to a certain MAG (blue to nitrifiers and yellow to denitrifiers) and the grey part corresponds to proteins belonging to the unsorted portion of the community. **Note:** enzymes are divided based on the reaction they perform, the guilds are distinguished by colour. For example, NirK is effectively a denitrifying enzyme but it was almost entirely expressed by nitrifiers (blue).

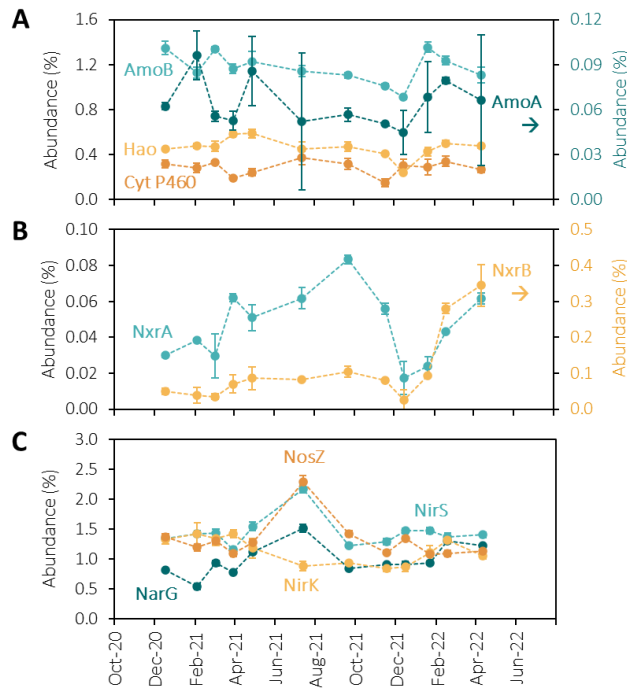


**Figure S3.17. Relative abundance of enzymes involved in ammonia (A) and nitrite oxidation (B), and in the reduction of nitrate, nitrite and nitrous oxide (C).** The symbols represent the mean and the error bars represent standard deviations of technical duplicates independently injected in the LC-MS/MS, some are smaller than the symbols. **(A)** Ammonia oxidation to nitrite: Alpha and beta subunits of the ammonia monooxygenase (AmoA on the right axis, and AmoB on the left axis), hydroxylamine oxidoreductase (Hao, left axis), and the cytochrome P460 (Cyt P460, left axis). **(B)** Nitrite oxidation to nitrate: Alpha and beta subunits of the nitrite oxidoreductase (NxrA on the left axis and NxrB on the right axis). **(C)** Nitrate reduction to dinitrogen gas: catalytic subunit of the membrane-bound nitrate reductase (NarG), Cu-type nitrite reductase (NirK), cd1-type nitrite reductase (NirS) and nitrous oxide reductase (NosZ). All abundances include MAG and unbinned proteins.

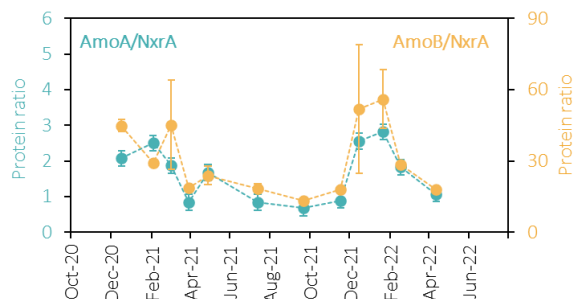


**Figure S3.18. Identical protein ratio profiles when using either the alpha or the beta subunits of AMO.** The beta subunit of the ammonia monooxygenase (AmoB) was used in all our analyses because the catalytic alpha subunit (AmoA) was detected in very low amounts. In any case, the protein profiles using either of the subunits is identical. All abundances include MAG and unbinned proteins. The symbols represent the mean

and the error bars represent standard deviations of technical duplicates independently injected in the LC-MS/MS.

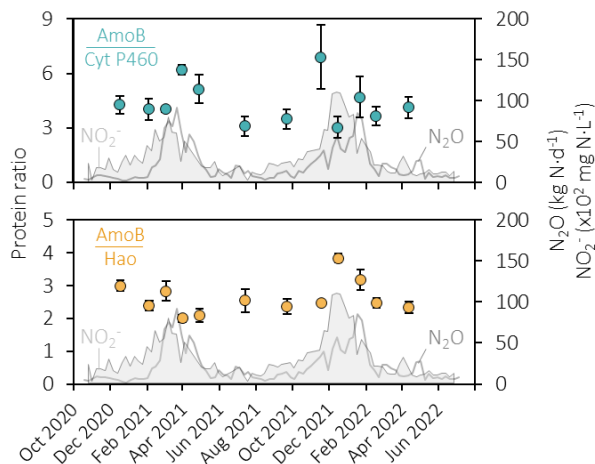


**Figure S3.19. Fluctuation of the ratio between hydroxylamine-producing (AmoB) and -consuming (Cyt P460 and Hao) enzymes.** The ratio between the beta-subunit of the ammonia monooxygenase (AmoB) and cytochrome P460 (Cyt P460) and the hydroxylamine oxidoreductase (Hao) represent the hydroxylamine flux balance. All abundances include MAG and unbinned proteins. The symbols represent the mean and the error bars represent standard deviations of technical duplicates independently injected in the LC-MS/MS, some are smaller than the symbols.

**Table S3.6. Pearson correlation coefficients between microbial ratios (DNA, protein, activities) and weekly averages of key WWTP parameters (temperature, ammonium, dissolved oxygen, nitrite, N<sub>2</sub>O).** Negative correlations are highlighted in red, and positive correlations are highlighted in green. Statistically significant correlations are indicated (\*\* for  $p < 0.05$  and \* for  $p < 0.10$ ). The corresponding degrees of freedom, two-sided t-statistics, p-values, and 95% confidence intervals are also represented.

	AOB/ NOB (DNA)	AOB/ NOB (Protein)	AmoB/ NxrA	Hao/ NxrA	NirK/ AmoB	NirK/ Hao	NirK/ NirS	NirK/ NxrA	NirK/ NosZ	$r_{NH_4^+}/$ $r_{NO_2^-}$
<b>Pearson correlation coefficients</b>										
T	-0.9 **	-0.4 **	-0.5 **	-0.5 **	-0.6 **	-0.6 **	-0.6 **	-0.6 **	-0.7 **	-0.4 **
NH <sub>4</sub> <sup>+</sup>	0.6	0.0	0.2	0.2	0.3	0.4 **	-0.1	0.3	0.0	0.2
DO	0.7	0.5 **	0.4 *	0.3	0.3	0.6 **	0.0	0.5 **	0.1	0.4 *
NO <sub>2</sub> <sup>-</sup>	0.3	0.4 *	0.5 **	0.3	0.1	0.7 **	-0.1	0.5 **	-0.1	-0.1
N <sub>2</sub> O	0.1	0.6 **	0.4 **	0.4 **	0.0	0.2	0.1	0.4 *	0.2	0.3
<b>Degrees of freedom</b>										
T	4	22	22	22	22	22	22	22	22	24
NH <sub>4</sub> <sup>+</sup>	4	22	22	22	22	22	22	22	22	24
DO	3	20	20	20	20	20	20	20	20	21
NO <sub>2</sub> <sup>-</sup>	4	22	22	22	22	22	22	22	22	24
N <sub>2</sub> O	4	22	22	22	22	22	22	22	22	24
<b>t-statistics</b>										
T	-3.8	-2.1	-2.4	-3.0	-3.2	-3.2	-3.1	-3.2	-5.2	-2.2
NH <sub>4</sub> <sup>+</sup>	1.5	-0.2	1.0	0.9	1.4	2.2	-0.4	1.4	0.0	1.1
DO	1.6	2.3	1.9	1.4	1.4	3.6	-0.1	2.3	0.6	2.0



NO <sub>2</sub> <sup>-</sup>	0.7	2.0	2.4	1.3	0.4	4.2	-0.5	2.5	-0.4	-0.5
N <sub>2</sub> O	0.1	3.3	2.4	2.1	-0.2	1.1	0.5	1.9	0.9	1.3
<b>p-values</b>										
T	0.02	0.05	0.03	0.007	0.004	0.004	0.005	0.004	0.00003	0.04
NH <sub>4</sub> <sup>+</sup>	0.2	0.8	0.3	0.4	0.2	0.04	0.7	0.2	1	0.3
DO	0.2	0.03	0.07	0.2	0.2	0.002	0.9	0.03	0.6	0.06
NO <sub>2</sub> <sup>-</sup>	0.5	0.06	0.03	0.2	0.7	0.0003	0.6	0.02	0.7	0.6
N <sub>2</sub> O	0.9	0.003	0.03	0.05	0.8	0.3	0.6	0.07	0.4	0.2
<b>Confidence intervals</b>										
T	[-1, -0.3]	[-0.7, 0]	[-0.7, -0.1]	[-0.8, -0.2]	[-0.8, -0.2]	[-0.8, -0.2]	[-0.8, -0.2]	[-0.8, -0.2]	[-0.9, -0.5]	[-0.7, 0]
NH <sub>4</sub> <sup>+</sup>	[-0.4, 0.9]	[-0.4, 0.4]	[-0.2, 0.6]	[-0.2, 0.5]	[-0.1, 0.6]	[0, 0.7]	[-0.5, 0.3]	[-0.1, 0.6]	[-0.4, 0.4]	[-0.2, 0.6]
DO	[-0.5, 1]	[0, 0.7]	[0, 0.7]	[-0.1, 0.6]	[-0.1, 0.6]	[0.3, 0.8]	[-0.4, 0.4]	[0, 0.7]	[-0.3, 0.5]	[0, 0.7]
NO <sub>2</sub> <sup>-</sup>	[-0.6, 0.9]	[0, 0.7]	[0.1, 0.7]	[-0.1, 0.6]	[-0.3, 0.5]	[0.4, 0.8]	[-0.5, 0.3]	[0.1, 0.7]	[-0.5, 0.3]	[-0.5, 0.3]
N <sub>2</sub> O	[-0.8, 0.8]	[0.2, 0.8]	[0.1, 0.7]	[0, 0.7]	[-0.4, 0.4]	[-0.2, 0.6]	[-0.3, 0.5]	[0, 0.7]	[-0.2, 0.6]	[-0.1, 0.6]

### 3.5.9. Balance of DEN at proteomic and kinetic levels

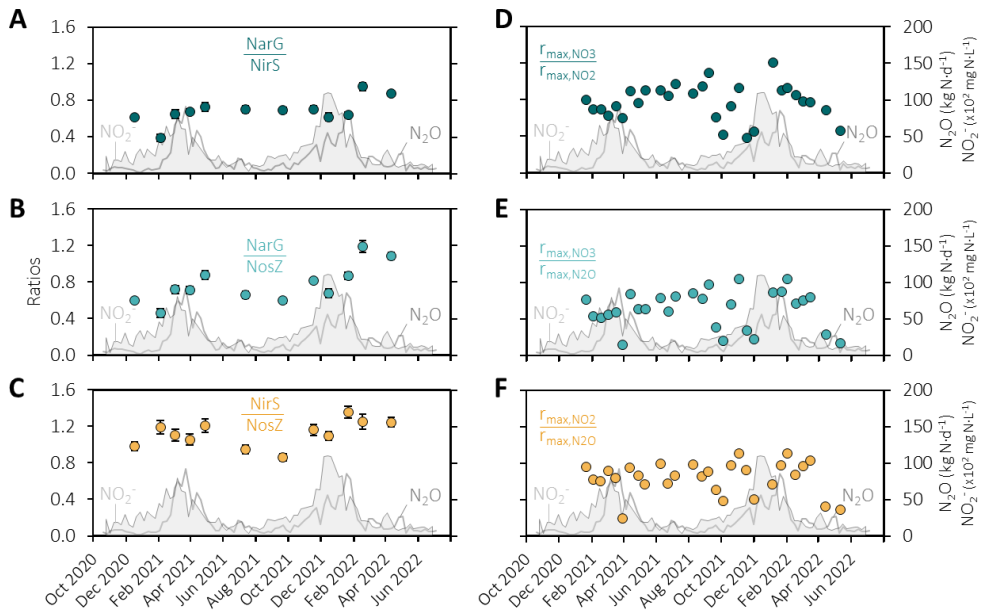


**Figure S3.20. Fluctuations in the balance of DEN fluxes in terms of protein abundances (A-C) and maximum activities (D-F).** (A) Ratio between the nitrite-producing and -consuming enzymes of DEN: membrane-bound nitrate reductase (NarG) and cd1-type nitrite reductase (NirS). (B) Ratio between membrane-bound nitrate reductase (NarG) and nitrous oxide reductase (NosZ). (C) Ratio between the N<sub>2</sub>O-producing and -consuming enzymes of DEN: NirS and NosZ. (A-C) The symbols represent the mean and the error bars represent standard deviations of technical duplicates independently injected in the LC-MS/MS, some are smaller than the symbols. All abundances include MAG and unbinned proteins. (D) Ratio between the nitrate and nitrite reduction potentials. (E) Ratio between the nitrate and nitrous oxide reducing potentials. (F) Ratio between the nitrite and nitrous oxide reduction potentials.

### 3.5.10. Free ammonia and free nitrous acid toxicity

The maximum possible concentration of free ammonia (FA,  $\text{NH}_3$ ) and free nitrous acid (FNA,  $\text{HNO}_2$ ) in the WWTP was calculated using the maximum pH and  $\text{NH}_4^+$  concentration for FA and the minimum pH and maximum  $\text{NO}_2^-$  concentration for FNA.

$$C_{\text{NH}_3} = 10^{\text{pH}-\text{pK}_a} \cdot C_{\text{NH}_4^+} \quad (\text{eq. S3.1})$$

$$C_{\text{HNO}_2} = 10^{\text{pK}_a-\text{pH}} \cdot C_{\text{NO}_2^-} \quad (\text{eq. S3.2})$$

**Table S3.7. Values used to calculate the maximum free ammonia concentration in the WWTP and the literature reported thresholds for AOB and NOB.**

Maximum pH	pKa	Maximum $\text{NH}_4^+$ (mg N·L <sup>-1</sup> )	Maximum $\text{NH}_3$ (mg N·L <sup>-1</sup> )	Threshold AOB <sup>105</sup> (mg $\text{NH}_3$ -N·L <sup>-1</sup> )	Threshold NOB <sup>105</sup> (mg $\text{NH}_3$ -N·L <sup>-1</sup> )
6.7	9.26	11	0.03	10	0.1

**Table S3.8. Values used to calculate the maximum free nitrous acid concentration in the WWTP and the literature reported thresholds for AOB and NOB.**

Minimum pH	pKa	Maximum $\text{NO}_2^-$ (mg N·L <sup>-1</sup> )	Maximum $\text{HNO}_2$ (mg N·L <sup>-1</sup> )	Threshold AOB <sup>103</sup> (mg $\text{HNO}_2$ -N·L <sup>-1</sup> )	Threshold NOB <sup>103</sup> (mg $\text{HNO}_2$ -N·L <sup>-1</sup> )
6.15	3.16	1.2	0.001	0.2	0.01

### 3.5.11. AOB and NOB growth stoichiometry and kinetics

**Table S3.9. Maximum specific growth rates and biomass yields of *Nitrosomonas* and *Nitrospira* cultures reported in literature.** The  $\mu_{\text{max}}$  values were normalised to 20 °C using the Arrhenius equation (eq. S3.5) and the experimentally determined coefficients for AOB and NOB (reported at the end of this page).

Guild	Species	$\mu_{\text{max}}$ (d <sup>-1</sup> )	$Y_{\text{X/N}}$ (gX/gN)	Conditions	$\mu_{\text{max}}$ 20 °C (d <sup>-1</sup> )	Ref.
AOB	<i>Nitrosomonas europaea</i>	0.84	0.063	30 °C, pH 7	0.27	144
	<i>Nitrosomonas spp.</i>	1.0	0.12	30 °C, pH 7	0.32	145
	<i>Nitrosomonas spp.</i>	0.54	0.14	24 °C, pH 7.8	0.34	146
	<i>Nitrosomonas europaea</i>	1.3	-	30 °C, pH 6.8	0.42	147
	<i>Nitrosomonas europaea</i>	1.3	0.36	28 °C, pH 7.9	0.53	148
Median		1.00	0.13		0.34	
NOB	<i>Nitrospira defluvii</i>	0.64	0.017*	28 °C, pH 7.5	0.30	149
	<i>Nitrospira moscoviensis</i>	0.75	0.030*	37 °C, pH 7.5	0.15	149
	<i>Nitrospira sp.</i>	0.64	0.020*	28 °C, pH 7.5	0.30	149
	<i>Nitrospira sp.</i>	0.32	-	29 °C, pH 8.0	0.14	150
	<i>Nitrospira japonica</i>	0.62	-	29 °C, pH 8.0	0.26	150
	<i>Nitrospira spp.</i>	0.69	0.09	22 °C, pH 7.5	0.57	151
Median		0.64	0.025		0.28	

\*Assuming a protein content of 50% the dry mass

The growth rates of AOB and NOB depend on the temperature and substrate concentration:

$$\mu_{\text{AOB}} = \mu_{\text{max,AOB}}(T) \cdot \frac{c_{\text{NH}_4^+}}{c_{\text{NH}_4^+} + K_{\text{NH}_4^+}} \cdot \frac{c_{\text{O}_2}}{c_{\text{O}_2} + K_{\text{O}_2,\text{AOB}}} \quad (\text{eq. S3.3})$$

$$\mu_{\text{NOB}} = \mu_{\text{max,NOB}}(T) \cdot \frac{c_{\text{NO}_2^-}}{c_{\text{NO}_2^-} + K_{\text{NO}_2^-}} \cdot \frac{c_{\text{O}_2}}{c_{\text{O}_2} + K_{\text{O}_2,\text{NOB}}} \quad (\text{eq. S3.4})$$

With  $\mu$  the specific growth rate,  $\mu_{\text{max}}$  the maximum specific growth rate (a function of temperature),  $c_i$  the concentrations of  $\text{NH}_4^+$ ,  $\text{NO}_2^-$  and  $\text{O}_2$  and  $K_i$  the half-saturation constants for each substrate.

The maximum specific growth rates depend on the temperature according to the Arrhenius equation:

$$\mu_{\text{max},i} = \mu_{\text{max},i}^{T_{\text{ref}}} \cdot \theta_i^{(T-T_{\text{ref}})}, \quad i = \text{AOB, NOB} \quad (\text{eq. S3.5})$$

With  $\theta$  the Arrhenius coefficient and  $T_{\text{ref}}$  a reference temperature for which we know  $\mu_{\text{max}}$ .

The Arrhenius coefficient for AOB and NOB was determined from five independent experiments with activated sludge, sampled between October 2021 and February 2022. The maximum  $\text{NH}_4^+$  and  $\text{NO}_2^-$  oxidation rates were determined at 10, 15, 20 and 25 °C. The Arrhenius coefficients, obtained from linear regressions of eq. S3.5 (Figure S3.21), were  $1.12 \pm 0.01$  for AOB and  $1.10 \pm 0.01$  for NOB.

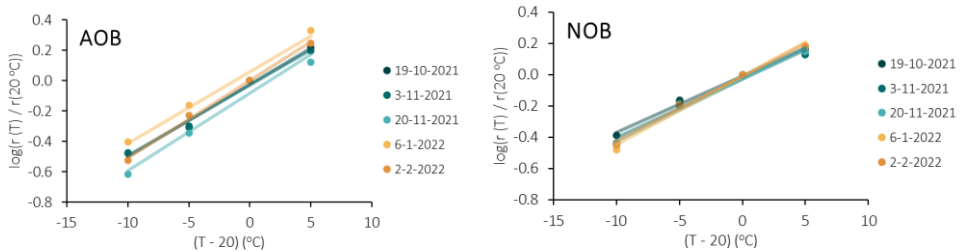


**Figure S3.21. Linear regressions between maximum activities and temperature to determine the Arrhenius coefficients of AOB and NOB in activated sludge.**

In the WWTP, when the growth rates of AOB and NOB drop below  $1/\text{SRT}$  the bacteria cannot grow as fast as they are removed from the system, so they start to washout, i.e. their concentration in the sludge slowly decreases. The variation of  $\mu_{\text{max}}$  with temperature was determined with eq. S3.5 and represented in Figure S3.22. The

temperature at which each guild starts to wash out, here named critical temperature ( $T_c$ ), is higher for NOB than AOB (Figure S3.22). This means that during winter, when the temperature progressively decreases, NOB starts washing out before AOB, resulting in a higher AOB/NOB ratio.

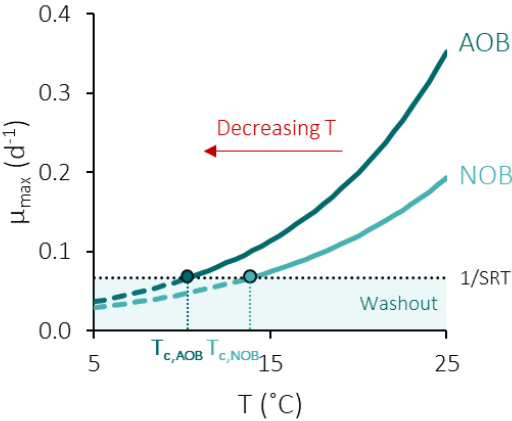


**Figure S3.22.** Variation of the  $\mu_{\max}$  of AOB and NOB with a decreasing temperature from 25 to 5 °C. The critical temperature ( $T_c$ ) represents the temperature below which each guild starts washing out.

### 3.5.12. Mathematical model replicating the seasonal peaks

A mathematical model describing the microbial and metabolite dynamics in a biological nutrient removal process was set up in Python v3.9.12 (Figure S3.23). The metabolic cascade was replicated by changing the temperature and the oxygen concentration, reproducing the WWTP dynamics.

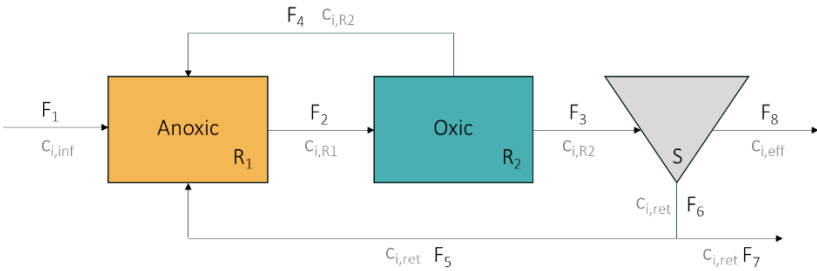


**Figure S3.23.** Simplified flowsheet of the biological nutrient removal process used in the mathematical model, comprising an anoxic ( $R_1$ ) and oxidic tank ( $R_2$ ), and a settler ( $S$ ). The flowrates are represented by  $F_i$  and the metabolite and biomass concentrations in each process unit and stream are represented by  $c_i$ .

The implemented model was adapted from a previously described model including the three known metabolic pathways of  $N_2O$  production: hydroxylamine oxidation, nitrifier

denitrification, and heterotrophic denitrification<sup>152</sup>. The volumetric process rates were described with Monod terms (Table S3.10). Nitrite and nitric oxide reduction by AOB were assumed not to be inhibited by oxygen, in line with their important role in regenerating electron carriers and avoiding the accumulation of NO and NH<sub>2</sub>OH during ammonia oxidation under oxic conditions<sup>118,119,122,123</sup>. The compound production and consumption rates were determined by multiplying the process rates with the stoichiometric table (Table S3.11). The fluctuation of  $\mu_{\max}$  with temperature was described with eq. S5.

**Table S3.10. Volumetric production and consumption rates of biomass and metabolites in the oxic and anoxic tanks.**

	Guild	Reaction	Rate formula (gCOD·m <sup>-3</sup> ·d <sup>-1</sup> )
<b>Growth</b>			
1	AOB	NH <sub>4</sub> <sup>+</sup> → NH <sub>2</sub> OH	$\mu_{\max, \text{AMO}}(T) \cdot c_{\text{AOB}} \cdot \frac{c_{\text{NH}_4^+}}{c_{\text{NH}_4^+} + K_{\text{NH}_4^+}} \cdot \frac{c_{\text{O}_2}}{c_{\text{O}_2} + K_{\text{O}_2, \text{AOB}}}$
2		NH <sub>2</sub> OH → NO <sub>2</sub> <sup>-</sup>	$(1 - \varepsilon) \cdot \mu_{\max, \text{HAO}}(T) \cdot c_{\text{AOB}} \cdot \frac{c_{\text{NH}_2\text{OH}}}{c_{\text{NH}_2\text{OH}} + K_{\text{NH}_2\text{OH}}} \cdot \frac{c_{\text{O}_2}}{c_{\text{O}_2} + K_{\text{O}_2, \text{AOB}}}$
3		NH <sub>2</sub> OH → NO	$\varepsilon \cdot \mu_{\max, \text{HAO}}(T) \cdot c_{\text{AOB}} \cdot \frac{c_{\text{NH}_2\text{OH}}}{c_{\text{NH}_2\text{OH}} + K_{\text{NH}_2\text{OH}}} \cdot \frac{c_{\text{O}_2}}{c_{\text{O}_2} + K_{\text{O}_2, \text{AOB}}}$
4		NO <sub>2</sub> <sup>-</sup> → NO	$\eta_{\text{AOB}} \cdot \mu_{\max, \text{HAO}}(T) \cdot c_{\text{AOB}} \cdot \frac{c_{\text{NH}_2\text{OH}}}{c_{\text{NH}_2\text{OH}} + K_{\text{NH}_2\text{OH}}} \cdot \frac{c_{\text{NO}_2^-}}{c_{\text{NO}_2^-} + K_{\text{NO}_2^-}}$
5		NO → N <sub>2</sub> O	$\eta_{\text{AOB}} \cdot \mu_{\max, \text{HAO}}(T) \cdot c_{\text{AOB}} \cdot \frac{c_{\text{NH}_2\text{OH}}}{c_{\text{NH}_2\text{OH}} + K_{\text{NH}_2\text{OH}}} \cdot \frac{c_{\text{NO}}}{c_{\text{NO}} + K_{\text{NO}}}$
6	NOB	NO <sub>2</sub> <sup>-</sup> → NO <sub>3</sub> <sup>-</sup>	$\mu_{\max, \text{NOB}}(T) \cdot c_{\text{NOB}} \cdot \frac{c_{\text{NO}_2^-}}{c_{\text{NO}_2^-} + K_{\text{NO}_2^-}} \cdot \frac{c_{\text{O}_2}}{c_{\text{O}_2} + K_{\text{O}_2, \text{NOB}}}$
7	HB	O <sub>2</sub> → H <sub>2</sub> O	$\mu_{\max, \text{HB}}(T) \cdot c_{\text{HB}} \cdot \frac{c_{\text{NH}_4^+}}{c_{\text{NH}_4^+} + K_{\text{NH}_4^+}} \cdot \frac{c_{\text{O}_2}}{c_{\text{O}_2} + K_{\text{O}_2, \text{HB}}} \cdot \frac{c_{\text{S}}}{c_{\text{S}} + K_{\text{S}, \text{HB}}}$
8		NO <sub>3</sub> <sup>-</sup> → NO <sub>2</sub> <sup>-</sup>	$\eta_{\text{HB}} \cdot \mu_{\max, \text{HB}}(T) \cdot c_{\text{HB}} \cdot \frac{c_{\text{NH}_4^+}}{c_{\text{NH}_4^+} + K_{\text{NH}_4^+}} \cdot \frac{c_{\text{NO}_2^-}}{c_{\text{NO}_2^-} + K_{\text{NO}_2^-}} \cdot \frac{c_{\text{S}}}{c_{\text{S}} + K_{\text{S}, \text{HB}}} \cdot \frac{K_{\text{I}, \text{O}_2}}{c_{\text{O}_2} + K_{\text{I}, \text{O}_2}}$
9		NO <sub>2</sub> <sup>-</sup> → NO	$\eta_{\text{HB}} \cdot \mu_{\max, \text{HB}}(T) \cdot c_{\text{HB}} \cdot \frac{c_{\text{NH}_4^+}}{c_{\text{NH}_4^+} + K_{\text{NH}_4^+}} \cdot \frac{c_{\text{NO}_2^-}}{c_{\text{NO}_2^-} + K_{\text{NO}_2^-}} \cdot \frac{c_{\text{S}}}{c_{\text{S}} + K_{\text{S}, \text{HB}}} \cdot \frac{K_{\text{I}, \text{O}_2}}{c_{\text{O}_2} + K_{\text{I}, \text{O}_2}}$
10		NO → N <sub>2</sub> O	$\eta_{\text{HB}} \cdot \mu_{\max, \text{HB}}(T) \cdot c_{\text{HB}} \cdot \frac{c_{\text{NH}_4^+}}{c_{\text{NH}_4^+} + K_{\text{NH}_4^+}} \cdot \frac{c_{\text{NO}}}{c_{\text{NO}} + K_{\text{NO}}} \cdot \frac{c_{\text{S}}}{c_{\text{S}} + K_{\text{S}, \text{HB}}} \cdot \frac{K_{\text{I}, \text{O}_2}}{c_{\text{O}_2} + K_{\text{I}, \text{O}_2}}$
11		N <sub>2</sub> O → N <sub>2</sub>	$\eta_{\text{HB}} \cdot \mu_{\max, \text{HB}}(T) \cdot c_{\text{HB}} \cdot \frac{c_{\text{NH}_4^+}}{c_{\text{NH}_4^+} + K_{\text{NH}_4^+}} \cdot \frac{c_{\text{N}_2\text{O}}}{c_{\text{N}_2\text{O}} + K_{\text{N}_2\text{O}}} \cdot \frac{c_{\text{S}}}{c_{\text{S}} + K_{\text{S}, \text{HB}}} \cdot \frac{K_{\text{I}, \text{O}_2}}{c_{\text{O}_2} + K_{\text{I}, \text{O}_2}}$
<b>Decay</b>			
12	AOB (oxic)	X <sub>AOB</sub> → X <sub>I</sub>	$0.05 \cdot \mu_{\max, \text{HAO}}(T) \cdot c_{\text{AOB}}$
	AOB (anoxic)	X <sub>AOB</sub> → X <sub>I</sub>	$\eta_{\text{AOB}} \cdot 0.05 \cdot \mu_{\max, \text{HAO}}(T) \cdot c_{\text{AOB}}$
13	NOB (oxic)	X <sub>NOB</sub> → X <sub>I</sub>	$0.05 \cdot \mu_{\max, \text{NOB}}(T) \cdot c_{\text{NOB}}$
	NOB (anoxic)	X <sub>NOB</sub> → X <sub>I</sub>	$\eta_{\text{NOB}} \cdot 0.05 \cdot \mu_{\max, \text{NOB}}(T) \cdot c_{\text{NOB}}$
14	HB (oxic)	X <sub>HB</sub> → X <sub>I</sub>	$0.05 \cdot \mu_{\max, \text{HB}}(T) \cdot c_{\text{HB}}$
	HB (anoxic)	X <sub>HB</sub> → X <sub>I</sub>	$\eta_{\text{HB}} \cdot 0.05 \cdot \mu_{\max, \text{HB}}(T) \cdot c_{\text{HB}}$

Table S3.11. Stoichiometric matrix.

S	NH <sub>4</sub> <sup>+</sup>	NH <sub>2</sub> OH	NO <sub>2</sub> <sup>-</sup>	NO <sub>3</sub> <sup>-</sup>	NO	N <sub>2</sub> O	AOB	NOB	HB	IN
$\frac{\text{gCOD} \cdot \text{gCOD}^{-1}}{\text{gCOD}^{-1}}$	$\frac{\text{gN} \cdot \text{gCOD}^{-1}}{\text{gCOD}^{-1}}$	$\frac{\text{gN} \cdot \text{gCOD}^{-1}}{\text{gCOD}^{-1}}$	$\frac{\text{gN} \cdot \text{gCOD}^{-1}}{\text{gCOD}^{-1}}$	$\frac{\text{gN} \cdot \text{gCOD}^{-1}}{\text{gCOD}^{-1}}$	$\frac{\text{gN} \cdot \text{gCOD}^{-1}}{\text{gCOD}^{-1}}$	$\frac{\text{gN} \cdot \text{gCOD}^{-1}}{\text{gCOD}^{-1}}$	$\frac{\text{gCOD} \cdot \text{gCOD}^{-1}}{\text{gCOD}^{-1}}$	$\frac{\text{gCOD} \cdot \text{gCOD}^{-1}}{\text{gCOD}^{-1}}$	$\frac{\text{gCOD} \cdot \text{gCOD}^{-1}}{\text{gCOD}^{-1}}$	$\frac{\text{gCOD} \cdot \text{gCOD}^{-1}}{\text{gCOD}^{-1}}$
1	-1	1								
2	$-i_{NXB}$	$-\frac{1}{Y_{AOB}}$	$\frac{1}{Y_{AOB}}$				1			
3	$-i_{NXB}$	$-\frac{1}{Y_{AOB}}$			$\frac{1}{Y_{AOB}}$		1			
4		-1	-3		4					
5		-1			-2	3				
6	$-i_{NXB}$		$-\frac{1}{Y_{NOB}}$	$\frac{1}{Y_{NOB}}$				1		
7	$-\frac{1}{Y_{HB}}$	$-i_{NXB}$							1	
8	$-\frac{1}{Y_{HB}}$	$-i_{NXB}$	$\frac{1 - Y_{HB}}{1.14 \cdot Y_{HB}}$	$-\frac{1 - Y_{HB}}{1.14 \cdot Y_{HB}}$					1	
9	$-\frac{1}{Y_{HB}}$	$-i_{NXB}$	$-\frac{1 - Y_{HB}}{0.57 \cdot Y_{HB}}$		$\frac{1 - Y_{HB}}{0.57 \cdot Y_{HB}}$				1	
10	$-\frac{1}{Y_{HB}}$	$-i_{NXB}$			$-\frac{1 - Y_{HB}}{0.57 \cdot Y_{HB}}$	$\frac{1 - Y_{HB}}{0.57 \cdot Y_{HB}}$			1	
11	$-\frac{1}{Y_{HB}}$	$-i_{NXB}$				$-\frac{1 - Y_{HB}}{0.57 \cdot Y_{HB}}$			1	
12	$1 - f_{XI}$	$i_{NXB} - i_{NXI} \cdot f_{XI}$					-1			$f_{XI}$
13	$1 - f_{XI}$	$i_{NXB} - i_{NXI} \cdot f_{XI}$						-1		$f_{XI}$
14	$1 - f_{XI}$	$i_{NXB} - i_{NXI} \cdot f_{XI}$							-1	$f_{XI}$

**Table S3.12. Process and microbial parameters used in the mathematical model.**

Parameter	Description	Value	Unit	Reference
<b>Process parameters</b>				
SRT	Sludge retention time	30	d	Assumed
V <sub>1</sub>	Volume of R <sub>1</sub> (anoxic)	11000	m <sup>3</sup>	This study
V <sub>2</sub>	Volume of R <sub>2</sub> (oxic)	5800	m <sup>3</sup>	This study
V <sub>s</sub>	Volume of the settler	18500	m <sup>3</sup>	This study
F <sub>1</sub>	Influent flow rate	26000	m <sup>3</sup> ·d <sup>-1</sup>	This study
F <sub>4</sub>	Flow rate from the recycling from oxic to anoxic tank	100000	m <sup>3</sup> ·d <sup>-1</sup>	This study
F <sub>5</sub>	Flow rate of the return sludge	26000	m <sup>3</sup> ·d <sup>-1</sup>	This study
C <sub>NH4,in</sub>	Influent ammonium concentration	70	gN·m <sup>-3</sup>	This study
C <sub>S,in</sub>	Influent organic substrate concentration	600	gCOD·m <sup>-3</sup>	This study
<b>Stoichiometric and kinetic parameters</b>				
K <sub>O2,AOB</sub>	O <sub>2</sub> half-saturation coefficient of AOB	0.7	gO <sub>2</sub> ·m <sup>-3</sup>	107,109
K <sub>NH4</sub>	NH <sub>4</sub> <sup>+</sup> half-saturation coefficient of AOB and HB	0.1	gN·m <sup>-3</sup>	153
K <sub>NH2OH</sub>	NH <sub>2</sub> OH half-saturation coefficient of AOB	0.2	gN·m <sup>-3</sup>	152
K <sub>NO2</sub>	NO <sub>2</sub> <sup>-</sup> half-saturation coefficient of all guilds	0.5	gN·m <sup>-3</sup>	154
K <sub>NO</sub>	NO half-saturation coefficient of AOB and HB	0.01	gN·m <sup>-3</sup>	152
μ <sub>max,AMO</sub>	Maximum specific AMO rate of AOB	2.9	d <sup>-1</sup>	155
μ <sub>max,HAO</sub>	Maximum specific HAO rate of AOB	2.2	d <sup>-1</sup>	155
η <sub>AOB</sub>	Anoxic rate reduction factor of AOB	0.2	-	152
ε	Fraction of NH <sub>2</sub> OH oxidation to NO	0.001	-	152
Y <sub>AOB</sub>	AOB biomass yield on NH <sub>4</sub> <sup>+</sup>	0.21	gCOD·gN <sup>-1</sup>	Table S3.9
θ <sub>AOB</sub>	Arrhenius coefficient of AOB	1.12	-	This study
K <sub>O2,NOB</sub>	O <sub>2</sub> half-saturation coefficient of NOB	0.1	gO <sub>2</sub> ·m <sup>-3</sup>	107,109
μ <sub>max,NOB</sub>	Maximum specific growth rate of NOB	1.4	d <sup>-1</sup>	155
Y <sub>NOB</sub>	NOB biomass yield on NO <sub>2</sub> <sup>-</sup>	0.04	gCOD·gN <sup>-1</sup>	Table S3.9
θ <sub>NOB</sub>	Arrhenius coefficient of NOB	1.10	-	This study
K <sub>O2,HB</sub>	O <sub>2</sub> half-saturation coefficient of HB	0.1	gO <sub>2</sub> ·m <sup>-3</sup>	156
K <sub>NO3</sub>	NO <sub>3</sub> <sup>-</sup> half-saturation coefficient of HB	0.2	gN·m <sup>-3</sup>	156
K <sub>N2O</sub>	N <sub>2</sub> O half-saturation coefficient of HB	0.05	gN·m <sup>-3</sup>	157
K <sub>S</sub>	Organic substrate half-saturation coefficient of HB	2	gCOD·m <sup>-3</sup>	158
K <sub>I,O2</sub>	O <sub>2</sub> inhibition coefficient of heterotrophic denitrification	0.03	gO <sub>2</sub> ·m <sup>-3</sup>	158
μ <sub>max,HB</sub>	Maximum specific growth rate of HB	12	d <sup>-1</sup>	158 *
η <sub>HB</sub>	Anoxic rate reduction factor of HB	0.2	-	152
Y <sub>HB</sub>	HB biomass yield on organic substrate	0.6	gCOD·gCOD <sup>-1</sup>	156
θ <sub>HB</sub>	Arrhenius coefficient of HB	1.05	-	Assumed
i <sub>NXB</sub>	Nitrogen content of biomass	0.09	gN·gCOD <sup>-1</sup>	156
i <sub>NXI</sub>	Nitrogen content of inerts	0.02	gN·gCOD <sup>-1</sup>	156
f <sub>XI</sub>	Fraction of inerts in biomass	0.08	gCOD·gCOD <sup>-1</sup>	156

\*Calculated oxic rate from denitrification rates reported in the reference and the reduction factor (η<sub>HB</sub>)

The unknown flow rates of the process were determined from the known flow rates with overall mass balances (Figure S3.23, Table S3.12).

**Table S3.13. Overall mass balances to determine the unknown volumetric flow rates.**

Flow rate	Description	Formula	Units
F <sub>2</sub>	Anoxic to oxic tank	F <sub>1</sub> + F <sub>4</sub> + F <sub>5</sub>	m <sup>3</sup>
F <sub>3</sub>	Oxic tank to settler	F <sub>2</sub> - F <sub>4</sub>	m <sup>3</sup>
F <sub>7</sub>	Purged sludge	$\frac{V_{R1} \cdot (c_{AOB,R1} + c_{NOB,R1} + c_{HB,R1}) + V_{R2} \cdot (c_{AOB,R2} + c_{NOB,R2} + c_{HB,R2})}{SRT \cdot (c_{AOB,ret} + c_{NOB,ret} + c_{HB,ret})}$	m <sup>3</sup>
F <sub>6</sub>	Sludge effluent from settler	F <sub>5</sub> + F <sub>7</sub>	m <sup>3</sup>
F <sub>8</sub>	Water effluent from settler	F <sub>3</sub> - F <sub>6</sub>	m <sup>3</sup>

Mass balances in each process unit described the dynamics in biomass and metabolite concentrations.

**Table S3.14. Mass balances (ordinary differential equations) of metabolites and biomass in each process unit.**

Process unit	Ordinary differential equation	Compounds	Units
R <sub>1</sub>	$\frac{dc_{i,R1}}{dt} = \frac{c_{i,in} \cdot F_1 + c_{i,R2} \cdot F_4 + c_{i,ret} \cdot F_5 - c_{i,R1} \cdot F_2}{V_{R1}} + r_{i,R1}$	Metabolites and biomass	g·m <sup>-3</sup> ·d <sup>-1</sup>
R <sub>2</sub>	$\frac{dc_{i,R2}}{dt} = \frac{c_{i,R1} \cdot F_2 - c_{i,R2} \cdot (F_3 + F_4)}{V_{R2}} + r_{i,R2}$	Metabolites and biomass	g·m <sup>-3</sup> ·d <sup>-1</sup>
S	$\frac{dc_{i,ret}}{dt} = \frac{c_{i,R2} \cdot F_3 + c_{i,ret} \cdot F_6}{V_S}$	Biomass	g·m <sup>-3</sup> ·d <sup>-1</sup>
	$\frac{dc_{i,ret}}{dt} = \frac{c_{i,R2} \cdot F_3 + c_{i,ret} \cdot (F_6 + F_8)}{V_S}$	Metabolites	g·m <sup>-3</sup> ·d <sup>-1</sup>

The ordinary differential equations were solved with the LSODA method of the solve\_ivp function of the SciPy v1.7.3 <sup>46</sup> package for a time span of 5 years. The oxygen concentration in the anoxic tank was set as 0. The seasonal fluctuations in the temperature in both anoxic and oxic tanks was replicated with a sinusoid as function of time and the concentration of oxygen in the oxic tank was set as function of the ammonium concentration, to replicate the WWTP operation mode:

$$T = A \cdot \sin(2\pi \cdot f \cdot t + \varphi) + B \quad (\text{eq. S3.6})$$

$$C_{O_2} = \frac{C_{O_2,max} - C_{O_2,min}}{0.4 \cdot C_{NH_4^+,in}} \cdot C_{NH_4^+} + C_{O_2,min} \quad (\text{eq. S3.7})$$



**Table S3.15. Parameters for the equations describing seasonal fluctuations in the oxygen concentration and the temperature.**

Parameter	Description	Value for T equation	Value for c <sub>O<sub>2</sub></sub> equation
Min	Minimum value	10 °C	0.5 g·m <sup>-3</sup>
Max	Maximum value	25 °C	3 g·m <sup>-3</sup>
A	Amplitude	$\frac{T_{\max} - T_{\min}}{2}$	-
f	Frequency	1/365	-
φ	Phase	0.5π	-
B	Axis shift	$\frac{T_{\max} + T_{\min}}{2}$	-
c <sub>NH<sub>4</sub>,in</sub>	Influent ammonium	-	70

The model replicated the ecophysiological cascade, with the accumulation of NH<sub>4</sub><sup>+</sup>, NO<sub>2</sub><sup>-</sup> and N<sub>2</sub>O and the increase in AOB/NOB ratio (Figure S3.23).

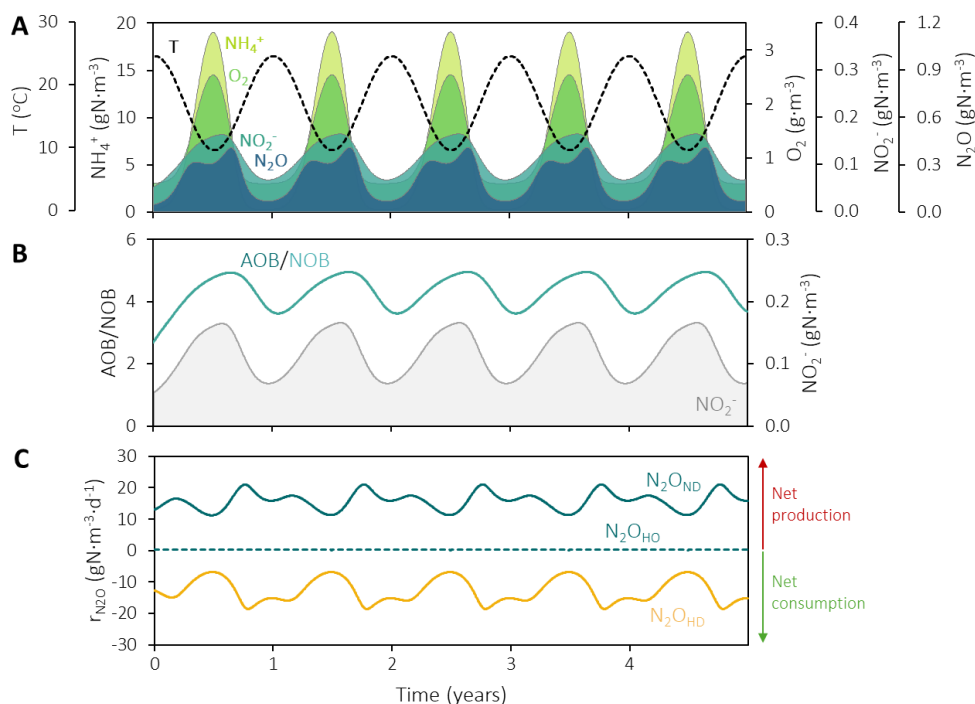


**Figure S3.24. Mathematical model simulating the seasonal nitrifiers and nitrogen metabolites dynamics.** In the model, the ecophysiological cascade was triggered with decreasing temperature and increasing dissolved O<sub>2</sub>, as hypothesised from the full-scale observations. **(A)** Temperature, and ammonium, dissolved oxygen, nitrite and nitrous oxide concentrations in the oxidic tank. **(B)** Ratio of the concentrations of AOB and NOB in the oxidic tank, alongside the nitrite concentration also represented in A. **(C)** N<sub>2</sub>O accumulation rates for each metabolic pathway: nitrifier denitrification (ND) and hydroxylamine oxidation (HO) by AOB and heterotrophic denitrification (HD) by heterotrophic bacteria. Positive values indicate that the pathway is an N<sub>2</sub>O source (net production) and negative values indicate the pathway is a sink (net consumption).

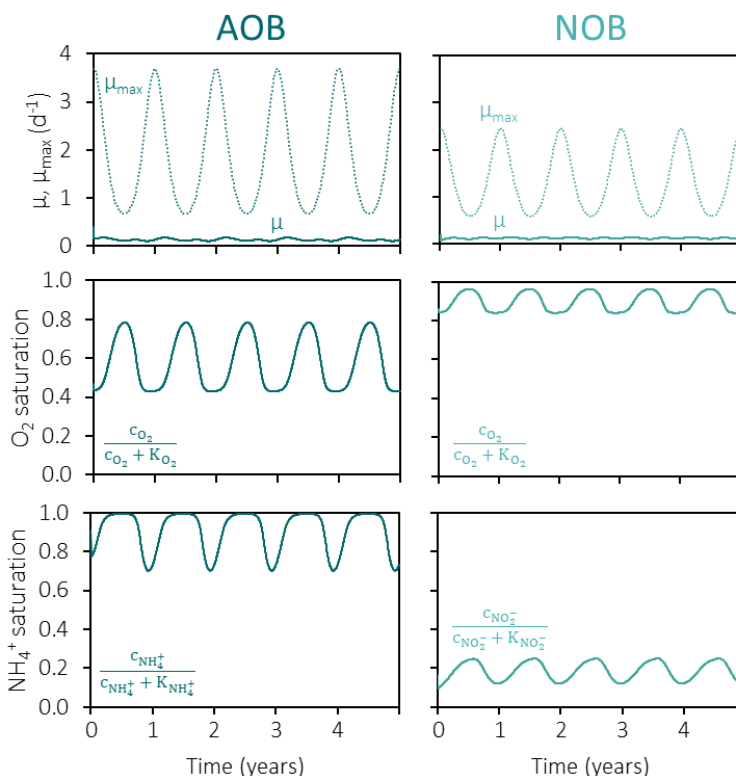


**Figure S3.25. Kinetic contributions of each element of the growth equations to the AOB and NOB growth rates (eq. S3.3-3.4) during temperature and dissolved oxygen fluctuations in the mathematical model represented in Figure S3.24. (A)** Fluctuation of the maximum ( $\mu_{\max}$ ) and actual specific growth rates ( $\mu$ ). While the  $\mu_{\max}$  of AOB decreases relatively more than the  $\mu_{\max}$  of NOB, the value for NOB achieves a much lower value, so the negative effect of temperature decrease harms NOB more than AOB. **(B)** Fluctuation in the dissolved oxygen saturation fraction. The relative increase in  $\mu_{\text{AOB}}$  is much higher than in  $\mu_{\text{NOB}}$ , so the  $\text{O}_2$  increase benefits AOB more than NOB. **(C)** Fluctuation in the ammonium (AOB) and nitrite (NOB) saturation fractions.

The python script with the mathematical model replicating the seasonal nitrite accumulation can be found online in the supplementary information of the article.

### 3.5.13. Calculation of the maximum $\text{N}_2\text{O}$ activities

#### Determination of the $\text{N}_2\text{O}$ mass transfer coefficient ( $k_{\text{La}}$ )

The  $\text{N}_2\text{O}$  volumetric mass transfer coefficient ( $k_{\text{La}}$ ) was determined to calculate the transfer rate during the  $\text{N}_2\text{O}$  batches. The  $k_{\text{La}}$  was determined under the same conditions as the activity tests (750 rpm stirring, no gas flow, 20 °C), with water instead of biomass.

The  $k_{LA}$  was obtained by taking the slope of the linearised integrated mass transfer equation fitted to the dissolved N<sub>2</sub>O concentration profile over time.

$$C_{N_2O} = C_{N_2O}^* \cdot (1 - e^{-k_{LA} \cdot t}) \quad (\text{eq. S3.8})$$

with  $C_{N_2O}^*$  the solubility of N<sub>2</sub>O at 20 °C. The obtained  $k_{LA}$  was 5 h<sup>-1</sup>.

The python script used to calculate the maximum N<sub>2</sub>O activities can be found online in the supplementary information of the article.

## 3.6. References

1. Intergovernmental Panel on Climate Change. *Climate Change 2014: Synthesis Report*. (Core Writing Team, Pachauri RK, Meyer LA, eds.). IPCC; 2015.
2. Tian H, Xu R, Canadell JG, et al. A comprehensive quantification of global nitrous oxide sources and sinks. *Nature*. 2020;586(7828):248-256. doi:10.1038/s41586-020-2780-0
3. Vasilaki V, Massara TM, Stanchev P, Fatone F, Katsou E. A decade of nitrous oxide (N<sub>2</sub>O) monitoring in full-scale wastewater treatment processes: A critical review. *Water Res*. 2019;161:392-412. doi:10.1016/j.watres.2019.04.022
4. Marchant HK, Ahmerkamp S, Lavik G, et al. Denitrifying community in coastal sediments performs aerobic and anaerobic respiration simultaneously. *ISME J*. 2017;11(8):1799-1812. doi:10.1038/ismej.2017.51
5. Freing A, Wallace DWR, Bange HW. Global oceanic production of nitrous oxide. *Philos Trans R Soc B*. 2012;367:1245-1255. doi:10.1098/rstb.2011.0360
6. Butterbach-Bahl K, Baggs EM, Dannenmann M, Kiese R, Zechmeister-Boltenstern S. Nitrous oxide emissions from soils: How well do we understand the processes and their controls? *Philos Trans R Soc B*. 2013;368(1621). doi:10.1098/rstb.2013.0122
7. Sabba F, Picioreanu C, Boltz JP, Nerenberg R. Predicting N<sub>2</sub>O emissions from nitrifying and denitrifying biofilms: A modeling study. *Water Sci Technol*. 2017;75(3):530-538. doi:10.2166/wst.2016.484
8. Schreiber F, Wunderlin P, Udert KM, Wells GF. Nitric oxide and nitrous oxide turnover in natural and engineered microbial communities: Biological pathways, chemical reactions, and novel technologies. *Front Microbiol*. 2012;3(OCT):1-24. doi:10.3389/fmicb.2012.00372
9. Wrage-Mönnig N, Horn MA, Well R, Müller C, Velthof G, Oenema O. The role of nitrifier denitrification in the production of nitrous oxide revisited. *Soil Biol Biochem*. 2018;123(April):A3-A16. doi:10.1016/j.soilbio.2018.03.020
10. Morley N, Baggs EM, Dörsch P, Bakken L. Production of NO, N<sub>2</sub>O and N<sub>2</sub> by extracted soil bacteria, regulation by NO<sub>2</sub>- and O<sub>2</sub> concentrations. *FEMS Microbiol Ecol*. 2008;65(1):102-112. doi:10.1111/j.1574-6941.2008.00495.x
11. Zhu-Barker X, Cavazos AR, Ostrom NE, Horwath WR, Glass JB. The importance of abiotic reactions for nitrous oxide production. *Biogeochemistry*. 2015;126(3):251-267. doi:10.1007/s10533-015-0166-4
12. Stein LY, Klotz MG, Lancaster KM, et al. Comment on "A Critical Review on Nitrous Oxide Production by Ammonia-Oxidizing Archaea" by Lan Wu, Xueming Chen, Wei Wei, Yiwen Liu, Dongbo Wang, and Bing-Jie Ni. *Environ Sci Technol*. 2021;55(1):797-798. doi:10.1021/acs.est.0c06792
13. Stieglmeier M, Mooshammer M, Kitzler B, et al. Aerobic nitrous oxide

- p>production through N-nitrosating hybrid formation in ammonia-oxidizing archaea.
- ISME J.*
- 2014;8(5):1135-1146. doi:10.1038/ismej.2013.220
14. Santoro AE, Buchwald C, McIlvin MR, Casciotti KL. Isotopic signature of N<sub>2</sub>O produced by marine ammonia-oxidizing archaea. *Science (80- )*. 2011;333:1282-1285. doi:10.1126/science.1208239
  15. Hink L, Gubry-Rangin C, Nicol GW, Prosser JL. The consequences of niche and physiological differentiation of archaeal and bacterial ammonia oxidisers for nitrous oxide emissions. *ISME J.* 2018;12(4):1084-1093. doi:10.1038/s41396-017-0025-5
  16. Hink L, Nicol GW, Prosser JL. Archaea produce lower yields of N<sub>2</sub>O than bacteria during aerobic ammonia oxidation in soil. *Environ Microbiol.* 2017;19(12):4829-4837. doi:10.1111/1462-2920.13282
  17. Kozłowski JA, Stieglmeier M, Schleper C, Klotz MG, Stein LY. Pathways and key intermediates required for obligate aerobic ammonia-dependent chemolithotrophy in bacteria and Thaumarchaeota. *ISME J.* 2016;10(8):1836-1845. doi:10.1038/ismej.2016.2
  18. Su Q, Domingo-Félez C, Jensen MM, Smets BF. Abiotic nitrous oxide (N<sub>2</sub>O) production is strongly pH dependent, but contributes little to overall N<sub>2</sub>O emissions in biological nitrogen removal systems. *Environ Sci Technol.* 2019;53(7):3508-3516. doi:10.1021/acs.est.8b06193
  19. Yang S, Chang BX, Warner MJ, et al. Global reconstruction reduces the uncertainty of oceanic nitrous oxide emissions and reveals a vigorous seasonal cycle. *Proc Natl Acad Sci U S A.* 2020;117(22). doi:10.1073/pnas.1921914117
  20. Wan XS, Lin H, Ward BB, Kao SJ, Dai M. Significant Seasonal N<sub>2</sub>O Dynamics Revealed by Multi-Year Observations in the Northern South China Sea. *Global Biogeochem Cycles.* 2022;36(10). doi:10.1029/2022GB007333
  21. Bremner JM, Robbins SG, Blackmer AM. Seasonal variability in emission of nitrous oxide from soil. *Geophys Res Lett.* 1980;7(9):641-644. doi:10.1029/GL007i009p00641
  22. Wagner-Riddle C, Congreves KA, Abalos D, et al. Globally important nitrous oxide emissions from croplands induced by freeze-thaw cycles. *Nat Geosci.* 2017;10(4):279-283. doi:10.1038/ngeo2907
  23. Wang X, Wang S, Yang Y, et al. Hot moment of N<sub>2</sub>O emissions in seasonally frozen peatlands. *ISME J.* 2023;17(6):792-802. doi:10.1038/s41396-023-01389-x
  24. Kortelainen P, Larmola T, Rantakari M, Juutinen S, Alm J, Martikainen PJ. Lakes as nitrous oxide sources in the boreal landscape. *Glob Chang Biol.* 2020;26(3):1432-1445. doi:10.1111/gcb.14928
  25. Liang X, Wang B, Gao D, et al. Nitrification Regulates the Spatiotemporal Variability of N<sub>2</sub>O Emissions in a Eutrophic Lake. *Environ Sci Technol.* 2022;56(23):17430-17442. doi:10.1021/acs.est.2c03992

26. Beaulieu JJ, Shuster WD, Rebholz JA. Nitrous oxide emissions from a large, impounded river: The Ohio river. *Environ Sci Technol*. 2010;44(19):7527-7533. doi:10.1021/es1016735
27. Brotto AC, Kligerman DC, Andrade SA, et al. Factors controlling nitrous oxide emissions from a full-scale activated sludge system in the tropics. *Environ Sci Pollut Res*. 2015;22(15):11840-11849. doi:10.1007/s11356-015-4467-x
28. Chen X, Mielczarek AT, Habicht K, Andersen MH, Thornberg D, Sin G. Assessment of Full-Scale N2O Emission Characteristics and Testing of Control Concepts in an Activated Sludge Wastewater Treatment Plant with Alternating Aerobic and Anoxic Phases. *Environ Sci Technol*. 2019;53(21):12485-12494. doi:10.1021/acs.est.9b04889
29. Valk L, Peces M, Singleton CM, et al. Exploring the microbial influence on seasonal nitrous oxide concentration in a full-scale wastewater treatment plant using metagenome assembled genomes. *Water Res*. 2022;219(May):118563. doi:10.1016/j.watres.2022.118563
30. Sieranen M, Hilander H, Haimi H, Larsson T, Kuokkanen A, Mikola A. Seasonality of nitrous oxide emissions at six full-scale wastewater treatment plants. *Water Sci Technol*. 2023;89(3):603-612. doi:10.2166/wst.2023.420
31. Daelman MRJ, van Voorthuizen EM, van Dongen UGJM, Volcke EIP, van Loosdrecht MCM. Seasonal and diurnal variability of N2O emissions from a full-scale municipal wastewater treatment plant. *Sci Total Environ*. 2015;536:1-11. doi:10.1016/j.scitotenv.2015.06.122
32. Bae W Bin, Park Y, Chandran K, et al. Temporal triggers of N2O emissions during cyclical and seasonal variations of a full-scale sequencing batch reactor treating municipal wastewater. *Sci Total Environ*. 2021;797:149093. doi:10.1016/j.scitotenv.2021.149093
33. Gruber W, Niederdorfer R, Ringwald J, Morgenroth E, Bürgmann H, Joss A. Linking seasonal N2O emissions and nitrification failures to microbial dynamics in a SBR wastewater treatment plant. *Water Res X*. 2021;11:100098. doi:10.1016/j.wroa.2021.100098
34. Gruber W, von Känel L, Vogt L, et al. Estimation of countrywide N2O emissions from wastewater treatment in Switzerland using long-term monitoring data. *Water Res X*. 2021;13(September). doi:10.1016/j.wroa.2021.100122
35. Daims H, Taylor MW, Wagner M. Wastewater treatment: a model system for microbial ecology. *Trends Biotechnol*. 2006;24(11):483-489. doi:10.1016/j.tibtech.2006.09.002
36. Gruber W, Villez K, Kipf M, et al. N2O emission in full-scale wastewater treatment: Proposing a refined monitoring strategy. *Sci Total Environ*. 2020;699:134157. doi:10.1016/j.scitotenv.2019.134157
37. Kosonen H, Heinonen M, Mikola A, et al. Nitrous Oxide Production at a Fully Covered Wastewater Treatment Plant:

- Results of a Long-Term Online Monitoring Campaign. *Environ Sci Technol.* 2016;50(11):5547-5554. doi:10.1021/acs.est.5b04466
38. Daelman MRJ, Van Voorthuizen EM, Van Dongen LGJM, Volcke EIP, Van Loosdrecht MCM. Methane and nitrous oxide emissions from municipal wastewater treatment - Results from a long-term study. *Water Sci Technol.* 2013;67(10):2350-2355. doi:10.2166/wst.2013.109
39. Chen H, Zeng L, Wang D, Zhou Y, Yang X. Recent advances in nitrous oxide production and mitigation in wastewater treatment. *Water Res.* 2020;184:116168. doi:10.1016/j.watres.2020.116168
40. Baggs EM. Soil microbial sources of nitrous oxide: recent advances in knowledge, emerging challenges and future direction. *Curr Opin Environ Sustain.* 2011;3(5):321-327. doi:10.1016/j.cosust.2011.08.011
41. Thomson AJ, Giannopoulos G, Pretty J, Baggs EM, Richardson DJ. Biological sources and sinks of nitrous oxide and strategies to mitigate emissions. *Philos Trans R Soc B Biol Sci.* 2012;367(1593):1157-1168. doi:10.1098/rstb.2011.0415
42. Pijuan M, Zhao Y. *Quantification and Modelling of Fugitive Greenhouse Gas Emissions from Urban Water Systems*; 2022. doi:10.2166/9781789060461
43. Vasilaki V, Volcke EIP, Nandi AK, van Loosdrecht MCM, Katsou E. Relating N<sub>2</sub>O emissions during biological nitrogen removal with operating conditions using multivariate statistical techniques. *Water Res.* 2018;140:387-402. doi:10.1016/j.watres.2018.04.052
44. Johnston J, LaPara T, Behrens S. Composition and Dynamics of the Activated Sludge Microbiome during Seasonal Nitrification Failure. *Sci Rep.* 2019;9(1):1-15. doi:10.1038/s41598-019-40872-4
45. Harris CR, Millman KJ, van der Walt SJ, et al. Array programming with NumPy. *Nature.* 2020;585(7825):357-362. doi:10.1038/s41586-020-2649-2
46. Virtanen P, Gommers R, Oliphant TE, et al. SciPy 1.0: fundamental algorithms for scientific computing in Python. *Nat Methods.* 2020;17(3):261-272. doi:10.1038/s41592-019-0686-2
47. McKinney W. pandas: a Foundational Python Library for Data Analysis and Statistics. *Python High Perform Sci Comput.* 2011;(January 2011):1-9.
48. Singleton CM, Petriglieri F, Kristensen JM, et al. Connecting structure to function with the recovery of over 1000 high-quality metagenome-assembled genomes from activated sludge using long-read sequencing. *Nat Commun.* 2021;12:2009. doi:10.1038/s41467-021-22203-2
49. Shen W, Le S, Li Y, Hu F. SeqKit: A cross-platform and ultrafast toolkit for FASTA/Q file manipulation. *PLoS One.* 2016;11(10). doi:10.1371/journal.pone.0163962
50. De Coster W, D'Hert S, Schultz DT, Cruts M, Van Broeckhoven C. NanoPack: visualizing and processing long-read sequencing data. *Bioinformatics.* 2018;34(15):2666-2669.

- doi:10.1093/bioinformatics/bty149
51. Bolger AM, Lohse M, Usadel B. Trimmomatic: a flexible trimmer for Illumina sequence data. *Bioinformatics*. 2014;30(15):2114-2120. doi:10.1093/bioinformatics/btu170
  52. Rodriguez-R LM, Konstantinidis KT. Nonpareil: a redundancy-based approach to assess the level of coverage in metagenomic datasets. *Bioinformatics*. 2014;30(5):629-635. doi:10.1093/bioinformatics/btt584
  53. Kolmogorov M, Bickhart DM, Behsaz B, et al. metaFlye: scalable long-read metagenome assembly using repeat graphs. *Nat Methods*. 2020;17(11):1103-1110. doi:10.1038/s41592-020-00971-x
  54. Li H. Minimap2: pairwise alignment for nucleotide sequences. *Bioinformatics*. 2018;34(18):3094-3100. doi:10.1093/bioinformatics/bty191
  55. Li H, Handsaker B, Wysoker A, et al. The Sequence Alignment/Map format and SAMtools. *Bioinformatics*. 2009;25(16):2078-2079. doi:10.1093/bioinformatics/btp352
  56. Kang DD, Li F, Kirton E, et al. MetaBAT 2: an adaptive binning algorithm for robust and efficient genome reconstruction from metagenome assemblies. *PeerJ*. 2019;7. doi:10.7717/peerj.7359
  57. Wu YW, Simmons BA, Singer SW. MaxBin 2.0: an automated binning algorithm to recover genomes from multiple metagenomic datasets. *Bioinformatics*. 2016;32(4):605-607. doi:10.1093/bioinformatics/btv638
  58. Alneberg J, Bjarnason BS, De Bruijn I, et al. Binning metagenomic contigs by coverage and composition. *Nat Methods*. 2014;11(11):1144-1146. doi:10.1038/nmeth.3103
  59. Sieber CMK, Probst AJ, Sharrar A, et al. Recovery of genomes from metagenomes via a dereplication, aggregation and scoring strategy. *Nat Microbiol*. 2018;3(7):836-843. doi:10.1038/s41564-018-0171-1
  60. Hyatt D, Chen GL, LoCascio PF, Land ML, Larimer FW, Hauser LJ. Prodigal: prokaryotic gene recognition and translation initiation site identification. *BMC Bioinformatics*. 2010;11. doi:10.1186/1471-2105-11-119
  61. Buchfink B, Xie C, Huson DH. Fast and sensitive protein alignment using DIAMOND. *Nat Methods*. 2014;12(1):59-60. doi:10.1038/nmeth.3176
  62. Olm MR, Brown CT, Brooks B, Banfield JF. DRep: a tool for fast and accurate genomic comparisons that enables improved genome recovery from metagenomes through de-replication. *ISME J*. 2017;11(12):2864-2868. doi:10.1038/ismej.2017.126
  63. Parks DH, Imelfort M, Skennerton CT, Hugenholtz P, Tyson GW. CheckM: assessing the quality of microbial genomes recovered from isolates, single cells, and metagenomes. *Genome Res*. 2015;25(7):1043-1055. doi:10.1101/gr.186072.114
  64. Chaumeil PA, Mussig AJ, Hugenholtz P, Parks DH. GTDB-Tk v2: memory friendly classification with the genome taxonomy database. *Bioinformatics*. 2022;38(23):5315-5316. doi:10.1093/bioinformatics/btac672



65. Parks DH, Chuvochina M, Rinke C, Mussig AJ, Chaumeil PA, Hugenholtz P. GTDB: an ongoing census of bacterial and archaeal diversity through a phylogenetically consistent, rank normalized and complete genome-based taxonomy. *Nucleic Acids Res.* 2022;50:785-794. doi:10.1093/nar/gkab776
66. Price MN, Dehal PS, Arkin AP. FastTree 2 - Approximately maximum-likelihood trees for large alignments. *PLoS One.* 2010;5(3). doi:10.1371/journal.pone.0009490
67. Smith M. TreeTools: create, modify and analyse phylogenetic trees. *Compr R Arch Netw.* Published online 2019. doi:10.5281/zenodo.3522725
68. RStudio Team. RStudio: integrated development environment for R. RStudio, PBC, Boston, MA. Published 2021. <https://www.rstudio.com/>
69. R Core Team. R: A language and environment for statistical computing. R Foundation for Statistical Computing, Vienna, Austria. Published 2022. <https://www.r-project.org/>
70. Letunic I, Bork P. Interactive tree of life (iTOL) v5: An online tool for phylogenetic tree display and annotation. *Nucleic Acids Res.* 2021;49(W1):W293-W296. doi:10.1093/nar/gkab301
71. Suzek BE, Wang Y, Huang H, McGarvey PB, Wu CH. UniRef clusters: A comprehensive and scalable alternative for improving sequence similarity searches. *Bioinformatics.* 2015;31(6):926-932. doi:10.1093/bioinformatics/btu739
72. Kanehisa M, Sato Y, Kawashima M, Furumichi M, Tanabe M. KEGG as a reference resource for gene and protein annotation. *Nucleic Acids Res.* 2016;44(D1):D457-D462. doi:10.1093/nar/gkv1070
73. Mistry J, Chuguransky S, Williams L, et al. Pfam: the protein families database in 2021. *Nucleic Acids Res.* 2021;49:412-419. doi:10.1093/nar/gkaa913
74. Haft DH, Selengut JD, Richter RA, Harkins D, Basu MK, Beck E. TIGRFAMs and genome properties in 2013. *Nucleic Acids Res.* 2013;41(D1):387-395. doi:10.1093/nar/gks1234
75. Boyd JA, Woodcroft BJ, Tyson GW. GraftM: a tool for scalable, phylogenetically informed classification of genes within metagenomes. *Nucleic Acids Res.* 2018;46(10):E59. doi:10.1093/NAR/GKY174
76. The UniProt Consortium. UniProt: the universal protein knowledgebase in 2023. *Nucleic Acids Res.* 2023;51:523-531. doi:doi.org/10.1093/nar/gkac1052
77. Zumft WG. Nitric oxide reductases of prokaryotes with emphasis on the respiratory, heme-copper oxidase type. *J Inorg Biochem.* 2005;99(1):194-215. doi:10.1016/j.jinorgbio.2004.09.024
78. Madeira F, Pearce M, Tivey ARN, et al. Search and sequence analysis tools services from EMBL-EBI in 2022. *Nucleic Acids Res.* 2022;50(W1):W276-W279. doi:10.1093/nar/gkac240
79. Wickham H. The split-apply-combine strategy for data analysis. *J Stat Softw.*

- 2011;40(1). doi:10.18637/jss.v040.i01
80. Wickham H, Averick M, Bryan J, et al. Welcome to the Tidyverse. *J Open Source Softw.* 2019;4(43):1686. doi:10.21105/joss.01686
  81. Wickham H, Bryan J. readxl: read excel files. Published 2023. <https://cran.r-project.org/package=readxl>
  82. Barrett T, Dowle M, Srinivasan A, Gorecki J, Chirico M, Hocking T. data.table: Extension of “data.frame.” Published online 2024. <https://rdatatable.gitlab.io/data.table>
  83. Yu G. aplot for decorating a plot with associated information. Published online 2023. <https://github.com/YuLab-SMU/aplot>
  84. Wickham H. Reshaping data with the reshape package. *J Stat Softw.* 2007;21(12):1-20. doi:10.18637/jss.v021.i12
  85. Kleikamp HBC, Grouzdev D, Schaasberg P, et al. Metaproteomics, metagenomics and 16S rRNA sequencing provide different perspectives on the aerobic granular sludge microbiome. *Water Res.* 2023;246. doi:10.1016/j.watres.2023.120700
  86. Musiani F, Broll V, Evangelisti E, Ciurli S. The model structure of the copper-dependent ammonia monooxygenase. *J Biol Inorg Chem.* 2020;25:995-1007. doi:10.1007/s00775-020-01820-0
  87. Bengtsson H, Ahlmann-Eltze C, Bravo HC, et al. matrixStats: Functions that Apply to Rows and Columns of Matrices (and to Vectors). Published online 2023. <https://github.com/HenrikBengtsson/matrixStats>
  88. Daims H, Lücker S, Wagner M. A new perspective on microbes formerly known as nitrite-oxidizing bacteria. *Trends Microbiol.* 2016;24(9):699-712. doi:10.1016/j.tim.2016.05.004
  89. Mündinger AB, Lawson CE, Jetten MSM, Koch H, Lücker S. Cultivation and transcriptional analysis of a canonical nitrospira under stable growth conditions. *Front Microbiol.* 2019;10(JUN):1-15. doi:10.3389/fmicb.2019.01325
  90. Starkenburg SR, Chain PSG, Sayavedra-Soto LA, et al. Genome sequence of the chemolithoautotrophic nitrite-oxidizing bacterium *Nitrobacter winogradskyi* Nb-255. *Appl Environ Microbiol.* 2006;72(3):2050-2063. doi:10.1128/AEM.72.3.2050-2063.2006
  91. Koch H, Lücker S, Albertsen M, et al. Expanded metabolic versatility of ubiquitous nitrite-oxidizing bacteria from the genus *Nitrospira*. *Proc Natl Acad Sci U S A.* 2015;112(36):11371-11376. doi:10.1073/pnas.1506533112
  92. Lücker S, Wagner M, Maixner F, et al. A *Nitrospira* metagenome illuminates the physiology and evolution of globally important nitrite-oxidizing bacteria. *Proc Natl Acad Sci U S A.* 2010;107(30):13479-13484. doi:10.1073/pnas.1003860107
  93. Shiro Y. Structure and function of bacterial nitric oxide reductases: Nitric oxide reductase, anaerobic enzymes. *Biochim Biophys Acta - Bioenerg.* 2012;1817(10):1907-1913. doi:10.1016/j.bbabi.2012.03.001

94. Wang Y, Ye J, Ju F, et al. Successional dynamics and alternative stable states in a saline activated sludge microbial community over 9 years. *Microbiome*. 2021;9(1):199. doi:10.1186/s40168-021-01151-5
95. Ju F, Guo F, Ye L, Xia Y, Zhang T. Metagenomic analysis on seasonal microbial variations of activated sludge from a full-scale wastewater treatment plant over 4 years. *Environ Microbiol Rep*. 2014;6(1):80-89. doi:10.1111/1758-2229.12110
96. Saunders AM, Albertsen M, Vollertsen J, Nielsen PH. The activated sludge ecosystem contains a core community of abundant organisms. *ISME J*. 2016;10(1):11-20. doi:10.1038/ismej.2015.117
97. Herold M, Martínez Arbas S, Narayanasamy S, et al. Integration of time-series meta-omics data reveals how microbial ecosystems respond to disturbance. *Nat Commun*. 2020;11(1). doi:10.1038/s41467-020-19006-2
98. Yu K, Zhang T. Metagenomic and metatranscriptomic analysis of microbial community structure and gene expression of activated sludge. *PLoS One*. 2012;7(5). doi:10.1371/journal.pone.0038183
99. Lu H, Chandran K, Stensel D. Microbial ecology of denitrification in biological wastewater treatment. *Water Res*. 2014;64:237-254. doi:10.1016/j.watres.2014.06.042
100. Castellano-Hinojosa A, Maza-Márquez P, Melero-Rubio Y, González-López J, Rodelas B. Linking nitrous oxide emissions to population dynamics of nitrifying and denitrifying prokaryotes in four full-scale wastewater treatment plants. *Chemosphere*. 2018;200:57-66. doi:10.1016/j.chemosphere.2018.02.102
101. Song MJ, Choi S, Bae W Bin, et al. Identification of primary effectors of N<sub>2</sub>O emissions from full-scale biological nitrogen removal systems using random forest approach. *Water Res*. 2020;184:116144. doi:10.1016/j.watres.2020.116144
102. Duan H, Gao S, Li X, et al. Improving wastewater management using free nitrous acid (FNA). *Water Res*. 2020;171. doi:10.1016/j.watres.2019.115382
103. Zhou Y, Oehmen A, Lim M, Vadivelu V, Ng WJ. The role of nitrite and free nitrous acid (FNA) in wastewater treatment plants. *Water Res*. 2011;45(15):4672-4682. doi:10.1016/j.watres.2011.06.025
104. Park S, Bae W. Modeling kinetics of ammonium oxidation and nitrite oxidation under simultaneous inhibition by free ammonia and free nitrous acid. *Process Biochem*. 2009;44(6):631-640. doi:10.1016/j.procbio.2009.02.002
105. Anthonisen AC, Srinath EG, Loehr RC, Prakasam TBS. Inhibition of nitrification and nitrous acid compounds. *J Water Pollut Control Fed*. 1976;48(5):835-852.
106. Cao Y, Kwok BH, Van Loosdrecht MCM, et al. The influence of dissolved oxygen on partial nitrification/ anammox performance and microbial community of the 200,000 m<sup>3</sup>/d activated sludge process at the Changi water reclamation plant (2011 to 2016).

- Water Sci Technol.* 2018;78(3):634-643. doi:10.2166/wst.2018.333
107. Law Y, Matysik A, Chen X, et al. High dissolved oxygen selection against nitrospira sublineage i in full-scale activated sludge. *Environ Sci Technol.* 2019;53(14):8157-8166. doi:10.1021/acs.est.9b00955
  108. Picioreanu C, Pérez J, van Loosdrecht MCM. Impact of cell cluster size on apparent half-saturation coefficients for oxygen in nitrifying sludge and biofilms. *Water Res.* 2016;106:371-382. doi:10.1016/j.watres.2016.10.017
  109. Regmi P, Miller MW, Holgate B, et al. Control of aeration, aerobic SRT and COD input for mainstream nitrification/denitrification. *Water Res.* 2014;57:162-171. doi:10.1016/j.watres.2014.03.035
  110. Terada A, Sugawara S, Hojo K, et al. Hybrid Nitrous Oxide Production from a Partial Nitrifying Bioreactor: Hydroxylamine Interactions with Nitrite. *Environ Sci Technol.* 2017;51(5):2748-2756. doi:10.1021/acs.est.6b05521
  111. Olaya-Abril A, Hidalgo-Carrillo J, Luque-Almagro VM, et al. Exploring the denitrification proteome of *Paracoccus denitrificans* PD1222. *Front Microbiol.* 2018;9. doi:10.3389/fmicb.2018.01137
  112. Zorz JK, Kozłowski JA, Stein LY, Strous M, Kleiner M. Comparative proteomics of three species of ammonia-oxidizing bacteria. *Front Microbiol.* 2018;9. doi:10.3389/fmicb.2018.00938
  113. Beaumont HJE, Lens SL, Reijnders WNM, Westerhoff H V., Van Spanning RJM. Expression of nitrite reductase in *Nitrosomonas europaea* involves NsrR, a novel nitrite-sensitive transcription repressor. *Mol Microbiol.* 2004;54(1):148-158. doi:10.1111/j.1365-2958.2004.04248.x
  114. Yu R, Chandran K. Strategies of *Nitrosomonas europaea* 19718 to counter low dissolved oxygen and high nitrite concentrations. *BMC Microbiol.* 2010;10(2). doi:10.1186/1471-2180-10-70
  115. Cua LS, Stein LY. Effects of nitrite on ammonia-oxidizing activity and gene regulation in three ammonia-oxidizing bacteria. *FEMS Microbiol Lett.* 2011;319(2):169-175. doi:10.1111/j.1574-6968.2011.02277.x
  116. Soler-Jofra A, Schmidtchen L, Olmo L, van Loosdrecht MCM, Pérez J. Short and long term continuous hydroxylamine feeding in a granular sludge partial nitrification reactor. *Water Res.* 2022;209. doi:10.1016/j.watres.2021.117945
  117. Perez-Garcia O, Villas-Boas SG, Swift S, Chandran K, Singhal N. Clarifying the regulation of NO/N2O production in *Nitrosomonas europaea* during anoxic-oxic transition via flux balance analysis of a metabolic network model. *Water Res.* 2014;60:267-277. doi:10.1016/j.watres.2014.04.049
  118. Cantera JLL, Stein LY. Role of nitrite reductase in the ammonia-oxidizing pathway of *Nitrosomonas europaea*. *Arch Microbiol.* 2007;188(4):349-354. doi:10.1007/s00203-007-0255-4
  119. Kozłowski JA, Price J, Stein LY. Revision

- of N<sub>2</sub>O-producing pathways in the ammonia-oxidizing bacterium *Nitrosomonas europaea* ATCC 19718. *Appl Environ Microbiol.* 2014;80(16):4930-4935. doi:10.1128/AEM.01061-14
120. Kozłowski JA, Dimitri Kits K, Stein LY. Comparison of nitrogen oxide metabolism among diverse ammonia-oxidizing bacteria. *Front Microbiol.* 2016;7(JUL):1-9. doi:10.3389/fmicb.2016.01090
121. Beaumont HJE, Hommes NG, Sayavedra-Soto LA, et al. Nitrite reductase of *Nitrosomonas europaea* is not essential for production of gaseous nitrogen oxides and confers tolerance to nitrite. *J Bacteriol.* 2002;184(9):2557-2560. doi:10.1128/JB.184.9.2557-2560.2002
122. Schmidt I, van Spanning RJM, Jetten MSM. Denitrification and ammonia oxidation by *Nitrosomonas europaea* wild-type, and NirK- and NorB-deficient mutants. *Microbiology.* 2004;150(12):4107-4114. doi:10.1099/mic.0.27382-0
123. Hink L, Lycus P, Gubry-Rangin C, et al. Kinetics of NH<sub>3</sub>-oxidation, NO<sub>2</sub>-turnover, N<sub>2</sub>O-production and electron flow during oxygen depletion in model bacterial and archaeal ammonia oxidisers. *Environ Microbiol.* 2017;19(12):4882-4896. doi:10.1111/1462-2920.13914
124. Morris RM, Nunn BL, Frazar C, Goodlett DR, Ting YS, Rocap G. Comparative metaproteomics reveals ocean-scale shifts in microbial nutrient utilization and energy transduction. *ISME J.* 2010;4(5):673-685. doi:10.1038/ismej.2010.4
125. Wilmes P, Heintz-Buschart A, Bond PL. A decade of metaproteomics: Where we stand and what the future holds. *Proteomics.* 2015;15(20):3409-3417. doi:10.1002/pmic.201500183
126. Vieira A, Galinha CF, Oehmen A, Carvalho G. The link between nitrous oxide emissions, microbial community profile and function from three full-scale WWTPs. *Sci Total Environ.* 2019;651:2460-2472. doi:10.1016/j.scitotenv.2018.10.132
127. Gruber W, Magyar PM, Mitrovic I, et al. Tracing N<sub>2</sub>O formation in full-scale wastewater treatment with natural abundance isotopes indicates control by organic substrate and process settings. *Water Res X.* 2022;15. doi:10.1016/j.wroa.2022.100130
128. Toyoda S, Suzuki Y, Hattori S, et al. Isotopomer analysis of production and consumption mechanisms of N<sub>2</sub>O and CH<sub>4</sub> in an advanced wastewater treatment system. *Environ Sci Technol.* 2011;45(3):917-922. doi:10.1021/es102985u
129. Wunderlin P, Lehmann MF, Siegrist H, et al. Isotope signatures of N<sub>2</sub>O in a mixed microbial population system: Constraints on N<sub>2</sub>O producing pathways in wastewater treatment. *Environ Sci Technol.* 2013;47(3):1339-1348. doi:10.1021/es303174x
130. Duan H, Ye L, Erler D, Ni B jie, Yuan Z. Quantifying nitrous oxide production pathways in wastewater treatment systems using isotope technology - A critical review. *Water Res.* 2017;122:96-113. doi:10.1016/j.watres.2017.05.054

131. Bakken LR, Frostegård Å. Sources and sinks for N<sub>2</sub>O, can microbiologist help to mitigate N<sub>2</sub>O emissions? *Environ Microbiol.* 2017;19(12):4801-4805. doi:10.1111/1462-2920.13978
132. Duan H, van den Akker B, Thwaites BJ, et al. Mitigating nitrous oxide emissions at a full-scale wastewater treatment plant. *Water Res.* 2020;185. doi:10.1016/j.watres.2020.116196
133. Yan X, Li L, Liu J. Characteristics of greenhouse gas emission in three full-scale wastewater treatment processes. *J Environ Sci.* 2014;26(2):256-263. doi:10.1016/S1001-0742(13)60429-5
134. van Dijk EJJ, van Loosdrecht MCM, Pronk M. Nitrous oxide emission from full-scale municipal aerobic granular sludge. *Water Res.* 2021;198:117159. doi:10.1016/j.watres.2021.117159
135. Seuntjens D, Han M, Kerckhof FM, et al. Pinpointing wastewater and process parameters controlling the AOB to NOB activity ratio in sewage treatment plants. *Water Res.* 2018;138:37-46. doi:10.1016/j.watres.2017.11.044
136. Winkler MKH, Bassin JP, Kleerebezem R, Sorokin DY, Van Loosdrecht MCM. Unravelling the reasons for disproportion in the ratio of AOB and NOB in aerobic granular sludge. *Appl Microbiol Biotechnol.* 2012;94(6):1657-1666. doi:10.1007/s00253-012-4126-9
137. Kleiner M, Thorson E, Sharp CE, et al. Assessing species biomass contributions in microbial communities via metaproteomics. *Nat Commun.* 2017;8(1). doi:10.1038/s41467-017-01544-x
138. Soliman M, Eldyasti A. *Ammonia-Oxidizing Bacteria (AOB): Opportunities and Applications—a Review.* Vol 17. Springer Netherlands; 2018. doi:10.1007/s11157-018-9463-4
139. Watson SW, Bock E, Valois FW, Waterbury JB, Schlosser U. *Nitrospira marina* gen. nov. sp. nov.: a chemolithotrophic nitrite-oxidizing bacterium. *Arch Microbiol.* 1986;144(1):1-7. doi:10.1007/BF00454947
140. Ehrich S, Behrens D, Lebedeva E, Ludwig W, Bock E. A new obligately chemolithoautotrophic, nitrite-oxidizing bacterium, *Nitrospira moscoviensis* sp. nov. and its phylogenetic relationship. *Arch Microbiol.* 1995;164(1):16-23. doi:10.1007/s002030050230
141. Spieck E, Hartwig C, McCormack I, et al. Selective enrichment and molecular characterization of a previously uncultured *Nitrospira*-like bacterium from activated sludge. *Environ Microbiol.* 2006;8(3):405-415. doi:10.1111/j.1462-2920.2005.00905.x
142. Lebedeva E V., Off S, Zumbrägel S, et al. Isolation and characterization of a moderately thermophilic nitrite-oxidizing bacterium from a geothermal spring. *FEMS Microbiol Ecol.* 2011;75(2):195-204. doi:10.1111/j.1574-6941.2010.01006.x
143. Daims H, Lebedeva E V., Pjevac P, et al. Complete nitrification by *Nitrospira* bacteria. *Nature.* 2015;528(7583):504-509. doi:10.1038/nature16461
144. Keen GA, Prosser JL. Steady state and

- transient growth of autotrophic nitrifying bacteria. *Arch Microbiol.* 1987;147(1):73-79.  
doi:10.1007/BF00492908
145. Vadivelu VM, Keller J, Yuan Z. Stoichiometric and kinetic characterisation of *Nitrosomonas* sp. in mixed culture by decoupling the growth and energy generation processes. *J Biotechnol.* 2006;126(3):342-356.  
doi:10.1016/j.jbiotec.2006.04.017
146. Blackburne R, Vadivelu VM, Yuan Z, Keller J. Determination of Growth Rate and Yield of Nitrifying Bacteria by Measuring Carbon Dioxide Uptake Rate. *Water Environ Res.* 2007;79(12):2437-2445.  
doi:10.2175/106143007x212139
147. Ramírez M, Gómez JM, Aroca G, Cantero D. Removal of ammonia by immobilized *Nitrosomonas europaea* in a biotrickling filter packed with polyurethane foam. *Chemosphere.* 2009;74(10):1385-1390.  
doi:10.1016/j.chemosphere.2008.11.061
148. Cruvellier N, Poughon L, Creuly C, Dussap CG, Lasseur C. Growth modelling of *Nitrosomonas europaea* ATCC® 19718 and *Nitrobacter winogradskyi* ATCC® 25391: A new online indicator of the partial nitrification. *Bioresour Technol.* 2016;220:369-377.  
doi:10.1016/j.biortech.2016.08.090
149. Nowka B, Daims H, Spieck E. Comparison of oxidation kinetics of nitrite-oxidizing bacteria: Nitrite availability as a key factor in niche differentiation. *Appl Environ Microbiol.* 2015;81(2):745-753.  
doi:10.1128/AEM.02734-14
150. Ushiki N, Jinno M, Fujitani H, Suenaga T, Terada A, Tsuneda S. Nitrite oxidation kinetics of two *Nitrospira* strains: The quest for competition and ecological niche differentiation. *J Biosci Bioeng.* 2017;123(5):581-589.  
doi:10.1016/j.jbiosc.2016.12.016
151. Park MR, Park H, Chandran K. Molecular and Kinetic Characterization of Planktonic *Nitrospira* spp. Selectively Enriched from Activated Sludge. *Environ Sci Technol.* 2017;51(5):2720-2728.  
doi:10.1021/acs.est.6b05184
152. Domingo-Félez C, Smets BF. Modelling N<sub>2</sub>O dynamics of activated sludge biomass: Uncertainty analysis and pathway contributions. *Chem Eng J.* 2020;379(April 2019):122311.  
doi:10.1016/j.cej.2019.122311
153. Manser R, Gujer W, Siegrist H. Consequences of mass transfer effects on the kinetics of nitrifiers. *Water Res.* 2005;39(19):4633-4642.  
doi:10.1016/j.watres.2005.09.020
154. Pérez J, Lotti T, Kleerebezem R, Picioreanu C, van Loosdrecht MCM. Outcompeting nitrite-oxidizing bacteria in single-stage nitrogen removal in sewage treatment plants: A model-based study. *Water Res.* 2014;66(ii):208-218.  
doi:10.1016/j.watres.2014.08.028
155. Ni BJ, Rusalleda M, Pellicer-Nàcher C, Smets BF. Modeling Nitrous Oxide Production during Biological Nitrogen Removal via Nitrification and Denitrification: Extensions to the General ASM Models. *Environ Sci*

- Technol.* 2011;45:7768-7776.  
doi:10.1021/es201489n
156. Hiatt WC, Grady CPL. An Updated Process Model for Carbon Oxidation, Nitrification, and Denitrification. *Water Environ Res.* 2008;80(11):2145-2156.  
doi:10.2175/106143008x304776
157. Henze M, Gujer W, Mino T, van Loosdrecht M. *Activated Sludge Models ASM1, ASM2, ASM2d and ASM3*. IWA Publishing; 2000.
158. von Schulthess R, Gujer W. Release of nitrous oxide (N<sub>2</sub>O) from denitrifying activated sludge: Verification and application of a mathematical model. *Water Res.* 1996;30(3):521-530.  
doi:10.1016/0043-1354(95)00204-9



# Metabolic labour division trade-offs in denitrifying microbiomes





#### 4.1. Division of labour in microbial ecosystems

Labour division is ubiquitous in complex communities, from human societies to bee and ant colonies <sup>1</sup>, multicellular organisms <sup>2</sup>, and microbial ecosystems <sup>3</sup>. Microbial communities benefit from dividing long and complex biochemical pathways among different species. Shorter pathways require less enzymes, allowing individual cells to allocate more of their limited resources (e.g. energy, elemental building blocks, synthesis machinery) and cellular space (e.g. cytoplasm, membrane, and periplasm) to energy conservation, cell growth, and metabolic adaptation <sup>4</sup>. Division of labour can also improve overall community function by facilitating complex substrate degradation, like carbohydrates in the human gut microbiome <sup>5</sup>; and by minimising the impacts of inhibitory intermediates such as hydrogen, which is cross-fed between secondary fermenters and hydrogenotrophic methanogens in anaerobic environments <sup>6</sup>. At the same time, shorter catabolic pathways yield less energy per unit of substrate metabolised, and cellular fitness may suffer from the reduced metabolic flexibility in dynamic environments where substrate availability fluctuates <sup>7</sup>. Division of labour may also result in inter-species competition for nutrients and space, and impact reaction efficiency due to the additional requirement of cross-membrane metabolite transport <sup>8</sup>. Trade-offs between growth, energy conservation, and metabolic flexibility drive the assembly and function of any microbiome occupying a specific environmental niche <sup>9</sup>.

Among global biogeochemical cycles, the network of nitrogen transforming organisms builds on modular metabolic pathways. Nitrification, the oxidation of ammonia ( $\text{NH}_3$ ) via nitrite ( $\text{NO}_2^-$ ) to nitrate ( $\text{NO}_3^-$ ), can be performed in two steps by separate guilds (ammonia oxidising bacteria or archaea – AOB or AOA – and nitrite oxidising bacteria – NOB) or by a single organism (complete ammonia oxidising – comammox – bacteria) <sup>10</sup>. Comammox was first theoretically proposed based on a trade-off between growth rate and biomass yield <sup>7</sup>, and was experimentally confirmed a decade later with enrichments from slow-growing (low nutrient flux) oligotrophic (low nutrient levels) biofilm systems <sup>11,12</sup>. The produced nitrate is reduced to nitrite, which can be reduced back to ammonia via dissimilatory nitrite reduction to ammonia (DNRA), or successively denitrified to gaseous nitric oxide (NO), nitrous oxide ( $\text{N}_2\text{O}$ ) and dinitrogen gas ( $\text{N}_2$ ). DNRA and denitrification thus compete for the same electron acceptor (nitrate or nitrite) and donor (commonly organic carbon) <sup>13</sup>. Denitrification can be catalysed by complete denitrifiers performing all reduction steps, or partial denitrifiers which divide the labour by performing only one or few reduction steps <sup>10</sup>. Complete and partial denitrifiers compete for the same substrates (organic carbon and nitrogen oxides), yet they occupy different ecological niches due to their distinct ecophysiological traits <sup>14–17</sup>. Most denitrifiers are facultative aerobes, mainly denitrifying under anoxic conditions, as commonly found in soil and ocean depths <sup>10,18</sup>. Despite their pivotal role in global

nitrogen turnover, biotechnological applications, and greenhouse gas emissions <sup>10</sup>, the factors controlling the dominance of complete or partial denitrifiers remain elusive, hindering the understanding and management of natural and engineered nitrogen-transforming microbiomes. In this work, we focus on the catabolic modularity of the denitrification pathway, and its ecological significance. We discuss the ecological drivers selecting for complete and partial denitrifiers by critically exploring current labour division theories, from individual enzyme properties and resource allocation to rate-yield trade-offs, intermediate toxicity, and substrate limitation, and by integrating the most recent experimental and theoretical insights.

## 4.2. Bridging species physiology to ecosystem phenotype

Denitrification has been studied for over a century <sup>19</sup>, and our physiological and biochemical knowledge builds primarily on pure cultures of complete denitrifiers, particularly model organisms like *Paracoccus denitrificans* and *Pseudomonas stutzeri* <sup>20</sup>. Model denitrifiers not only allowed identifying the nitrate transporter and determining the cytoplasmic orientation of the nitrate reductase <sup>21</sup>, but also led to the first identification of a nitric oxide reductase <sup>22,23</sup> and the inhibitory role of oxygen <sup>24</sup>. Additionally, the electron transport chain of *P. denitrificans* has been used as the basis for the general biochemical architecture of the denitrification respiratory network <sup>20</sup>. Yet, *P. denitrificans* and *P. stutzeri* hardly dominate natural and engineered ecosystems <sup>25–28</sup>, and denitrifiers are biochemically, physiologically, and ecologically very diverse, as exemplified by the existence of partial and aerobically denitrifying organisms <sup>17,18,29</sup>. Insights gained from complete denitrifying model organisms can thus not be extrapolated to all denitrifiers, and their generalisability to more complex ecosystems remains limited. The historical focus on complete denitrifiers likely results from the enrichment and isolation methods used in the past: nitrate was provided as the sole substrate, restricting the isolation to nitrate reducers; and the production of bubbles was often used as a denitrification selection criterium, excluding single-step nitrate reducers <sup>17,30</sup>. Moreover, partial denitrifiers accumulating toxic denitrification intermediates (e.g. NO) as end products are unlikely to survive in pure cultures <sup>17</sup>. This limitation has recently been addressed through the development of new protocols, resulting in the isolation and characterisation of 61 partial denitrifiers from soil <sup>17</sup>. These advances hold promise to dramatically expand our repertoire of physiologically characterised partial denitrifiers. However, cultivation methods alone cannot capture the full breadth of denitrifying organisms nor resolve their ecological role, highlighting the complementary need for more *in situ* ecological studies.

Natural communities are inherently complex, challenging their taxonomic and functional characterisation. Rapid advancements in genome-resolved metagenomics

allow now to recover near-complete draft genomes from complex microbiomes and more accurately identify organisms genetically encoding the complete or partial denitrification pathway. We analysed the genetic functional profiles of 1571 published metagenome-assembled genomes (MAGs) containing at least one denitrification gene (encoding a catalytic subunit) across ecosystems. Given the challenge of distinguishing the physiological roles of denitrification – such as energy conservation in canonical denitrifiers vs. redox balancing or detoxification in organisms like ammonia oxidisers – based solely on genomic data, our analysis includes also 24 MAGs identified as nitrifiers. Nearly 60% of all MAGs were high-quality (HQ,  $\geq 90\%$  complete,  $\leq 5\%$  contaminated) (Figure 4.1; Supplementary Table S4.1). It is evident that labour-dividing partial denitrifiers predominate in complex environments, featuring dynamic availability of multiple substrates and high microbial diversity, and being often spatially stratified. Conversely, complete denitrifiers seem to be favoured in continuous suspended cultures characterised by stable availability of one or few substrates, homogeneity, and low microbial diversity. MAGs recovered from soils <sup>25,31–33</sup>, river sediments <sup>34–36</sup>, oceanic oxygen deficient zones <sup>15,26</sup> and wastewater treatment systems <sup>27,37–39</sup> are mostly partial, often single-step, denitrifiers (Figure 4.1). Similarly, biofilm systems, which closely resemble natural environments in their complexity, stratification, and metabolic diversity, were dominated by organisms encoding one or two denitrification steps <sup>40–42</sup> (Figure 4.1). In contrast, continuous suspended laboratory cultures predominantly selected for denitrifiers with genes encoding three or four steps <sup>29,43–46</sup>; the relatively lower number of recovered MAGs also reflects the limited complexity of these ecosystems (Figure 4.1). Although one might argue that the reported prevalence of partial denitrifiers in complex environments is due to the challenge of recovering near-complete MAGs, the increasing number of high-quality denitrifying MAGs from natural environments <sup>15,32</sup> and wastewater treatment plants <sup>27,39</sup> (Figures 4.1 and 4.2A-B) rules out methodological biases. Besides, most gene-centric metagenomic studies find unbalanced abundances of denitrification genes, with *nar* and *nor* often being the most abundant in ocean and soil microbiomes <sup>47–49</sup>, further supporting the low frequency of complete denitrifiers in natural environments. The clear prevalence of partial denitrifiers across all studied complex environments suggests a competitive advantage of dividing labour over performing complete denitrification, yet the underlying selection principles remain unclear. Expanding the current database of HQ MAGs is paramount, specially to enable functional analyses at transcriptional and translational levels (Box 4.1). Nevertheless, the experimental data available to date already provide important insights to explore the ecological drivers explaining the diversity of denitrifying microbiomes.

### Box 4.1. Denitrification genotype vs. phenotype

The distinction between complete and partial denitrifiers is here based on currently available medium and high-quality denitrifying MAGs (Figures 4.1 and 4.2). The presence of a gene, however, does not imply its transcription or translation under a given condition, let alone provide information on the activity of the encoded protein and the organism itself<sup>17</sup>. For instance, in a wastewater treatment microbiome, the *nirK* and *nirS* genes were both widespread in non-nitrifying MAGs (Figure 4.2B), yet we only detected the NirS enzyme from these MAGs<sup>39</sup>. The expression of denitrification enzymes in model denitrifiers like *P. denitrificans* has been shown to be controlled by environmental factors – typically activated by nitrate, nitrite, and nitric oxide, and repressed by oxygen and nitric oxide – whereas the expression of different reductases is not necessarily coordinated<sup>20,50–52</sup>. Complete denitrifiers may exhibit a partial denitrifying phenotype under certain conditions, or express all reductases even in the absence of their substrates. For example, all denitrification enzymes were detected in enrichments solely fed with NO or N<sub>2</sub>O<sup>46,53</sup>. On these grounds, it is clear that the genetic fingerprint of denitrifying communities represents only the first step in resolving their assembly and function. We advocate for more studies recovering HQ MAGs from complex and cultured nitrogen-converting communities as solid reference for the integration of metatranscriptomic and metaproteomic analysis in answering ecologically focused mechanistic questions.

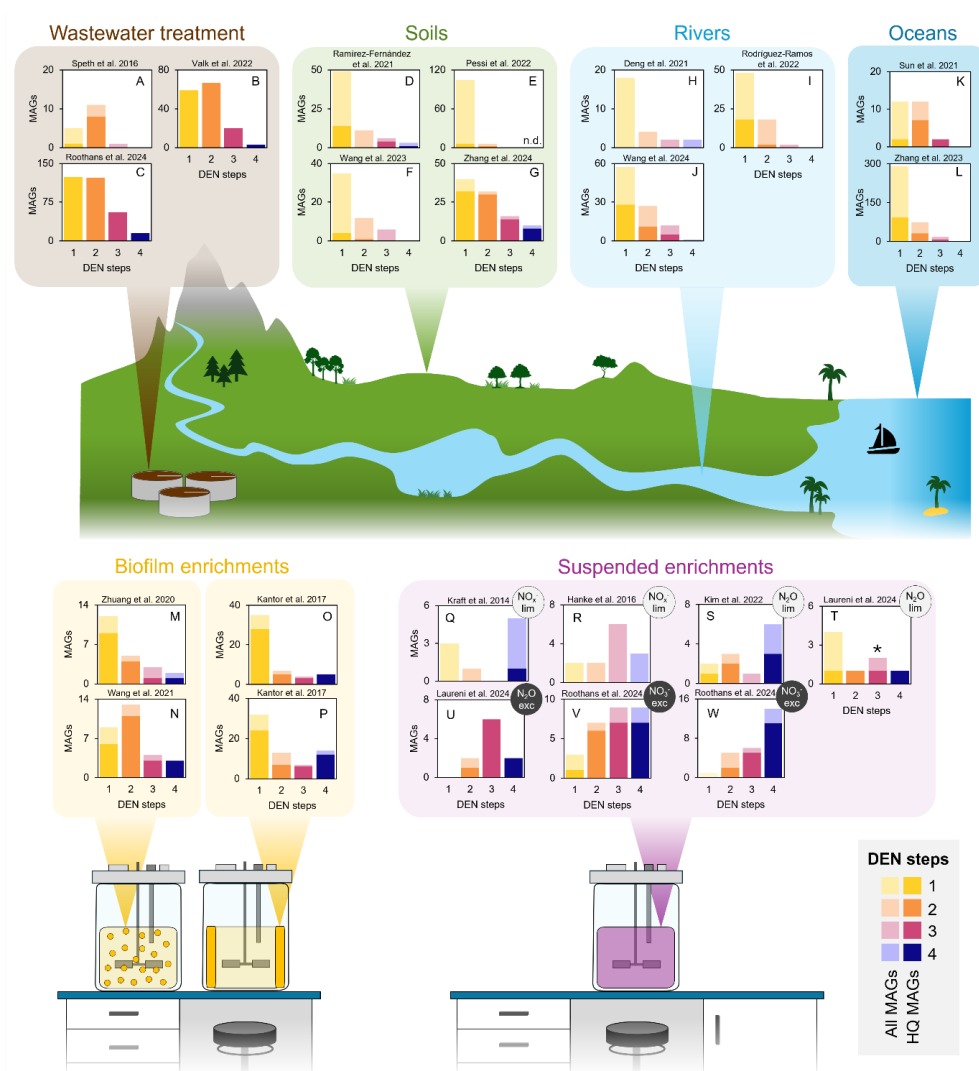


**Figure 4.1. Summary of the distribution of complete and partial denitrifiers from 1571 published metagenome-assembled genomes: dynamic engineered and natural environments (top), and laboratory experiments (bottom).** Each graph represents the number of MAGs containing genes encoding the catalytic subunit of 1, 2, 3, or 4 denitrification steps (*narG/Z*, *napA*, *nirK*, *nirS*, *norZ*, *norB*, *nosZ*). The HQ MAGs in each study are highlighted with darker colours. The dynamic environments included i) wastewater treatment plants: full-scale partial nitrification-anammox (A [38]) and two activated sludge systems (B [27,37], C [39]; 83 MAGs are the same in these two studies); ii) soils: coastal soil (D [31]), heathlands and meadows (E [25] – did not report the presence or absence of *nar/nap* in the MAGs), wetland (F [33]), and agricultural soil (G [32]); iii) rivers: sediments and surface water (H [34]), and sediments (I [35], J [36]); iv) oceans: oxygen deficient zones (K [26], L [15]). The biofilm laboratory enrichments included two granular reactors performing anammox (M [40]) and phosphate removal (N [41]), and two biofilms growing on reactor walls removing ammonium sulphate (O) and thiocyanate (P) [42] (34 MAGs are the same in these two reactors). The continuous suspended laboratory enrichment cultures include two supplied with limiting nitrate and nitrite

(Q [43], R [44]), two with limiting N<sub>2</sub>O (S [45], T [46]), one with excess N<sub>2</sub>O (U [46]), and two with excess nitrate (V, W [29]). \*Where available, the distribution of MAGs in terms of relative abundance profiles was similar to the frequency profiles represented here [15,26,29,39,40,46]; culture T was the only exception as it was dominated by a single 3-step denitrifier HQ MAG [46] (Supplementary Table S4.2). The quality and functional annotations (i.e. the identification of the catalytic subunit of the genes of interest) of all MAGs were taken from the corresponding literature studies.

### 4.3. Denitrification gene patterns and physiological diversity

The publicly available 878 unique denitrifier HQ MAGs allow to explore associations between functionally homologous denitrification genes and denitrification pathway completeness (Figure 4.2; Supplementary Table S4.3). Across natural environments, out of the 128 HQ MAGs with differentiated nitrate reductases, 84 contained the *narG/Z* gene, but none was a complete denitrifier (Figure 4.2A). Almost two thirds of the HQ MAGs lacked genes for any other denitrification step (Figure 4.2A). The only two complete denitrifiers contained *napA*. Similarly, most *nirK*-harbouring MAGs lacked other denitrification genes, whereas the two *napA*-harbouring complete denitrifiers contained *nirS* (Figure 4.2A). The *napA/narGZ* and *nirS/K* partitioning between complete and partial denitrifiers, respectively, was observed across all environments, even if the proportion of complete denitrifiers increased from natural environments to wastewater treatment plants, biofilms, and suspended cultures (Figure 4.2A-D). Another study also observed a higher occurrence of *nirS* in complete denitrifiers when comparing genomes from natural environments, wastewater, and animal and plant hosts, yet nitrate reductase homologues were not included in their analysis<sup>16</sup>. The functionally homologous genes *norZ/norB* and *nosZ I/nosZ II* are seldomly differentiated in metagenomic studies (Figure 4.2A-D). Nevertheless, based on the wastewater treatment microbiomes and laboratory cultures (Figure 4.2B and 4.2D), *norZ* and *norB* genes appear to be equally distributed between complete and partial denitrifiers, whereas 80% of all identified complete denitrifiers harboured the *nosZ* clade I genes. All N<sub>2</sub>O-reducing specialists contained the *nosZ* clade II genes (Figure 4.2B and 4.2D), confirming the previously suggested higher occurrence of *nosZ* I and *nosZ* II in complete and partial denitrifiers, respectively<sup>16</sup>. This pattern may be associated with a potential incompatibility between nitrate and *nosZ* II expression, recently observed in a *Thauera* species<sup>54</sup>. Taxonomically, among the 318 denitrifying HQ MAGs we recovered from wastewater treatment microbiomes, *napA*, *nirS* and *nosZ* I, and complete denitrifiers clustered predominantly within the *Proteobacteria* phylum (Figure 4.2E). This taxonomic clustering aligns with prior findings<sup>16,55–57</sup>, and suggests that evolutionary and physiological mechanisms shape denitrification gene patterns. The physiological difference between the nitrate reductases is relatively well established, with Nap-expressing cells often featuring higher nitrate affinities and Nar providing more energy and a potentially faster turnover of nitrate (Box 4.2)<sup>47,56,58,59</sup>, yet this is currently not the



case for the other reductases. NirK, taxonomically more dispersed<sup>57</sup> and less resource demanding to produce than NirS<sup>60</sup>, has been hypothesised to provide a higher physiological adaptability in dynamic environments<sup>57,61</sup>, yet this remains to be experimentally verified<sup>57</sup>. Both NirS and NosZ II have been hypothesised to have a higher affinity for their substrates and a higher tolerance to oxygen compared to their counterparts NirK and NosZ I<sup>60–62</sup>, yet these observations are limited to a few strains and have been contradicted by other studies<sup>63–65</sup>.

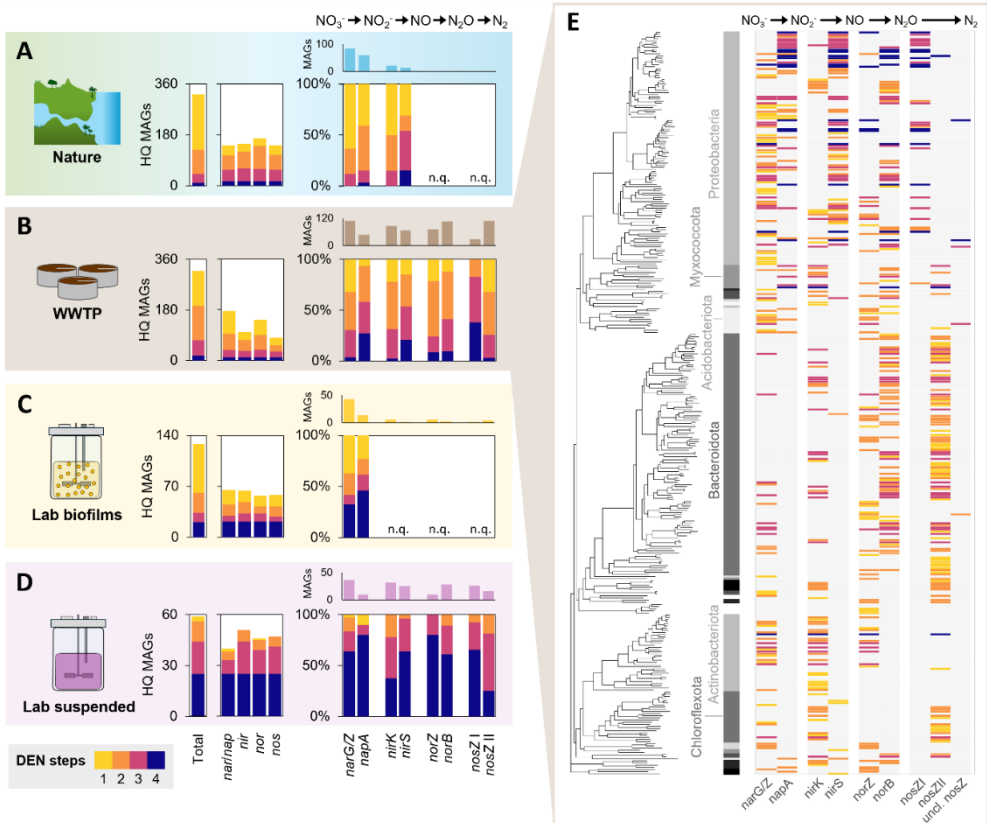


**Figure 4.2. Denitrification gene partitioning in natural and engineered ecosystems.** The colours from light to dark represent denitrifiers with genes encoding one, two, three, or four denitrification steps. **(A–D)** The left bar charts represent the total number of unique denitrifying HQ MAGs recovered from natural environments (A, including soils [31,33], rivers [35,36], and oceans [15]), wastewater treatment plants (B, [39] – taken as representative considering that over half of the MAGs from [37] overlapped with this study), laboratory biofilms (C [40,42]) and suspended cultures (D [29,43,45,46]), and the number of HQ MAGs encoding each of the four denitrification steps (*nar/nap*, *nir*, *nor*, *nos*). On the right, the total amount (top) and proportion of one-, two-, three-, and four-step denitrifying HQ MAGs (bottom) are distributed over the gene homologues. The quality and functional annotations (i.e. the identification of the catalytic subunit of the genes of interest) of all MAGs were taken from the corresponding literature studies. Some studies made no distinction between *nirK/S*, *norZ/B*, and *nosZ I/II* or did not recover enough HQ MAGs, so these gene distributions appear as not quantified (n.q.) in nature (A) and biofilms (C). **(E)** 349 high-quality MAGs

recovered from wastewater treatment microbiomes, 14 nitrifying and 304 non-nitrifying MAGs contained at least one denitrification gene. The heatmap shows the gene distribution among complete and partial denitrifiers: cytoplasmic- (*narG*, *narZ*) and periplasmic nitrate reductase (*napA*); copper-based (*nirK*) and cytochrome *cd1* nitrite reductase (*nirS*); quinol- (*norZ*) and cytochrome *c*-dependent nitric oxide reductase (*norB*); nitrous oxide reductase clade I (*nosZ* I), clade II (*nosZ* II), and unclassified (uncl. *nosZ*). The MAGs are ordered according to the phylogenetic tree and the six most frequent phyla are highlighted. Data were adapted from [39].

## 4

Beyond individual enzymes, a physiological yield-rate trade-off has been proposed to govern the competition between generalists (complete denitrifiers) and specialists (partial denitrifiers) <sup>66</sup>, so it is here also discussed in analogy to nitrification <sup>7</sup>. As facultative aerobes, denitrifiers normally conserve energy by oxidising organic carbon and reducing nitrogen oxides in the absence of (sufficient) oxygen. Complete denitrification effectively yields more energy, i.e. generates more proton motive force, per mole of nitrogen oxides than partial denitrification (Box 4.2). Complete denitrifiers are thus expected to feature higher biomass yields, in analogy to the higher yield of comammox on ammonia <sup>7</sup>. In turn, a shorter catabolic pathway allows partial denitrifiers to increase the concentration of each denitrification reductase, increasing the ATP production rate and potentially resulting in higher growth rates like AOB <sup>4,7</sup>. On these grounds, with a higher growth yield on nitrogen oxides and lower maximum growth rates, one would expect complete denitrifiers to dominate slower-growing, nitrogen-limited systems, where an efficient use of available resources is more beneficial than faster growth <sup>67</sup>. Yet, complete denitrifiers appear to dominate faster-growing well-mixed continuous suspended laboratory cultures <sup>29,43,53</sup>, whereas they are outnumbered by partial denitrifiers in most slower-growing ecosystems including oceans <sup>15,26</sup>, freshwater systems <sup>34–36</sup>, soils <sup>25,32,33</sup>, wastewater treatment plants <sup>27,38,39</sup>, and laboratory biofilm systems <sup>40–42</sup> (Figure 4.1). Organic carbon is often limiting in these complex environments <sup>14,35,68,69</sup>, so the dominance of partial denitrifiers could simply be determined by the limiting substrate (nitrogen oxides or organic carbon) (Box 4.2), as recently proposed by a theoretical modelling study <sup>14</sup>. However, the available experimental evidence is limited and seems to refute this hypothesis, as two carbon-limited laboratory cultures enriched for complete denitrifiers (Figure 4.1V–W) <sup>29</sup> and a largely nitrogen-limited soil enriched for partial denitrifiers (Figure 4.1E) <sup>25</sup>. Additionally, DNRA-performing bacteria have been shown to outcompete denitrifiers in nitrogen-limited laboratory cultures and soils <sup>13,70,71</sup>, potentially further narrowing the ecological niche for complete denitrifiers. This may also underly the higher frequency of DNRA-performing bacteria over complete denitrifiers in most environments, e.g. 51 and 17 DNRA vs. 6 and 0 complete denitrifier MAGs in wastewater treatment <sup>39</sup> and ocean microbiomes <sup>15</sup>, respectively. Nevertheless, other factors – such as generation time, nitrite/nitrate ratio, and type of carbon source – affect the competition between DNRA and denitrification <sup>13,72</sup>, and may also influence the prevalence of partial over complete

denitrifiers. Future experiments are needed to confirm the validity of this observation across different conditions and multiple organic substrates. An alternative hypothesis considers the benefit for complete denitrifiers of minimising the accumulation of toxic intermediates, such as free nitrous acid ( $\text{HNO}_2$ ) disrupting the transmembrane proton gradient<sup>73,74</sup>; nitric oxide potentially inactivating key enzymes<sup>75</sup>; and nitrous oxide inactivating vitamin B12<sup>76</sup>. Though interesting, the only two studies comparing intermediate accumulation by complete and partial denitrifiers reached contradicting results. Experiments with *P. stutzeri* mutants found lower nitrite accumulation during cross-feeding<sup>77</sup>, whereas identical experiments with *Pseudomonas aeruginosa* mutants observed lower accumulation when a single strain produced and consumed nitrite<sup>78</sup>. Ultimately, though further experimental confirmations are warranted, the currently available ecophysiological data do not seem to support any of the hypotheses put forward to explain the distribution of functional homologues nor the selection of microbiomes dominated by complete or partial denitrifiers.

#### Box 4.2. Denitrification bioenergetics

The proton motive force driving ATP synthesis is generated during the transfer of electrons from a donor (e.g. organic carbon) to an acceptor (e.g. nitrogen oxides). Energy conservation in denitrifying and DNRA-performing organisms depends on the availability of organic carbon and nitrogen oxides, and the configuration of the nitrogen oxide reductase modules. Apart from Nar, none of the denitrification enzymes directly contributes to proton motive force. However, for all denitrification steps, protons are translocated by NADH dehydrogenase and/or cytochrome *bc1* during the electron transport from the donor to the reductase (Table 4.1). Therefore, respiration with the terminal reductases Nar, Nir, cNor, or Nos translocates the same amount of protons across the cell membrane, generating an equivalent amount of ATP per electron pair transferred, despite the potentially higher thermodynamic driving force of nitric and nitrous oxide reduction (Table 4.1)<sup>18,20,79</sup>. Nap and qNor in denitrifiers or Nrf in DNRA-performing bacteria result in the translocation of only four protons per electron pair, instead of six (Table 4.1). Under carbon-limited conditions, the energy yield is constrained by the amount of electrons available, so both complete and partial denitrifiers obtain the same energy ( $6 \text{ H}^+ / 2 \text{ e}^-$  if Nar, Nir, cNor, and Nos are used). Conversely, in nitrogen-limited environments, complete denitrifiers and DNRA-performing bacteria are in principle favoured as they accept more electrons per mole nitrogen, which is fully reduced to dinitrogen gas or ammonia, resulting in a higher energy yield (up to 15 and 18  $\text{H}^+ / \text{NO}_3^-$ , respectively). Compared to partial denitrifiers, complete denitrifiers can also benefit from using multiple nitrogen oxides as electron acceptors, and, the potential electron

competition between reductases has been shown not to impact the overall electron consumption and energy conservation rate in a mixed culture <sup>80</sup>.

**Table 4.1. Proton translocation across the cell membrane for each nitrogen oxide reduction step.** The proton translocation was determined considering NADH as the electron donor, and was normalised for two electrons accepted by each enzyme complex. Denitrification and DNRA: Nar – cytoplasmic nitrate reductase; Nap – periplasmic nitrate reductase. Denitrification: Nir – copper or cytochrome *cd1* nitrite reductase; cNor – cytochrome *c*-type nitric oxide reductase; qNor – quinol-dependent nitric oxide reductase; Nos – nitrous oxide reductase. DNRA: Nrf – cytochrome *c* nitrite reductase. In each nitrogen oxide reduction step, protons are translocated during the oxidation of NADH and the quinol pool. The total proton translocation ( $\Delta H^+$ ) of each step and the standard potential ( $E^0$ ) of each redox pair are presented. <sup>18,20,79</sup>

Redox reaction (2 e <sup>-</sup> transfer)	$E^0$ (V)	Enzyme complex	NADH oxidation ( $\Delta H^+ / 2 e^-$ )	Quinol pool oxidation ( $\Delta H^+ / 2 e^-$ )					Total $\Delta H^+ / 2e^-$	Total $\Delta H^+ / N$
			NADH dehydrogenase (complex I)	Cyt <i>bc1</i> (complex III)	Nar	Nap	qNor	Nrf		
$NO_3^- \rightarrow NO_2^-$	+0.43	Nar	4	-	2	-	-	-	6	6
		Nap	4	-	-	0	-	-	4	4
$2 NO_2^- \rightarrow 2 NO$	+0.36	Nir	4	2	-	-	-	-	6	3
$2 NO \rightarrow N_2O$	+1.18	cNor	4	2	-	-	-	-	6	3
		qNor	4	-	-	-	0	-	4	2
$N_2O \rightarrow N_2$	+1.36	Nos	4	2	-	-	-	-	6	3
$1/3 NO_2^- \rightarrow 1/3 NH_4^+$	+0.34	Nrf	4	-	-	-	-	0	4	12

#### 4.4. Metabolic adaptability beyond respiratory flexibility

The growing evidence of partial denitrifiers being the rule rather than the exception in almost all environments cannot be explained by current labour division theories centred around catabolic pathways. Beyond the availability of nitrogen oxides and electron donors, dynamic denitrifying ecosystems experience frequent fluctuations in temperature, pH, oxygen, and nutrient levels, only to name a few environmental variables <sup>10,39,81,82</sup>. So, we argue that resource allocation trade-offs between growth efficiency and adaptability control the selection of complete and partial denitrifiers, in analogy to other microbial systems. For example, *E. coli* cells are capable of increasing substrate flexibility and affinity under substrate-limited conditions by directing resources and membrane space towards porin production <sup>83,84</sup>. Slower-growing natural *Saccharomyces cerevisiae* strains switch among substrates more quickly than lab-grown strains in dynamic environments by having reduced gene regulation mechanisms, enabling the constant expression of metabolic machinery for multiple carbon sources <sup>85</sup>. Slower-growing bacteria are also reported to often exhibit greater antibiotic tolerance by prioritising resistance mechanisms over growth <sup>86</sup>. By specialising in a few denitrification steps, partial denitrifiers require fewer resources and cellular space for

denitrification, which can instead be invested in the uptake of organic carbon, cofactors and micronutrients, metabolic flexibility, and stress response mechanisms, including cross-membrane transporters, alternative metabolic enzymes, and specialised RNA and protein synthesis machinery such as sigma factors and chaperones<sup>87</sup>. This potentially gives them a competitive advantage in complex, dynamic, oligotrophic, and carbon-limited ecosystems (Figure 4.3). Conversely, in stable and nutrient-rich laboratory cultures, where metabolic flexibility and rapid adaptation requirements are reduced, complete denitrifiers likely outcompete partial denitrifiers by maximising energy conservation through denitrification (Figure 4.3). Metabolic trade-offs are emerging as key to explain the observed functional diversity and microbial fluctuations across ecosystems. Microorganisms in soil were proposed to excel either at growth, resource acquisition, or stress tolerance depending on environmental conditions, each contributing to the accumulation of organic matter, breakdown of complex resources through extracellular enzymes, or production of osmolytes and extracellular polymeric substances for protection<sup>88</sup>. Resource allocation balances have been suggested to explain patterns in stream biofilms: organisms that invest in cell adhesion and extracellular polymeric substances dominate during biofilm formation, whereas faster-growing organisms appear only in mature biofilms<sup>89</sup>. Similarly, a defence-growth trade-off explained the seasonal shifts in lake phytoplankton, where organisms with stronger defences but slower growth dominate during periods of increased grazing<sup>90</sup>.

Experimentally testing how resource allocation controls the assembly and function of denitrifying microbiomes in response to environmental fluctuations remains a challenge. Recovering HQ MAGs and differentiating functionally homologous reductases is rapidly becoming the norm, and will allow to quantify and characterise complete and partial denitrifiers in complex ecosystems. Descriptive analyses of denitrifying communities are essential to continue populating the evidence on the distribution of denitrification labour division across various environments and are key to generate novel hypotheses. However, they fall short in explaining the mechanisms driving the observed patterns. We advocate for more ecologically driven mechanistic studies based on open continuous culture approaches, alongside targeted physiological and enzymatic characterisations of the growing number of denitrifiers isolated from diverse ecosystems. Non-axenic continuous enrichments allow microbial communities to evolve to a steady-state under strictly controlled operational conditions, mimicking natural environments<sup>91</sup>. The enriched microorganisms are, by definition, the fittest for the imposed conditions, having outcompeted all others. Combined with genome-resolved metatranscriptomic and metaproteomic analyses, mixed culture enrichments will prove essential to resolve the ecological significance of metabolic trade-offs in denitrifying microbiomes, greatly advancing our understanding of global nitrogen turnover and N<sub>2</sub>O emissions.

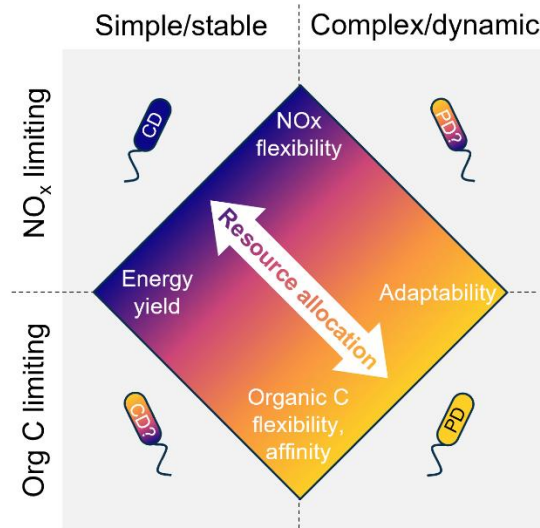


**Figure 4.3. Proposed niche partitioning drivers between complete (CD) and partial denitrifiers (PD).** Resource allocation trade-offs drive the selective advantage along two axes: environmental complexity (horizontal) and limiting substrate (vertical). Complete denitrifiers dominate nitrogen-limited stable laboratory cultures (top left) by prioritising energy yield and nitrogen oxide ( $\text{NO}_x$ ) catabolic diversity. In contrast, partial denitrifiers dominate complex environments (bottom right), which are often carbon-limited, likely due to resource allocation towards organic carbon (Org C) and other nutrient transporters, electron donor catabolic diversity, and stress response mechanisms. Nitrogen-limited complex environments (top right) and carbon-limited laboratory cultures (bottom left) remain largely unexplored, though they seem to favour partial and complete denitrifiers, respectively. Future studies should focus on these underrepresented conditions to refine this framework.

## 4.5. Supplementary information

**Table S4.1. Number of MAGs in publicly available literature distributed by the number of denitrification steps encoded in their genomes.** The genes encoding the catalytic subunit of each enzyme was considered as proxy for the enzyme complex. The high-quality MAGs ( $\geq 90\%$  completeness,  $\leq 5\%$  contamination) are represented on the right. The corresponding plot label for each dataset in Figure 4.1 is also indicated. The annotations and quality of the MAGs were taken from the literature studies.

Plot	Reference	Environment	Details	All MAGs					HQ MAGs ( $\geq 90\%$ completeness, $\leq 5\%$ contamination)				
				Total	1 step	2 steps	3 steps	4 steps	Total	1 step	2 steps	3 steps	4 steps
A	Speth et al. 2016	WWTP	Anammox granules	17	5	11	1	0	11	1	8	0	0
B*	Valk et al. 2022	WWTP	Activated sludge	149	59	67	20	3	149	59	67	20	3
C*	Roothans, Pabst, et al. 2024	WWTP	Activated sludge	318	124	122	56	16	318	124	122	56	16
D	Ramírez-Fernández et al. 2021	Soil	Coastal soil	69	49	11	6	3	19	14	0	4	1
E	Pessi et al. 2022	Soil	Heathlands and meadows	110	104	6	0	-	8	6	2	0	-
F	Wang et al. 2023	Soil	Wetland	53	35	12	6	0	5	4	1	0	0
G	Zhang et al. 2024	Soil	Agricultural soils	98	40	32	16	10	84	32	30	14	8
H	Deng et al. 2024	River	Riparian soils, channel sediments, and surface water	26	18	4	2	2	0	0	0	0	0
I	Rodríguez-Ramos et al. 2022	River	Sediments	68	48	18	2	0	20	18	2	0	0
J	Wang et al. 2024	River	Sediments	97	57	27	12	1	44	28	11	5	0
K	Sun et al. 2021	Ocean	Oxygen deficient zones	26	12	12	2	0	11	2	7	2	0
L	Zhang et al. 2023	Ocean	Oxygen deficient zones	383	291	73	18	1	132	92	31	8	1
M	Zhuang et al. 2020	Lab biofilm	Anammox	22	12	5	3	2	15	9	4	1	1
N	Wang et al. 2021	Lab biofilm	Enhanced biological phosphorus removal	29	9	13	4	3	23	6	11	3	3
O**	Kantor et al. 2017	Lab biofilm	Ammonium sulfate	51	35	7	4	5	41	28	5	3	5
P**	Kantor et al. 2017	Lab biofilm	Thiocyanate	66	32	13	7	14	49	24	7	6	12
Q	Kraft et al. 2014	Lab suspended	NOx limiting	9	3	1	0	5	1	0	0	0	1
R	Hanke et al. 2016	Lab suspended	NOx limiting	13	2	2	6	3	0	0	0	0	0
S	Kim et al. 2022	Lab suspended	N2O limiting	12	2	3	1	6	6	1	2	0	3
T	Laureni et al. 2024	Lab suspended	N2O limiting	8	4	1	2	1	4	1	1	1	1
U	Laureni et al. 2024	Lab suspended	N2O excess	10	0	2	6	2	9	0	1	6	2
V	Roothans, Gabriëls, et al. 2024	Lab suspended	NO3 excess	28	3	7	9	9	21	1	6	7	7
W	Roothans, Gabriëls, et al. 2024	Lab suspended	NO3 excess	26	1	5	6	14	18	0	2	5	11

\* 83 HQ MAGs overlapped in these two studies, \*\* 34 MQ and 27 HQ MAGs overlapped in these two reactors

**Table S4.2. Relative abundance of MAGs in the analysed ecosystems in publicly available literature, distributed by the number of denitrification steps encoded in their genomes.** The genes encoding the catalytic subunit of each enzyme was considered as proxy for the enzyme complex. The high-quality MAGs ( $\geq 90\%$  completeness,  $\leq 5\%$  contamination) are represented on the right. The corresponding plot label for each dataset in Figure 4.1 is also indicated. The annotations and quality of the MAGs were taken from the literature studies.

Plot	Reference	Environment	Details	All MAGs					HQ MAGs ( $\geq 90\%$ completeness, $\leq 5\%$ contamination)				
				Total (%)	1 step (%)	2 steps (%)	3 steps (%)	4 steps (%)	Total (%)	1 step (%)	2 steps (%)	3 steps (%)	4 steps (%)
A	Speth et al. 2016	WWTP	Anammox granules	-	-	-	-	-	-	-	-	-	-
B	Valk et al. 2022	WWTP	Activated sludge	-	-	-	-	-	-	-	-	-	-
C	Roothans, Pabst, et al. 2024	WWTP	Activated sludge	21.3	10.9	5.8	4.0	0.7	21.3	10.9	5.8	4.0	0.7
D	Ramírez-Fernández et al. 2021	Soil	Coastal soil	-	-	-	-	-	-	-	-	-	-
E	Pessi et al. 2022	Soil	Heathlands and meadows	-	-	-	-	-	-	-	-	-	-
F	Wang et al. 2023	Soil	Wetland	-	-	-	-	-	-	-	-	-	-
G	Zhang et al. 2024	Soil	Agricultural soils	-	-	-	-	-	-	-	-	-	-
H	Deng et al. 2024	River	Riparian soils, channel sediments, and surface water	-	-	-	-	-	-	-	-	-	-
I	Rodríguez-Ramos et al. 2022	River	Sediments	-	-	-	-	-	-	-	-	-	-
J	Wang et al. 2024	River	Sediments	-	-	-	-	-	-	-	-	-	-
K	Sun et al. 2021	Ocean	Oxygen deficient zones	18.0	11.8	5.6	0.6	0.0	6.1	3.2	2.3	0.6	0.0
L	Zhang et al. 2023	Ocean	Oxygen deficient zones	10.5	8.0	2.4	0.2	0.0	3.7	2.4	1.1	0.2	0.0
M	Zhuang et al. 2020	Lab biofilm	Anammox	22.9	17.2	2.4	2.0	1.2	15.1	12.7	1.4	0.6	0.4
N	Wang et al. 2021	Lab biofilm	Enhanced biological phosphorus removal	-	-	-	-	-	-	-	-	-	-
O	Kantor et al. 2017	Lab biofilm	Ammonium sulfate	-	-	-	-	-	-	-	-	-	-
P	Kantor et al. 2017	Lab biofilm	Thiocyanate	-	-	-	-	-	-	-	-	-	-
Q	Kraft et al. 2014	Lab suspended	NOx limiting	-	-	-	-	-	-	-	-	-	-
R	Hanke et al. 2016	Lab suspended	NOx limiting	-	-	-	-	-	-	-	-	-	-
S	Kim et al. 2022	Lab suspended	N2O limiting	-	-	-	-	-	-	-	-	-	-
T	Laureni et al. 2024	Lab suspended	N2O limiting	71.1	1.0	0.3	67.9	1.9	3.2	0.2	0.3	0.8	1.9
U	Laureni et al. 2024	Lab suspended	N2O excess	94.5	0.0	0.7	87.9	5.9	94.1	0.0	0.3	87.9	5.9
V	Roothans, Gabriëls, et al. 2024	Lab suspended	NO3 excess	82.0	1.7	12.5	22.4	45.3	80.6	1.2	12.4	22.1	44.8
W	Roothans, Gabriëls, et al. 2024	Lab suspended	NO3 excess	66.7	0.9	2.7	6.9	56.2	58.0	0.0	1.6	6.9	49.5



**Table S4.3. Number of high-quality MAGs recovered from literature distributed by the number of denitrification steps encoded in their genomes and the different denitrification genes.** The corresponding plot label for each dataset in Figure 4.1 is also indicated. Studies B,C and O,P have MAGs in common, as indicated in the last rows of this table. The annotations and quality of the MAGs were taken from the literature studies.

Plot	Reference	Environment	Details	Den steps	HQ MAGs (≥90% completeness, ≤5% contamination)												Total
					Total nar/nap	Total nir	Total nor	Total nos	narG/Z	napA	nirK	nirS	norZ	norB	nosZI	nosZII	
A	Speth et al. 2016	WWTP	Anammox granules	1	0	0	0	1	0	0	0	0	0	0	-	-	1
A	Speth et al. 2016	WWTP	Anammox granules	2	3	3	5	5	3	1	3	0	2	3	-	-	8
A	Speth et al. 2016	WWTP	Anammox granules	3	0	0	0	0	0	0	0	0	0	0	-	-	0
A	Speth et al. 2016	WWTP	Anammox granules	4	0	0	0	0	0	0	0	0	0	0	-	-	0
B	Valk et al. 2022	WWTP	Activated sludge	1	13	14	9	23	13	0	10	4	-	-	-	-	59
B	Valk et al. 2022	WWTP	Activated sludge	2	27	32	39	36	17	12	14	19	-	-	-	-	67
B	Valk et al. 2022	WWTP	Activated sludge	3	13	15	17	15	9	6	7	8	-	-	-	-	20
B	Valk et al. 2022	WWTP	Activated sludge	4	3	3	3	3	0	3	0	3	-	-	-	-	3
C	Roothans, Pabst, et al. 2024	WWTP	Activated sludge	1	35	28	26	35	35	3	19	10	15	13	0	35	124
C	Roothans, Pabst, et al. 2024	WWTP	Activated sludge	2	51	59	82	52	41	17	40	21	39	50	5	46	122
C	Roothans, Pabst, et al. 2024	WWTP	Activated sludge	3	40	45	43	40	29	15	25	22	11	34	13	25	56
C	Roothans, Pabst, et al. 2024	WWTP	Activated sludge	4	16	16	16	16	4	13	2	14	6	10	11	3	16
D	Ramírez-Fernández et al. 2021	Soil	Coastal soil	1	11	1	2	0	11	0	0	1	-	-	-	-	14
D	Ramírez-Fernández et al. 2021	Soil	Coastal soil	2	0	0	0	0	0	0	0	0	-	-	-	-	0
D	Ramírez-Fernández et al. 2021	Soil	Coastal soil	3	4	2	2	4	4	0	0	2	-	-	-	-	4
D	Ramírez-Fernández et al. 2021	Soil	Coastal soil	4	1	1	1	1	0	1	0	1	-	-	-	-	1
E	Pessi et al. 2022	Soil	Heathlands and meadows	1	0	2	2	2	-	-	2	1	-	-	-	-	6
E	Pessi et al. 2022	Soil	Heathlands and meadows	2	0	0	2	2	-	-	0	0	-	-	-	-	2
E	Pessi et al. 2022	Soil	Heathlands and meadows	3	0	0	0	0	-	-	0	0	-	-	-	-	0
E	Pessi et al. 2022	Soil	Heathlands and meadows	4	-	-	-	-	-	-	-	-	-	-	-	-	-
F	Wang et al. 2023	Soil	Wetland	1	0	2	0	2	0	0	2	0	-	-	-	-	4
F	Wang et al. 2023	Soil	Wetland	2	0	1	0	1	0	1	0	0	-	-	-	-	1
F	Wang et al. 2023	Soil	Wetland	3	0	0	0	0	0	0	0	0	-	-	-	-	0
F	Wang et al. 2023	Soil	Wetland	4	0	0	0	0	0	0	0	0	-	-	-	-	0
G	Zhang et al. 2024	Soil	Agricultural soils	1	8	12	5	7	-	-	-	-	-	-	-	-	32
G	Zhang et al. 2024	Soil	Agricultural soils	2	13	21	18	8	-	-	-	-	-	-	-	-	30
G	Zhang et al. 2024	Soil	Agricultural soils	3	9	12	12	9	-	-	-	-	-	-	-	-	14

G	Zhang et al. 2024	Soil	Agricultural soils	4	8	8	8	8	-	-	-	-	-	-	-	-	8
H	Deng et al. 2024	River	Riparian soils, channel sediments, surface water	1	0	0	0	0	-	-	-	-	-	-	-	-	0
H	Deng et al. 2024	River	Riparian soils, channel sediments, surface water	2	0	0	0	0	-	-	-	-	-	-	-	-	0
H	Deng et al. 2024	River	Riparian soils, channel sediments, surface water	3	0	0	0	0	-	-	-	-	-	-	-	-	0
H	Deng et al. 2024	River	Riparian soils, channel sediments, and surface water	4	0	0	0	0	-	-	-	-	-	-	-	-	0
I	Rodríguez-Ramos et al. 2022	River	Sediments	1	4	5	5	4	4	0	5	0	-	-	-	-	18
I	Rodríguez-Ramos et al. 2022	River	Sediments	2	2	2	0	0	2	0	2	0	-	-	-	-	2
I	Rodríguez-Ramos et al. 2022	River	Sediments	3	0	0	0	0	0	0	0	0	-	-	-	-	0
I	Rodríguez-Ramos et al. 2022	River	Sediments	4	0	0	0	0	0	0	0	0	-	-	-	-	0
J	Wang et al. 2024	River	Sediments	1	17	1	7	3	14	4	-	-	-	-	-	-	28
J	Wang et al. 2024	River	Sediments	2	8	4	6	4	4	7	-	-	-	-	-	-	11
J	Wang et al. 2024	River	Sediments	3	4	1	5	5	2	2	-	-	-	-	-	-	5
J	Wang et al. 2024	River	Sediments	4	0	0	0	0	0	0	-	-	-	-	-	-	0
K	Sun et al. 2021	Ocean	Oxygen deficient zones	1	1	1	0	0	-	-	-	-	-	-	-	-	2
K	Sun et al. 2021	Ocean	Oxygen deficient zones	2	7	3	2	2	-	-	-	-	-	-	-	-	7
K	Sun et al. 2021	Ocean	Oxygen deficient zones	3	2	2	1	1	-	-	-	-	-	-	-	-	2
K	Sun et al. 2021	Ocean	Oxygen deficient zones	4	0	0	0	0	-	-	-	-	-	-	-	-	0
L	Zhang et al. 2023	Ocean	Oxygen deficient zones	1	41	6	35	10	24	20	3	3	-	-	-	-	92
L	Zhang et al. 2023	Ocean	Oxygen deficient zones	2	27	7	23	5	15	18	5	2	-	-	-	-	31
L	Zhang et al. 2023	Ocean	Oxygen deficient zones	3	8	6	8	2	4	5	3	3	-	-	-	-	8
L	Zhang et al. 2023	Ocean	Oxygen deficient zones	4	1	1	1	1	0	1	0	1	-	-	-	-	1
M	Zhuang et al. 2020	Lab biofilm	Anammox	1	2	1	4	2	0	2	1	0	4	0	0	2	9
M	Zhuang et al. 2020	Lab biofilm	Anammox	2	2	3	1	2	1	1	3	0	1	0	1	1	4
M	Zhuang et al. 2020	Lab biofilm	Anammox	3	1	1	1	0	0	1	1	0	0	1	0	0	1
M	Zhuang et al. 2020	Lab biofilm	Anammox	4	1	1	1	1	0	1	0	1	0	1	0	1	1
N	Wang et al. 2021	Lab biofilm	Enhanced biological phosphorus removal	1	1	2	0	3	-	-	-	-	-	-	-	-	6
N	Wang et al. 2021	Lab biofilm	Enhanced biological phosphorus removal	2	5	5	4	8	-	-	-	-	-	-	-	-	11
N	Wang et al. 2021	Lab biofilm	Enhanced biological phosphorus removal	3	2	3	2	2	-	-	-	-	-	-	-	-	3
N	Wang et al. 2021	Lab biofilm	Enhanced biological phosphorus removal	4	3	3	3	3	-	-	-	-	-	-	-	-	3
O	Kantor et al. 2017	Lab biofilm	Ammonium sulfate	1	12	6	6	4	11	1	-	-	-	-	-	-	28

O	Kantor et al. 2017	Lab biofilm	Ammonium sulfate	2	4	2	2	2	3	1	-	-	-	-	-	-	5
O	Kantor et al. 2017	Lab biofilm	Ammonium sulfate	3	1	3	3	2	1	0	-	-	-	-	-	-	3
O	Kantor et al. 2017	Lab biofilm	Ammonium sulfate	4	5	5	5	5	4	2	-	-	-	-	-	-	5
P	Kantor et al. 2017	Lab biofilm	Thiocyanate	1	5	7	5	7	5	0	-	-	-	-	-	-	24
P	Kantor et al. 2017	Lab biofilm	Thiocyanate	2	5	5	2	2	5	0	-	-	-	-	-	-	7
P	Kantor et al. 2017	Lab biofilm	Thiocyanate	3	4	5	6	3	3	1	-	-	-	-	-	-	6
P	Kantor et al. 2017	Lab biofilm	Thiocyanate	4	12	12	12	12	10	3	-	-	-	-	-	-	12
Q	Kraft et al. 2014	Lab suspended	NOx limiting	1	0	0	0	0	0	0	-	-	-	-	-	-	0
Q	Kraft et al. 2014	Lab suspended	NOx limiting	2	0	0	0	0	0	0	-	-	-	-	-	-	0
Q	Kraft et al. 2014	Lab suspended	NOx limiting	3	0	0	0	0	0	0	-	-	-	-	-	-	0
Q	Kraft et al. 2014	Lab suspended	NOx limiting	4	1	1	1	1	1	0	-	-	-	-	-	-	1
R	Hanke et al. 2016	Lab suspended	NOx limiting	1	0	0	0	0	-	-	-	-	-	-	-	-	0
R	Hanke et al. 2016	Lab suspended	NOx limiting	2	0	0	0	0	-	-	-	-	-	-	-	-	0
R	Hanke et al. 2016	Lab suspended	NOx limiting	3	0	0	0	0	-	-	-	-	-	-	-	-	0
R	Hanke et al. 2016	Lab suspended	NOx limiting	4	0	0	0	0	-	-	-	-	-	-	-	-	0
S	Kim et al. 2022	Lab suspended	N2O limiting	1	1	0	0	0	0	1	0	0	-	-	-	-	1
S	Kim et al. 2022	Lab suspended	N2O limiting	2	1	1	1	1	1	0	1	0	-	-	-	-	2
S	Kim et al. 2022	Lab suspended	N2O limiting	3	0	0	0	0	0	0	0	0	-	-	-	-	0
S	Kim et al. 2022	Lab suspended	N2O limiting	4	3	3	3	3	1	2	0	3	-	-	-	-	3
T	Laureni et al. 2024	Lab suspended	N2O limiting	1	0	0	1	0	0	0	0	0	-	-	0	0	1
T	Laureni et al. 2024	Lab suspended	N2O limiting	2	0	1	1	0	0	0	1	0	-	-	0	0	1
T	Laureni et al. 2024	Lab suspended	N2O limiting	3	0	1	1	1	0	0	1	0	-	-	0	1	1
T	Laureni et al. 2024	Lab suspended	N2O limiting	4	1	1	1	1	1	1	0	1	-	-	0	1	1
U	Laureni et al. 2024	Lab suspended	N2O excess	1	0	0	0	0	0	0	0	0	-	-	0	0	0
U	Laureni et al. 2024	Lab suspended	N2O excess	2	0	0	1	1	0	0	0	0	-	-	0	1	1
U	Laureni et al. 2024	Lab suspended	N2O excess	3	2	6	4	6	1	1	3	3	-	-	2	4	6
U	Laureni et al. 2024	Lab suspended	N2O excess	4	2	2	2	2	2	0	2	0	-	-	0	2	2
V	Roothans, Gabriëls, et al. 2024	Lab suspended	NO3 excess	1	1	0	0	0	1	0	0	0	0	0	0	0	1
V	Roothans, Gabriëls, et al. 2024	Lab suspended	NO3 excess	2	3	3	2	4	3	0	3	1	0	2	2	2	6
V	Roothans, Gabriëls, et al. 2024	Lab suspended	NO3 excess	3	4	7	5	5	4	0	5	3	0	5	3	2	7
V	Roothans, Gabriëls, et al. 2024	Lab suspended	NO3 excess	4	7	7	7	7	7	3	4	5	3	7	6	1	7
W	Roothans, Gabriëls, et al. 2024	Lab suspended	NO3 excess	1	0	0	0	0	0	0	0	0	0	0	0	0	0
W	Roothans, Gabriëls, et al. 2024	Lab suspended	NO3 excess	2	1	2	1	0	1	0	2	0	0	1	0	0	2
W	Roothans, Gabriëls, et al. 2024	Lab suspended	NO3 excess	3	2	5	4	4	2	0	4	2	2	3	2	2	5
W	Roothans, Gabriëls, et al. 2024	Lab suspended	NO3 excess	4	11	11	11	11	11	2	6	7	5	10	11	0	11
B, C	Valk et al. 2022; Roothans, Pabst, et al. 2024	WWTP	Overlapping MAGs in the two studies	1	7	8	4	10	7	0	5	4	-	-	-	-	29
B, C	Valk et al. 2022; Roothans, Pabst, et al. 2024	WWTP	Overlapping MAGs in the two studies	2	14	21	19	14	10	7	9	13	-	-	-	-	68

B, C	Valk et al. 2022; Roothans, Pabst, et al. 2024	WWTP	Overlapping MAGs in the two studies	3	11	13	13	14	7	6	6	7	-	-	-	-	51
B, C	Valk et al. 2022; Roothans, Pabst, et al. 2024	WWTP	Overlapping MAGs in the two studies	4	3	3	3	3	0	3	0	3	-	-	-	-	12
O, P	Kantor et al. 2017	Lab biofilm	Overlapping MAGs in the two reactors	1	13	7	7	8	12	1	-	-	-	-	-	-	35
O, P	Kantor et al. 2018	Lab biofilm	Overlapping MAGs in the two reactors	2	7	5	3	3	6	1	-	-	-	-	-	-	18
O, P	Kantor et al. 2019	Lab biofilm	Overlapping MAGs in the two reactors	3	4	6	7	4	3	1	-	-	-	-	-	-	21
O, P	Kantor et al. 2020	Lab biofilm	Overlapping MAGs in the two reactors	4	12	12	12	12	10	3	-	-	-	-	-	-	48

**Table S4.4. Characteristics from the ecosystems included in Figures 4.1 and 4.2.** The studies are ordered based on Figure 4.1, and the corresponding plot number is indicated. The organic carbon and nitrogen oxides supplied to the systems, and the biomass retention times were mainly defined for the laboratory studies. The annotations and quality of the MAGs were taken from the literature studies.

Plot	Reference	Environment	Details	Organic carbon	NO <sub>x</sub>	Biomass retention (d)
A	Speth et al. 2016	WWTP	Anammox granules	-	Mix <sup>a</sup>	-
B	Valk et al. 2022	WWTP	Activated sludge	-	Mix <sup>a</sup>	11-15
C	Roothans, Pabst, et al. 2024	WWTP	Activated sludge	-	Mix <sup>a</sup>	11-15
D	Ramírez-Fernández et al. 2021	Soil	Coastal soil	-	Mix	-
E	Pessi et al. 2022	Soil	Heathlands and meadows	-	Mix	-
F	Wang et al. 2023	Soil	Wetland	-	Mix	-
G	Zhang et al. 2024	Soil	Agricultural soils	-	Mix	-
H	Deng et al. 2024	River	Riparian soils, channel sediments, and surface water	-	Mix	-
I	Rodríguez-Ramos et al. 2022	River	Sediments	-	Mix	-
J	Wang et al. 2024	River	Sediments	-	Mix	-
K	Sun et al. 2021	Ocean	Oxygen deficient zones	-	Mix	-
L	Zhang et al. 2023	Ocean	Oxygen deficient zones	-	Mix	-
M	Zhuang et al. 2020	Lab biofilm	Anammox	-	Mix <sup>a</sup>	-
N	Wang et al. 2021	Lab biofilm	Enhanced biological phosphorus removal	Acetate, propionate	NO <sub>2</sub> <sup>-</sup>	-
O	Kantor et al. 2017	Lab biofilm	Ammonium sulfate	Molasses	Mix <sup>a</sup>	-
P	Kantor et al. 2017	Lab biofilm	Thiocyanate	Molasses	Mix <sup>a</sup>	-
Q	Kraft et al. 2014	Lab suspended	NO <sub>x</sub> limiting	Glucose, acetate, aminoacids	Mainly NO <sub>2</sub> <sup>-</sup> , some NO <sub>3</sub> <sup>-</sup>	0.6
R	Hanke et al. 2016	Lab suspended	NO <sub>x</sub> limiting	Glucose, acetate, aminoacids	Mainly NO <sub>2</sub> <sup>-</sup> , some NO <sub>3</sub> <sup>-</sup>	2.8
S	Kim et al. 2022	Lab suspended	N <sub>2</sub> O limiting	Acetate	N <sub>2</sub> O	1.6
T	Laureni et al. 2024	Lab suspended	N <sub>2</sub> O limiting	Acetate	N <sub>2</sub> O	7
U	Laureni et al. 2024	Lab suspended	N <sub>2</sub> O excess	Acetate	N <sub>2</sub> O	7
V	Roothans, Gabriëls, et al. 2024	Lab suspended	NO <sub>3</sub> <sup>-</sup> excess	Acetate, propionate, butyrate	NO <sub>3</sub> <sup>-</sup>	2
W	Roothans, Gabriëls, et al. 2024	Lab suspended	NO <sub>3</sub> <sup>-</sup> excess	Acetate, propionate, butyrate	NO <sub>3</sub> <sup>-</sup>	2

## 4.6. References

1. Oster GF, Wilson EO. *Caste and Ecology in the Social Insects*. Princeton University Press; 1978. doi:10.2307/j.ctvx5wb34
2. Smith JM, Szathmari E. *The Major Transitions in Evolution*. Oxford University Press; 1997. doi:10.1093/oso/9780198502944.001.0001
3. West SA, Cooper GA. Division of labour in microorganisms: An evolutionary perspective. *Nat Rev Microbiol*. 2016;14(11):716-723. doi:10.1038/nrmicro.2016.111
4. Pfeiffer T, Bonhoeffer S. Evolution of cross-feeding in microbial populations. *Am Nat*. 2004;163(6):126-135. doi:10.1086/383593
5. Wardman JF, Bains RK, Rahfeld P, Withers SG. Carbohydrate-active enzymes (CAZymes) in the gut microbiome. *Nat Rev Microbiol*. 2022;20(9):542-556. doi:10.1038/s41579-022-00712-1
6. Müller N, Timmers P, Plugge CM, Stams AJM, Schink B. Syntrophy in methanogenic degradation. In: Hackstein J, ed. *(Endo)Symbiotic Methanogenic Archaea*. Springer; 2018:153-192. doi:10.1007/978-3-319-98836-8\_9
7. Costa E, Pérez J, Kreft JU. Why is metabolic labour divided in nitrification? *Trends Microbiol*. 2006;14(5):213-219. doi:10.1016/j.tim.2006.03.006
8. Tsoi R, Wu F, Zhang C, Bewick S, Karig D, You L. Metabolic division of labor in microbial systems. *Proc Natl Acad Sci U S A*. 2018;115(10):2526-2531. doi:10.1073/pnas.1716888115
9. Zhu M, Dai X. Shaping of microbial phenotypes by trade-offs. *Nat Commun*. 2024;15:4238. doi:10.1038/s41467-024-48591-9
10. Kuypers MMM, Marchant HK, Kartal B. The microbial nitrogen-cycling network. *Nat Rev Microbiol*. 2018;16(5):263-276. doi:10.1038/nrmicro.2018.9
11. Daims H, Lebedeva E V., Pjevac P, et al. Complete nitrification by *Nitrospira* bacteria. *Nature*. 2015;528(7583):504-509. doi:10.1038/nature16461
12. Van Kessel MAHJ, Speth DR, Albertsen M, et al. Complete nitrification by a single microorganism. *Nature*. 2015;528(7583):555-559. doi:10.1038/nature16459
13. Kraft B, Tegetmeyer HE, Sharma R, et al. The environmental controls that govern the end product of bacterial nitrate respiration. *Science (80- )*. 2014;345(6197):676-679. doi:10.1126/science.1254070
14. Sun X, Buchanan P, Zhang I, Babbitt A, Zakem E. Ecological dynamics explain modular denitrification in the ocean. *Proc Natl Acad Sci U S A*. 2024;121(52):e2417421121. doi:10.1073/pnas.2417421121
15. Zhang IH, Sun X, Jayakumar A, Fortin SG, Ward BB, Babbitt AR. Partitioning of the denitrification pathway and other nitrite metabolisms within global oxygen deficient zones. *ISME Commun*. 2023;3(1):76. doi:10.1038/s43705-023-00284-y
16. Graf DRH, Jones CM, Hallin S. Intergenomic comparisons highlight modularity of the denitrification pathway and underpin the importance of community structure for N2O

- emissions. *PLoS One*. 2014;9(12):e114118. doi:10.1371/journal.pone.0114118
17. Lycus P, Bøthun KL, Bergaust L, Shapleigh JP, Bakken LR, Frostegård Å. Phenotypic and genotypic richness of denitrifiers revealed by a novel isolation strategy. *ISME J*. 2017;11(10):2219-2232. doi:10.1038/ismej.2017.82
  18. Chen J, Strous M. Denitrification and aerobic respiration, hybrid electron transport chains and co-evolution. *Biochim Biophys Acta*. 2013;1827(2):136-144. doi:10.1016/j.bbabi.2012.10.002
  19. Broadbent FE, Clark F. Denitrification. In: Bartholomew W V., Clark FE, eds. *Soil Nitrogen*. American Society of Agronomy; 1965:344-359. doi:10.2134/agronmonogr10.c9
  20. van Spanning RJM, Richardson DJ, Ferguson SJ. Introduction to the biochemistry and molecular biology of denitrification. In: Bothe H, Ferguson SJ, Newton WE, eds. *Biology of the Nitrogen Cycle*. Elsevier B.V.; 2007. doi:10.1016/B978-044452857-5.50002-3
  21. John P. Aerobic and anaerobic bacterial respiration monitored by electrodes. *J Gen Microbiol*. 1977;98(1):231-238. doi:10.1099/00221287-98-1-231
  22. Braun C, Zumft WG. Marker exchange of the structural genes for nitric oxide reductase blocks the denitrification pathway of *Pseudomonas stutzeri* at nitric oxide. *J Biol Chem*. 1991;266(34):22785-22788. doi:10.1016/s0021-9258(18)54420-3
  23. Carr GJ, Ferguson SJ. The nitric oxide reductase of *Paracoccus* denitrificans. *Biochem J*. 1990;269(2):423-429. doi:10.1042/bj2690423
  24. Alefounder PR, McCartthy JEG, Ferguson SJ. The basis of the control of nitrate reduction by oxygen in *Paracoccus* denitrificans. *FEMS Microbiol Lett*. 1981;12:321-326. doi:10.1111/j.1574-6968.1981.tb07666.x
  25. Pessi IS, Viitamäki S, Virkkala AM, et al. In - depth characterization of denitrifier communities across different soil ecosystems in the tundra. *Environ Microbiome*. 2022;17:30. doi:10.1186/s40793-022-00424-2
  26. Sun X, Ward BB. Novel metagenome-assembled genomes involved in the nitrogen cycle from a Pacific oxygen minimum zone. *ISME Commun*. 2021;1:26. doi:10.1038/s43705-021-00030-2
  27. Singleton CM, Petriglieri F, Kristensen JM, et al. Connecting structure to function with the recovery of over 1000 high-quality metagenome-assembled genomes from activated sludge using long-read sequencing. *Nat Commun*. 2021;12:2009. doi:10.1038/s41467-021-22203-2
  28. Wang Y, Ye J, Ju F, et al. Successional dynamics and alternative stable states in a saline activated sludge microbial community over 9 years. *Microbiome*. 2021;9(1):199. doi:10.1186/s40168-021-01151-5
  29. Roothans N, Gabriëls M, Abeel T, Pabst M, Van Loosdrecht MCM, Laureni M. Aerobic denitrification as an N<sub>2</sub>O source from microbial communities. *ISME J*. 2024;18(1):wrae116. doi:doi.org/10.1093/ismejo/wrae116
  30. Tiedje JM. Denitrifiers. In: Weaver

- RW, Angle S, Bottomley P, et al., eds. *Methods of Soil Analysis: Part 2 - Microbiological and Biochemical Properties*. Soil Science Society of America; 1994. doi:10.2136/sssabookser5.2.c14
31. Ramírez-Fernández L, Orellana LH, Johnston ER, Konstantinidis KT, Orlando J. Diversity of microbial communities and genes involved in nitrous oxide emissions in Antarctic soils impacted by marine animals as revealed by metagenomics and 100 metagenome-assembled genomes. *Sci Total Environ*. 2021;788:147693. doi:10.1016/j.scitotenv.2021.147693
  32. Zhang L, Zhao H, Qin S, et al. Genome-resolved metagenomics and denitrifying strain isolation reveal new insights into microbial denitrification in the deep dadose zone. *Environ Sci Technol*. 2024;58(5):2323-2334. doi:10.1021/acs.est.3c06466
  33. Wang X, Wang S, Yang Y, et al. Hot moment of N<sub>2</sub>O emissions in seasonally frozen peatlands. *ISME J*. 2023;17(6):792-802. doi:10.1038/s41396-023-01389-x
  34. Deng D, Yang Z, Yang Y, Wan W, Liu W, Xiong X. Metagenomic insights into nitrogen-cycling microbial communities and their relationships with nitrogen removal potential in the Yangtze River. *Water Res*. 2024;265:122229. doi:10.1016/j.watres.2024.122229
  35. Rodríguez-Ramos J, Borton MA, McGivern BB, et al. Genome-resolved metaproteomics decodes the microbial and river sediments. *mSystems*. 2022;7(4):e00516-22.
  36. Wang S, Lan B, Yu L, et al. Ammonium-derived nitrous oxide is a global source in streams. *Nat Commun*. 2024;15(1):4085. doi:10.1038/s41467-024-48343-9
  37. Valk L, Peces M, Singleton CM, et al. Exploring the microbial influence on seasonal nitrous oxide concentration in a full-scale wastewater treatment plant using metagenome assembled genomes. *Water Res*. 2022;219(May):118563. doi:10.1016/j.watres.2022.118563
  38. Speth DR, In'T Zandt MH, Guerrero-Cruz S, Dutilh BE, Jetten MSM. Genome-based microbial ecology of anammox granules in a full-scale wastewater treatment system. *Nat Commun*. 2016;7:11172. doi:10.1038/ncomms11172
  39. Roothans N, Pabst M, van Diemen M, et al. Long-term multi-metagenomics resolves the ecophysiological controls of seasonal N<sub>2</sub>O emissions. *bioRxiv*. Published online 2024:2024.04.17.589950. doi:10.1101/2024.04.17.589950
  40. Zhuang J long, Zhou Y yuan, Liu Y di, Li W. Flocs are the main source of nitrous oxide in a high-rate anammox granular sludge reactor: insights from metagenomics and fed-batch experiments. *Water Res*. 2020;186:116321. doi:10.1016/j.watres.2020.116321
  41. Wang Y, Gao H, F. Wells G. Integrated omics analyses reveal differential gene expression and potential for cooperation between denitrifying polyphosphate and glycogen accumulating organisms. *Environ Microbiol*. 2021;23(6):3274-3293. doi:10.1111/1462-2920.15486
  42. Kantor RS, Huddy RJ, Iyer R, et al. Genome-resolved meta-omics ties microbial dynamics to process performance in biotechnology for



- thiocyanate degradation. *Environ Sci Technol.* 2017;51(5):2944-2953.  
doi:10.1021/acs.est.6b04477
43. Kraft B, Tegetmeyer HE, Meier D, Geelhoed JS, Strous M. Rapid succession of uncultured marine bacterial and archaeal populations in a denitrifying continuous culture. *Environ Microbiol.* 2014;16(10):3275-3286.  
doi:10.1111/1462-2920.12552
  44. Hanke A, Berg J, Hargesheimer T, Tegetmeyer HE, Sharp CE, Strous M. Selective pressure of temperature on competition and cross-feeding within denitrifying and fermentative microbial communities. *Front Microbiol.* 2016;6:1461.  
doi:10.3389/fmicb.2015.01461
  45. Kim DD, Han H, Yun T, et al. Identification of nosZ-expressing microorganisms consuming trace N<sub>2</sub>O in microaerobic chemostat consortia dominated by an uncultured Burkholderiales. *ISME J.* 2022;16(9):2087-2098.  
doi:10.1038/s41396-022-01260-5
  46. Laurenzi M, Corbera Rubio F, Kim DD, et al. Selective enrichment of high-affinity clade II N<sub>2</sub>O-reducers in a mixed culture. *bioRxiv.* Published online 2024:2024.02.09.579283.  
doi:10.1101/2024.02.09.579283
  47. Crocker K, Lee K, Chakraverti-Wuerthwein M, et al. Environmentally dependent interactions shape patterns in gene content across natural microbiomes. *Nat Microbiol.* 2024;9:2022-2037.  
doi:10.1038/s41564-024-01752-4
  48. Fuchsman CA, Devol AH, Saunders JK, McKay C, Rocap G. Niche partitioning of the N cycling microbial community of an offshore oxygen deficient zone. *Front Microbiol.* 2017;8(DEC):2384.  
doi:10.3389/fmicb.2017.02384
  49. Nadeau SA, Roco CA, Debenport SJ, et al. Metagenomic analysis reveals distinct patterns of denitrification gene abundance across soil moisture, nitrate gradients. *Environ Microbiol.* 2019;21(4):1255-1266.  
doi:10.1111/1462-2920.14587
  50. Gaimster H, Alston M, Richardson DJ, Gates AJ, Rowley G. Transcriptional and environmental control of bacterial denitrification and N<sub>2</sub>O emissions. *FEMS Microbiol Lett.* 2018;365:fnx277.  
doi:10.1093/femsle/fnx277
  51. Qu Z, Bakken LR, Molstad L, Frostegård Å, Bergaust LL. Transcriptional and metabolic regulation of denitrification in *Paracoccus denitrificans* allows low but significant activity of nitrous oxide reductase under oxic conditions. *Environ Microbiol.* 2016;18(9):2951-2963.  
doi:10.1111/1462-2920.13128
  52. Lycus P, Soriano-Laguna MJ, Kjos M, et al. A bet-hedging strategy for denitrifying bacteria curtails their release of N<sub>2</sub>O. *Proc Natl Acad Sci U S A.* 2018;115(46):11820-11825.  
doi:10.1073/pnas.1805000115
  53. Garrido-Amador P, Stortenbeker N, Wessels HJCT, Speth DR, Garcia-Heredia I, Kartal B. Enrichment and characterization of a nitric oxide-reducing microbial community in a continuous bioreactor. *Nat Microbiol.* 2023;8(8):1574-1586.  
doi:10.1038/s41564-023-01425-8
  54. Semedo M, Wittorf L, Hallin S, Song B. Differential expression of clade I and II N<sub>2</sub>O reductase genes in denitrifying *Thauera linaloolentis* 47LoIT under different nitrogen conditions.

- FEMS Microbiol Lett.*  
2020;367(24):fnaa205.  
doi:10.1093/femsle/fnaa205
55. Jones CM, Graf DRH, Bru D, Philippot L, Hallin S. The unaccounted yet abundant nitrous oxide-reducing microbial community: A potential nitrous oxide sink. *ISME J.* 2013;7(2):417-426. doi:10.1038/ismej.2012.125
  56. Richardson DJ, Berks BC, Russell DA, Spiro S, Taylor CJ. Functional, biochemical and genetic diversity of prokaryotic nitrate reductases. *Cell Mol Life Sci.* 2001;58(2):165-178. doi:10.1007/PL00000845
  57. Pold G, Bonilla-Rosso G, Saghai A, Strous M, Jones CM, Hallin S. Phylogenetics and environmental distribution of nitric oxide-forming nitrite reductases reveal their distinct functional and ecological roles. *ISME Commun.* 2024;4(1):ycae020. doi:10.1093/ismeco/ycae020
  58. Wang H, Tseng CP, Gunsalus RP. The napF and narG nitrate reductase operons in *Escherichia coli* are differentially expressed in response to submicromolar concentrations of nitrate but not nitrite. *J Bacteriol.* 1999;181(17):5303-5308. doi:10.1128/jb.181.17.5303-5308.1999
  59. Potter LC, Millington P, Griffiths L, Thomas GH, Cole JA. Competition between *Escherichia coli* strains expressing either a periplasmic or a membrane-bound nitrate reductase: does Nap confer a selective advantage during nitrate-limited growth? *Biochem J.* 1999;344(1):77-84. doi:10.1042/0264-6021:3440077
  60. Zumft WG. Cell biology and molecular basis of denitrification. *Microbiol Mol Biol Rev.* 1997;61(4):533-616. doi:10.1128/mmbr.61.4.533-616.1997
  61. Liu RR, Tian Y, Zhou EM, Xiong MJ, Xiao M, Li WJ. Distinct expression of the two NO-forming nitrite reductases in *Thermus antranikianii* DSM 12462T improved environmental adaptability. *Microb Ecol.* 2020;80(3):614-626. doi:10.1007/s00248-020-01528-3
  62. Suenaga T, Riya S, Hosomi M, Terada A. Biokinetic characterization and activities of N2O-reducing bacteria in response to various oxygen levels. *Front Microbiol.* 2018;9:697. doi:10.3389/fmicb.2018.00697
  63. Wang Z, Vishwanathan N, Kowaliczko S, Ishii S. Clarifying microbial nitrous oxide reduction under aerobic conditions: tolerant, intolerant, and sensitive. *Microbiol Spectr.* 2023;11(2):e04709-22. doi:doi.org/10.1128/spectrum.04709-22
  64. Wittorf L, Jones CM, Bonilla-Rosso G, Hallin S. Expression of nirK and nirS genes in two strains of *Pseudomonas stutzeri* harbouring both types of NO-forming nitrite reductases. *Res Microbiol.* 2018;169(6):343-347. doi:10.1016/j.resmic.2018.04.010
  65. Otte S, Grobбен NG, Robertson LA, Jetten MSM, Kuenen JG. Nitrous oxide production by *Alcaligenes faecalis* under transient and dynamic aerobic and anaerobic conditions. *Appl Environ Microbiol.* 1996;62(7):2421-2426. doi:10.1128/aem.62.7.2421-2426.1996
  66. Stump SM, Klausmeier CA. Competition and coexistence between a syntrophic consortium and a metabolic generalist, and its effect on productivity. *J Theor Biol.* 2016;404:348-360. doi:10.1016/j.jtbi.2016.06.019

67. Kreft JU. Biofilms promote altruism. *Microbiology*. 2004;150(8):2751-2760. doi:10.1099/mic.0.26829-0
68. Lu H, Chandran K, Stensel D. Microbial ecology of denitrification in biological wastewater treatment. *Water Res*. 2014;64:237-254. doi:10.1016/j.watres.2014.06.042
69. Chen S, Wang F, Zhang Y, et al. Organic carbon availability limiting microbial denitrification in the deep vadose zone. *Environ Microbiol*. 2018;20(3):980-992. doi:10.1111/1462-2920.14027
70. Putz M, Schleusner P, Rütting T, Hallin S. Relative abundance of denitrifying and DNRA bacteria and their activity determine nitrogen retention or loss in agricultural soil. *Soil Biol Biochem*. 2018;123(February):97-104. doi:10.1016/j.soilbio.2018.05.006
71. Van Den Berg EM, Van Dongen U, Abbas B, Van Loosdrecht MCM. Enrichment of DNRA bacteria in a continuous culture. *ISME J*. 2015;9(10):2153-2161. doi:10.1038/ismej.2015.26
72. Carlson HK, Lui LM, Price MN, et al. Selective carbon sources influence the end products of microbial nitrate respiration. *ISME J*. 2020;14(8):2034-2045. doi:10.1038/s41396-020-0666-7
73. Almeida JS, Júlio SM, Reis MAM, Carrondo MJT. Nitrite inhibition of denitrification by *Pseudomonas fluorescens*. *Biotechnol Bioeng*. 1995;46(3):194-201. doi:10.1002/bit.260460303
74. Sijbesma WFH, Almeida JS, Reis MAM, Santos H. Uncoupling effect of nitrite during denitrification by *Pseudomonas fluorescens*: An in vivo 31P-NMR study. *Biotechnol Bioeng*. 1996;52(1):176-182. doi:10.1002/(SICI)1097-0290(19961005)52:1<176::AID-BIT18>3.0.CO;2-M
75. Zumft WG. The biological role of nitric oxide in bacteria. *Arch Microbiol*. 1993;160:253-264. doi:10.1007/BF00292074
76. Sullivan MJ, Gates AJ, Appia-Ayme C, Rowley G, Richardson DJ. Copper control of bacterial nitrous oxide emission and its impact on vitamin B12-Dependent metabolism. *Proc Natl Acad Sci U S A*. 2013;110(49):19926-19931. doi:10.1073/pnas.1314529110
77. Lilja EE, Johnson DR. Segregating metabolic processes into different microbial cells accelerates the consumption of inhibitory substrates. *ISME J*. 2016;10(7):1568-1578. doi:10.1038/ismej.2015.243
78. Zhang IH, Mullen S, Ciccacese D, et al. Ratio of electron donor to acceptor influences metabolic specialization and denitrification dynamics in *Pseudomonas aeruginosa* in a mixed carbon medium. *Front Microbiol*. 2021;12(3):711073. doi:10.3389/fmicb.2021.711073
79. Simon J, Klotz MG. Diversity and evolution of bioenergetic systems involved in microbial nitrogen compound transformations. *Biochim Biophys Acta*. 2013;1827(2):114-135. doi:10.1016/j.bbabbio.2012.07.005
80. Pan Y, Ni BJ, Bond PL, Ye L, Yuan Z. Electron competition among nitrogen oxides reduction during methanol-utilizing denitrification in wastewater treatment. *Water Res*. 2013;47(10):3273-3281. doi:10.1016/j.watres.2013.02.054
81. Daniel R. The metagenomics of soil. *Nat Rev Microbiol*. 2005;3(6):470-478. doi:10.1038/nrmicro1160
82. Sunagawa S, Coelho LP, Chaffron S,

- et al. Structure and function of the global ocean microbiome. *Science*. 2015;348(6237):1261359. doi:10.1126/science.1261359
83. Senn H, Lendenmann U, Snozzi M, Hamer G, Egli T. The growth of *Escherichia coli* in glucose-limited chemostat cultures: a re-examination of the kinetics. *Biochim Biophys Acta*. 1994;1201:424-436. doi:10.1111/j.1462-2920.2005.00846.x
  84. Ihssen J, Egli T. Global physiological analysis of carbon- and energy-limited growing *Escherichia coli* confirms a high degree of catabolic flexibility and preparedness for mixed substrate utilization. *Environ Microbiol*. 2005;7(10):1568-1581. doi:10.1111/j.1462-2920.2005.00846.x
  85. Roop JI, Chang KC, Brem RB. Polygenic evolution of a sugar specialization trade-off in yeast. *Nature*. 2016;530(7590):336-339. doi:10.1038/nature16938
  86. Andersson DI, Levin BR. The biological cost of antibiotic resistance. *Curr Opin Microbiol*. 1999;2(5):489-493. doi:10.1016/S1369-5274(99)00005-3
  87. de Bruijn FJ. *Stress and Environmental Regulation of Gene Expression and Adaptation in Bacteria*. (de Bruijn FJ, ed.). John Wiley & Sons, Inc.; 2016. doi:10.1002/9781119004813
  88. Malik AA, Martiny JBH, Brodie EL, Martiny AC, Treseder KK, Allison SD. Defining trait-based microbial strategies with consequences for soil carbon cycling under climate change. *ISME J*. 2020;14(1):1-9. doi:10.1038/s41396-019-0510-0
  89. Niederdorfer R, Besemer K, Battin TJ, Peter H. Ecological strategies and metabolic trade-offs of complex environmental biofilms. *npj Biofilms Microbiomes*. 2017;3(1):21. doi:10.1038/s41522-017-0029-y
  90. Ehrlich E, Kath NJ, Gaedke U. The shape of a defense-growth trade-off governs seasonal trait dynamics in natural phytoplankton. *ISME J*. 2020;14(6):1451-1462. doi:10.1038/s41396-020-0619-1
  91. Kuenen JG. Continuous cultures (chemostats). In: Schmidt TM, ed. *Encyclopedia of Microbiology*. 4th ed. Elsevier Inc.; 2019:743-761. doi:10.1016/B978-0-12-801238-3.02490-9

# Outlook





The research presented in this thesis aimed to deepen our understanding of the ecophysiology of N<sub>2</sub>O-emitting microbial communities. By studying these communities across varying degrees of complexity (laboratory vs. *in situ* environments) and different cellular levels (genomic, proteomic, kinetic), we were able to draw three key conclusions:

1. Aerobic denitrification can be significant under dynamic oxygen conditions.
2. Seasonal N<sub>2</sub>O emissions in a WWTP are primarily driven by unbalanced nitrification.
3. Resource allocation trade-offs may explain the widespread denitrification labour division.

Several broader reflections emerged from the research, which have been divided into three fundamental questions.

## 5.1. How do we deal with our growing knowledge of the complexity of the microbial nitrogen network?

### 5.1.1. Importance of metabolic adaptability in dynamic ecosystems

As our knowledge of the microbial nitrogen network expands, so does its complexity. For example, heterotrophic denitrification can remain significantly active at high oxygen concentrations (Chapter 2). Decades of research into aerobic denitrification have often reported negligible rates, likely because earlier studies focused on denitrifiers cultivated under constant oxic conditions, in contrast to the dynamic conditions used in Chapter 2. These contrasting findings highlight how stable and dynamic environments differently influence microbial behaviour, highlighting the advantage of metabolic preparedness in aerobic denitrifying organisms. This metabolic adaptability may also explain the dominance of partial denitrifiers over complete denitrifiers in natural ecosystems (Chapter 4). These insights emphasise the importance of studying microbiome selection and activity in reproducible dynamic conditions under laboratory conditions and characterise microbiomes *in situ*.

### 5.1.2. Yet unanswered questions about aerobic denitrification

Several key questions about aerobic denitrification remain. First, *can all heterotrophic denitrifiers perform aerobic denitrification under alternating oxic-anoxic conditions, or is this ability limited to certain species?* Past research suggests that only specific denitrifiers are capable of this, but I hypothesise that many denitrifiers may be able to aerobically

denitrify to some extent if exposed to fluctuating oxygen availability. This ability will likely depend on the oxygen inhibition of their denitrification enzymes or the electron distribution to the respiratory enzymes, rather than transcriptional regulation mechanisms. This can be tested by exposing different denitrifying species to alternating oxic-anoxic conditions.

Another open question is: *How do aerobic denitrification rates vary with different frequencies of oxic-anoxic cycling?* The research developed in Chapter 2 addressed this by exposing denitrifying cultures to different cycling frequencies. Though no significant rate differences were observed, it would be good to test a wider range of cycle frequencies. I hypothesise that the rates will not be significantly affected by the cycling frequency as long as it exceeds protein turnover rates. This naturally raises the question: *What is the lowest cycling frequency at which we can still observe aerobic denitrification?* The answer to this question may also provide some insights into how significant aerobic denitrification is in different environments.

Aerobic denitrification alters our understanding of denitrification, but it also reshapes how we (should) interpret N<sub>2</sub>O emission data. Previously, it was reasonable to assume that all N<sub>2</sub>O emissions in oxic environments were attributed to ammonia oxidising bacteria (AOB), as denitrification was considered inactive. However, aerobic denitrification may be a significant source of N<sub>2</sub>O in environments frequently subjected to oxic-anoxic fluctuations (Chapter 2), such as soils, marine sediments, and wastewater treatment plants. A key question remains: *To what extent does aerobic denitrification occur in these environments, and how much does it contribute to N<sub>2</sub>O production (and consumption)?* Obtaining the answer to this question remains challenging. The most accurate quantification of aerobic denitrification in natural environments would involve studying microbial communities *in situ*, potentially by combining multi-omics (to resolve key microbial players) with isotope tracing (to follow the conversions of nitrogen compounds). However, current isotope-based methods still fall short of differentiating nitrifier and heterotrophic denitrification, making it challenging to quantify the contribution of aerobic denitrification to N<sub>2</sub>O emissions. Besides, it may be difficult to ensure highly oxygenated conditions *in situ*. Instead, *ex situ* incubations of soil, marine, and activated sludge samples with nitrate may be necessary, similarly to experiments performed by Gao et al. (2010), Marchant et al. (2017), and Morley et al. (2008). In all experiments, incubations should be performed under fluctuating oxic-anoxic conditions and care must be taken to ensure that there are no anoxic niches in the oxic phase. Incubations with and without ammonia oxidation inhibitors (such as ATU) could help distinguish between AOB and denitrifiers as N<sub>2</sub>O-producing organisms.



### 5.1.3. Classification of microbial guilds

The growing complexity of the nitrogen cycle challenges not only our understanding of microbial systems but also the classification of nitrogen-converting processes and organisms. Definitions of “denitrification” range from the complete reduction of nitrate to dinitrogen gas <sup>4</sup> to partial reductions like nitrite to nitric oxide or nitrous oxide <sup>5,6</sup>. Aerobic denitrification adds further complexity, with some researchers including nitrifier denitrification under this term. As a result, it often falls upon the reader to interpret the terminology used in research articles.

5

The wide distribution of denitrification genes across various taxa and functional groups further complicates classifying organisms as “denitrifiers”. Typically, denitrifiers are defined as organisms using nitrogen oxides for energy conservation, separating them from organisms like AOB. However, this raises the question: *Can we be certain that AOB do not conserve energy through denitrification, and if they do, would that qualify them as denitrifiers?* While Hink et al. (2017) suggested that denitrification contributes minimally to respiration in one AOB species, evidence is still lacking to definitively rule out the possibility of energy conservation through nitrifier denitrification. Additionally, in complex ecosystems, determining the physiological role of denitrification for each organism would require cultivating thousands of species, making it impractical to identify “true” denitrifiers. Given these limitations, our analysis of denitrification labour division (Chapter 4) adopted a broader approach by including all organisms with at least one denitrification gene.

As an alternative solution to the somewhat ambiguous microbial guild definitions, Kuypers et al. (2018) proposed to “refrain from classifying organisms” by function (e.g. nitrifiers, denitrifiers) and instead focus on the processes (e.g. nitrification, denitrification). Though this better reflects the complexity within the nitrogen cycle, in practice, it remains challenging to discuss microbial roles without grouping organisms. Even Kuypers et al. (2018) continue to refer to “denitrifying microorganisms”, effectively reintroducing the classification under a different term. There is thus a pressing need to standardise terminology as new metabolic pathways and organisms continue to emerge and blur existing definitions. For now, it is essential to remember that organisms within the same functional group are not physiologically identical, and generalising findings from single species to entire guilds risks oversimplification in ecological contexts.

## 5.2. What further steps are needed to mitigate N<sub>2</sub>O emissions in WWTPs?

### 5.2.1. Determine universality of mechanisms driving seasonal N<sub>2</sub>O emissions

In Chapter 3, we identified the balance between AOB and NOB as a key factor underlying seasonal nitrite accumulation and subsequent N<sub>2</sub>O emissions at the Amsterdam-West WWTP. We hypothesised that nitrifier denitrification by AOB is the main N<sub>2</sub>O-producing pathway during seasonal emissions. Yet, *are these mechanisms observed in all wastewater treatment plants with seasonal N<sub>2</sub>O emissions?* To develop universal mitigation strategies, it is essential to confirm that similar dynamics occur in other plants. This requires comparing operational data and microbial dynamics across multiple WWTP, including both activated and granular sludge plants. WWTPs without seasonal emissions should also be studied to identify potential solutions to mitigate these emissions in other plants.

The insights from Chapter 3 can help streamline future microbial characterisations across different WWTPs. By analysing only a few DNA samples from each plant, metagenome-assembled genomes (MAGs) representing a large portion of the microbiome can be obtained. Several MAGs will overlap across WWTPs, so they can be combined with those from this thesis and public datasets (as was done in Chapter 3), to create a single collection of activated sludge MAGs. When using MAGs from different sources, it is important to use consistent software and databases for taxonomic and functional annotation to avoid discrepancies. The unbinned DNA portion should not be disregarded, as it may hold valuable genetic information, especially if it is used as database for metaproteomics. Aside from MAG reconstruction, time-based microbial DNA dynamics can be captured by more frequent sampling using, for example, lower sequencing depths or 16S rRNA amplicon sequencing, and linking this information to the MAGs (similar to what was done by Valk et al. (2022)). However, despite the importance of detailed genomic characterisations, insights into the dynamics of specific nitrogen-converting enzymes are indispensable to further study the mechanisms underlying N<sub>2</sub>O emissions. As for the activity tests, though useful to support DNA and protein observations, they were laborious and less informative compared to metaproteomics. Therefore, metaproteomics combined with metagenomics, should be prioritised for future studies. The profiles in Chapter 3 can be used as guideline to choose sample frequency and timepoints in other WWTPs. Metatranscriptomics may offer an alternative proxy for microbial activity, yet seasonal transcript dynamics of activated sludge may be masked by daily variations.

Besides looking at daily averages, monitoring profiles of nitrogen intermediates (ammonia, nitrite, nitrate, nitric oxide, and nitrous oxide) throughout the day in both oxic and anoxic tanks may also prove very informative. It is important to identify where

nitrite and nitrous oxide accumulate during the seasonal peaks to confirm that nitrifiers are indeed the main source. Online monitoring of key parameters such as dissolved oxygen, temperature, and pH, alongside nitrogen intermediates, can provide key insights of microbial processes at larger timescales. The focus should not lie on every little fluctuation in these profiles, but on how the profiles change seasonally. For example, in Chapter 3, the daily patterns showed that  $\text{N}_2\text{O}$  emissions strongly correlated with dissolved oxygen during peak periods, suggesting oxygen as the limiting nutrient for AOB.

### 5.2.2. Practical solutions to minimise $\text{N}_2\text{O}$ emissions

To minimise  $\text{N}_2\text{O}$  emissions in WWTPs, seasonal peaks should be prioritised, as they account for most of the annual emissions – 65% in the case of the Amsterdam-West WWTP. Testing full-scale mitigation strategies is essential, but *which approaches do we test?* Since nitrite accumulation drives  $\text{N}_2\text{O}$  emissions, reducing nitrite is key. The balance between AOB and NOB largely determines nitrite levels, yet this balance is challenging to maintain (Chapter 3).

One potential solution is to increase dissolved oxygen levels before temperature drops, preventing ammonia accumulation and selective NOB washout (Chapter 3). The seasonal accumulation of nitrite results from amplified daily nitrite peaks, so applying similar oxygen control on a daily basis could contribute to overall seasonal nitrite reduction. Increasing the SRT (and sludge concentration) ahead of peak months could enhance the ammonia and nitrite oxidation capacity and prevent NOB washout <sup>10</sup>, potentially avoiding the need for increased oxygen input while saving energy. However, a combination of strategies is likely the most effective. Implementing these strategies proactively, before the seasonal peak arises, is essential, as microbial communities require time to respond.

Optimising denitrification offers another potential solution. Increasing denitrification capacity by extending anoxic HRT or raising sludge concentrations could enhance nitrite consumption. However, this may not fully compensate for nitrite buildup from AOB/NOB imbalances. Besides, as most  $\text{N}_2\text{O}$  is produced in the oxic tank and stripped before reaching the denitrification tank, preventing its formation is likely the most effective strategy. Nonetheless, maximising denitrification capacity can further contribute to reducing emissions <sup>11–13</sup>.

### 5.2.3. To what extent can emissions be mitigated?

During this research, I was often asked: *Will we be able to bring N<sub>2</sub>O emissions to zero?* In my (possibly pessimistic) opinion, probably not. The complexity of WWTPs and their microbiomes, along with fluctuating conditions, makes it unlikely that we will be able to completely eliminate N<sub>2</sub>O emissions. However, with an improved understanding of microbial mechanisms and advances in operational and microbial monitoring technologies, significant reductions to negligible levels are possible.

Additionally, covered WWTPs may implement end-of-pipe technologies to remove or recover N<sub>2</sub>O from the off-gas. Promising options include bioscrubbers and biofilters, which can denitrify N<sub>2</sub>O to N<sub>2</sub> <sup>14,15</sup>. However, these technologies only remove part of the N<sub>2</sub>O, challenged by factors such as low N<sub>2</sub>O concentrations, limited gas-liquid transfer, high oxygen concentrations, organic carbon supply, and the fluctuating availability of N<sub>2</sub>O in full-scale systems. Physical-chemical technologies, often applied in chemical industries, are limited by the low N<sub>2</sub>O concentrations and require chemicals, expensive catalysts, and high energy inputs, counteracting the benefits of removing N<sub>2</sub>O <sup>16</sup>. Recovery of N<sub>2</sub>O as an energy source is also under investigation, but current off-gas concentration are too low to make this approach feasible <sup>17,18</sup>. Besides, only a small fraction of WWTPs worldwide are covered, so even if these approaches prove effective, they would not be applicable to most plants.

### 5.3. Do omics tools live up to the hype in microbial ecology research?

*Short answer:* it depends. *Long answer:* absolutely, but we must be aware of their limitations and carefully align their use with our research questions.

#### 5.3.1. Limitations and opportunities of meta-omics in complex microbiomes

Meta-omics technologies have revolutionised our understanding of microbial communities, both *in situ* and in the lab. They offer unparalleled insight into microbial taxonomic and functional diversity, as demonstrated throughout this thesis. However, their application to complex microbiomes still faces challenges.

Metagenomics enables the analysis of the entire DNA from a community, yet information is lost during DNA sequencing, assembly, and binning <sup>19</sup>. For example, in Chapter 3, a large portion of DNA fragments could not be assigned to any MAGs. In complex communities like WWTPs, lower-abundance species are often not covered and it is difficult to differentiate closely related strains, potentially obscuring functional differences. Additionally, interpretation of metagenomic data relies on existing

biochemical knowledge, i.e. genes with unknown functions will remain unidentified. Even well-characterised genes may have varying, yet unknown, roles across different organisms. For example, the NirK protein typically reduces nitrite to nitric oxide but may catalyse the reverse reaction in AOB <sup>20</sup>.

Metaproteomics, combined with metagenomics, offers valuable insight into the active functions of microbial communities, capturing changes that may not be evident at the DNA level. However, it requires specialised facilities and expertise, low-abundant proteins are often not detected, and proteins from closely related organisms may be indistinguishable <sup>21</sup>. For example, in Chapter 3, the NirK proteins of two *Nitrospira* MAGs could not be differentiated. Membrane proteins, essential for understanding processes like nitric oxide reduction, respiratory processes, and nutrient transport are also often not detected using standard protein extraction protocols (Chapters 2 and 3). Despite these challenges, the accessibility and effectiveness of metaproteomics will improve with time, making it an indispensable tool in microbial ecophysiology. In the meantime, metatranscriptomics could help overcome some of these limitations. For example, metatranscriptomics could help identify active denitrifiers and the extent of denitrification labour division in WWTPs (Chapters 3 and 4).

For all omics techniques, differences in extraction methods, sequencing approaches, and bioinformatic analyses can lead to inconsistent results <sup>22,23</sup>. Future advances in omics technologies will likely overcome many of the challenges listed here, but until then, researchers must be mindful of these limitations and select research questions that can be addressed within these constraints. Additionally, traditional physiological and biochemical studies remain crucial to resolve the roles of key organisms and enzymes in nitrogen conversions.

### 5.3.2. Data handling: the next big challenge in microbial ecology research

As omics tools become more accessible, microbial ecology studies are generating vast amounts of data. This presents two key challenges: data management and interpretation. First, the large volumes of data often overwhelm the storage capacity, processing power, and bioinformatics expertise available to many labs. Instead of generating excessive data, researchers should focus on using appropriate tools for specific research questions and make use of existing public repositories. Standardisation in data generation and reporting, including detailed metadata, is critical to facilitate this. Second, large datasets increase the risk of overemphasising correlations, particularly with the rise of machine learning techniques <sup>24</sup>. While useful to explore data and generate hypotheses, correlations may arise even when variables are not causally related <sup>25</sup>. Researchers must critically assess whether these correlations have real

biological significance. Ultimately, the mechanistic interpretation of data is vital to convert large-scale data into practical applications, such as mitigating N<sub>2</sub>O emissions.

## 5.4. References

1. Morley N, Baggs EM, Dörsch P, Bakken L. Production of NO, N<sub>2</sub>O and N<sub>2</sub> by extracted soil bacteria, regulation by NO<sub>2</sub><sup>-</sup> and O<sub>2</sub> concentrations. *FEMS Microbiol Ecol.* 2008;65(1):102-112. doi:10.1111/j.1574-6941.2008.00495.x
2. Marchant HK, Ahmerkamp S, Lavik G, et al. Denitrifying community in coastal sediments performs aerobic and anaerobic respiration simultaneously. *ISME J.* 2017;11(8):1799-1812. doi:10.1038/ismej.2017.51
3. Gao H, Schreiber F, Collins G, et al. Aerobic denitrification in permeable Wadden Sea sediments. *ISME J.* 2010;4(3):417-426. doi:10.1038/ismej.2009.127
4. Sanford RA, Wagner DD, Wu Q, et al. Unexpected nondenitrifier nitrous oxide reductase gene diversity and abundance in soils. *Proc Natl Acad Sci U S A.* 2012;109(48):19709-19714. doi:10.1073/pnas.1211238109
5. Zumft WG. Cell biology and molecular basis of denitrification. *Microbiol Mol Biol Rev.* 1997;61(4):533-616. doi:10.1128/mmbr.61.4.533-616.1997
6. Lycus P, Bøthun KL, Bergaust L, Shapleigh JP, Bakken LR, Frostegård Å. Phenotypic and genotypic richness of denitrifiers revealed by a novel isolation strategy. *ISME J.* 2017;11(10):2219-2232. doi:10.1038/ismej.2017.82
7. Hink L, Lycus P, Gubry-Rangin C, et al. Kinetics of NH<sub>3</sub>-oxidation, NO<sub>2</sub><sup>-</sup>-turnover, N<sub>2</sub>O-production and electron flow during oxygen depletion in model bacterial and archaeal ammonia oxidisers. *Environ Microbiol.* 2017;19(12):4882-4896. doi:10.1111/1462-2920.13914
8. Kuypers MMM, Marchant HK, Kartal B. The microbial nitrogen-cycling network. *Nat Rev Microbiol.* 2018;16(5):263-276. doi:10.1038/nrmicro.2018.9
9. Valk L, Peces M, Singleton CM, et al. Exploring the microbial influence on seasonal nitrous oxide concentration in a full-scale wastewater treatment plant using metagenome assembled genomes. *Water Res.* 2022;219(May):118563. doi:10.1016/j.watres.2022.118563
10. Gruber W, Niederdorfer R, Ringwald J, Morgenroth E, Bürgmann H, Joss A. Linking seasonal N<sub>2</sub>O emissions and nitrification failures to microbial dynamics in a SBR wastewater treatment plant. *Water Res X.* 2021;11:100098. doi:10.1016/j.wroa.2021.100098
11. Desloover J, Vlaeminck SE, Clauwaert P, Verstraete W, Boon N. Strategies to mitigate N<sub>2</sub>O emissions from biological nitrogen

- removal systems. *Curr Opin Biotechnol.* 2012;23(3):474-482. doi:10.1016/j.copbio.2011.12.030
12. Gruber W, von Känel L, Vogt L, et al. Estimation of countrywide N<sub>2</sub>O emissions from wastewater treatment in Switzerland using long-term monitoring data. *Water Res X.* 2021;13(September). doi:10.1016/j.wroa.2021.100122
  13. Conthe M, Lycus P, Arntzen M, et al. Denitrification as an N<sub>2</sub>O sink. *Water Res.* 2019;151:381-387. doi:10.1016/j.watres.2018.11.087
  14. Yoon H, Song MJ, Yoon S. Design and Feasibility Analysis of a Self-Sustaining Biofiltration System for Removal of Low Concentration N<sub>2</sub>O Emitted from Wastewater Treatment Plants. *Environ Sci Technol.* 2017;51(18):10736-10745. doi:10.1021/acs.est.7b02750
  15. Frutos OD, Quijano G, Pérez R, Muñoz R. Simultaneous biological nitrous oxide abatement and wastewater treatment in a denitrifying off-gas bioscrubber. *Chem Eng J.* 2016;288:28-37. doi:10.1016/j.cej.2015.11.088
  16. Frutos OD, Quijano G, Aizpuru A, Muñoz R. A state-of-the-art review on nitrous oxide control from waste treatment and industrial sources. *Biotechnol Adv.* 2018;36(4):1025-1037. doi:10.1016/j.biotechadv.2018.03.004
  17. Duan H, Zhao Y, Koch K, et al. Recovery of Nitrous Oxide from Wastewater Treatment: Current Status and Perspectives. *ACS ES T Water.* 2021;1(2):240-250. doi:10.1021/ACSESTWATER.0C00140
  18. Zhang M, Gu J, Liu Y. Engineering feasibility, economic viability and environmental sustainability of energy recovery from nitrous oxide in biological wastewater treatment plant. *Bioresour Technol.* 2019;282(March):514-519. doi:10.1016/j.biortech.2019.03.040
  19. Quince C, Walker AW, Simpson JT, Loman NJ, Segata N. Shotgun metagenomics, from sampling to analysis. *Nat Biotechnol.* 2017;35(9):833-844. doi:10.1038/nbt.3935
  20. Stein LY. Insights into the physiology of ammonia-oxidizing microorganisms. *Curr Opin Chem Biol.* 2019;49:9-15. doi:10.1016/j.cbpa.2018.09.003
  21. Lohmann P, Schäpe SS, Haange SB, et al. Function is what counts: how microbial community complexity affects species, proteome and pathway coverage in metaproteomics. *Expert Rev Proteomics.* 2020;17(2):163-173. doi:10.1080/14789450.2020.1738931
  22. Van Den Bossche T, Kunath BJ, Schallert K, et al. Critical Assessment of MetaProteome Investigation (CAMPI): a multi-laboratory comparison of established workflows. *Nat Commun.* 2021;12(1):1-15.



- doi:10.1038/s41467-021-27542-8
23. Sczyrba A, Hofmann P, Belmann P, et al. Critical Assessment of Metagenome Interpretation - A benchmark of metagenomics software. *Nat Methods*. 2017;14(11):1063-1071. doi:10.1038/nmeth.4458
  24. Hernández Medina R, Kutuzova S, Nielsen KN, et al. Machine learning and deep learning applications in microbiome research. *ISME Commun*. 2022;2(1):1-7. doi:10.1038/s43705-022-00182-9
  25. Carr A, Diener C, Baliga NS, Gibbons SM. Use and abuse of correlation analyses in microbial ecology. *ISME J*. 2019;13(11):2647-2655. doi:10.1038/s41396-019-0459-z



## ACKNOWLEDGEMENTS

This book and, most importantly, my scientific and personal growth would not exist without the wonderful people I was lucky enough to meet and work with over these four years.

I only made it because of all of you.

**Michele**, thank you for opening every possible and impossible door for me ever since we met. Every achievement of this PhD was possible because of you. Thank you for pushing me into uncomfortable situations, for being able to motivate me even at my lowest with your endless enthusiasm, for feeding my perfectionism (and for teaching me that there is always another level for it!), for teaching me to set and meet high-quality standards in everything I do, and for investing so much time and energy into this. Thank you for driving me crazy with all your writing feedback, for spending half our meetings chitchatting and venting about life as much as science, for making me feel like I could ask and tell you anything, and for making me believe in myself. I could fill a whole book with thank-yous for you alone. I could not have asked for a better supervisor, and I truly believe the academic world needs more Micheles.

**Mark**, thank you for building such a wonderful group and for creating an atmosphere where I felt at home from day one. I feel incredibly lucky to have done my PhD under your guidance. Thank you for teaching me to put healthy limits on my perfectionism, for reminding me that overthinking is not always the answer, and for giving me the freedom to explore my own ideas. Thank you for embracing every bit of the craziness that came from Michele and me, for constantly amazing me with your creativity, for always making time to help despite your overflowing schedule, and for having Friday beers with us. You are an example of the kind of leader I hope to work with, and maybe become, one day.

When it comes to supervisees, I won the lottery. Working with you was the most fun part of my PhD. **Claudia**, your incredible level of organisation and meticulousness did not just improve our work, it defined how I approached the rest of my PhD. **Menno**, your creativity and efficiency are something I can only strive for. **Minke**, Chapter 2 exists only because of your endless persistence and determination. **Nienke**, I also place you in this category because working with you was just as joyful and enlightening. Your “doer” spirit is still something I look up to. Thank you all for always showing up with a smile, for making it so much fun to work together, for keeping both your motivation and mine high,

for teaching me so much, for making our research a success, and for being my partners in crime through every high and low.

**Martin**, thank you for so diligently and persistently working on developing a method for our samples, for always being so kind and enthusiastic, and for welcoming my million questions with a smile. **Thomas**, I wish we had had more chances to meet, because every time we did, it was a pleasure. Your openness, (pleasant) directness, and your refreshing “can do” attitude are exactly the kind of energy academia needs more of. **Marcel**, thank you for being my go-to wastewater treatment supervisor, for saying “yes” to all my requests, and for guiding me in the right direction. Your curiosity, knowledge, and incredible intuition never ceased to amaze me. I am so glad I got to work with you. **Maaïke**, thank you for all the emotional and managerial support, and for always staying so involved. I loved being surrounded by your enthusiasm. **Alexandra, Cora, Floris, Inge, Mariska, Maurice, Robert**, thank you for showing up to every project meeting with genuine interest, advice, and a willingness to listen to my complicated stories. You kept me motivated and reminded me why this research actually matters. Your curiosity and your commitment to research are exactly what is needed to push water technologies forward. **Adrien, Alex, Eddie, Hidde, Marga, Nick, Remmie, Ron, Willem**, thank you for being so helpful with the sludge sampling. Your small acts of kindness were a huge help for me. Everyone from the **CoP lachgas**, thank you for valorising my research and for letting me take a peek into the real-world side of solving the N<sub>2</sub>O problem. It was an absolute pleasure working with you all.

My paranympths, my unconditional cheerleaders, and the ones who carried me through this PhD. I honestly cannot imagine embarking on new adventures without you by my side. I wish I could carry you around in my pocket wherever life takes me next.

**Francesc**, you are probably one of the people most different from me, and yet one of the people I admire most, learned the most from, and teamed up with the best. Your unmatched efficiency, assertiveness, no-bullshit attitude, and genuine curiosity about everything and everyone make me want to be more like you. Thank you for always checking in on me, for turning every trip into an adventure, for introducing me to half the academic world at conferences, for handling my moods, for motivating me, for always finding something interesting to talk about, for boosting my ego when I needed it, for challenging me, for helping me come out of my shell, and for being such a great friend.

**Timmy**, you have a unique capability of putting me in a good mood no matter how shitty I feel (and we both know how hard that is). Our early-morning chats were often the motivational boost that got me through the day. Thank you for bringing so much positivity into my life, for making me feel completely at ease around you, for listening to

all my complains, for making lunch breaks so much fun, for organising the best activities, for being the life of every party, for asking me questions about my research, for inspiring me to be more enthusiastic and social, and for amazing me with your natural talent for teaching and exciting students.

**Venda**, my unofficial paranymp and my endless conversation partner, I don't think we have ever run out of things to talk about. Thank you for the crazy sleepovers and the intense online workout sessions during covid, for always being so easy-going, for cooking amazing food and taking me to the best restaurants, for our birthday lunches, for singing *Tusa* and *Payphone* with me on karaoke nights, for not holding my mood swings against me, for giving the best advice, for dealing with my indecisiveness, for sharing my obsession with being overly prepared, and for turning me into a climbing addict.

To the friends this PhD brought me, each wonderful in their own way, and even better as a group. **Ali**, thank you for entertaining us with your dancing pecs (we are all jealous), and for staying our friend even after the PhD. **Angelos**, thank you for the best hugs and for your contagious smile. **David**, thank you for effortlessly making every encounter a fun one, and for introducing me to the best song in the world. **Jan**, thank you for always being so enthusiastic, and for making me the best coffee in the world (setting impossible standards for any future coffee I will drink). **Lemin**, thank you for your infinite sweetness, contagious positivity, and nutritional lessons. **Mariana** thank you for being unapologetically you, and for shamelessly (yet tastefully) making fun of everyone. **Maxim**, thank you for being the sunshine on the other side of the wall, hearing you sing or watching you slam yourself against the window always made my day. **Rodoula**, thank you for being so much fun, for making the boys' office so welcoming, and for being my fashion icon. **Sam**, thank you for bravely embracing your role as the group's roast target and for bringing some much-needed maturity to the group. **Sergio**, thank you for your never-ending energy, and of course, for the unforgettable *Toxic* performances. **Stefan**, thank you for being the perfect mix of calm, open, and crazy, sharing so many climbing sessions with you was so much fun. Thank you all for filling this journey with laughter, craziness, inside jokes, and unforgettable moments.

**Zeja**, you deserve a special spot in these acknowledgements. I do not think I have ever met anyone with a heart as big as yours, being around you is pure joy. Thank you for all the amazing food you cooked for me, for the lovely chats, and for sharing beers on sunny afternoons.

I feel incredibly lucky to have done my PhD in such a warm and supporting group as EBT. To my many officemates, **Beck, Carlota, Changlin, Daphne, David, Eloi, Emine, Karel**,

**Martijn, Meryem, Sara, Sofia, Timo, Vittoria** (I hope I did not forget anyone...), thank you for the lovely chats and for brightening up the office every day. To my fellow EBTers, **Alba, Beatriz, Chris, Claudia, Diana, Gerben, Goncalo, Heike, Hugo, Ingrid, Ismail, Jelle, Jelmer, Ji, Jisk, Jitske, João, Jules, Jure, Linghang, Luz, Mario, Marit, Marta, Marte, Miguel, Morez, Natalia, Patricia, Phillip, Pim, Puck, Ramon, Rebeca, Robbert, Samarpita, Sebastian, Siem, Sirous, Sofia, Viktor, Yubo, Yuemei**, thank you for all the fun lunches, Friday drinks, barbecues, coffees, cakes, defence parties, corridor chats, and conferences. A big thank you the EBTers (**Ben, Carol, Dirk, Dita, Miranda, Zita**) and non-EBTers (**Anita, Apilena, Astrid, Gea, Jannie, Kawieta, Marinka, Miranda, Nayyar**) that were always ready to help, kept things running smoothly in- and outside the lab, and brought so much positive energy to the group. And to all the lovely people outside EBT who I had the pleasure of sharing meetings, teaching duties, parties, coffees, dinners, and barbecues with, **Alexandra, Cees, Chiara, Chiel, Georg, Esther, Hector, Hugo, Ilse, Koen, Lars, Marina, Roos, Roxana, Simon, Stephanie**, thank you for making every experience so much more fun!

**Cristian**, a special thanks to you for letting me help with your teaching, and for all the lovely catch-ups when you are back in Delft. I learned so much and had such a good time. Your passion, dedication, and talent for captivating students is hard to find, and deserves much more appreciation than it gets. **David**, thank for always being such a fun person to be around, for introducing me to so many people at conferences, and for your constant support and belief that I can do anything. I hope to keep in touch. **Dimitry**, thank you for always making time for our incredibly enjoyable chats, for making me think critically about my work, and for sharing your knowledge and opinions so generously. Having you around these years was an absolute privilege. **Gijs**, thank you for your invaluable insights and for your excitement about our research. Our conversations were always such a pleasure and so helpful. Your genuine passion for microorganisms and science is something rare and incredibly inspiring.

To my non-PhD friends, thank you for your invaluable support over these years, it truly made all the difference.

To my “weekend friends”, thank you for the most fun dinners, boardgames, go-karting sessions, trips, and best birthday gifts. **Álvaro**, thank you for your positive energy and endless jokes. **Fernanda**, for bringing so much sweetness to the group. **Jorge**, for turning every activity into a blast. **Melina**, for your positivity, honesty, and for showing us the very best of Greek hospitality. **Ricardo**, for always making me feel at home no matter how long we have not seen each other, I miss you. **Sara**, for helping me bring some much-needed order to this chaotic group, and for preparing the loveliest brunches, lunches, and afternoon snacks.

To my Leiden friends, **Bernardo, Carlo, Ezgi, Matej, Tim**, thank you for making every climbing session, trip, cooking adventure, dinner, concert, and sunny walk so much fun. And a special thank you for your invaluable support during the seemingly never-ending design of the cover of this dissertation.

To my Erasmus friends, **Amy, Axel, Elio, Josema, Nico, Ramona, Volker**, thank you for the incredibly fun reunions every year, here's to many more in the future.

To my master friends, **Britt, Julia, Guillaume, Sasha, Shupan**, thank you for keeping in touch and for making every catch-up just as fun as our time together in Delft.

E aos meus amigos em Portugal, porque quando estou com vocês, estou em casa. **Inês**, reencontrar-te é sempre uma alegria como nenhuma outra. **Lu**, os nossos jantarinhos são sempre o ponto alto das minhas visitas a Lisboa. **Simone**, obrigada por trazeres um bocadinho do sol Português à minha via na Holanda. Aos meus amigos de infância, **Ana, André, Andreia, Antónia, António, Carina, Cláudia, Fatinha, Helena, Joana, Mariana, Fatinha**, obrigada pela animação, pelas recordações, e por me fazerem doer as bochechas de tanto rir sempre que nos reencontramos.

**Mama, Papa, Paul, Laura**, omdat jullie me alle kansen van de wereld hebben gegeven om te worden wie ik wilde zijn, en omdat ik bij jullie altijd thuis ben en helemaal mezelf kan zijn, waar we ook zijn. Zonder jullie was dit nooit gelukt.

**Matteo**, my support, my sun, my favourite person in the world. Thank you for wanting to celebrate even my tiniest achievements, for always being up for ice cream, for our endless boardgame battles, for being excited to jump into new adventures with me, for accepting every one of my moods, for knowing exactly when to help me and when to leave me alone, for making me a better person, and for making me so happy every single day. **Diego, Manuela, Rebecca, Paolo**, grazie per avermi dato il più caloroso benvenuto nella vostra famiglia, siete le persone più dolci che abbia mai incontrato. Grazie per avermi insegnato che il vero stress non è un dottorato, ma giocare a *Ligretto* con voi.





# CURRICULUM VITAE

13-12-1996 Born in Veldhoven, the Netherlands

## Education

2020-2025 **PhD Environmental Biotechnology**  
*Delft University of Technology, the Netherlands*  
**Thesis:** Ecophysiology of N<sub>2</sub>O-emitting microbial communities  
**(Co)promoters:** prof. dr. ir. M. C. M. van Loosdrecht and dr. M. Laurení



2017-2019 **MSc Life Science and Technology**  
Biochemical Engineering, *cum laude*  
*Delft University of Technology, the Netherlands*  
**Thesis:** Novel insights into the nitrogen cycle: integrating thermodynamics, modelling, and laboratory enrichments  
**Supervisors:** prof. dr. D. Weissbrodt and dr. M. Laurení

2014-2017 **BSc Biological Engineering Sciences**  
*Instituto Superior Técnico, Universidade de Lisboa, Portugal*

## Work experience

2020-2025 **PhD Researcher**  
*Delft University of Technology, the Netherlands*  
Ecophysiology of N<sub>2</sub>O-emitting microbial communities

2019-2020 **Intern & Junior Research Assistant**  
*Nestlé Research, Switzerland*  
Enzymatic degradation of packaging materials

2018-2019 **Master Student Researcher**  
*Delft University of Technology, the Netherlands*  
**Project 1:** Novel insights into the nitrogen cycle: integrating thermodynamics, modelling, and laboratory enrichments  
**Project 2:** *Saccharomyces cerevisiae* engineering with CRISPR-Cas

2017 **Laboratory Summer Intern**  
*Instituto Gulbenkian da Ciência*  
Quantitative analysis of GFP-tagged cohesion in *Drosophila melanogaster*



# SCIENTIFIC CONTRIBUTIONS

## Journal articles

**Roothans N**, Pabst M, van Diemen M, Herrera Mexicano C, Zandvoort M, Abeel T, van Loosdrecht MCM, Laureni M. Long-term multi-meta-omics resolves the ecophysiological controls of seasonal N<sub>2</sub>O emissions during wastewater treatment. *Nat Water* 2025 (*manuscript accepted*)

**Roothans N**, van Loosdrecht MCM, Laureni, M. Metabolic labour division trade-offs in denitrifying microbiomes. *ISME J* 2025;19:wraf020, <https://doi.org/10.1093/ismejo/wraf020>

Laureni M, Corbera Rubio F, Kim DD, Browne S, **Roothans N**, Weissbrodt DG, Olavarria K, de Jonge N, Yoon S, Pabst M, van Loosdrecht MCM, Selective enrichment of high-affinity clade II N<sub>2</sub>O-reducers in a mixed culture, *ISME Comm* 2025; ycaf022, <https://doi.org/10.1093/ismeco/ycaf022>

**Roothans N**, Gabriëls M, Abeel T, Pabst M, van Loosdrecht MCM, Laureni M. Aerobic denitrification as an N<sub>2</sub>O source from microbial communities. *ISME J* 2024;18:wrae116, <https://doi.org/10.1093/ismejo/wrae116>

## Patents

Börner T, Srebny V, **Roothans N**. Enzymatic recycling of polyurethanes by a combination of cutinases and esterases. *U.S. Patent and Trademark Office* 2024, US20240084094A1. (Nestlé SA)

Börner T, Srebny V, **Roothans N**. Enzymatic recycling of polyurethanes by a combination of cutinases and lipases. *U.S. Patent and Trademark Office* 2024, US20240067793A1. (Nestlé SA)

Börner T, **Roothans N**. Enzymatic recycling of recycled polyethylene terephthalate by cutinases. *U.S. Patent and Trademark Office* 2024, US20240301160A1. (Nestlé SA)

Börner T, Srebny V, **Roothans N**. Enzymatic recycling of polyurethanes by cutinases. *U.S. Patent and Trademark Office* 2023, US20230391978A1. (Nestlé SA)

## Conference proceedings

Presenting author in **bold**:

**Roothans N**, Pabst M, van Diemen M, Herrera Mexicano C, Zandvoort M, Abeel T, van Loosdrecht MCM, Laureni M. Meta-omics resolves the microbial mechanisms underlying seasonal N<sub>2</sub>O emissions. *Scientific Spring Meeting KNVM & NVMM*, Papendal (Netherlands) 2025

**Roothans N**, Pabst M, van Diemen M, Herrera Mexicano C, Zandvoort M, Abeel T, van Loosdrecht MCM, Laureni M. Long-term ecophysiological profiling of the wastewater microbiome underlying N<sub>2</sub>O emissions. *10th Microbial Ecology and Water Engineering Specialist Conference*, Brisbane (Australia) 2023, International Water Association

Roothans N, Gabriëls M, Abeel T, Pabst M, van Loosdrecht MCM, **Laureni M**. Aerobic heterotrophic denitrification as N<sub>2</sub>O source in mixed communities. *26th European Nitrogen Cycle Meeting*, Oslo (Norway) 2023

**Roothans N**, Pabst M, van Diemen M, Herrera Mexicano C, Zandvoort M, Abeel T, van Loosdrecht MCM, Laureni M. Long-term ecophysiological profiling of the wastewater microbiome underlying N<sub>2</sub>O emissions. *25th European Nitrogen Cycle Meeting*, Rome (Italy) 2022

**Roothans N**, Pabst M, van Diemen M, Herrera Mexicano C, Zandvoort M, Abeel T, van Loosdrecht MCM, Laureni M. Proteome-based wastewater microbiome dynamics underlying N<sub>2</sub>O emissions. *18th International Symposium on Microbial Ecology*, Lausanne (Switzerland) 2022, International Society for Microbial Ecology

**Roothans N**, Corbera Rubio F, Weissbrodt DG, Picioreanu C, van Loosdrecht MCM, Laureni M. The role of Dissimilatory Nitrite Reduction to Ammonium (DNRA) in anammox-based biofilm systems at high influent COD/NO<sub>2</sub><sup>-</sup>. *Nutrient Removal and Recovery Conference*, 2020 (online), International Water Association

## Awards

Kiem award, Best first publication by young microbiologists, *Koninklijke Nederlandse Vereniging voor Microbiologie (KNVM) & Nederlandse Vereniging voor Medische Microbiologie (NVMM)*, 2025.